PERFORMANCE EVALUATION OF FRICTION

DAMPED BRACED STEEL FRAMES UNDER SIMULATED EARTHQUAKE LOADS

by

ANDRE FILIATRAULT

B.A.Sc., University of Sherbrooke, 1983

A THESIS SUBMITTED IN PARTIAL FULFILLMENT OF

THE REQUIREMENTS FOR THE DEGREE OF

MASTER OF APPLIED SCIENCE

in

THE FACULTY OF GRADUATE STUDIES

Department of Civil Engineering

We accept this thesis as conforming

to the required standard

THE UNIVERSITY OF BRITISH COLUMBIA

October 1985

Department of _____Civil Engineering_____

The University of British Columbia
1956 Main Mall
Vancouver, Canada
V6T 1Y3

Date _____October, 1985_____

ABSTRACT

This thesis presents the results obtained from qualification tests of a new friction damping system, which has been proposed in order to improve the response of Moment Resisting Frames and Braced Moment Resisting Frames during severe earthquakes. The system basically consists of a special inexpensive mechanism containing friction brake lining pads introduced at the intersection of frame cross-braces. The main objective is to study the performance of a 3 storey Friction Damped Braced Frame model under simulated earthquake loads.

The main members of the test frame were chosen from available hot-rolled sections and the mass selected to provide the expected fundamental frequency of a three storey Moment Resisting Frame. The seismic testing was performed on an earthquake simulator table. The experimental results are compared with the findings of an inelastic time-history dynamic analysis. Two different computer models were used for this purpose. The first one is based on an equivalent hysteretic model and is only approximate, since it does not take into account the complete behaviour of the friction devices. A more refined computer model was then developed and the results from the two models are compared. It is found that the simpler approximate model overestimates the energy dissipated by the devices, but the inaccuracy is relatively small (10-20% in resulting member forces).

To quantify the performance of the Friction Damped Braced Frame relative to conventional aseismic systems, an equivalent viscous damping study is made. Viscous damping is added to the Moment Resisting Frame and the Braced Moment Resisting Frame until their responses become similar to the

response of the Friction Damped Braced Frame. The results show that for
this purpose 38% of critical damping must be added to the Moment Resisting
Frame and 12% to the Braced Moment Resisting Frame. The new system becomes
more efficient as the intensity of the earthquake increases.

The economical potential of the new damping system is investigated by
designing a reduced size Friction Damped Braced Frame having response
characteristics which are similar to those of conventional structural
systems with heavier members. For the model frames studied, the results
show that if the effects of wind, live and torsion loads are neglected, it
is possible to reduce the members sizes of the Friction Damped Braced Frame
by 47% and still achieve a superior performance under strong earthquake, in
comparison to the seismic response of the two other conventional frames
with their original, heavier members.

The results, both analytical and experimental, clearly indicate the
superior performance of the friction damped braced frame compared to
conventional building systems. Even an earthquake record with a peak
acceleration of 0.9 g causes no damage to the Friction Damped Braced Frame,
while the Moment Resisting Frame and the Braced Moment Resisting frame
undergo large inelastic deformations.

TABLE OF CONTENTS

TABLE OF CONTENTS (Continued)

TABLE OF CONTENTS (Continued)

LIST OF FIGURES

LIST OF FIGURES (Continued)

LIST OF FIGURES (Continued)

LIST OF TABLES (Continued)

ACKNOWLEDGEMENTS

<div style="text-align: right">André Filiatrault</div>

October 1985

Vancouver, British Columbia

1. INTRODUCTION

1.1 Background

Earthquake loading is unique among the types of loads that a structural engineer must consider because a great earthquake may cause greater stresses and deflections in various critical components of a structure than all the other loadings combined. From an energy point of view, earthquakes induce kinetic energy in a structure. The amount of energy fed into the structure depends greatly on the natural frequency of the structure compared to the energy distribution of the ground motion expressed in terms of the frequency content of that motion. The level of damage is determined by the manner in which this kinetic energy is absorbed by the structure.

Generally it is not economically feasible to design a structure to resist a major earthquake within the elastic range of the construction materials. The philosophy of most building codes, including the National Building Code of Canada, is based on a criterion of ductility in which the demand on a structure must be balanced by its ductility capacity, i.e. the capacity of the members to safely absorb the induced energy while undergoing inelastic deformations. In this context, the following design criteria are usually adopted:

1. A minor earthquake at the building site should not cause any structural or non-structural damage.

2. A moderate earthquake which may reasonably be expected at the building site during the life of the structure should be taken as the basis of

design. The building should be proportioned to resist this intensity of ground motion without significant damage to the basic structure.

3. During the most severe earthquake that could possibly be expected to occur at the building site during the life of the structure, it is economically justified to permit significant structural damage. However, collapse and loss of life must be avoided.

To meet these design criteria, traditional methods of aseismic design place reliance on the ductility of the structural elements. To optimize the energy absorption without producing a plastic collapse mechanism, it is necessary to consider the yielding pattern of a structure. The "weak beams-strong columns" design philosophy is a typical example of the control of this pattern: the beams are sacrificed first, since local yielding of the beams does not seriously affect the vertical-load-carrying capacity of the structure, whereas local column yielding could easily lead to collapse.

For steel construction, current aseismic structural systems can be grouped into two categories:

1) Braced Moment Resisting Frames;

2) Moment Resisting Frames.

Braced Moment Resisting Frames, where the braces are designed in tension only, are known to be economical and are effective in controlling lateral deflections due to wind and moderate earthquakes; but during extreme earthquakes these structures do not perform well. Being stiffer, they tend to attract higher seismic forces, and their energy dissipation is very poor due to the deteriorating hysteresis loops of the braces.

Figure 1.1 shows a typical hysteresis loop of a tension brace[3]. This kind of hysteresis is called "pinched hysteresis". During a severe shock the tension brace first stretches and subsequently buckles in

compression during reversal of load. On the next application of load in the same direction, the elongated brace is not effective in tension until it is taut again. Therefore, energy dissipation degrades very quickly and this kind of structural system is viewed with suspicion for earthquake resistance.

Moment Resisting Frames are known for their earthquake resistance capability due to their stable ductile behaviour under repeated reversing loads. These structures are very flexible and tend to induce lower seismic forces. However, their great flexibility leads to economical problems since interstorey drift and deflections must be controlled to prevent non-structural damage. Furthermore, because of their large deflections, structural stability is often jeopardized by the P-Δ factor.

In recent years, many authors have shown great interest in the development of structural systems which combine the ductile behaviour of Moment Resisting Frames and the stiffness of Braced Moment Resisting Frames. In Japan, designers often employ Braced Moment Resisting Frames in which the braces are designed to carry only a portion of the lateral loads[1]. An eccentric braced frame is a further step in this direction[2]. In this system the diagonal brace joints are made eccentric to force the beams to yield and dissipate more energy. The structure is saved from collapse during a major earthquake, but the beams are sacrificed and major, costly repairs are needed. Another approach makes use of a base isolation system[12]. In this technique the structure is uncoupled from the earthquake excitation, and its lateral stiffness is thereby reduced, such that its first natural frequency is well below the frequency content of most typical earthquakes. None of these systems are intended to resist major earthquakes within the elastic limit of the materials and will require post-earthquake repairs.

Recently a novel structural system for aseismic design of steel framed buildings has been proposed and patented by A.S. Pall[3]. The system basically consists of an inexpensive mechanism containing friction brake lining pads introduced at the intersection of frame cross-braces. Figure 1.2 shows the location of the friction devices in a typical steel frame. The device is designed not to slip under normal service loads and moderate earthquakes. During severe seismic excitations, the device slips at a predetermined load, before any yielding and cracking of the main members has occurred. Slipping of a device changes the natural frequency of the structure and allows the structure to alter its fundamental mode shape during a severe earthquake. The phenomenon of quasi-resonance between the structure and the earthquake excitation is prevented because of this de-tuning capability of the structure.

1.2 Object and Scope

Although the response of Friction Damped Braced Frames has been studied analytically[3], qualification tests of these structures are lacking. The main objective of the investigation reported in this thesis is to study experimentally the seismic performance of Friction Damped Steel Braced Frame structures. This was done by placing a 3 storey scale model of the structure on a shaking table and subjecting it to representative ground motion time-histories.

A dimensional analysis was first performed to develop a 1/3 scale model of a Moment Resisting Frame. The frame was then designed according to the National Building Code of Canada 1980 and the CAN3 S16.1-M78 "Limit State Design-Steel Structures for Building" Code. The seismic loads were taken into account using the static method. A static, linear analysis was

made and the members were chosen from available hot-rolled sections. The connections of the test frame were designed so that the model could easily be transformed into a Braced Moment Resisting Frame or a Friction Damped Braced Frame as desired. By a proper choice of the test sequence, it was possible to carry out a comparative study of the 3 model types using only a single frame.

Two identical frames were fabricated for this study. The second frame was used as a backup for the primary tests and/or for undertaking further studies, depending on the results of the initial experiments.

All the seismic testing was carried out on the Earthquake Simulator Table in the Civil Engineering Department of the University of British Columbia.

The experimental results are compared to the predictions of an inelastic time-history dynamic analysis using the computer program "DRAIN-2D", which was developed at the University of California in Berkeley. This program consists of a series of subroutines which carry out a step-by-step integration of the dynamic equilibrium equations using a constant acceleration algorithm within any time step.

Two different computer models were used to predict analytically the response of the Friction Damped Braced Frame. The first one, originally proposed by A.S. Pall[3], is based on an equivalent hysteretic model and is only approximate, since it does not take into account the complete behaviour of the friction devices. As a result, a new, refined computer model was developed and the results obtained from analyses using both models are compared.

The friction devices were fabricated at a machine shop in Montreal to develop the optimum slip load as determined from the above noted model

analyses. The optimum slip load is the load which leads to maximum energy dissipation in the friction device.

Quality control testing under cyclic loading is necessary to calibrate the friction devices; these tests were carried out at the University of British Columbia.

An equivalent viscous damping analysis is used to quantify the performance of the Friction Damped Braced Frame relative to the behaviour of conventional aseismic structural systems. In this analysis, viscous damping is added to the Moment Resisting Frame and the Braced Moment Resisting until their responses become similar to the response of the Friction Damped Braced Frame.

Finally, the economical potential of the new damping system is evaluated by designing a reduced size Friction Damped Braced Frame having a response which is similar to the response of conventional structural systems with heavier members.

2. DAMPING SYSTEM

2.1 Description

The proposed damping system uses friction pads to develop additional energy dissipating sources which can be marshalled to protect the main members from structural damage. To be effective the slip joints must present very stable, non-deteriorating hysteresis loops.

Several static and dynamic friction tests on slip joints having different surface treatments have been conducted under repeated reversals of loads and are reported in the literature (4,5,6). Figure 2.1 reproduces the hysteresis loops obtained from a variety of these slip joint surfaces clamped together by 12.7 mm diameter ASTM A325 high strength bolts. Note that the best results are obtained with heavy duty brake lining pads inserted between the sliding steel surfaces. The performance is reliable and repeatable, and the hysteresis loops are rectangular with negligible fade over many more cycles than are encountered in successive earthquakes. For these reasons, this type of slip joint was used in the present study.

If the diagonal braces of an ordinary braced frame structure were designed not to buckle in compression, a simple friction joint could be inserted in each diagonal. In this case each slip joint would act independently of the other. The slip load should be lower than the yield load of the braces so that the joint can be activated before the member yields. However, it is not economical to design the braces in compression and, more often, the braces are quite slender and are designed to be effective in tension only. In such cases a simple friction joint would slip in tension but would not slip back during reversal of the tension load and in the compression (buckled) regime. The energy absorption would be

relatively poor since the brace would not slip again until it was stretched beyond the previous elongated length, as shown in Figure 2.2.

The braces can be made to slip both in tension and compression by connecting a special mechanism at the intersection of frame cross-braces as indicated in Figure 1.2. The details of this mechanism are shown schematically in Figure 2.3. When a seismic lateral load is induced in the frame, one of the braces goes into tension while the other brace buckles very early in compression. If the slip load of the friction joint is lower than the yield load of the brace, when the load in the tension brace reaches the slip load it forces the joint to slip and activates the four links. This in turn, forces the joint in the other brace to slip simultaneously. In this manner, energy is dissipated in both braces in each half cycle. Moreover, in each half cycle, the mechanism straightens the buckled brace and makes it ready to absorb energy immediately when the load is reversed. In this way the energy dissipation of this system is comparable with that of a simple friction joint used with braces which are designed not to buckle in compression.

The friction devices can be used in any configuration of the bracing system. Some possible bracing arrangements are shown in Figure 2.4. These devices also can be conveniently incorporated in existing framed buildings to upgrade their earthquake resistance.

2.2 Simplified Model

Consider the hysteretic behaviour of a simple Friction Damped Braced Frame under seismic load as shown on Figure 2.5. Let

V   = Lateral load at the girder representing the seismic load

Δ_1 = Relative displacement of node C with respect to node A (defined positive in figure)

Δ_2 = Relative displacement of node B with respect to node D (defined positive in figure)

P_1 = Load in brace 1 (positive in tension)

P_2 = Load in brace 2 (positive in tension)

Figure 2.5 also illustrates five stages during a typical load cycle. For each stage the load-deformation curves of both braces and the associated deformed shape of the frame are shown. The following points should be noted during the cycle:

1) In the early stages of loading both braces are active and behave elastically in tension and compression.

2) At very low load the compression brace buckles while the tension brace still stretches elastically in tension.

3) The slip load is reached before yielding occurs in the tension brace. As a result, the four links of the special mechanism are activated and deform into the rhomboid form, which eliminates the buckled shape of the compressive brace under the same buckling load. At the end of the slippage P_2 is still the buckling load but now the compression brace is straight.

4) When the load is reversed the buckled brace is straight and can immediately absorb energy in tension.

5) After the completion of one cycle, the resulting areas of the hysteresis loops are identical for both braces.

The program "Drain-2D" contains truss elements which may be arbitrarily oriented in the x,y plane, but which can transmit axial load only. Two alternative modes of inelastic behaviour may be specified, namely (a)

yielding in both tension and compression and (b) yielding in tension with elastic buckling in compression.

"Drain-2D" can be used in a very simple way to model a Friction Damped Braced Frame. For this prupose we need only replace the friction device by two normal braces which can yield both in tension and compression as shown in Figure 2.6. We define a fictitious yield stress in tension, which corresponds to the stress in the tension brace when the device slips. We also assign a very low fictitious compression yield stress to the material, corresponding to the buckling stress of the compression brace. This simple model was originally proposed and used by A.S. Pall[3].

The Pall model is only approximate since it does not adequately account for the complete deformation pattern of the friction device. The assumed hysteresis behaviour is accurate only if the device slips at every cycle, which is not the case in an actual earthquake. In many cycles the tension brace will not slip but the compression brace will buckle. Under such conditions, the assumed hysteresis behaviour is no longer valid, since the mechanism has not activated the links to pull back the buckled brace.

The simple model also assumes that the slippage of the device is large enough to straighten completely the buckled brace. If in a given cycle the slippage is not large enough to achieve this condition, parts of the energy stored in the compression brace will be restored to the structure (see Figure 2.2). Therefore this simple model overestimates the energy absorption of the friction device. For this reason a more accurate or refined model was developed to evaluate the significance of these simplifying assumptions on the overall response of the structure under a major earthquake.

2.3 Refined Model

To eliminate the assumptions used with the simple model, each member of the mechanism in the Friction Damped Braced Frame is taken as a individual element. Truss elements, each with their individual stress-strain curves, were initially used in this new model. However, assuming pinned connections at the four corners of the mechanism leads to an unstable condition, as shown on Figure 2.7. Therefore these four mechanism connections must be rigid and carry a small amount of bending to ensure stability.

The program "Drain-2D" contains beam-column elements which may be arbitrarily oriented in the xy plane. These elements possess flexural and axial stiffness. Yielding may take place only in concentrated plastic hinges at the element ends. The yield moments may be specified to be different at the two element ends, and for positive and negative bending. The interaction between axial force and moment in producing yield is taken into account approximately by interaction surfaces. However, inelastic axial deformations are assumed not to occur in beam-column elements, because of the difficulty of considering the interaction between axial and flexural deformations after yield. Hence, we cannot use this type of element alone to model the friction device, since we would loose track of the inelastic axial deformations during slippage.

A refined model which accurately reflects the true behaviour of the friction device can be developed by superposing truss and beam-column elements for the diagonal braces. This proposed model is shown in Figure 2.8. We first model all the members by truss elements with their own stress-strain curves. The four outside diagonal braces are allowed to buckle elastically in compression and the two inside diagonal pads slip in

tension and compression. For the diagonal braces we superpose beam-column elements with a zero cross-sectional area such that they can carry bending moment only, which is required to ensure stability. To represent the pinned connections at the four corners of the frame we specify zero plastic moments capacity for the beam-column elements.

With this refined model we can accurately represent the real behaviour of a Friction Damped Braced Frame. However, it requires many more elements and degrees of freedom than the simplified model and the computer time is increased significantly. In the analytical study the two models will be compared and a conclusion drawn on the validity of the approximate model.

3. DESIGN OF MODEL FRAME

3.1 Dimensional Analysis

Any structural model should be designed, loaded, and interpreted according to a set of similitude requirements that relate the model to the real structure. These similitude requirements are based upon the theory of modeling, which can be derived from a dimensional analysis of the physical phenomena involved in the behaviour of the structure.

The three general classes of physical problems, namely, mechanical (static and dynamic), thermodynamic, and electical, are conveniently described qualitatively in terms of the following fundamental measures:

1. Length

2. Force (or mass)

3. Time

4. Temperature

5. Electric charge.

Most structural modeling problems are mechanical; thus the measures of length, force, and time are most important in structural work.

Keeping the above definitions of measure in mind, the theory of dimensions can be summarized by a general theorem stated by Buckingham in 1914:

> "Any dimensionally homogeneous equation involving certain physical quantities can be reduced to an equivalent equation involving a complete set of dimensionless products."

This theorem states that the solution equation for some physical quantity of interest, i.e.,

$$F(X_1, X_2, \ldots, X_n) = 0 \tag{3.1}$$

can equivalently be expressed in the form

$$G(\pi_1, \pi_2, \ldots, \pi_m) = 0 \tag{3.2}$$

The Pi terms are dimensionless products of the physical quantities $X_1, X_2, \ldots, X_n$. Generally, it can be stated that the number of dimensionless products (m) is equal to the difference between the number of physical variables (n) and the number of fundamental measures (r) that are involved.

The main question to be resolved in applying the Buckingham Pi theorem pertains to the formation of appropriate Pi terms. The best method for arriving at the groupings of Pi terms is open to personal preference; there are a number of rather formal techniques which involve setting up the appropriate dimensional equations. One less formal approach involves the following steps:

1. Choose r variables that embrace the r dimensions (fundamental measures) required to express all variables of the problem, and that are dimensionally independent. This means that if a problem involves the dimensions of force F, length L, and time T, then the three variables chosen must collectively have dimensions which include F, L and T, but no two variables can have the same dimensions. Variables that are in themselves dimensionless (strain, Poisson's ratio, angles) cannot be chosen in the set of r variables.

2. Form the m Pi terms by taking the remaining (n-r) variables and grouping them with the r variables in such a fashion that all groups

are dimensionless. This procedure will guarantee a set of independent, dimensionless terms.

A consideration of the variables that govern the behaviour of vibrating structures reveals that in addition to length (L) and force (F), which are considered in static loading situations, we must also include time (T) as one of the fundamental quantities before we proceed with dimensional analysis.

Consider an elastic structure made of a homogeneous isotropic material whose vibration conditions are to be determined. A typical length in the structure is designated by ℓ and a typical force by Q. The materials of both the model and prototype can be characterized by the material constants: the modulus of elasticity E, the Poisson's ratio ν, and the mass density ρ. The important parameters to be determined from the structural vibration are the deflected shape δ, the natural frequency f, and the dynamic stresses σ. The acceleration due to gravity g must also be included since it is common to both model and prototype structures. The dimensions of the governing variables in both absolute and common engineering units are shown in Table 3.1.

For the problem of vibration of an elastic structure, the number of variables and dimensions are:

$$n = 9 \text{ variables } (\ell, Q, E, \nu, \rho, \delta, \sigma, f, g)$$
$$r = 3 \text{ dimensions } (F, L, T)$$

The number of Pi terms that can be formed is then:

$$m = n-r = 6 \text{ Pi terms}$$

To apply the Buckingham Pi theorem we choose 3 variables that contain the 3 dimensions of the problem (F,L,T). For example we can choose: $\ell(L)$, $E(FL^{-2})$ and $g(LT^{-2})$.

We then group the remaining 6 variables ($\delta,\sigma,\nu,\rho,Q,f$) with the primary variables (ℓ,E,g) such that all groups are dimensionless. For a true model, dimensionless parameters that govern the behaviour will then be:

$$\phi(\frac{\delta}{\ell}, \frac{\sigma}{E}, \frac{f^2\ell}{g}, \frac{\rho g\ell}{E}, \frac{Q}{E\ell^2}, \nu) = 0 \qquad (3.3)$$

Equation (3.3) means that we can determine the dynamic characteristics of the structure by means of a model test by forcing the dimensionless products of the left-hand side of Equation (3.3) to be identical in model and prototype. To impose these restrictions on the model design we normally choose the scaling factors for length and modulus of elasticity:

$$S_\ell = \frac{\text{length of model}}{\text{length of prototype}} = \frac{\ell_m}{\ell_p} \qquad (3.4)$$

$$S_E = \frac{\text{Modulus of Elasticity of Model}}{\text{Modulus of Elasticity of Prototype}} = \frac{E_m}{E_p} \qquad (3.5)$$

We can then express all the other scaling factors as a function of S_E and S_ℓ. The implied scale factors that govern these relationships are summarized in Table 3.2.

As we can see from this Table, the density scale is equal to S_E/S_ℓ for a true elastic model and is usually different from one. This means that the model should be made of a different material than the prototype. In practice this is usually very expensive and often the effect of gravity

forces is neglected. Table 3.2 gives also the scaling factors for the case when the gravity forces are neglected.

In the Table note that the time scale is equal to $S_\ell^{-1/2}$ for a true elastic model and to S_ℓ in the case of a model where gravity loading effects can be neglected. This means that an actual earthquake record should have a different time scale when used as the input for the test of a model. The frequency of vibration of the model, which is inversely proportional to the period, will be $S_\ell^{-1/2}$ and S_ℓ^{-1} considering and neglecting gravity, respectively. This means that the model will have higher frequencies than the prototype structure.

3.2 Practical Design

The first step in the design of the model frame was to choose a full scale prototype structure. It was decided to choose the first 3 floors of the frame used by Workman[8] as the prototype structure. The dimensions, member sizes, and other properties of all the Moment Resisting Frame members and braces are shown in Figure 3.1. The total height of the prototype structure is 10.98 m. Considering the vertical clearance of the Earthquake Simulator Room (4 m), a 1/3 scaling factor was selected for length. Also, since available hot-rolled section were to be used for the main members, the scaling factor for modulus of elasticity was fixed as unity. Thus

$$S_\ell = 1/3 \tag{3.6}$$

$$S_E = 1 \tag{3.7}$$

To represent a true model the scaling factor for density should be:

$$S_\rho = \frac{S_E}{S_\ell} = 3 \qquad (3.8)$$

Thus theoretically we should use a model material having 3 times the density of steel. Practically, this could be achieved by attaching a large number of lumped masses to the main steel members. However, this procedure would be very expensive and tedious. Furthermore hot-rolled sections meeting the similitude requirements for cross-sectional area and moment of inertia ($S\ell^2$ and $S\ell^4$) do not exist. For these reasons, it was not possible to follow the requirements of the dimensional analysis. However it is not necessary to represent an exact model since the study will compare the response behaviour of the Moment Resisting Frame, the Braced Moment Resisting Frame and the Friction Damped Braced Frame. Therefore it was decided to select the fundamental frequency of the model frame on the basis of the National Building Code suggestion:

$$T = \frac{N}{10} = \frac{3}{10} = 0.30 \text{ sec. (or } f = 3\text{Hz)} \qquad (3.9)$$

where

N = Number of storey

T = Fundamental period in seconds

The main members were chosen from available hot-rolled sections and the connections designed according to the CAN3 S16.1-M78 "Limit State Design-Steel Structures for Buildings" code. Figure 3.2 shows the general arrangement of the resulting model frame.

The overall dimensions of the model frame are 2.05 × 1.4 m in plan and 3.53 m in height. The frame is composed of several separate assemblages which are bolted together for ease of handling. The side frames, oriented parallel to the direction of the excitation, represent a Moment Resisting Construction. The frames in the direction perpendicular to the excitation, are bolted. The first two floors are loaded with two concrete blocks, each weighing 1700 kg., while the third floor is loaded with a 1150 kg concrete block. The frame was analyzed and its fundamental frequency was found to be 2.83 Hz.

The frame is mounted on a rigid base beam to facilitate the installation on the shaking table. The total weight of the model frame with the base beam and the concrete blocks is 6000 kg.

3.3 Remarks on Final Design

Figures 3.3, 3.4 and 3.5 show the details of the model frame. All the main beams and columns are made of the smallest S shapes (S75×8) available. The cross-section has a depth of 75 mm and flange width of 59 mm. The column cross-sections are reinforced at their bases by 2 plates, each of 6 mm thickness and over a length of 400 mm, in order to delay the formation of plastic hinges at the column bases.

The beam-column connections were designed such that the Moment Resisting Frame could be transformed easily into a Braced Moment Resisting Frame or a Friction Damped Braced Frame as needed.

The cross-section of the braces for the Braced Moment Resisting Frame and the Friction Damped Braced Frame was designed such that the following similitude is respected:

$$\frac{\text{Brace Cross-Section of Model}}{\text{Column Cross-Section of Model}} = \frac{\text{Brace Cross-Section of Prototype}}{\text{Column Cross-Section of Prototype}} \quad (3.8)$$

This led to the choice of a 6 mm square bar ($A = 36$ mm^2) for the bracing members.

In the direction perpendicular to the excitation, heavy cross-braces were installed to separate the translational frequencies in each direction and thus reduce the problem of torsional resonance. As noted above, the fundamental frequency in the direction parallel to the excitation was found by calculation to be 2.83 Hz; in the direction perpendicular to the excitation the analysis yielded a much higher fundamental frequency of 14.31 Hz.

The dead load of each concrete block is transmitted to its supporting beams through the flanges of 6 channels welded to these main members (see Figure 3.2). With this system, representing point loads, the diaphragm effect of the concrete blocks is reduced.

Figure 3.6 shows the actual model of the Moment Resisting Frame mounted on the shaking table.

4. ANALYTICAL STUDY

4.1 Concept of Optimum Slip Load

The energy dissipation of a friction device is equal to the product of slip load by the total slip travel. For very high slip loads the energy dissipation in friction will be zero, as there will be no slippage. In this situation the structure will behave exactly as a normal Braced Moment Resisting Frame. If the slip load is very low, large slip travels will occur but the amount of energy dissipation again will be negligible. Between these extremes, there is an intermediate value of the slip load which results in the maximum energy dissipation. This intermediate value is defined as the "Optimum Slip Load". This concept of optimum slip load is illustrated on Figure 4.1.

As noted in Chapter 2, when tension in one of the braces forces the joint to slip, it activates the four links which forces the joint in the other brace to slip simultaneously. Figure 4.2 shows a free body diagram of a friction device when slippage occurs. We define the "Global Slip Load (P_g)" as the load in the tension brace when slippage occurs; also, the "Local Slip Load (P_ℓ)" is defined as the load in each friction pad when slippage occurs.

As can be seen from equilibrium in Figure 4.2, the relation between the Global Slip Load and the Local Slip Load is given by:

$$P_g = 2P_\ell - P_{cr} \qquad\qquad (4.1)$$

where P_{cr} is the critical buckling load of the compression brace.

Usually the buckling load is very small and can be neglected; in this case we obtain:

$$P_g = 2P_\ell \qquad\qquad (4.2)$$

These two definitions of slip load must be differentiated since they control the different computer models used. The simplified model is based on an equivalent hysteretic behaviour and the Global Slip Load is the governing parameter. The refined model considers each joint separately and the Local Slip Load governs in this case.

4.2 Optimum Slip Load Study

To determine the optimum slip load of the model frame, inelastic time history dynamic analyses were performed for different values of the slip load. The computer program "Drain-2D", was used for this purpose. This program consists of series of subroutines which carry out a step-by-step integration of the dynamic equilibrium equations:

$$[M]\{\ddot{x}\} + [C]\{\dot{x}\} + [K]\{x\} = -[M]\{I\}\,\ddot{x}_g \qquad\qquad (4.3)$$

where

$[M]$ = global mass matrix

$[C]$ = global damping matrix

$[K]$ = global stiffness matrix

$\{x\}$ = vector of mass displacements relative to the moving base

$\ddot{x}_g$ = ground acceleration

$\{I\}$ = influence vector coupling the input ground motion to each degree of freedom

The constant acceleration method is used within each time step and provides an unconditional stable solution. The global mass matrix is assumed to remain constant during the earthquake. However, the damping and

stiffness matrices may change at the beginning of a time step, depending on the plastic deformation state of the structure at the end of the previous time step. The global mass matrix and the global stiffness matrix are formed by the direct method.

The damping matrix is described by considering Rayleigh type damping:

$$[C] = \alpha[M] + \beta[K] + \beta_o[K_o] \qquad (4.4)$$

where:

$[K]$ = Updated global stiffness matrix

$[K_o]$ = Initial elastic global stiffness matrix

α, β, β_o = Damping coefficients

Flexural and axial deformations are considered and the interaction between axial forces and moments at yield are taken into account by means of yield interaction surfaces. Figure 4.3 shows the yield interaction surfaces used in the analyses. The yield stress of the steel is assumed to be 300 MPa in tension and compression. The P-Δ effect is considered approximately by adding the global geometric stiffness matrix from static loading to the updated global stiffness matrix. No viscous damping is considered in the optimum slip load study; the value of this parameter is essentially negligible compared to the very much greater friction damping mechanism. Rigid foundations are assumed and soil-structure interaction is neglected. The static dead loads are considered by means of initial forces on the elements.

It is known that different earthquake records, even when normalized to the same intensity, give widely varying structural response, and the

results obtained using a single record may not be conclusive. For this reason, the optimum slip load study was carried out for 3 different earthquake records as follows:

1)   El-Centro earthquake 1940, component S00E, 0-6 seconds, scaled to a peak acceleration of 0.52 g.

2)   Parkfield earthquake 1966, component N65E, 0-9 seconds, scaled to a peak acceleration of 0.52 g.

3)   Newmark-Blume-Kapur artificial earthquake, 0-15 seconds, scaled to a peak acceleration of 0.30 g.

The acceleration records and the amplitudes of the Fourier spectra for these three earthquakes are shown on Figure 4.4

To save computation costs, the simplified computer model described in Chapter 2 was used for all the analyses. Preliminary analyses were made to determine the proper time step to be used. An integration time step of 0.005 sec was found to be sufficient and was used in all the analyses.

The results of the optimum slip load study are given in Figures 4.5, 4.6, and 4.7. Deflection envelopes, maximum moments in the beams and columns and maximum shear forces in the columns are plotted for different values of the global slip load. The results are given for global slip loads ranging from 0 to 10 kN, representing the elastic region of the cross-braces. Results for zero global slip load represent the response of a Moment Resisting Frame.

The figures clearly show the effectiveness of the friction devices in improving the seismic response of the frame. As we increase the global slip load the deflections, moments and shear forces decrease steadily up to a global slip load of 6 kN. For a global slip load between 6 kN and 10 kN,

there is very little variation in the response. The results indicate that during a major earthquake, the devices extract enough energy to prevent yielding in structural members.

This lower bound value of 6 kN for the global slip load is observed for the 3 different earthquakes studied. This suggests that the optimum value of the global slip load may be independent of the ground motion input. If this is found to hold true for all cases, the optimum slip load can be considered as a structural property. This observation may greatly simplify the development of a design procedure for the friction devices.

On the basis of the results obtained, an optimum global slip load value of 7 kN was subsequently used for the study of the Friction Damped Braced Frame model. From equation 4.2, the corresponding local slip load will be 3.5 kN if the buckling load of the brace is neglected. It is interesting to note that this global slip load is 20% of the weight of the model. It might be expected that the same percentage would also apply to the prototype structure.

4.3 Comparison Between Simplified and Refined Models

The simplified computer model is based on an equivalent hysteretic model and is only approximate, since it does not take into account the complete behaviour of the friction devices. The refined model considers each element of the friction device as an individual member with its own material (stress-strain) properties. It can therefore represent the complete behaviour of the friction devices but requires many more degrees of freedom and is much more expansive to run than the simplified model. For this reason, the results of the two models are compared for the El-Centro 1940 earthquake only.

An optimum global slip load of 7 kN was used with the simplified model

and an optimum local slip load of 3.5 kN was used with the refined model.
Some trial analyses were made to determine the proper integration time step
to be used with the refined model. It was found that a much lower time
step than used with the simplified model was needed in order to obtain
accurate results; a time step of 0.0015 second was used in the analysis.
The response parameters obtained using the two models of the Friction
Damped Braced Frame are also compared to the corresponding responses of the
Moment Resisting Frame and the Braced Moment Resisting Frame.

The structural damage in the various members of the different frames
at the end of the El-Centro (0-6 sec.) earthquake is illustrated in Figure
4.8. Significant damage occurs in the Moment Resisting Frame, in which the
first and second floor beams reach their plastic moment capacity. All the
cross-braces of the Braced Moment Resisting Frame have yielded in tension
and will need replacement. Furthermore, the level of damage in the Braced
Moment Resisting Frame is a lower bound, since the computer program
neglects the effect of the degrading stiffness of the braces (pinched
hysteresis). All the members remain elastic for the simplified and refined
models of the Friction Damped Braced Frame.

The envelopes of the response parameters for the different frames are
given in Figure 4.9. It can be seen that the deflection at the top of the
Friction Damped Braced Frame is about 20% of the equivalent deflection in
the Moment Resisting Frame and about 55% of the deflection in the normal
Braced Moment Resisting Frame. All the beams, except those in the top
storey, have yielded in the Moment Resisting Frame, and all the braces have
yielded in the Braced Moment Resisting Frame; but none of the beams or
braces have yielded in the Friction Damped Braced Frame. The maximum shear
at the base of the Friction Damped Braced Frame is only 55% and 32% of the
corresponding shear in the Braced Moment Resisting Frame and the Moment
Resisting Frame respectively.

The maximum moment at the base of the Friction Damped Braced Frame is 26% and 51% of the corresponding moment in the Moment Resisting Frame and the Braced Moment Resisting Frame, respectively.

The results of the simplified and refined models of the Friction Damped Braced Frame are compared in Table 4.1. The refined model gives higher member forces and deflections than the simplified model since the refined model takes into account the real deformation pattern of the friction devices; as discussed in Chapter 2, the approximate model over-estimates the energy dissipated by the friction devices. However the results are reasonably close for practical application.

The simplified model will give exact results under extreme excitations, when the devices are slipping at every cycle. This means that the two models will converge to the same response as the ground motion gets more severe.

From the above comparison it can be concluded that the simplified model is simpler and cheaper to use than the refined model. Its application in the study of Friction Damped Braced Frames is satisfactory for all practical purposes, leading to results which are within the variations typically expected in earthquake analysis.

4.4   Response Under Random White Noise Excitation

When using a particular earthquake record as ground motion input, the energy transmitted to the structure is different for each type of frame (F.D.B.F., B.M.R.F., M.R.F.), since the natural frequencies of these frames are all different. However the energy input for the three different model frames can be made identical by using band limited white noise as the excitation source.

Band limited white noise is defined as a random variable having a
constant Power Spectral Density Function over a certain frequency range.
It is possible to generate a band limited white noise signal by the tech-
nique of summation of sinusoids (16). In our case, to make the energy
input identical for the three test frames, the frequency band of the white
noise signal must span the estimated natural frequency range of the three
different model frames. The computer program SIMU.S, developed at the
University of British Columbia, was used to generate a band limited (0-25
Hz) white noise signal. The acceleration record and its normalized Power
Spectral Density Function is presented in Figure 4.10. The record has a
duration of 20 seconds with a peak acceleration of 1 g (9810 mm/s^2). The
amplitude of the Power Spectral Density Function is constant for frequen-
cies from 0 to 25 Hz. When this record is used as a ground motion input to
the model frames, all the frequencies within the range of 0 to 25 Hz are
excited with equal intensity.

This band limited white noise record, scaled to a peak ground accel-
eration of 0.50 g, was used to study the performance of the Friction Damped
Braced Frame. The simplified model was used with a global slip load of 7
kN. The response parameters obtained with the Friction Damped Braced Frame
are compared to the corresponding responses of the Moment Resisting Frame
and the Braced Moment Resisting Frame.

The structural damage in the various members of the three model frames
after the end of the white noise record (i.e. resulting from the 20 seconds
excitation) is illustrated in Figure 4.11. Serious damage occurs in the
Moment Resisting Frame, in which the first and second floor beams and both
base columns reach their plastic moment capacity. Significant structural
damage also occurs in the Braced Moment Resisting Frame, where all the

cross-braces have yielded in tension. Notice that all the structural members of the Friction Damped Braced Frame remain elastic.

The envelopes of the response parameters for the different model frames are presented in Figure 4.12. The deflection at the top of the Friction Damped Braced Frame is 12% of the equivalent deflection in the Moment Resisting Frame and 25% of the deflection in the Braced Moment Resisting Frame. The maximum shear at the base of the Friction Damped Braced Frame is only 21% and 45% of the corresponding shear in the Moment Resisting Frame and the Braced Moment Resisting Frame respectively. The maximum moment at the base of the Friction Damped Braced Frame is 20% and 43% of the corresponding values in the Moment Resisting Frame and the Braced Moment Resisting Frame respectively.

Time-histories of the deflection at the top of building for the three frames are shown in Figure 4.13. The peak amplitude of the Friction Damped Braced Frame is far less than the corresponding amplitude of the two other model frames. Notice that the vibrations at the end of the excitation are almost negligible for the Friction Damped Braced Frame compared with the vibrations of the other two frames. This indicates that the building recovers with almost no permanent deformation. As suggested by A.S. Pall (3), if the building is slightly out of alignment, it can be corrected by loosening the bolts in the device and then retightening.

The results of this investigation clearly indicate the superior performance of the Friction Damped Braced Frame compared to conventional aseismic building systems. By performing this study under conditions which ensure that the energy induced in the structures is the same for all frames, it has been shown that the frequency content of a particular earthquake, in relation to the different frame frequencies, is not the underlying source of this difference in structural response.

4.5 <u>Equivalent Viscous Damping Study</u>

The results of the previous sections have shown that the use of inexpensive friction devices in the bracings of steel framed buildings can significantly enhance their earthquake resistance. One method to quantify the performance of the Friction Damped Braced Frame relative to conventional aseismic systems is by means of an equivalent viscous damping study. Viscous damping was added to the Moment Resisting Frame and the Braced Moment Resisting Frame until their responses become similar to the response of the Friction Damped Braced Frame. The maximum deflection at the top of the building was choosen as the comparative response parameter.

The program "Drain-2D" assumes that the viscous damping results from a combination of mass-dependent and stiffness-dependent effects, so that if $\beta_0 = 0$ (see Equation (4.4)):

$$[C] = \alpha[M] + \beta[K] \qquad (4.5)$$

in which α and β are constants to be specified by the program user. To ensure the existence of classical normal modes, the viscous damping ratios must be defined in the following way (14);

$$\zeta_r = \frac{\alpha}{2\omega_r} + \frac{\beta\omega_r}{2} \qquad (4.6)$$

where:

$\quad \zeta_r \quad$ = viscous damping ratio of the rth mode

$\quad \omega_r \quad$ = undamped natural frequency of the rth mode (rad/s)

$\quad \alpha,\beta \quad$ = damping coefficients

Considering only the first two modes of vibrations, the damping coefficients α,β can be determined:

$$\alpha = \frac{4\pi(T_2\zeta_2 - T_1\zeta_1)}{T_2{}^2 - T_1{}^2} \qquad (4.7a)$$

$$\beta = \frac{T_1T_2(T_2\zeta_1 - T_1\zeta_2)}{T_2{}^2 - T_1{}^2} \qquad (4.7b)$$

where:

T_1, T_2 = Undamped periods of the first and second modes.

To make the equivalent viscous damping study dependent on a single variable, it was assumed that the viscous damping ratios are the same for the first and second modes:

$$\zeta_1 = \zeta_2 = \zeta \qquad (4.8)$$

Hence:

$$\alpha = \frac{4\pi \zeta(T_2 - T_1)}{T_2{}^2 - T_1{}^2} \qquad (4.9a)$$

$$\beta = \frac{T_1T_2 \zeta(T_2 - T_1)}{T_1{}^2 - T_1{}^2} \qquad (4.9b)$$

The first two natural periods of both the Moment Resisting Frame and the Braced Moment Resisting Frame were calculated and found to be (see Sections 9.1 and 10.1):

1) <u>Moment Resisting Frame</u>

T_1 = 0.3532 sec.

T_2 = 0.1090 sec.

2) <u>Braced Moment Resisting Frame</u>

T_1 = 0.1966 sec.

T_2 = 0.0686 sec.

Therefore:

    1)   <u>Moment Resisting Frame</u>

         α = 27.1882 ζ

         β = 0.0833 ζ

    2)   <u>Braced Moment Resisting Frame</u>

         α = 47.3845 ζ

         β = 0.0509 ζ

Several inelastic time-history dynamic analyses were performed for the Moment Resisting Frame and the Braced Moment Resisting Frame with different values of the viscous damping ratio until their responses become similar to the response of the Friction Damped Braced Frame. The Newmark-Blume-Kapur artificial earthquake scaled to peak accelerations of 0.05, 0.10 and 0.30 g was used in the analyses.

The results of the analyses are shown in Figure 4.14. The equivalent viscous damping ratio necessary to match the response of the Friction Damped Braced Frame is plotted vs. the ground peak acceleration. As expected, less viscous damping is needed for the Braced Moment Resisting Frame than the Moment Resisting Frame. Notice that the equivalent viscous damping ratio increases with the ground peak acceleration. This indicates that the Friction Damped Braced Frame becomes more efficient as the intensity of the ground motion increases; this is due to the fact that the energy is dissipated mechanically throughout the height of the building rather than by localized inelastic action of the main structural members. For a peak ground acceleration of 0.30 g, 38% of critical damping is needed for the Moment Resisting Frame and 12% for the Braced Moment Resisting Frame.

5.   CALIBRATION AND QUALITY CONTROL OF FRICTION DEVICES

5.1 General

In the last chapter, the optimum global slip load of the Friction

Damped Braced Frame was found to be 7 kN. Based on this value, seven

friction devices were fabricated in a machine shop in Montreal.

This chapter is concerned with the cyclic load tests performed at

different frequencies on the friction devices in order to calibrate these

units for the optimum slip load. The tests also verify the reliability of

the hysteresis loops after many cycles.

The general arrangement of an actual friction device is presented in

Figure 5.1. Note that the overall dimensions of the mechanism are 355×200

mm. The four connections between the pads and the braces are made with two

20 mm diameter ASTM A325 high strength bolts, representing moment

connections.

For research purposes, each friction device is provided with a

compression spring (Korfund & Simpson Ltd., Type WSCB K = 1950 lbs/in)

which allows adjustments to be made to the clamping force and therefore the

slip load. The free length of the compression spring is 146 mm. Springs

will not be used in the prototype structure; the clamping force will be

developed by a bolt torqued to the proper value.

Figure 5.2 shows the details of a friction device. The mechanism is

made from 50×8 mm mild steel plates. The friction surfaces are 3 mm thick

heavy duty brake lining pads (No. 55B by "ASBESTONOS"), which are glued to

the steel plates with plasti-lock glue. Each device is provided with four

friction surfaces: one friction surface in each joint and one common fric-

tion surface between the joints in the form of a washer, to which brake

lining pads are glued on each side. A view of the different friction surfaces is shown in Figure 5.3. The fabrication tolerances were specified according to the CSA standard CAN3-S16.1-M78. The nominal diameter of the holes were drilled 2 mm greater than the nominal bolt sizes.

Figure 5.4 shows an actual friction device mounted on the model frame.

5.2 Experimental Set Up

The cyclic load tests on the friction devices were carried out in the Structural Laboratory of the Civil Engineering Department at the University of British Columbia. The general experimental set up for the tests is shown in Figure 5.5.

One end of a diagonal link of the friction device was bolted to a rigid testing bench while the opposite end was attached to a 50 kN capacity vertical hydraulic actuator having a piston area of 2400 mm^2 and a maximum stroke of 250 mm. The servo valve of the actuator has a flow rate of 20 gallons/minute.

The movement of the piston was controlled by an MTS console which contains an oscillator that allows controlled cyclic displacement tests to be performed with variable amplitudes and frequencies. The displacement of the piston was monitored by a LVDT (Linear Variable Displacement Transducer) mounted inside the actuator. The load was measured by a 5 metric ton capacity load cell.

The analog signals from the LVDT and the load cell were fed into a Philips analog-analog tape recorder. The data were stored directly on tape for subsequent reduction and manipulation. A Hewlett-Packard X-Y Plotter was connected in parallel with the tape recorder so that a permanent record of the hysteresis loops could be obtained on paper as the tests were

performed. A storage oscilloscope was also connected in parallel with the tape recorder in order to visualize immediately the hysteresis loops on the screen; this served to monitor the plots desired for the permanent record.

5.3 Stability Tests

The first series of tests on the friction devices were performed with a simple friction joint (2 friction surfaces) in order to verify the stability and reliability of the brake lining pads under repetitive cyclic loads. The experimental set up for this series of tests is presented in Figure 5.6.

The tests were conducted with different values of the slip load and also at various frequencies. The range of frequencies covered was from 0.2 Hz to 4.0 Hz. Each test was subjected to 50 cycles of loading.

Figure 5.7 shows a typical load-displacement curve obtained from this series of tests. The performance of the brake lining pads is seen to be reliable and repeatable. The hysteresis loop is very nearly a perfect rectangle and exhibits negligible fade even after 50 cycles.

It may be seen that two distinct plateaus occur at two opposite corners of the hysteresis loop, where the transition between tension-compression and compression-tension takes places. The first plateau is due to the eccentricity of the friction joint which results in a small out-of-plane movement of the central bolt and spring unit when the load is applied. The second plateau is due to the clearance provided between the central bolt and the washer onto which the brake lining pads are glued. The 2 mm tolerance on the hole size was found to be too large and, as a result, the central bolt initially moved without contacting the washer and thus friction resistance was not fully developed in the early stage of the loading.

Figure 5.8 shows typical hysteresis loops obtained at various frequencies of loading. For the range of frequencies studied (0.2-4.0 Hz), it seems that the slip load remains constant. Because of the physical limitations of the actuator, the total movement of the piston is reduced as the excitation frequency increases. This leads to an apparent reduction in the efficiency of the friction joint at high frequency loading since, although the total movement of the piston is reduced, the two plateau displacements remain constant. To be fully effective, the friction joint must slip more than a certain threshold necessary to overcome the tolerance of the hole size. This problem may be encountered during an earthquake characterized by a high frequency input, since the resulting structural displacements will usually remain small.

Note that for a frequency of 4 Hz the slip load is not reached. This is due to the fact that the slippage is too small to overcome the tolerance of the hole size and not because the friction properties of the pads are altered. As noted below, this problem was solved by adjusting the hole size of the washer.

5.4 Tests of Complete Device

The tests described in Section 5.3 were used to verify the reliability of the brake lining pads; it was demonstrated that the hysteresis loops developed by these pads do not degrade and remain stable even after 50 cycles. This section deals with a series of tests which were performed on the complete friction devices.

As mentioned earlier, the diameter of all the bolt holes were specified 2 mm greater than the nominal bolt size. This fabrication tolerance was found to be too large and, as a result, a rectangular

hysteresis loop was not obtained, as shown in Figure 5.9. This is due to the fact that, when the loaded link slips, the 4 corner bolts of the mechanism (see Figure 5.1) first slide in their holes without developing any bearing resistance. During this interval, the mechanism is not activated and energy is not absorbed in the friction joint of the other link. This problem occurs in both tension and compression. The displacement required to get both joints to slip is so large that the value of the global slip load cannot be reached, as shown in Figure 5.9.

The results of these tests clearly indicate that a rectangular load-deformation curve can only be obtained if the fabrication tolerances of the friction devices are minimized. This was achieved by inserting steel bushings in the 4 corner holes of the mechanism and also in the center slots of the friction pads. As a result, the fabrication tolerance was reduced from 2 mm to 0.25 mm. These steel bushings were fabricated in the Civil Engineering Workshop at the University of British Columbia.

A typical hysteresis loop developed with the modified device is shown in Figure 5.10. Note that the incorporation of the steel bushings dramatically improves the performance of the friction devices. Because the fabrication tolerances are minimized, both friction joints slip simultaneously; this results in an almost perfectly rectangular hysteresis loop.

Notice, however, that some imperfections still remain at two opposite corners of the hysteresis loop. A perfectly rectangular hysteresis loop presumably could be obtained by completely eliminating the fabrication tolerance; however, it was decided that the results obtained with these modified devices are satisfactory for practical applications.

Again, the hysteresis loop associated with the complete device is very stable and displays negligable fade. For high slip loads (> 5 kN) the

pads and the central portion of the mechanism become very hot after 50
cycles. However, the slip load is not influenced by the elevation in
temperature. A test was performed when the pads were very hot, and another
at room temperature with the same spring load; no difference was observed
in the load-deformation curves.

5.5 Calibration Curves

In order to calibrate the friction devices for the desired global slip
load, all 7 devices were tested under repeated cyclic loads with different
values of the spring load.

Before each test, the length of the compression spring was measured
with a precision vernier. It was then possible to establish a correlation
between the global slip load and the length of the compression spring. For
each device a linear regression analysis was performed to obtain an equa-
tion relating the global slip load and the length of the spring.

The resulting equations represent calibration curves for the friction
devices. These curves are plotted with the experimental data in Figure
5.11. The results of all the linear regression analyses are shown in Table
5.1. Note that the correlation coefficients are very close to unity; this
is to be expected since the relation between the global slip load and
spring length should be linear according to the conventional friction law.

Once these calibration curves are available, it is very easy to set
each device for the optimum slip load of 7 kN (see Chapter 4) by simply
adjusting the length of the spring with a precision vernier.

6. DETERMINATION OF MATERIAL PROPERTIES

6.1 General

This chapter describes the procedures followed to determine the physical properties of the materials used in the fabrication of the model frames. These values are needed in the non-linear, time-history dynamic analysis program, from which analytical solutions were generated for comparison with the experimental results.

For the main members used in the construction of the model frame (S75×8), the following properties must be determined:

Young's Modulus, E

Tangent Modulus, E'

Plastic Moment, M_p

For the cross-braces used in the Braced Moment Resisting Frame and in the Friction Damped Braced Frame, the following properties must be determined:

Young's Modulus, E

Tangent Modulus, E'

Yield Stress, σ_y

Buckling Stress, σ_{cr}

To estimate these material properties, a series of uniaxial tests were carried out on steel specimens in the Structural Laboratory of the Civil Engineering Department at the University of British Columbia.

6.2 Tests of Cross-Braces

For the cross-braces, these tests were conducted on a complete brace unit as used with the Friction Damped Braced Frame. The unit consists of a 6 mm square bar made of AINSI C-1018 cold formed steel, which was welded to 2 plates of mild steel, as shown in Figure 6.1.

Two uniaxial tests were conducted on 2 different specimens. In the first test, the specimen was loaded through one cycle of tension and compression without rupture. Figure 6.2 shows the permanent deformation of the specimen at the end of this test. The load deformation curve obtained from this test is shown in Figure 6.3. The slope (m) of the initial elastic part of the curve can be measured from the graph and is equal to:

$$m = \frac{AE}{L} \qquad (6.1)$$

where:

A   = cross-sectional area of the specimen

E   = Young's Modulus

L   = Length of the specimen

Young's Modulus can then be evaluated from:

$$E = \frac{mL}{A} \qquad (6.2)$$

Similarly the tangent modulus can be estimated by:

$$E' = \frac{m'L}{A} \qquad (6.3)$$

where m' is the slope of the inelastic part of the curve determined from a linear regression analysis.

The yield load (P_y) is determined directly from the curve and the yield stress (σ_y) can then be found since:

$$\sigma_y = \frac{P_y}{A} \tag{6.4}$$

The critical buckling load (P_{cr}) can be determined directly from the load-deformation curve and is equal to:

$$P_{cr} = \frac{\pi^2 EI}{(KL)^2} \tag{6.5}$$

from which the effective length factor can be estimated:

$$K = \frac{\pi}{L} \sqrt{\frac{EI}{P_{cr}}} \tag{6.6}$$

where:

    K = 1   for a perfectly pin-pin brace

    K = 0.5   for a perfectly fix-fix brace.

The effective length factor can be expected to lie between these two values, since the end conditions of the brace unit are not clearly defined.

The second uniaxial tensile test on a brace unit was carried out up to rupture of the specimen. Figure 6.4 shows the load-deformation curve obtained from this test. The ultimate load (P_u) can be determined from the curve; the resulting ultimate stress is given by:

$$\sigma_u = \frac{P_u}{A} \tag{6.7}$$

Also, the ultimate strain (ε_u) can be calcualted from:

$$\varepsilon_u = \frac{\Delta \ell_u}{\ell} \tag{6.8}$$

where

$\Delta \ell_u$ = ultimate elongation of the brace.

Based on these uniaxial tests, the following materials properties were obtained for the braces:

Young's Modulus, E = 180,000 MPa

Tangent Modulus, E' = 58,000 MPa

Yield Stress, σ_y = 495 MPa

Ultimate Stress, σ_u = 720 MPa

Ultimate Strain, ε_u = 0.0074

Effective Length Factor K = 0.65

Critical Buckling Stress σ_{cr} = 74 MPa for F.D.B.F.

σ_{cr} = 4 MPa for B.M.R.F.

6.3 Tests of Main Members

The material properties of the main members (S75×8) were evaluated by performing a uniaxial compression test on a complete S75×8 section 300 mm long. The load-deformation curve obtained from this test is shown in Figure 6.5.

Following the same procedure described in Section 6.2, the material properties of the main members were determined as follows:

Young's Modulus, E = 170,000 MPa

Tangent Modulus, E' = 0

Yield Stress, σ_y = 400 MPa

Yield Strain, ε_y = 0.0024

The plastic moment is given by:

$$M_p = Z \, \sigma_y \qquad\qquad (6.9)$$

where

Z = plastic section modulus = 31.9×10^3 mm^3 for S75×8

Therefore, M_p = 12.76 kN-m.

7. EXPERIMENTAL SET UP ON SHAKING TABLE

7.1 Shaking Table

All the seismic tests reported in this thesis were carried out on the Earthquake Simulator in the Earthquake Engineering Laboratory of the Civil Engineering Department at the University of British Columbia. The shake table is 3 m × 3 m in plan and is fabricated as a cellular box from welded aluminum plate. The table is mounted on four pedestal legs with universal joints at each end to ensure linear horizontal motion. Lateral movement of the table (or yaw) is restrained by three hydrostatic bearings. Test specimens are attached to the table by steel bolts which thread into steel inserts arranged in a grid. Figure 7.1 shows the general arrangement of the shaking table.

The shaking table is activated by an MTS hydraulic power supply which provides regulated hydraulic pressure and flow to the servo valve and actuator. The hydraulic fluid is supplied at a pressure of 3000 psi and at a flow rate of up to 70 gpm. The MTS hydraulic jack is a double acting linear actuator. A manifold supplies surges in hydraulic fluid demand and reduces fluctuations in line pressure during dynamic conditions. A three stage servo valve is used to control electrically the direction and magnitude of the hydraulic flow. The third stage of the servo valve is position controlled by electric feedback from a spool linear variable displacement transducer (LVDT) and a valve controller.

The simulator can be programmed by a Digital PDP 11/04 mini-computer to excite the test specimens with very generalized functions, including seismic ground motions. Some of the system specifications are as follows: maximum specimen weight equals 16000 kg; maximum horizontal acceleration equals 2.5 g; and maximum peak-to-peak horizontal displacement is 150 mm. The mass of the empty table is 2090 kg.

7.2 Data Acquisition

The data acquisition system of the Earthquake Engineering Laboratory
is controlled by a Digital PDP11/04 mini-computer having 56K bytes of
memory, a RT11 operating software system and two RX01 disk drives. The
physical arrangement of the data acquisition system is shown in Figure
7.2.

During an experiment, the analog signals coming from the different
sensors mounted on the test structure are fed into a 16 channel multi-
plexed Analog-Digital converter. Data is stored directly onto floppy disks
for later reduction and manipulation.

A direct line links the mini-computer to the University's main
(Amdahl) computer, thereby assuring powerful data processing capability at
the convenience of a main frame system. Facilities also exist to display
test data on storage oscilloscopes, on chart recorders and X-Y plotters,
and on a Calcomp plotter and Tektronix graphics terminals equipped with
hard copy units.

The Earthquake Simulator at the University of British Columbia is
probably the most sophisticated test facility of its kind in Canada. Its
ability to command the table and to handle test data by means of a mini-
computer allows for accuracy and efficiency when dealing with earthquake
generated excitations.

7.3 Instrumentation

A variety of sensors were mounted on the structures and on the shaking
table in order to measure the response of the model frames due to earth-
quake ground motion excitations.

Four accelerometers were used to measure the horizontal acceleration at various levels of the structure. A Kistler servo accelerometer was clamped under the shaking table in order to monitor the table acceleration. Two Statham model A514TC strain gage accelerometers, with a working range of ± 2.5 g, were installed on the first and second floor cross-beams of the model frame. Figure 7.3 shows the first floor accelerometer bolted on the cross-beam. To monitor the third floor horizontal acceleration, a Statham model 1525 strain gage accelerometer, with a working range of ± 20 g, was mounted on the third floor cross-beam. The analog signals from these four accelerometers were fed into amplifiers and to the multi-plexed Analog-Digital converter.

Six linear potentiometers were connected to a fixed panel situated beyond the table; these were used to measure the absolute displacements of the frame. Two potentiometers were attached to each floor, one to each side frame parallel to the direction of the excitation. By analysing the phase shift between the two displacement records at each floor, it was possible to measure and detect any torsional motion developed in the structure. Figure 7.4 shows one potentiometer mounted on the fixed panel located outside the table. All the potentiometers were excited by one D.C. power supply, whose excitation voltage was 9 volts. The analog signals from the potentiometers were fed directly into the multi-plexed Analog-Digital converter.

The absolute displacement of the table was measured by a Linear Variable Displacement Transducer (LVDT) mounted inside the table actuator. The relative displacement of each floor of the structure with respect to its moving base (i.e., the table) was obtained by subtracting the digitized record of the table displacement from each corresponding potentiometer record.

Four sets of strain gages were installed to monitor the strain-time history at various locations in the model. Each set consisted of two strain gages, which were glued to the outer faces of each flange of the main members. Half bridge circuits were used, so that only bending strains were recorded. One set of strain gages was mounted just above the reinforcing plate of one of the base colums, as shown in Figure 7.5. The remaining three pairs of strain gages were mounted at one end of each floor beam, so that the strains in the beams could be monitored. Figure 7.6 shows the set of strain gages mounted on the first floor beam. The analog signals from the strain gages were fed through amplifiers to the multiplexed Analog-Digital converter. All the strain gages were calibrated by connecting a calibration resistance simulating a known change of strain in parallel with the bridge.

Linear Variable Displacement Transducers (LVDT) were used to record the slippage-time history of the friction pads. In the first series of tests only one of the second floor friction devices was instrumented for slippage, because the 15 other recording channels of the data acquisition system were otherwise occupied. However, in the second test series three of the six potentiometers were disconnected, since it was found that torsional motion was negligible; this allowed a total of four friction devices to be instrumented.

All the LVDT's on the friction devices were excited by a single D.C. power supply having an excitation voltage of 6 volts.

Finally, Tens-Lac brittle lacquer was sprayed on various parts of the frame to detect the strain (stress) patterns. The brittle lacquer cracks at a certain strain level; the cracks occur perpendicular to the maximum tensile strains and are present at locations where the strain level has exceeded a certain threshold strain. For the brittle lacker used, this threshold was nominally 500 microstrain ($\mu\varepsilon$).

8. SYSTEM IDENTIFICATION THEORY

8.1 General

Dynamic tests of the model frames were divided into two parts: determination tests, and evaluation tests. The purpose of the determination tests was to obtain the dynamic characteristics of the model frames. Natural frequencies, damping parameters, mode shapes, and frequency-response functions of each model frame were obtained from the determination tests. Determination tests were conducted at low excitation levels. Evaluation tests were later used to study the performance of the model frames under specific ground motion time-histories. Evaluation tests were conducted at relatively high excitation levels.

Determination tests are based upon system identification theory. Two basic approaches can be used to estimate the dynamic characteristics of a test structure:

1) Time-response method

2) Frequency response method.

The choice of the method used to estimate the dynamic characteristics of a model structure depends on many factors: capability of the shaking table and the data acquisition system, instrumentation available, degree of non-linearity of the test structure, etc. Often, a combination of the two methods is used in a determination test program.

In this chapter the parameter estimation theory of linear elastic systems is reviewed and the methods necessary to determine the dynamic characteristics of the model frames are developed taking into account the instrumentation described in Chapter 7 and the capabilities of the Earthquake Simulator Table.

8.2 Undamped Free Vibration Analysis

The basic differential equation for the undamped free vibrations of a linear elastic system is given by:

$$[M]\{\ddot{x}\} + [K]\{x\} = \{0\} \qquad (8.1)$$

In steady-state conditions, the following solution is assumed:

$$\{x\} = \{A\} \sin(\omega t + \phi)$$

Substituting into (8.1) yields:

$$\left[[K] - \omega^2 [M] \right] \{A\} \sin(\omega t + \phi) = \{0\}$$

This equation must be satisfied for every value of t, therefore:

$$\left[[K] - \omega^2 [M] \right] \{A\} = \{0\} \qquad (8.2)$$

or

$$[K][I]\{A\} = \omega^2 [M]\{A\} \qquad (8.2a)$$

Assuming a diagonal mass matrix we can write:

$$[M] = [M]^{1/2} [M]^{1/2}$$

$$(8.2b)$$

$$[I] = [M]^{-1/2} [M]^{1/2}$$

Substituting into (8.2a) leads to:

$$[K][M]^{-1/2} [M]^{1/2} \{A\} = \omega^2 [M]^{1/2} [M]^{1/2} \{A\}$$

Pre-multiplying by $[M]^{-1/2}$ yields:

$$\left[[M]^{-1/2} [K][M]^{-1/2} \right] \left\{ [M]^{1/2} \{A\} \right\} = \omega^2 \left\{ [M]^{1/2} \{A\} \right\} \qquad (8.3)$$

Equation (8.3) is a classical eigenvalue problem of the form: $[B]\{y\} = \lambda\{y\}$, which leads to a set of n eigenvalues (natural frequencies) and n eigenvectors (mode shapes). The frequency matrix is defined as:

$$\lceil \omega_i^2 \rfloor = \begin{bmatrix} \omega_1^2 & & 0 \\ & \omega_2^2 & \\ 0 & & \omega_n^2 \end{bmatrix} \qquad (8.4)$$

where $\lceil \ \rfloor$ represents a diagonal matrix

By substituting each value of ω^2 in turn into Equation (8.3), we can solve for the corresponding set of $\{A\}$, i.e. $\left(\{A^{(1)}\}, \{A^{(2)}\}, \ldots \{A^{(n)}\} \right)$. These corresponding $\{A\}$ can be arranged in a modal matrix:

$$[A] = \left[\{A^{(1)}\}, \{A^{(2)}\}, \ldots \{A^{(n)}\} \right] \qquad (8.5)$$

Since the $\{A\}$ vectors are eigenvectors, they do not have an absolute value; only their shapes are determined. If the normal vectors are normalized such that:

$$\{A^{(r)}\}^T [M] \{A^{(r)}\} = 1 \qquad (8.6)$$

The following orthogonality properties of the normal modes can be shown (14) to exist:

$$[A]^T [M][A] = [I] \tag{8.7}$$

$$[A]^T [K][A] = \lceil \omega_i{}^2 \rfloor \tag{8.8}$$

The undamped natural frequencies and mode shapes of the different model frames were predicted using the computer program "DYNA" from the University of British Columbia Civil Engineering Program Library. "DYNA" is an interactive graphics program which performs linear elastic small deformation dynamic analysis of plane frame problems. The structure may be formed from pinned-pinned, fixed-fixed and fixed-pinned members.

"DYNA" reads the structural data from a data file and assembles the global stiffness and mass matrices. The global stiffness matrix is constructed from standard plane frame beam stiffness matrices as described in any introductory structural analysis reference. For modelling the mass distribution, half of the weight of each member may be concentrated at each end of the member, and point masses may be superimposed at any node. The resulting global mass matrix is diagonal.

The undamped natural frequencies and mode shapes are found by solving Equation (8.3). A modified iterative (power) method is used. The solution is performed in double precision.

8.3 Fourier Spectrum Analysis For Frequency Determination

The first step in the parameter estimation of a test structure is to measure experimentally the natural frequencies of the system. One standard method of exhibiting the frequency content of a time-history record involves the use of a Fourier Amplitude Spectrum.

The ith coordinate acceleration response of a lightly damped multi-degree of freedom system subjected to initial conditions $\{x_0\}$ and $\{\dot{x}_0\}$ is given by (14):

$$\ddot{x}_i(t) = \sum_r \left[A_i^{(r)} e^{-\zeta_r \omega_r t} \left(L^{(r)} \cos \omega_r t + N^{(r)} \sin \omega_r t \right) \right] \qquad (8.9)$$

where $L^{(r)}$ and $N^{(r)}$ are modal constants which depend on the initial conditions and on the modal natural frequency and damping value.

Note that $\ddot{x}_i(t)$ is a sum of simple harmonic signals whose frequencies correspond to the natural frequencies of the system. The Fourier Amplitude Spectrum of this signal, which illustrates its frequency content, therefore will exhibit a "spike" at each of the frequency components of the signal (the natural frequencies of the system). The amplitudes of the spikes will depend on the damping characteristic of the system and also on the initial conditions.

A very simple method of measuring experimentally the natural frequencies of the three different model frames was adopted using the Fourier Amplitude Spectrum. The model frames were excited under a harmonic base motion having a frequency well separated from the calculated resonant frequencies. The ground motion was then stopped suddenly and the third floor horizontal acceleration-time decay was recorded for a sufficient period of time. The Fourier Amplitude Spectrum of this recorded motion was calculated using the Earthquake Simulator Laboratory software program "EDSPEC". "EDSPEC" allows the Fourier Amplitude Spectrum to be plotted from formatted data files. Generated spectral values may be Hanned (18), and can be stored in a print file for later hard copy printout.

The natural frequencies of each model frame correspond to the frequencies defining the maximum spectral values (the 'spikes') of the Fourier Amplitude Spectrum.

8.4 Complex Frequency Response or Mobility Function

One convenient way to determine the dynamic characteristics of a test structure is to find the magnitude of its complex frequency response function (or mobility function $|H(\bar{\omega})|$) under harmonic base motion. The governing differential equation for a base motion problem can be written in the following form:

$$[M]\{\ddot{x}\} + [C]\{\dot{x}\} + [K]\{x\} = -[M]\{I\}\ddot{x}_g \qquad (8.10)$$

where

$[M]$ = global mass matrix

$[C]$ = global damping matrix

$[K]$ = global stiffness matrix

$\{x\}$ = vector of displacements relative to the moving base

$\{I\}$ = influence vector coupling the input ground motion to each degree of freedom

$\ddot{x}_g$ = ground acceleration

Assume that the ground acceleration is a known harmonic function:

$$\ddot{x}_g = a \sin \bar{\omega} t \qquad (8.11)$$

Under steady state conditions, the following solution of Equation (8.10) can be assumed:

$$\{x\} = \{P\} \cos \bar{\omega} t + \{Q\} \sin \bar{\omega} t \qquad (8.12)$$

Substituting into (8.10) yields:

$$\left[\left([K] - \bar{\omega}^2[M]\right)\{P\} + \bar{\omega}[C]\{Q\}\right] \cos \bar{\omega}t \; +$$

$$\left[\left([K] - \bar{\omega}^2[M]\right)\{P\} - \bar{\omega}[C]\{Q\}\right] \sin \bar{\omega}t \; = -[M]\{I\} \, a \sin \bar{\omega}t$$

This equation must be satisfied for any time t. Therefore:

$$\left([K] - \bar{\omega}^2[M]\right)\{P\} + \bar{\omega}[C]\{Q\} \; = \; \{0\} \qquad (8.13a)$$

$$\left([K] - \bar{\omega}^2[M]\right)\{P\} - \bar{\omega}[C]\{Q\} \; = \; -[M]\{I\} \, a \qquad (8.13b)$$

By using the orthogonality properties of the mode shapes as given by Equations (8.7) and (8.8), we may write:

$$[M] \; = \; [A]^{-T} \, [I] \, [A]^{-1} \qquad (8.14)$$

$$[K] \; = \; [A]^{-T} \, \lceil \omega_i^2 \rfloor \, [A]^{-1} \qquad (8.15)$$

Assuming modal damping, the damping matrix is also orthogonal (14) to the modal matrix:

$$[C] \; = \; [A]^{-T} \, \lceil 2\zeta_i \omega_i \rfloor \, [A]^{-1} \qquad (8.16)$$

Substituting Equations (8.14-8.16) into Equations (8.13a) and (8.13b):

$$[A]^{-T} \, \lceil \omega_i^2 - \bar{\omega}^2 \rfloor [A]^{-1}\{P\} + [A]^{-T} \, \lceil 2\zeta_i \omega_i \bar{\omega} \rfloor [A]^{-1}\{Q\} = \{0\} \qquad (8.17a)$$

$$[A]^{-T} \, \lceil \omega_i^2 - \bar{\omega}^2 \rfloor [A]^{-1}\{P\} - [A]^{-T} \, \lceil 2\zeta_i \omega_i \bar{\omega} \rfloor [A]^{-1}\{Q\} = -[A]^{-T}[I][A]^{-1} \, \{I\}a$$
$$\qquad (8.17b)$$

From which {P} and {Q} are solved:

$$\{P\} = [A] \left\lceil 2\zeta_i\omega_i\bar{\omega}/\left((\omega_i^2-\bar{\omega}^2)^2 + (2\zeta_i\omega_i\bar{\omega})^2\right)\right\rfloor [A]^{-1} \{I\}a \qquad (8.18)$$

$$\{Q\} = -[A] \left\lceil (\omega_i^2-\bar{\omega}^2)/\left((\omega_i^2-\bar{\omega}^2)^2 + (2\zeta_i\omega_i\bar{\omega})^2\right)\right\rfloor [A]^{-1} \{I\}a \qquad (8.19)$$

For the experimental set-up on the shaking table, the displacements were measured relative to a fixed reference. The vector of total displacement from the fixed reference, $\{x_T\}$, is expressed as

$$\{x_T\} = \{x\} + \{I\}\, x_g \qquad (8.20)$$

where x_g is the harmonic displacement of the table. Then

$$\{\ddot{x}_T\} = \{\ddot{x}\} + \{I\}\, \ddot{x}_g$$

$$\{\ddot{x}_T\} = \left(a\{I\} - \bar{\omega}^2\{H\}\right) \sin \bar{\omega}t - \bar{\omega}^2 \{P\} \cos \bar{\omega}t \qquad (8.21)$$

The vector of the mobility functions at any forcing frequency of the table can be defined as the ratio of the resulting vector of absolute maximum acceleration amplitudes to the absolute maximum amplitude of the ground motion acceleration (i.e. the magnification factors or maximum ratio of response to excitation for any forcing frequency):

$$\{|H(\bar{\omega})|\} = \frac{\{|\ddot{x}_T|\}}{|\ddot{x}_g|} \qquad (8.22)$$

The mobility function for the rth degree of freedom of the system is:

$$|H^{(r)}(\bar{\omega})| = \frac{|\ddot{x}_T^{(r)}|}{|\ddot{x}_g|} \qquad (8.23)$$

Substituting Equation (8.21) yields:

$$|H^{(r)}(\bar{\omega})| = \frac{[(-\bar{\omega}^2 \ P^{(r)})^2 + (a-\bar{\omega}^2 \ Q^{(r)})^2]^{1/2}}{a} \qquad (8.24)$$

Define:

$$\bar{P}^{(r)} = \frac{Q^{(r)}}{a} \qquad (8.25a)$$

$$\bar{P}^{(r)} = \frac{Q^{(r)}}{a} \qquad (8.25b)$$

Substituting into Equation (8.24) yields:

$$|H^{(r)}(\bar{\omega})| = (1 - 2\bar{\omega}^2 \ \bar{Q}^{(r)} + \bar{\omega}^4[(\bar{P}^{(r)})^2 + (\bar{Q}^{(r)})^2])^{1/2} \qquad (8.26)$$

Knowing the natural frequencies and mode shapes given by the program "DYNA" (see Section 8.2) and using the measured damping ratios (see Section 8.8), the vector of mobility functions can be calculated for various forcing frequencies. For this purpose, the computer program "VIBRATION" was created. A listing of the program is given in Appendix A. The program "VIBRATION" reads the natural frequencies, mode shapes and damping ratios of the system in a data file and uses Equation (8.26) to generate the mobility functions (magnification factors) in a given range of forcing frequencies for all the degrees of freedom considered.

The magnitudes of the mobility functions are expressed in decibles (db); this is accomplished by multiplying the $\log_{10}$ (magnitude) by the factor 20. This facilitates the use of the Half-Power method with the mobility functions for estimating damping ratios (see Section 8.8).

The mobility functions for each floor of the model frames can be generated experimentally by exciting the structure with various harmonic base motions and recording, at steady state, the acceleration amplification factors between the table and each floor (harmonic excitation method). The experimental mobility functions are generated by plotting these magnification factors (in db) as a function of the forcing frequencies.

8.5 Frequency Assurance Criteria

The natural frequencies of the different model frames can be predicted by the computer program "DYNA" which solves the classical eigenvalue problem (Equation (8.3)). The natural frequencies can also be measured experimentally by performing a Fourier Spectrum Analysis on the third floor time-acceleration decay record. It is necessary to establish a systematic method of comparing these two results in order to judge the accuracy of the analytical model.

The most obvious comparison of the measured and predicted natural frequencies can be made by a simple tabulation of the two sets of results. A more useful format involves plotting the experimental value against the predicted one for each of the modes included in the comparison. In this way, it is possible to see not only the degree of correlation between the two sets of results, but also the nature (and possible cause) of any discrepancies which do exist. Ideally, the points plotted should lie on or close to a straight line of slope 1. If they lie close to a line of

different slope then almost certainly the cause of the discrepancy is an erroneous material property used in the analytical model. If the points lie scattered widely about a straight line then the analytical model seriously fails to represent the test structure and a fundamental re-evaluation is called for. For a satisfactory model, it may be expected that the scatter will be small and randomly distributed about a 45° line.

If a linear regression analysis is performed on the plotted points, the correlation coefficient is expected to be close to unity for a suitable model. The correlation coefficient is defined as the "Frequency Assurance Criteria" (F.A.C.) and can be used to indicate the degree of agreement between the measured natural frequencies and the analytical natural frequencies.

8.6 Determination of Mode Shapes

Consider a base motion problem in which the system is excited at its rth natural frequency:

$$\ddot{x}_g(t) = a \sin \omega_r t$$

The steady state solution for the floor displacements relative to the moving base has been derived in Section 8.4 and is given by:

$$\{x\} = \{G\} \cos \omega_r t + \{H\} \sin \omega_r t \qquad (8.12)$$

where $\{G\}$ and $\{H\}$ are defined by Equations (8.18) and (8.19).

Since the system is excited at its rth natural frequency, the response will be primarily in its rth mode and therefore we can neglect the influence of the other modes (for $\zeta_i < 0.20$):

$$\{P\} = \frac{a}{2\zeta_r\omega_r^2} [\{0\},\{0\},\ldots,\{A^{(r)}\},\ldots,\{0\}][A]^{-1}\{I\} \quad (8.27)$$

$$\{Q\} = \{0\} \quad (8.28)$$

Let

$$\{D\} = [A]^{-1}\{I\} = \{D_1,D_2,\ldots,D_r,\ldots,D_n\}^T \quad (8.29)$$

Then setting (8.27) and (8.28) into (8.12) yields:

$$\{x\} = \frac{a\,D_r}{2\zeta_r\omega_r^2}\{A^{(r)}\}\cos\omega_r t \quad (8.30)$$

Similarly the accelerations relative to the moving base are given by:

$$\{\ddot{x}\} = -\frac{a\,D_r}{2\zeta_r}\{A^{(r)}\}\cos\omega_r t \quad (8.31)$$

Notice that $\{\ddot{x}\}$ is proportional to the rth mode shape $\{A^{(r)}\}$; this means that system accelerations can be used to define its rth mode shape when a system is excited by a harmonic base motion at a frequency which equals its rth natural frequency.

The mode shapes of the model frames were measured experimentally by exciting the structure at its different natural frequencies and recording the absolute horizontal acceleration at each floor $\{\ddot{x}_T\}$. The structure was considered as a three degree of freedom system, as shown in Figure 8.1. The relative acceleration at each floor of the structure with respect to its moving base (i.e. the table) $\{\ddot{x}\}$, was obtained by subtracting the digitized record of the table acceleration from each corresponding accelerometer record. The mode shapes were then obtained by normalizing to a unit length the vector containing the amplitudes of the relative acceleration at each floor.

8.7 <u>Modal Assurance Matrix</u>

The analytical mode shapes of the different model frames can be determined by using the computer program "DYNA" which solves the classical eigenvalue problem (Equation (8.3)). The experimental mode shapes can be found by exciting the frames at their various natural frequencies and recording the horizontal acceleration at each floor. It is also necessary to establish a systematic way of comparing these two results in order to judge the accuracy of the analytical model.

First consider a plot of the rth experimental mode shape vs. the sth analytical mode shape. If a linear regression analysis is performed on the data points, the resulting correlation coefficient is defined as the "Modal Assurance Criteria" (M.A.C.). The expected values of the M.A.C. are:

$$M.A.C. = 1 \quad \text{for two corresponding modes } (r = s)$$
$$M.A.C. = 0 \quad \text{for two uncorrelated modes } (r \neq s)$$

Having m_X experimental mode shapes and m_A analytical mode shapes, it is possible to construct a matrix $m_X \times m_A$ which contains all the possible correlation coefficients. This matrix is defined as the "Modal Assurance Matrix" [M.A.M.]. For perfect correlation, the [M.A.M.] should be equal to the identity matrix, i.e. ideally:

$$[M.A.M.] = \begin{bmatrix} 1 & 0 & 0 \\ 0 & 1 & 0 \\ 0 & 0 & 1 \end{bmatrix}$$

Some authors (15) suggest that the analytical model is accurate enough if:

M.A.C. > 0.9   for corresponding modes (r = s)

M.A.C. < 0.05   for uncorrelated modes (r ≠ s)

The Model Assurance Matrix was used to compare the measured and predicted mode shapes of the three different model frames.

8.8 Experimental Determination of Damping

In the program "Drain-2D", the damping matrix is described by considering Rayleigh type damping:

$$[C] = \alpha[M] + \beta[K] + \beta_0[K_0]$$ (8.32)

where:

$[M]$ = Global mass matrix

$[K]$ = Updated global stiffness matrix

$[K_0]$ = Initial elastic global stiffness matrix

α, β, β_0 = Damping coefficients

The first term on the right-hand side of Equation (8.36) is known as the inertial damping matrix. The corresponding damping force on each concentrated mass is proportional to its momentum. It represents the energy loss associated with change in momentum (for example, during an impact). The second and third terms are known as the stiffness damping matrices. The corresponding damping force is proportional to the rate of change of the deformation forces at the joints.

If the damping matrix is orthogonal to the model matrix [A], as expressed by Equation (8.16), it follows that the damped motion can be uncoupled into its individual modal responses. This means that the damped system (as well as the undamped system) possesses classical normal modes.

Assuming $\beta_0 = 0$, it can be shown (14) that, in the case of Rayleigh type damping, the damping matrix is orthogonal to the modal matrix if the damping ratios are defined such that:

$$\zeta_r = \frac{\alpha}{2\omega_r} + \frac{\beta\omega_r}{2}$$ (8.33)

where:

ζ_r = Damping ratio of the rth mode

ω_r = Undamped natural frequency of the rth mode

α, β = Damping coefficients

Knowing the damping ratios in the first two modes (ζ_1, ζ_2), the damping coefficients (α, β) can be determined from:

$$\alpha = \frac{4\pi(T_2\zeta_2 - T_1\zeta_1)}{T_2^2 - T_1^2}$$ (8.34a)

$$\beta = \frac{T_1T_2(T_2\zeta_1 - T_1\zeta_2)}{T_2^2 - T_1^2}$$ (8.34b)

where:

T_1, T_2 = Undamped periods of the first and second modes.

Two different methods were used to measure the damping ratios of the different model frames:

1) Half-Power (Bandwidth) Method

2) Logarithmic Decrement Method

1) Half-Power (Bandwidth) Method

First consider the mobility function of a lightly damped ($\zeta < 0.2$) single-degree-of-freedom-system. Using the result of Equation (8.26):

$$|H(\bar{\omega})| \quad = \quad \frac{\omega^2}{\sqrt{(\omega^2-\bar{\omega}^2)^2 + (2\zeta\omega\bar{\omega})^2}} \tag{8.35}$$

The peak amplification occurs when the denominator of Equation (8.35) is a minimum:

$$\frac{\partial}{\partial\bar{\omega}} \left[(\omega^2-\bar{\omega}^2)^2 + (2\zeta\omega\bar{\omega})^2 \right] = 0 \tag{8.36}$$

from which it follows that

$$\bar{\omega} \quad = \quad \omega\sqrt{1 - 2\zeta^2} \tag{8.37}$$

Substituting (8.37) into Equation (8.35), the peak magnification can be found as

$$|H(\bar{\omega})|_{max} \quad = \quad Q \quad = \quad \frac{1}{2\zeta\sqrt{1-2\zeta^2}} \tag{8.38}$$

For a lightly damped system ($\zeta < 0.2$)

$$Q = \frac{1}{2\zeta} \qquad (8.39)$$

The bandwidth (half-power) is defined as the width of the mobility curve when the magnitude is $1/\sqrt{2}$ times the peak value (Q). This bandwidth is denoted by $\Delta\omega = \omega_2 - \omega_1$, where ω_1, ω_2 are given by the roots of

$$\frac{\omega^2}{\sqrt{(\omega^2 - \bar{\omega}^2)^2 + (2\zeta\omega\bar{\omega})^2}} = \frac{1}{\sqrt{2}} \cdot \frac{1}{2\zeta} \qquad (8.40)$$

Expanding Equation (8.40) yields for a lightly damped system ($\zeta < 0.2$):

$$\zeta = \frac{\Delta\omega}{2\omega} \qquad (8.41)$$

This method can be extended to multi-degree-of-freedom systems having widely spaced resonance frequencies. For the rth mode of vibration the damping ratio is given by:

$$\zeta_r = \frac{1}{2} \frac{\Delta\omega_r}{\omega_r} \qquad (8.42)$$

If the mobility function is plotted in decibels (see Section 8.4), the bandwidth corresponding to a resonance is given by the width of the magnitude plot at 3 db below that resonance peak, as shown in Figure 8.3.2

2) Logarithmic Decrement Method

Consider a viscously damped single-degree-of-freedom system excited by some initial condition. The displacement response of this system takes the form of a time decay:

$$x_T(t) = x(t) = x_0 \, e^{-\zeta\omega t} \sin \omega_D t \qquad (8.43)$$

where:

$$\omega_D = \omega\sqrt{1 - \zeta^2} = \text{damped natural frequency} \qquad (8.44)$$

The acceleration response of the system is given by:

$$\ddot{x}(t) = x_0 \, e^{-\zeta\omega t} \left[(\zeta^2\omega^2-\omega_D^2) \sin \omega_D t - 2\zeta\omega\omega_D \cos \omega_D t\right] \qquad (8.45)$$

If the acceleration response at $t = t_i$ is denoted by $\ddot{x}_i$ and the response at $t = t_i+2\pi r/\omega_D$ is denoted by $\ddot{x}_{i+r}$ then it can be shown:

$$\frac{\ddot{x}_{i+r}}{\ddot{x}_i} = e^{-\zeta \frac{\omega}{\omega_D} 2\pi r} \qquad (8.46)$$

If $\ddot{x}_i$ corresponds to a peak point on the acceleration decay record with magnitude A_i, then $\ddot{x}_{i+r}$ corresponds to the peak point r cycles later in the acceleration-time history and its magnitude is denoted by A_{i+r} as shown in Figure 8.4.

It follows that

$$\frac{A_{i+r}}{A_i} = e^{-\zeta \frac{\omega}{\omega_D} 2\pi r} \qquad (8.47)$$

Substituting Equation (8.44) and eliminating the exponential leads to

$$\ln \left[\frac{A_{i+r}}{A_i}\right] = \frac{-\zeta}{\sqrt{1-\zeta^2}} \cdot 2\pi r \qquad (8.48)$$

For a lightly damped system ($\zeta < 0.2$)

$$\ln \left[\frac{A_{i+r}}{A_i}\right] = -\zeta \cdot 2\pi r \qquad (8.49)$$

from which

$$\zeta = \frac{1}{2\pi r} \ln \left[\frac{A_i}{A_{i+r}}\right] \qquad (8.50)$$

For multi-degree-of-freedom systems, the modal damping ratio for each mode can be determined using this method if the initial excitation is such that the decay takes place primarily in one mode of vibration.

There are limitations (in accuracy) of damping values that are experimentally determined by these two methods. In the logarithmic decrement method, the procedure is first to excite the model frame at the desired resonant frequency and then to cease suddenly the excitation; it is tacitly assumed that the model frame can be excited in a single mode. The resulting transient vibrations are invariably influenced by modal interaction. This introduces a certain amount of error into the measured damping values.

In the half-power (bandwidth) method, the accuracy of the damping ratio becomes poor at very low damping ratios ($<1\%$). The main reason for this is the difficulty in obtaining a sufficient number of experimental data points on the mobility curve in the vicinity of a resonance frequency of a lightly damped system. As a result, the mobility curve is poorly

defined in the neighbourhood of a weakly damped resonance peak. To reduce this problem, the mobility functions of the model frames were determined experimentally with the best frequency resolution that could be achieved with the oscillator of the Earthquake Simulator (i.e., 0.01 Hz increments).

The expressions used in computing the damping parameters of the model frames are based on linear system theory. However, during the evaluation tests the Moment Resisting Frame and the Braced Moment Resisting Frame will undergo inelastic deformations and will exhibit some non-linear behaviour. If the degree of non-linearity is high, the measured damping values will not be representative of the actual damping values. Measured viscous damping in the model frames should increase with the amplitude of motion (13).

9. SYSTEM IDENTIFICATION OF THE MOMENT RESISTING FRAME

9.1 Free Vibration Analysis

The first model frame considered represents the standard construction of a Moment Resisting Frame, as shown in Figure 9.1. The computer program "DYNA" (see Chapter 8) was used to predict the natural frequencies and mode shapes of this frame. A refined lumped mass system was developed to model the structure as illustrated in Figure 9.2. The mass matrix was formed by lumping the mass of the concrete blocks and the structure at the indicated nodes. The lumped masses were assumed to be active in the x and y directions, but rotational masses were neglected. The material properties determined from uniaxial tests on steel specimens (see Chapter 6) were used in the program. Shear deformations were not considered in the analysis.

The first six natural frequencies and mode shapes resulting from the analysis are shown in Figure 9.3. Notice that the third, fourth and fifth modes of vibration correspond to vertical deformations of the beams. In the test program, vertical excitation of the base is needed in order to measure these three mode shapes. Since the shaking table input is only quasi-horizontal, these three mode shapes do not contribute to the horizontal response of the structure and therefore they were discarded.

For purposes of comparison of the predicted and measured natural frequencies, the predicted horizontal natural frequencies of the Moment Resisting Frame are:

$$f_1 = 2.831 \text{ Hz} \qquad \omega_1 = 17.788 \text{ rad/s}$$

$$f_2 = 9.174 \text{ Hz} \qquad \omega_2 = 57.642 \text{ rad/s}$$

$$f_3 = 15.930 \text{ Hz} \qquad \omega_3 = 100.091 \text{ rad/s}$$

Considering only 3 degrees-of-freedom (see Figure 8.1), the predicted mode shapes of the Moment Resisting Frame are:

$$\{A^{(1)}\}^T = \{0.21, 0.57, 0.80\}$$
$$\{A^{(2)}\}^T = \{0.57, 0.46, -0.68\}$$
$$\{A^{(3)}\}^T = \{0.75, -0.58, 0.32\}$$

where $\{A^{(i)}\}^T$ represents the transposed matrix of the ith mode shape.

9.2 Harmonic Forced Vibration Test

The natural frequencies of the Moment Resisting Frame were measured experimentally by first exciting the structure with harmonic base motions having frequencies which differed significantly from the natural frequencies of the structure and then suddenly stopping the base excitations. The third floor time-acceleration decays were recorded at this stage and a standard Fast Fourier Transform program was used to convert these records into Fourier Amplitude Spectra, from which the natural frequencies of the Moment Resisting were determined.

Three different tests were made with base harmonic motions having frequencies of 5, 11, and 20 Hz (31.42, 69.12, 125.66 rad/s). The resulting Fourier Amplitude Spectra are shown in Figure 9.4. From these Spectra, the measured natural frequencies of the Moment Resisting Frame were found to be:

$$f_1 = 2.86 \text{ Hz} \qquad \omega_1 = 17.97 \text{ rad/s}$$
$$f_2 = 9.08 \text{ Hz} \qquad \omega_2 = 57.05 \text{ rad/s}$$
$$f_3 = 14.4 \text{ Hz} \qquad \omega_3 = 89.22 \text{ rad/s}$$

The predicted and measured natural frequencies of the Moment Resisting Frame are tabulated in Table 9.1. Figure 9.5 shows a plot of the measured vs. predicted natural frequencies of the Moment Resisting Frame. Notice that the scatter of the points is small. As a result, no change was made to the analytical model. The Frequency Assurance Criteria (F.A.C.) was found to be equal to 0.9980, which is very close to the expected value of 1.

9.3 Experimental Determination of Mode Shapes

The horizontal mode shapes of the Moment Resisting Frame were measured experimentally by exciting the structure at the desired natural frequencies and recording the acceleration of each floor relative to the moving base (i.e. table).

Figure 9.6 shows the steady-state, time-acceleration records of each floor for the first three horizontal modes considered. Notice the following characteristics of classical normal modes:

Mode 1 (ω_1 = 17.97 rad/s): All the floor records are in phase.

Mode 2 (ω_2 = 57.05 rad/s): The first and second floor records are in phase while the third floor record is out-of-phase by 180°.

Mode 3 (ω_3 = 89.22 rad/s): The first and third floor records are in phase while the second floor record is out-of-phase by 180°.

The measured mode shapes of the Moment Resisting Frame were normalized by equating the vector containing the amplitudes of the relative acceleration at each floor to a unit length; this leads to the following result:

$$\{A^{(1)}\}^T = \{0.22, \ 0.56, \ 0.80\}$$

$$\{A^{(2)}\}^T = \{0.55, \ 0.41, \ -0.72\}$$

$$\{A^{(3)}\}^T = \{0.86, \ -0.47, \ 0.21\}$$

Table 9.2 shows the comparison between the measured and predicted mode shapes of the Moment Resisting Frame. Notice that the Modal Assurance Criteria (M.A.C.) are very close to the expected value of 1 for corresponding modes. The measured vs. predicted mode shapes are plotted in Figure 9.7. The scatter of the points is small and randomly distributed about the expected 45° line. The resulting Modal Assurance Matrix (M.A.M.) was found to be:

$$[M.A.M] = \begin{bmatrix} 0.9996 & -0.5251 & -0.2634 \\ -0.4947 & 0.9998 & 0.0813 \\ -0.1632 & -0.0889 & 0.9823 \end{bmatrix}$$

As mentioned earlier (see Section 8.7), some authors suggest that the off-diagonal terms of the Modal Assurance Matrix should be smaller than 0.05 for satisfactory results. However this was not obtained for the M.A.M. of the Moment Resisting Frame since only 3 degrees of freedom were considered for defining the mode shapes (see Figure 8.2). If more degrees of freedom are used to determine the mode shapes, the off-diagonal terms of the M.A.M. should converge to zero.

9.4 Mobility Function

The mobility functions for each floor of the Moment Resisting Frame were determined experimentally by exciting the structure with various base harmonic motions and recording, at steady state, the amplifications of the acceleration responses between the table and each floor. The resulting

experimental Mobility Functions (in db) are shown in Figure 9.8. The first
two natural frequencies of the moment Resisting Frame (17.97 and 57.05
rad/s) are easily recognizable and correlate very well with the results of
the Fourier Spectrum Analysis (Section 9.2). However the third natural
frequency is not clearly defined, as two peaks arise around 90 rad/s. By
observation of the frame behaviour, it was found that the first peak is the
result of an interaction between horizontal and vertical modes due to the
rocking of the table. Since the shaking table is mounted on four vertical
legs with universal joints at each end, a small vertical excitation is
transmitted to the structure due to the arcing motion of the table as it is
excited horizontally. This motion causes the table to rock slightly, and
because the vertical natural frequencies of the Moment Resisting Frame are
very close to the third classical horizontal natural frequency, an
interaction occurs in the Mobility Functions. This effect can be elimina-
ted by installing two accelerometers (in opposite directions) at each floor
and subtracting the records to cancel the vertical component. The second
peak at 89.22 rad/s corresponds to the third classical horizontal natural
frequency of the Moment Resisting Frame.

9.5 Experimental Determination of Damping

As mentioned earlier (see Section 8.8), two different methods were
used to estimate the modal damping ratios of the Moment Resisting Frame:

1)   Half-Power (Bandwidth) Method

2)   Logarithmic Decrement Method

The Half-Power Method was used directly on the experimental mobility
functions (see Figure 9.8). Figure 9.9 illustrates the method on a

typical detail of the first floor mobility function of the Moment Resisting Frame.

The damping ratios were also estimated by the Logarithmic Decrement Method after exciting the structure in each mode and recording the time-acceleration decays at each floor. Figure 9.10 illustrates the method on a typical first floor time-acceleration decay in the first mode of vibration.

The damping ratios determined from the two methods are compared in Table 9.3. The two methods give damping ratios which are of the same order of magnitude. Notice that the values obtained by the Bandwidth Method are generally higher than those obtained by the Logarithmic Decrement Method. The Bandwidth Method tends to overestimate damping because of the difficulty in obtaining a sharp experimental peak at resonance. Based on these results, the following damping ratios were used for the Moment Resisting Frame:

$$\zeta_1 = 0.0028 \quad (0.28\%)$$
$$\zeta_2 = 0.0021 \quad (0.21\%)$$
$$\zeta_3 = 0.0074 \quad (0.74\%)$$

By considering only the above first two modal damping ratios (ζ_1, ζ_2), the damping coefficients for Rayleigh type damping, as obtained from Equations (8.34a) and (8.34b) are:

$$\alpha = 0.0853$$
$$\beta = 0.00015$$

These two damping coefficients were used in the non-linear, time-history dynamic analysis program to generate analytical solutions for the Moment Resisting Frame.

The modal damping ratios and the results of the Free Vibration Analysis (see Section 9.1) were used in the program "Vibration" (see Section 8.4) to predict the mobility functions of the Moment Resisting Frame. The predicted and measured mobility functions of the Moment Resisting Frame are plotted in Figure 9.11. The two curves correlate very well, especially for the first two modes of vibrations. The amplitudes of the resonant peaks are closely matched, indicating a good estimation of the modal damping ratios.

10.   SYSTEM IDENTIFICATION OF THE BRACED MOMENT RESISTING FRAME

10.1 Free Vibration Analysis

The second type of frame considered represents a Braced Moment Resisting construction for which the braces were designed to be effective in tension only. The braces were made of 6 mm square bars (AINSI C-1018 cold formed steel). They were not connected together at mid-length, so that their effective length is essentially the total length of a brace. This reduces the buckling load of the braces and allows the structure to be modelled as a linear system in which the braces act in tension only.

The computer program "DYNA" was used to predict the natural frequencies and mode shapes of the Braced Moment Resisting Frame. Figure 10.1 illustrates the computer model employed for the free vibration analysis. Only one brace was considered at each storey, since the compression braces were neglected.

The first six natural frequencies and mode shapes resulting from the analysis are shown in Figure 10.2. As expected, the first natural frequency of the Braced Moment Resisting Frame is higher than the corresponding frequency of the Moment Resisting Frame (see Figure 9.3), since the braces have stiffened the structure. Notice that the same three vertical modes encountered with the Moment Resisting Frame are also present with the Braced Moment Resisting Frame; the incorporation of the braces does not affect the bending stiffness of the beams. The three natural frequencies corresponding to the vertical modes (87.336, 95.756 and 99.965 rad/s) are very close to the classical horizontal second natural frequency (91.61 rad/s) and therefore we expect some difficulty in clearly differentiating

the classical second mode in the Fourier Spectrum Analysis (see Section 10.2).

For purposes of comparison, the predicted horizontal natural frequencies of the Braced Moment Resisting Frame are:

$$f_1 = 5.087 \text{ Hz} \qquad \omega_1 = 31.962 \text{ rad/s}$$

$$f_2 = 14.581 \text{ Hz} \qquad \omega_2 = 91.617 \text{ rad/s}$$

$$f_3 = 22.025 \text{ Hz} \qquad \omega_3 = 138.389 \text{ rad/s}$$

Considering only 3 degrees-of-freedom (see Figure 8.1), the predicted mode shapes of the Braced Moment Resisting Frame are:

$$\{A^{(1)}\}^T = \{0.27, \ 0.59, \ 0.76\}$$

$$\{A^{(2)}\}^T = \{0.63, \ 0.32, \ -0.71\}$$

$$\{A^{(3)}\}^T = \{0.65, \ -0.64, \ 0.40\}$$

10.2 Harmonic Forced Vibration Test

Two tests were performed in order to measure the natural frequencies of the Braced Moment Resisting Frame using the Fourier Amplitude Spectrum method. These were carried out with harmonic base motions having excitation frequencies of 8 and 18 Hz. The resulting Fourier Amplitude Spectra are presented in Figure 10.3.

The fundamental natural frequency of the Braced Moment Resisting Frame, which can easily be established from the Fourier Spectrum of the first test, was found to be:

$$f_1 = 5.29 \text{ Hz} \qquad \omega_1 = 33.24 \text{ rad/s}$$

However the second and third natural frequencies are not easily differentiable. The Fourier Amplitude Spectrum of the second test shows many peaks between 13 and 20 Hz (81.68 - 125.66 rad/s). These peaks correspond to the closely spaced natural frequencies found through the Free Vibration Analysis (see Figure 10.2) and are present in the Spectrum because of the interaction between vertical and horizontal modes due to the rocking of the table.

The investigation of the natural frequencies of the Braced Moment Resisting Frame was not pursued further, since the contributions of the second and higher modes to the response of the structure will be negligible.

10.3 Experimental Determination of Mode Shapes

Since it was difficult to separate the higher modes of the Braced Moment Resisting Frame, only the first mode shape was measured experimentally. The structure was excited at its first natural frequency (5.29 Hz) and the steady-state relative accelerations at each floor were recorded.

Figure 10.4 shows the time-acceleration records for the three floors. Again, the characteristic of a classical first normal mode can be observed, since all the floor records are in phase. The measured first mode shape of the Braced Moment Resisting Frame was found to be

$$\{A^{(1)}\}^T = \{0.34, 0.60, 0.72\}$$

A comparison of the measured and predicted first mode shape of the Braced Moment Resisting Frame (see Section 10.1) led to a Modal Assurance Criterion equal to 0.9994.

10.4 <u>Experimental Determination of Damping</u>

In the last chapter, the Bandwidth method and the Logarithmic Decrement method were used to estimate the modal damping ratios of the Moment Resisting Frame. The two methods gave results which correlated very well. Therefore, it was decided to use only the Logarithmic Decrement method to estimate the damping characteristics of the Braced Moment Resisting Frame. This avoided the need to generate experimental mobility functions, which require repetitive testing.

Since it was difficult to separate the higher modes of the Braced Moment Resisting Frame (see Section 10.2), only the first modal damping ratio was measured. To determine the values of the damping coefficients used in the Rayleigh type damping (Equations (8.34a) and (8.34b)), it was assumed that the two lower modal damping ratios were equal ($\zeta_1 = \zeta_2$).

Figure 10.5 illustrates the Logarithmic Decrement method as applied to the first floor acceleration-time decay in the first mode of vibration. Table 10.1 shows the different damping ratios measured. Based on these tests, the following (average) damping ratios were used for the Braced Moment Resisting Frame:

$$\zeta_1 = \zeta_2 = 0.0127 \quad (1.27\%)$$

Notice that the incorporation of the braces changes the damping characteristics of the structure:

$$\frac{\zeta_1 \ (\text{Braced Moment Resisting Frame})}{\zeta_1 \ (\text{Moment Resisting Frame})} = \frac{0.0127}{0.0028} = 4.54$$

The damping coefficients defining the Rayleigh type damping and obtained by Equations (8.34a) and (8.34b) were:

$$\alpha = 0.6195$$

$$\beta = 0.00064$$

These two damping coefficients were used in the non-linear, time-history dynamic analysis to generate analytical solutions for the Braced Moment Resisting Frame.

Assuming the same damping ratios in the first three horizontal modes of vibrations ($\zeta_1 = \zeta_2 = \zeta_3$) and using the results of the free vibration analysis (see Section 10.1), the predicted mobility functions of the Braced Moment Resisting Frame were generated by the program "Vibration" (see Section 8.4). The predicted mobility functions are shown in Figure 10.6.

11. SYSTEM IDENTIFICATION OF THE FRICTION DAMPED BRACED FRAME UNDER LOW AMPLITUDE EXCITATIONS

11.1 Free Vibration Analysis

The third type of frame considered in this investigation represents a Friction Damped Braced Frame as shown in Figure 11.1. Because of the incorporation of the friction devices, the structure can no longer be modelled as a linear system. The non-linearity of the structure basically results from two sources:

1)   Slipping of the Friction Devices

2)   Buckling of the Compression Braces

The dynamic characteristics of the Friction Damped Braced Frame (natural frequencies, damping parameters, mode shapes, mobility functions) therefore are a function of the amplitude of the excitation. Two extreme fundamental frequencies can be obtained for a Friction Damped Braced Frame as follows: the lowest natural frequency will happen when all the devices are slipping and will be identical to the fundamental frequency of the Moment Resisting Frame (2.86 Hz); the highest natural frequency will occur under very low amplitude excitations when none of the devices slip and all the braces behave elastically in tension and compression. For any combination of slippage of the devices and buckling of the compression braces, the fundamental natural frequency of the Friction Damped Braced Frame will lie between these two extreme values.

Similarly, the viscous damping characteristics of the structure will vary with the amplitude of the excitation. However, the viscous damping will be very small compared to the hysteretic damping dissipated by the devices and therefore can be assumed constant. For this reason, it was

decided to estimate the dynamic parameters of the Friction Damped Braced

Frame under low amplitude excitations, during which none of the devices

slip and all the braces behave elastically in tension and compression.

Under such conditions, the structure can be modelled as a linear system.

Figure 11.2 illustrates the computer model developed for the free vibra-

tions analysis using the computer program "DYNA". Since the compression

braces were assumed not to buckle under low amplitude excitations, two

elastic braces were considered at each storey. The friction pads were

modelled by elastic bars since it was assumed that no slippage takes place.

The mass of the devices were considered and lumped at the four corner nodes

of the mechanism.

The first nine natural frequencies and mode shapes resulting from the

analysis are shown in Figures 11.3 and 11.4. The first three natural

frequencies are closely spaced (24.448, 24.746 and 24.829 rad/s) and

correspond to rotational modes of the devices due to the bending of the

braces. A rotational excitation is needed to be able to measure these

three modes and since the motion of the table is quasi-horizontal, they

will not contribute to the horizontal response of the frame and therefore

they were considered as higher modes and neglected. In a real building

these three modes of vibrations will occur at much higher frequencies,

since the mass of the devices would be negligible compared to the mass of

the structure.

The first classical horizontal mode of the structure occurs at a

frequency of 44.059 rad/s; this is higher than the corresponding frequency

for the normal Braced Moment Resisting Frame (see Figure 10.2), since the

braces are assumed to be effective both in tension and compression under

low amplitude excitations. Notice, that the devices also rotate at this

same frequency; this deformation is caused by the bending of the braces.

The next three modes are vertical modes and they are identical to the ones obtained with the Moment Resisting Frame (see Figure 9.3) and the Braced Moment Resisting Frame (see Figure 10.2); incorporation of the friction devices does not alter the bending stiffness of the beams. Again, these three modes were considered as higher modes and neglected.

Finally, the second and third horizontal modes were obtained at frequencies of 122.348 and 177.919 rad/s.

For purposes of comparison with subsequent experimental results, the predicted horizontal natural frequencies of the Friction Damped Braced Frame under low amplitude excitations can be summarized as follows:

$$f_1 = 7.012 \text{ Hz} \qquad \omega_1 = 44.059 \text{ rad/s}$$
$$f_2 = 19.472 \text{ Hz} \qquad \omega_2 = 122.348 \text{ rad/s}$$
$$f_3 = 28.316 \text{ Hz} \qquad \omega_3 = 177.919 \text{ rad/s}$$

Considering only 3 degrees-of-freedom (see Figure 8.1), the predicted mode shapes of the Friction Damped Braced Frame under low amplitude excitations are:

$$\{A^{(1)}\}^T = \{0.29, \ 0.60, \ 0.75\}$$
$$\{A^{(2)}\}^T = \{0.66, \ 0.27, \ -0.70\}$$
$$\{A^{(3)}\}^T = \{0.60, \ -0.67, \ 0.44\}$$

11.2 Harmonic Forced Vibration Test

To measure the natural frequencies of the Friction Damped Braced Frame under low amplitude excitations, two harmonic tests were performed with

base motions having frequencies of 8 and 35 Hz. The resulting Fourier
Amplitude Spectra are shown in Figure 11.5. The first two horizontal
natural frequencies of the Friction Damped Braced Frame under low amplitude
excitations correspond to the frequencies at which the main spikes occur on
the spectra; these take place at:

$$f_1 = 7.03 \text{ Hz} \qquad \omega_1 = 44.17 \text{ rad/s}$$

$$f_2 = 18.4 \text{ Hz} \qquad \omega_2 = 115.6 \text{ rad/s}$$

The investigation of the third horizontal natural frequency becomes
very difficult in terms of the table capabilities because of the high value
of this frequency ($\approx$ 28 Hz) relative to the frequency range of the table.
Since only 2 modal damping ratios are needed to determine the damping
coefficients used in the Rayleigh type damping, no experimental attempt was
made to verify this third natural frequency.

The predicted and measured natural frequencies of the Friction Damped
Braced Frame under low amplitude excitations are tabulated in Table 11.1.
Figure 11.6 shows a plot of the measured vs. predicted natural frequencies.
The data points are very close to the expected 45° line and therefore no
change was made to the analytical model.

11.3 Experimental Determination of Mode Shapes

The first two horizontal mode shapes of the Friction Damped Braced
Frame under low amplitude excitations were measured experimentally. The
structure was excited at the desired natural frequencies and the horizontal
accelerations of each floor (relative to the table) were recorded under
steady-state conditions.

Figure 11.7 shows the relative time-acceleration records for the three floors of the model frame. Again notice that the results exhibit the same characteristics of classical normal modes as were discussed earlier in Section 9.3. From these records, the measured first two horizontal mode shapes of the Friction Damped Braced Frame under low amplitude excitations are:

$$\{A^{(1)}\}^T = \{0.40, \ 0.50, \ 0.77\}$$
$$\{A^{(2)}\}^T = \{0.58, \ 0.19, \ -0.79\}$$

Table 11.2 shows the comparison between the measured and predicted mode shapes. The Modal Assurance Criteria (M.A.C.) are very close to the expected value of 1 for the first two modes, hence confirming the validity of the analytical model. The measured vs. predicted mode shapes are plotted in Figure 11.8. Notice that the scatter of the data points is small and randomly distributed about the expected 45° line. The Modal Assurance Matrix (M.A.M.) was calculated to be:

$$[M.A.M.] = \begin{bmatrix} 0.9661 & -0.5235 \\ -0.4301 & 0.9972 \end{bmatrix}$$

11.4 Experimental Determination of Damping

The first two modal damping ratios of the Friction Damped Braced Frame under low amplitude excitations were estimated by the Logarithmic Decrement Method. The structure was excited in turn in its first two modes and the floor time-acceleration decays were recorded. Figure 11.9 illustrates the results obtained for the first floor time-acceleration decay corresponding to the first mode of vibration. Table 11.3 summarizes the different

damping ratios measured. Note that a damping result is missing for the second mode; this is due to the fact that a malfunction of the second floor amplifier was experienced during the test.

Based on these results, the following modal damping ratios were assigned to the Friction Damped Braced Frame:

$$\zeta_1 = 0.0060 \quad (0.60\%)$$

$$\zeta_2 = 0.0039 \quad (0.39\%)$$

The damping coefficients defining the Rayleigh type damping were calculated from Equations (8.34a) and (8.34b) to yield:

$$\alpha = 0.4667$$

$$\beta = 0.0001$$

These two damping coefficients were used in the non-linear, time-history dynamic analysis to generate analytical solutions for the Friction Damped Braced Frame.

12. SEISMIC TESTS ON SHAKING TABLE

12.1 Seismic Testing Program, Model Frame #1

It was decided to use the Newmark-Blume-Kapur artificial earthquake described in Chapter 4, for the test of the first model frame on the shaking table. This earthquake record provides a response spectrum which matches the Newmark-Blume-Kapur design spectrum and represents an average of many earthquake records.

As mentioned earlier, the connections of the test frame were designed so that the model could easily be transformed into any of the three structural configurations to be investigated (M.R.F., B.M.R.F., F.D.B.F.). By a proper choice of the intensity of the ground motion and the test sequence, it was possible to carry out a comparative study of the three model types using only a single frame.

Three different earthquake intensities, expressed in terms of the peak acceleration of the ground motion, were used to study the performance of the model frames in both the elastic and inelastic ranges. In order to accommodate the testing of the three structural configurations with a single frame, the three intensities of the ground motion were chosen to meet the following requirements:

Intensity 1

- The maximum stress in the Moment Resisting Frame should be less than 50% of the yield stress.
- All members remain elastic for the Braced Moment Resisting Frame and the Friction Damped Braced Frame.

Intensity 2

- The maximum stress in the Moment Resisting Frame should be between 50 and 75% of the yield stress.

- All members remain elastic for the Braced Moment Resisting Frame and the Friction Damped Braced Frame.

Intensity 3

- Some yielding should occur in the Moment Resisting Frame.

- Some of the cross-braces of the Braced Moment Resisting Frame should yield but all the other structural elements should remain elastic; all members remain elastic in the Friction Damped Braced Frame.

For any given earthquake, the maximum ground motion intensity which can be delivered by the shaking table is limited. Considering the maximum possible displacement of the table (±75 mm), it was found that the peak acceleration that can be developed by the table with the Newmark-Blume-Kapur artificial earthquake is 0.34 g.

To determine the appropriate earthquake accelerations corresponding to the intensities noted above, several non-linear time-history dynamic analyses were performed with different peak ground accelerations. The computer model used for this purpose was similar to the one described in Chapter 4. Viscous damping was considered using the measured damping coefficients determined experimentally (see Chapter 9 and 10). From the results of these analyses the following ground motion accelerations were found to satisfy the intensity requirements stated above and were used for the seismic tests of the first model frame:

Intensity	Peak Ground Acceleration (g)
1	0.05
2	0.10
3	0.30

The predicted structural damage resulting from the Newmark-Blume-Kapur artificial earthquake is shown in Figure 12.1 for the Moment Resisting Frame and the Braced Moment Resisting Frame under these intensities. Notice that these three intensities meet the requirements formulated above.

The following testing sequence was adopted in order to test all three structural configurations using only a single frame.

Test Sequence	Frame Type	Intensity	Structural Damage
1	F.D.B.F.	1	None
2	F.D.B.F.	2	None
3	B.M.R.F.	1	None
4	B.M.R.F.	2	None
5	M.R.F.	1	None
6	M.R.F.	2	None
7	F.D.B.F.	3	None
8	B.M.R.F.	3	Only cross-braces yield
9	M.R.F.	3	Main members yield

Some preliminary tests were performed at low acceleration amplitudes to verify the table performance in reproducing the Newmark-Blume-Kapur artificial earthquake. Figure 12.2 compares the acceleration records and

the Fourier Amplitude Spectra of the actual earthquake and the shaking table motions. Notice that the Fourier Amplitude Spectrum of the actual earthquake contains a large peak at very low frequency (≈ 0.2 Hz) which is not reproduced in the table record. For mechanical reasons, the integrating circuit for evaluating the table displacement corresponding to the acceleration input has a roll off at frequencies lower than 1 Hz and therefore filters the low frequencies; the table is displacement controlled.

12.2 Test Results, Model Frame #1

The experimental results presented in this section are compared to the predictions of the inelastic time-history dynamic analysis. The material properties determined from the uniaxial tests on steel specimens (see Chapter 6) were used in the analytical model. Also, the damping values measured at low amplitude vibrations (see chapters 9-11) were used to predict the responses of the frames.

The envelopes of the measured horizontal accelerations for the three intensities of the ground motion are shown in Figure 12.3. (The program Drain-2D does not provides results in terms of acceleration; the analytical values of acceleration are therefore not shown here). For the Intensity 3 earthquake (peak acceleration = 0.30 g), a peak horizontal acceleration of 2.00 g and 1.51 g was experienced at the top of the Moment Resisting Frame and the Braced Moment Resisting Frame respectively; the measured peak horizontal acceleration at the top of the Friction Damped Braced Frame was only 0.59 g. The influence of the new damping system in reducing seismic response can be visualized by comparing the maximum acceleration amplifications experienced by the three frames under the Intensity 3 earthquake:

Frame	Maximum Amplification
M.R.F.	6.63
B.M.R.F.	5.08
F.D.B.F.	1.98

Figure 12.4 shows the envelopes of lateral deflections for the three intensities of the ground motion. Good agreement is observed between the experimental results and the predictions of the inelastic time-history dynamic analysis. Notice that the smallest deflections were always obtained with the Friction Damped Braced Frame. The responses of the Friction Damped Braced Frame and the Braced Moment Resisting Frame are very similar for low intensity earthquakes, when there is no slippage of the friction devices. As the intensity of the ground motion increases, the friction devices become active and improve the performance of the Friction Damped Braced Frame compared to the two other frames.

The analytical model underestimates the deflections of the Braced Moment Resisting Frame for the Intensity 3 earthquake. This result was expected since the analytical model does not consider the stiffness degradation of the braces when they undergo several inelastic loops (pinched hysteresis). The predictions of the Moment Resisting Frame deflections are not very accurate for the Intensity 3 earthquake since the damping values, measured at very low amplitude excitations, and used in the analysis, are not representative of the frame behaviour under large inelastic vibrations. The influence of damping is illustrated in Figure 12.4 by showing the change in the deflections resulting from the use of a damping value which is 5 times the actual damping measured at low intensities.

No certain explanation can be offered for the apparent excessive

difference between the measured third floor deflection and its predicted value. It is possible that the calibration of the analog-digital converter for that recording channel was set in error in the test; the displacement appears to be excessive by a factor of two.

The envelopes of the bending moments in the beams are presented in Figure 12.5. The experimental bending moments were obtained from readings of the strain gages. Good agreement is observed between the measured and predicted values. However, the analytical prediction overestimates the actual damage in the beams of the Moment Resisting Frame under the Intensity 3 earthquake. Only slight yielding was measured in the first floor beam while the second floor beam remained elastic. This is again related to the fact that the measured damping values are not representative of the actual frame behaviour under large amplitude vibrations. The damping values of the model frames should increase with the amplitude of motion.

Table 12.1 compares the measured and predicted maximum bending moments in the base column at the location of the strain gages. Again good agreement is observed except for the Moment Resisting Frame under Intensity 3 earthquake, where the analytical model overestimates the bending moments in the base column.

The time-histories of the deflections at the top of the frames for the Intensity 3 earthquake are presented in Figure 12.6. The analytical model predicts reasonably well the responses of the frames. Notice that the amplitudes of the vibrations for the Friction Damped Braced Frame are far less than the corresponding vibrations of the two other model frames.

Figure 12.7 shows the measured and predicted slippage time-histories of the second floor device during the first 9 seconds of the Intensity 3

earthquake. The slippage predicted by the refined analytical model is of the same order of magnitude as the measured values. However, notice that the signal from the measured slippage is very noisy. This was due to the lateral vibrations of the devices, which influenced the readings of the L.V.D.T.'s. These lateral vibrations mainly occur because of the weight of the devices compared to the weight of the model frame; in a real building these lateral vibrations will be practically non-existent.

The torsional motion developed in the structure was measured by analyzing the phase shift between the displacement records given by the two potentiometers at each floor. Figure 12.8 shows the time-history of the third floor deflection recorded from both potentiometers for the Friction Damped Braced Frame during the Intensity 3 earthquake. The two signals are exactly in phase with similar amplitudes and therefore no significant torsional stresses were induced in the structure.

The results of this first series of tests clearly indicate the superior performance of the Friction Damped Braced Frame compared to the two frames, which represent a class of conventional building systems. From these results the following conclusions can be drawn:

1. The amplitudes of the displacements and accelerations are considerably reduced for the Friction Damped Braced Frame relative to the corresponding responses of the two other building systems; thus nonstructural damaged is minimized.

2. When subjected to the Intensity 3 earthquake many cross-braces of the Braced Moment Resisting Frame yielded in tension and the first floor beams of the Moment Resisting Frame reached their yield moment. No material yielding was involved in the process of energy dissipation in the Friction Damped Braced Frame; since this frame was not damaged

during the earthquake, it was able to face future earthquakes with the same efficiency.

3. No significant torsional motion of the Friction Damped Braced Frame was observed.

4. The deformations of the Friction Damped Braced Frame at the end of the earthquakes were negligible, indicating that the structure recovered from these shocks without any permanent set.

12.3 Supplementary Tests, Model Frame #1

At the end of the first series of tests, the first model frame had slightly yielded in the first floor beams. But a full plastic hinge had not been formed and the permanent set was very small. Therefore it was decided to test again the Moment Resisting Frame and the Friction Damped Braced Frame with a different earthquake record despite the small plastic deformation which was present. The Braced Moment Resisting Frame was not re-tested, since many of its cross-braces had yielded in tension in the first series of tests, and could not be used again.

The choice of the new earthquake record was based on the following requirements:

1. Its frequency content must be higher than that of the artificial earthquake so that a higher peak acceleration can be achieved with the same displacement of the shaking table.

2. Its Fourier amplitude spectrum should be relatively constant over the range of natural frequencies of the model frames so that the energy input is almost constant for the three types of construction.

Based on these requirements the following earthquake record was chosen:

Kern County California Earthquake (Taft Lincoln School Tunnel), July 21, 1952, Comp. Vert., 0-25 sec.

This earthquake does not completely satisfy the second requirement; however, an analytical study using 'white noise' as the excitation source was also performed (see Section 4.4) to fulfill that requirement.

Some preliminary tests were performed at low intensity to verify the ability of the shaking table to reproduce the Taft earthquake. The acceleration record and the Fourier Amplitude Spectrum of the actual earthquake and the shaking table are presented in Figure 12.9. On the basis of these tests, it was found that the peak acceleration which can be developed on the shaking table with the Taft earthquake is 0.90 g. Notice this value is much higher than the 0.34 g obtained with the Newmark-Blume-Kapur Artificial Earthquake. For the actual tests, it was decided to scale the earthquake record to a peak acceleration of 0.60 g. Again the experimental results were compared with the predictions of the inelastic time-history dynamic analysis. The slight damage which had been induced in the Moment Resisting Frame by the earlier test was ignored when making this comparison.

The envelope of the measured horizontal accelerations are shown in Figure 12.10. As expected, smaller accelerations were induced in the Friction Damped Braced Frame where, at the top storey, an acceleration of 1.10 g was experienced compared to 2.23 g for the corresponding value in the Moment Resisting Frame.

Figure 12.11 shows the envelope of lateral deflections. It can be seen that the measured deflection at the top of the Friction Damped Braced

Frame is only 31% of the equivalent deflection in the Moment Resisting Frame. The analytical predictions overestimate the deflections of the Moment Resisting Frame; again it is believed that the damping values, determined at low amplitude excitations, are smaller than the actual values for high amplitude vibrations. An analytical solution including 8 times the initial viscous damping is also shown in Figure 12.11 for the Moment Resisting Frame.

The envelopes of beam bending moments are shown in Figure 12.12. Notice that the first floor beam of the Moment Resisting Frame reaches its plastic moment capacity under this earthquake, whereas the equivalent moment in the Friction Damped Braced Frame is only 39% of the plastic moment.

Table 12.2 compares the measured and predicted maximum bending moments in the base columns of the three frames at the location of the strain gages. The measured maximum moment in the Friction Damped Braced Frame is only 28% of the value in the Moment Resisting Frame.

The time-histories of the deflections at the top of the frames are presented in Figure 12.13. The measured amplitudes of the vibrations of the Friction Damped Braced Frame are far less than the values obtained with the Moment Resisting Frame.

Figure 12.14 presents the measured slippage time-history of the second floor friction device. Significant slippage occurs in the device; the maximum recorded value is 7.64 mm. The maximum slippage occurred at the same time as the maximum ground acceleration (see Figure 12.9) and hence as the maximum inertia forces developed in the structure.

The torsional motion of the Friction Damped Braced Frame was checked again. Figure 12.5 shows the time-history of the third floor deflection

recorded from both potentiometers for the Friction Damped Braced Frame.
The two signals are exactly in phase with similar amplitudes and, there-
fore, it can be concluded again that no significant torsional stresses were
induced in the structure.

12.4 Seismic Testing Program, Model Frame #2

The results presented in the last section clearly show the superior
performance of the Friction Damped Braced Frame compared to the conven-
tional seismic structural systems. Even the Taft record scaled to a peak
acceleration of 0.6 g caused no damage in the Friction Damped Braced Frame,
while the Moment Resisting Frame underwent large inelastic deformations.

For the series of tests on the second model frame, it was decided to
study the performance of the three structural configurations when subjected
to the Taft Earthquake scaled to the maximum intensity that can be physic-
ally realized by the shaking table (peak acceleration = 0.9 g) for this
particular excitation.

Initially the second model frame was mounted on the shaking table and
some preliminary tests were performed to verify its fundamental dynamic
properties. The natural frequencies and damping characteristics of the
three different types of construction are compared in Tables 12.3 and 12.4
for both model frames. It can be seen that good agreement was obtained for
the two model frames.

From the results of the first tests series, it was found that
torsional motion was negligible; therefore, in the second test series three
of the six potentiometers were disconnected and three more friction devices
were instrumented for slippage.

12.5 Test Results, Model Frame #2

The Moment Resisting Frame and the Braced Moment Resisting Frame did
not perform well during the tests. Very large strains occurred in the base

column, and in the first and second floor beams of the Moment Resisting Frame, indicating that the full plastic moment capacity was reached at these locations. Although the main structural members of the Braced Moment Resisting Frame remained elastic, many cross-braces yielded in tension. The elongation of the braces was very large and they buckled significantly in the compression regime; this indicates that heavy non-structural damage would have occurred in a real building (cracks in walls, broken glass, etc.). However, the Friction Damped Braced Frame performed very well; no damage occurred in any member and the deflections and accelerations were far less than the values measured in the two other types of construction.

Figure 12.16 illustrates the superior performance of the Friction Damped Braced, expressed in terms of the envelope of the measured horizontal accelerations. A peak acceleration of 1.42 g was measured at the top of the Friction Damped Braced Frame compared to peak acceleration values of 2.24 g and 2.67 g for the Braced Moment Frame and the Moment Resisting Frame respectively. Notice that some variations occurred in the peak table acceleration (input) to which the frames were subjected. Although the intent was to apply the same base motion intensity to all three frames, it is believed that a frame-table interaction occurred as a result of the very large base shears which were developed at this strong level of excitation. However, the input variations were small and the results are still comparable.

Figure 12.17 shows the time-histories of the measured third floor accelerations. The trends noted in the first series of tests are also evident here, alhtough in a more exaggerated sense.

Since the excitations developed were extremely severe, it was possible to measure significant slippage in the friction devices of the Friction Damped Braced Frame. Figure 12.18 shows the slippage time-histories of these devices. Peak slippages of 5.89 mm, 10.16 mm and 4.91 mm were

recorded with the first, second and third floor devices respectively.

Notice that all the friction devices experienced peak slippage at a time

which coincided with time at which the peak ground acceleration occurred

(see Figure 12.9).

In this test series the two second floor friction devices were

instrumented; Figure 12.19 compares their slippage time-histories. It can

be seen that the signals are exactly in phase and have the same amplitude.

This confirms that the devices dissipated energy simultaneously and, there-

fore, that no significant torsional stresses were induced in the structure

even under the extreme ground excitation used in this experiment.

12.6 Energy Balance

As mentioned in Section 5.4, some imperfections were noted in the

hysteresis loops of even the modified devices. If Figure 5.10 is examined,

it can be seen that a minimum slippage of about 6 mm is required to develop

the full slip load of the friction devices. Since at many times during the

test the slippage of the devices was less than 6 mm, it is of interest to

evaluate the equivalent effective constant slip load of the friction

devices developed during the last test on the Friction Damped Braced Frame.

This can be achieved by considering an energy balance of the system.

From Newton's second law, the energy input (E_{in}) to the structure

during a ground motion of duration t_1 is the product of the base shear and

the ground displacement and can be expressed as

$$E_{in} = \sum_{i=1}^{N.D.O.F.} \int_0^{t_1} m_i \, \ddot{x}_i \, \frac{dx_g}{dt} \, dt \qquad (12.1)$$

where

N.D.O.F.   = number of degrees of freedom considered

m_i = lumped mass at the ith degree of freedom

$\ddot{x}_i$ = total acceleration of the ith degree of freedom

x_g = displacement of the ground.

The increment of energy input $\left(\Delta E_{in}^{(j)}\right)$ during a time step of finite length can be calculated on the basis of the average total acceleration during the time step for each degree of freedom:

$$\Delta E_{in}^{(j)} = \sum_{i=1}^{N.D.O.F.} \left[m_i \frac{\left(\ddot{x}_i^{(j)} + \ddot{x}_i^{(j-1)}\right)}{2} \left(x_g^{(j)} - x_g^{(j-1)}\right) \right] \quad (12.2)$$

Having N points in each time-history, the total energy input can be written as:

$$E_{in} = \sum_{j=2}^{N} \sum_{i=1}^{N.D.O.F.} m_i \frac{\left(\ddot{x}_i^{(j)} + \ddot{x}_i^{(j-1)}\right)}{2} \left(x_g^{(j)} - x_g^{(j-1)}\right) \quad (12.3)$$

The number of degrees of freedom can be reduced to three by considering only the lateral movement of each floor of the Friction Damped Braced Frame (see Figure 8.1). Therefore the total energy input can be written as:

$$E_{in} = \frac{1}{2} \sum_{j=2}^{N} \left[m_1\left(\ddot{x}_1^{(j)} + \ddot{x}_1^{(j-1)}\right) + m_2\left(\ddot{x}_2^{(j)} + \ddot{x}_2^{(j-1)}\right) \right.$$
$$\left. + m_3\left(\ddot{x}_3^{(j)} + \ddot{x}_3^{(j-1)}\right) \right] \left(x_g^{(j)} - x_g^{(j-1)}\right) \quad (12.4)$$

where:

$$m_1, m_2, m_3 \quad = \quad \text{mass of the concrete blocks}$$

$$\ddot{x}_1, \ddot{x}_2, \ddot{x}_3 \quad = \quad \text{absolute acceleration at each floor}$$

$$x_g \quad = \quad \text{ground displacement}$$

Note that when the inertia forces and ground displacement are of opposite sign energy is being radiated from the structure back into the ground. Hence at the end of the earthquake the total energy input to the system represents the net energy that the system must dissipate.

Since all the floors of the Friction Damped Braced Frame were instrumented for total acceleration, and the shaking table for ground displacement, it is possible to calculate the energy input during an actual test on the shaking table by simple numerical integration of the measured records. For this purpose, the computer program "Energy" was created; a listing of this program is provided in Appendix B.

The energy absorbed through friction by all the friction devices (E_D) can also be calculated by a numerical integration of the slippage time-histories:

$$E_D = 4P_\ell \sum_{j=2}^{N} \left[(s_1^{(j)} - s_1^{(j-1)}) + (s_2^{(j)} - s_2^{(j-1)}) + (s_3^{(j)} - s_3^{(j-1)}) \right]$$

(12.5)

where

$$P_\ell \quad = \text{local slip load}$$

$$s_1, s_2, s_3 \quad = \text{slippage time-history at each floor.}$$

It is assumed that the local slip load (P_ℓ) is constant and is the same for all the friction devices.

Neglecting viscous damping, it is possible to determine an upper bound value for the equivalent effective local slip load (P_ℓ) by comparing the energy input and the energy dissipated through friction at the end of each time step and imposing:

$$\frac{E_D}{E_{in}} < 1 \qquad\qquad (12.6)$$

In other words, the maximum percentage of energy dissipated was normalized to a unit value. The program "Energy" carries out the necessary steps to determine the equivalent effective local slip load (P_ℓ) during a test on the shaking table.

The experimental results of the last test series (Taft Earthquake (0.90 g)) were used with the program "Energy" to determine the equivalent effective local slip load for that test. A value of 1.7 kN was found for this load, which corresponds to a value of only 3.4 kN for the global slip load instead of the calibrated value of 7 kN (see Section 5.5). This same value of the slip load was also found by considering the requirements for horizontal dynamic equilibrium at each level of the frame and at a particular time when slippage occurs. The resulting time-history of the percentage of energy absorbed by the friction devices is presented in Figure 12.20.

These results confirm that the friction devices were not acting at the optimum slip load of the structure (7 kN), apparently due to the fact that the construction tolerance was still too large. In order to be fully effective, the friction devices should be fabricated in a precision shop with minimum construction tolerance. However, even though the optimum slip load was not obtained, the structural response of the Friction Damped Braced Frame was demonstratively superior to the responses of the two other types of frame construction.

The results of the experimental investigations involving seismic tests on the shaking table clearly demonstrate that the new damping system has the ability to dramatically increase the earthquake resistance and damage control capability of conventional framed buildings.

13.   ECONOMIC POTENTIAL OF FRICTION DAMPED BRACED FRAME

13.1 Introduction

The economical benefits achieved through the use of the new damping system can be evaluated by comparing the design requirements of a Friction Damped Braced Frame to those of conventional structural systems under conditions of similar response behaviour. We want to know what savings of materials can be derived by designing a reduced size frame equipped with friction devices which will approach the responses of the two other types of aseismic structural systems. In the analysis used for this purpose it was assumed that the observed behaviour of the Moment Resisting Frame and of the Braced Moment Resisting Frame is acceptable during a severe earthquake.

13.2 Analysis for Different Section Sizes

Several inelastic time-history dynamic analyses were performed with three different trial member sections. The dead load of the concrete blocks and the slip load of the devices were assumed similar for all frames.

Table 13.1 presents the results of the analyses for the Newmark-Blume-Kapur Artifical Earthquake scaled to a peak acceleration of 0.30 g. By examining the M_d/M_p ratio, it may be seen that there is a limit to which the cross-section can be reduced because of the requirement that the dead load be carried safely. Notice that the ratio of the bending moment induced by the inertia forces to the fully plastic bending moment in any reduced size Friction Damped Braced Frame is always smaller than the corresponding ratio of the two other conventional building systems. This

result is very important because it seems to indicate that, if earthquake loading is neglected in the design of a structure equipped with friction devices, its seismic response will always be superior to a conventional structure for which earthquake loading has been taken into account in the design. Assuming this to be true, a possible design procedure for a structure incorporating these friction devices is:

1) Design the structure so that its main members can carry safely all the possible load combinations but ignoring earthquake loading.

2) Determine the optimum slip load of the devices.

3) Provide the structure with friction devices at the optimum slip load.

If the preceding observation is valid for all cases, this approach should guarantee that the dynamic response of the designed structure with reduced member sizes would be less than the response of a conventional building system (with larger member sizes) designed by the code and including earthquake loading.

For the model frame (and member sizes) tested, the material savings possible using this design approach was examined by designing the structure to carry the dead load only according to the National Building Code of Canada. This resulted in the following cross-section being selected for the main members:

Special Light Profile SLP-3"
(from Cockerill-Belgium)

$$A = 565 \text{ mm}^2$$

$$I_x = 0.56 \times 10^6 \text{ mm}^4$$

$$M_p = 4.42 \text{ kN-m}$$

From Table 13.1, it can be seen that the performance of this reduced size
Friction Damped Braced Frame under a strong earthquake is superior to the
performance of the conventional building systems with heavier members.

The material savings is proportional to the reduction in cross-
sectional area:

$$\frac{A_{(reduced\ size)}}{A_{(actual)}} = \frac{565}{1070} = 0.528$$

In this example this represents a 47% savings in material cost. The
proposed damping system therefore appears to offer savings in material
costs while assuring added security against collapse. However it should be
noted that the effects of wind loads, live loads and torsion have been
neglected in this example and therefore the reduction in member sizes will
be less for a real building.

14. <u>CONCLUSIONS</u>

14.1 <u>Summary and Conclusions</u>

1. A refined computer model of a Friction Damped Braced Frame was developed to eliminate the non-conservative assumptions used with the simplified model originally proposed by A.S. Pall (3). It was found that this refined model can accurately represent the real behaviour of a Friction Damped Braced Frame. However, it requires many more elements and degrees of freedom than the simplified model and its use in analysis increases the computer time significantly. By comparing these two models it was concluded that the simplified model is simpler and cheaper to use than the refined model and yields results which satisfy the accuracy normally associated with earthquake analysis. Furthermore, the two models will provide results which converge to the same response as the ground motion becomes more severe.

2. To study the performance of the Friction Damped Braced Frame, a model of a 3-storey frame was designed. Two model frames were subsequently fabricated for use in the experimental program.

3. An optimum slip load study was performed to determine the value of the slip load which optimized the energy dissipation of the friction devices. The results seem to indicate that the optimum slip load is independent of the ground motion time-history and is rather a structural property. The global slip load for the fabricated model frames was found to be 7 kN.

4. Seven friction devices were fabricated for use with the model frames. Each device was provided with a compression spring in order to adjust the desired slip load The devices were first tested under cyclic loads in order to study the stability of the brake lining pads and to calibrate their slipping loads. The results of the tests clearly indicate that the behaviour of the pads is very stable even after 50 cycles. However, a rectangular load-deformation curve can only be obtained if the fabrication tolerances of the friction devices are minimized. This problem was partly solved by inserting steel bushings in the 4 corner holes of the mechanism and also in the centre slots of the friction pads. However, an energy balance calculation showed that during an actual seismic test on the shaking table the friction devices were still not operating at their optimum slip load.

5. Different analytical studies were made as follows to quantify the performance of the Friction Damped Braced Frame relative to conventional aseismic structural systems. (i) In an equivalent viscous damping study, viscous damping was added to the Moment Resisting Frame and to the Braced Moment Resisting Frame until their dynamic responses became similar to the response of the Friction damped Braced Frame. This equality was achieved by introducing 38% critical viscous damping to the Moment Resisting Frame and 12% to the Braced Moment Resisting Frame. It was found that the new damping system becomes more efficient as the intensity of the earthquake increases. (ii) The economical potential of the new damping system was evaluated by designing a reduced size Friction Damped Braced Frame whose seismic response is at least as good as the response of a conventional building system with heavier members. It was found that

a saving of 47% in material cost could be achieved with the actual model frames considered. Furthermore, the performance of this reduced size Friction Damped Braced Frame was demonstrably far superior to the performances of conventional aseismic building systems with heavier members. However the effects of wind loads and torsion were neglected in this analysis and it is expected that savings of material will be less in a real building.

6. Finally, seismic testing of the model frames on the shaking table under simulated earthquake loads confirmed the superior performance of the Friction Damped Braced Frame compared to conventional aseismic building systems. Even an earthquake record with a peak acceleration of 0.90 g did not cause any damage to the Friction Damped Braced Frame, while the Moment Resisting Frame and the Braced Moment Resisting Frame underwent large inelastic deformations. Under that same earthquake (0.90 g), a peak acceleration of 2.67 g and 2.24 g were measured at the top of the Moment Resisting Frame and the Braced Moment Resisting Frame respectively, while only a peak acceleration of 1.42 g was experienced by the Friction Damped Braced Frame at the same location.

14.2 Future Research

The work reported in this thesis should be viewed as as preliminary study. It is presented as a first step in examining the potential of structures equipped with friction devices. Although the proposed damping system was experimentally shown to be reliable and to perform satisfactorily, and as such might lead to a breakthrough in earthquake resistant design, extensive future research is needed before these friction devices can be safely used.

A simple design method for evaluating the optimum slip load must be developed; inelastic time-history dynamic computer analyses are much too expensive to be used for calculating the slip load on a regular basis in design offices. Therefore, a detailed parametric study should be undertaken in order to determine the parameters which govern the optimum slip load of a structure and to develop a simplified design method to calculate this load. The first step would be to verify whether the optimum slip load is indeed a structural property and is independent of the ground motion time-history. If this is found to be true, the development of a design procedure could possibly be based on a fundamental parameter of the structure, such as its fundamental mode shape, for example.

Each friction device used in this research project was provided with a compression spring which allows adjustments to be made to the clamping force and therefore the slip load. However, springs will not be used in a real structure; the clamping force will be developed by a bolt torqued to the proper value. Therefore, more experimental work is needed to develop a rational method of calibration for the friction devices. Also, long term studies should be undertaken to verify if the devices creep and are still in working condition after many years of service; maintenance methods should be developed to ensure that there is no deterioration in the long-term operability of the devices.

Finally, the performance of a three-dimensional model of a Friction Damped Braced Frame should be examined to provide a more realistic assessment of its behaviour. The computer program "Drain-Tabs", developed at the University of California, Berkeley, could be used for this purpose.

BIBLIOGRAPHY

1. POPOV, E.P., TAKANASHI, K. and ROEDER, C.W., "Structural Steel Bracing Systems: Behaviour Under Cyclic Loading," E.E.R.C. Report 76-17, Earthquake Engineering Research Center, University of California, Berkeley, California, June, 1976.

2. POPOV, E.P. and ROEDER, C.W., "Eccentrically Braced Steel Frames for Earthquakes," ASCE, Journal of Structural Division, March 1978.

3. PALL, A.S. and MARSH, C., "Response of Friction Damped Braced Frames," ASCE, Journal of Structural Division, June 1982.

4. PALL, A.S., "Limited Slip Bolted Joints - A Device to Control the Seismic Response of Large Panel Structures," Ph.D. Thesis presented to the Centre for Building Studies, Concordia University, Montreal, Canada, 1979.

5. PALL, A.S., MARSH, C., and FAZIO, P., "Friction Joints for Seismic Control of Large Panel Structures," Journal of the Prestressed Concrete Institute, Nov./Dec., 1980, Vol. 25, No. 6, pp. 38-61.

6. PALL, A.S., and MARSH, C., "Optimum Seismic Response of Large Panel Structures Using Limited Slip Bolted Joints," Proceedings, Seventh World Conference on Earthquake Engineering, Istanbul, Turkey, Sept., 1980, Vol. 4, pp. 177-184.

7. SABNIS, G.M., HARRIS, H.G., WHITE, R.N., and MIRZA, M.S., "Structural Modeling and Experimental Techniques", Prentice-Hall Civil Engineering and Engineering Mechanics Series, 1983.

8. WORKMAN, G.H., "The Inelastic Behavior of Multistory Braced Frame Structures Subjected to Earthquake Excitation", Research Report, University of Michigan, Ann Arbor, Michigan, September, 1969.

9. PICARD, A. and BEAULIEU, D., "Calcul aux Etats Limites des Charpentes d'Acier", Institut Canadien de la Construction d'Acier, 1981.

10. CANADIAN INSTITUTE OF STEEL CONSTRUCTION, "Handbook of Steel Construction", Willowdale, Ontario, December, 1980.

11. NATIONAL RESEARCH COUNCIL OF CANADA, "National Building Code of Canada", Ottawa, Ontario, 1980.

12. LEE, D.M. and MEDLAND, I.C., "Estimation of Base Isolated Structure Responses" Bulletin of the New Zealand National Society for Earthquake Engineering, No. 4, December 1978.

13. DE SILVA, C.W., "Dynamic Testing and Seismic Qualification Practice", Lexington Books, D.C. Heath and Company, Lexington, Massachusetts, 1983.

14. CLOUGH, R.W. and PENZIEN, J., "Dynamics of Structures", McGraw-Hill Book Company, 1975.

15. EWINS, D.J., "Model Testing: Theory and Practice", Research Studies Press, John Wiley & Sons, Inc., 1984.

16. LAM, C.F., "Analytical and Experimental Studies of the Behaviour of Equipment Vibration Isolators Under Seismic Conditions", M.A.Sc. Thesis submitted to the Department of Civil Engineering and the Faculty of Graduate Studies, University of British Columbia, Vancouver, Canada, April, 1985.

17. KANNAN, A.E. and POWELL, G.H., "Drain-2D, A General Purpose Computer Program for Dynamic Analysis of Inelastic Plane Structures", A computer program distributed by NISEE/Computer Applications, College of Engineering, University of California, Berkeley, California, August 1975.

18. KANASEWICH, E.R., "Time Sequence Analysis in Geophysics", The University of Alberta Press, 1975.
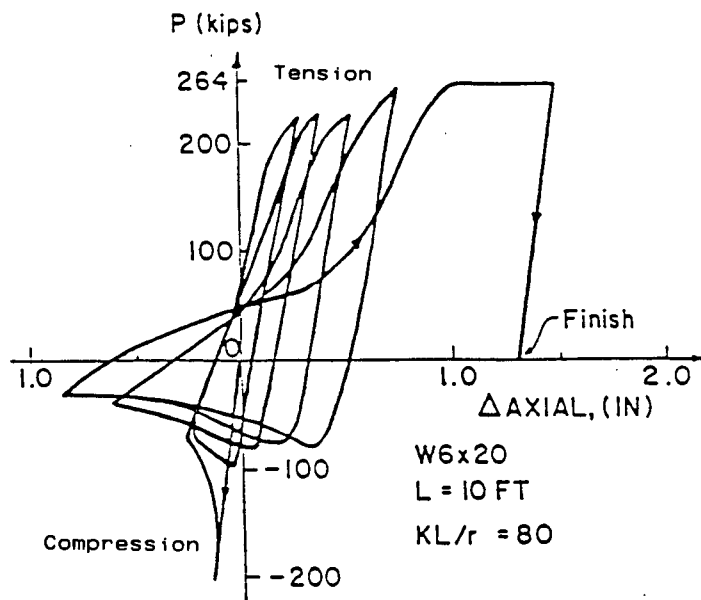
Figure 1.1 Typical Hysteresis Loops of a Tension Brace (from Ref.:3)
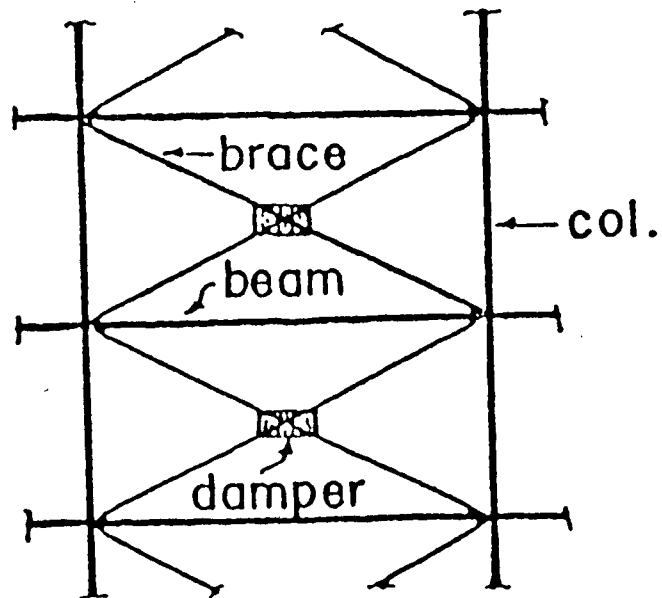
Figure 1.2 Location of Friction Device (from Ref.:3)
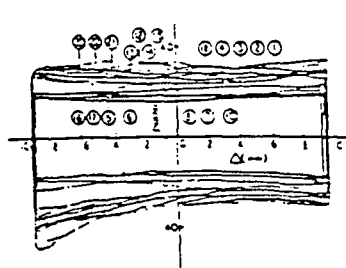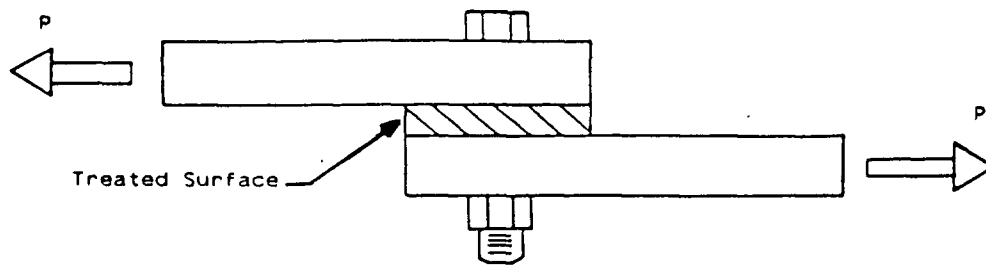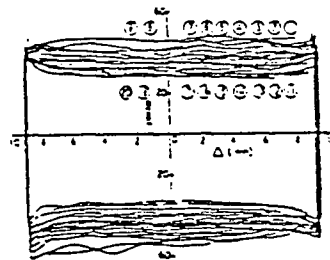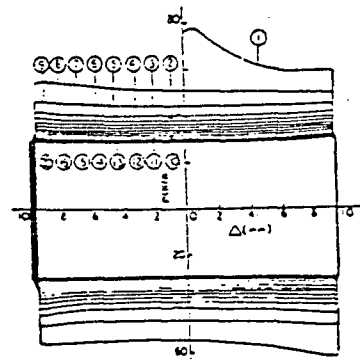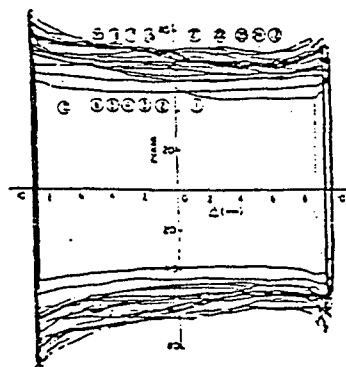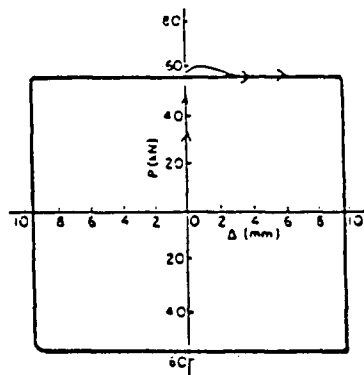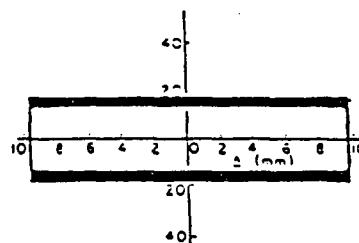
Figure 2.1 Hysteresis Loops of Simple Friction Joints (from Ref.:3)
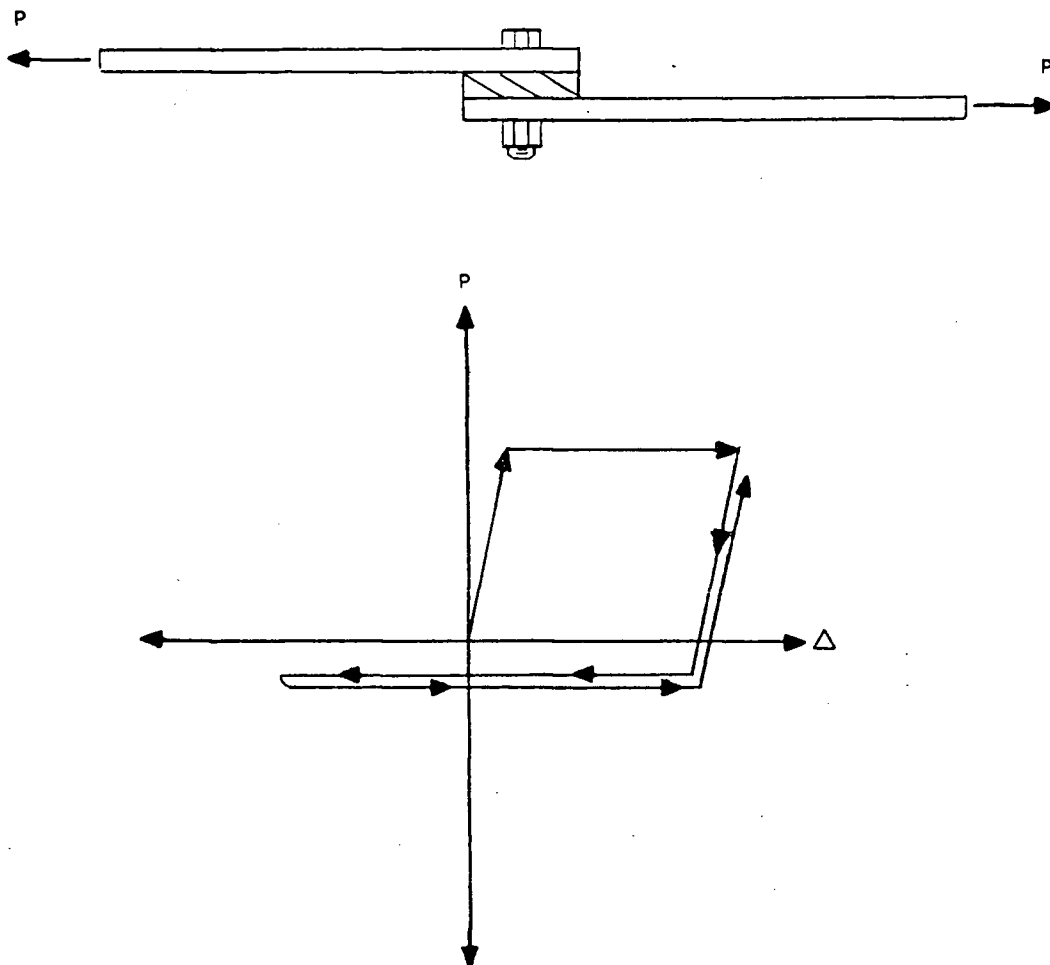
Figure 2.2 Hysteresis Loop of a Friction Joint where the Braces are Designed in Tension Only
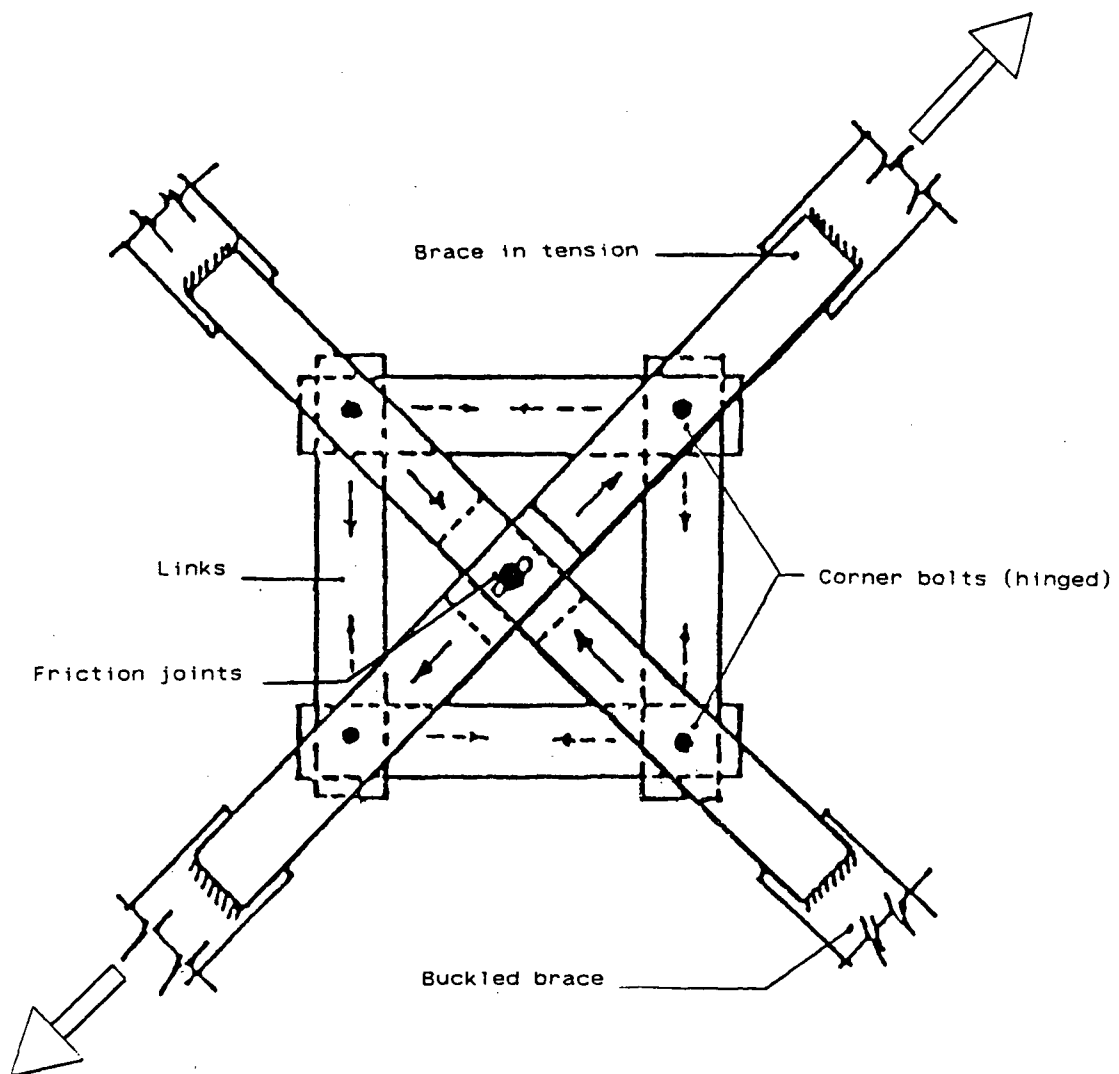
Figure 2.3 Mechanism of Friction Device (after Ref.:3)

(a)

(b)

(c)

(d)
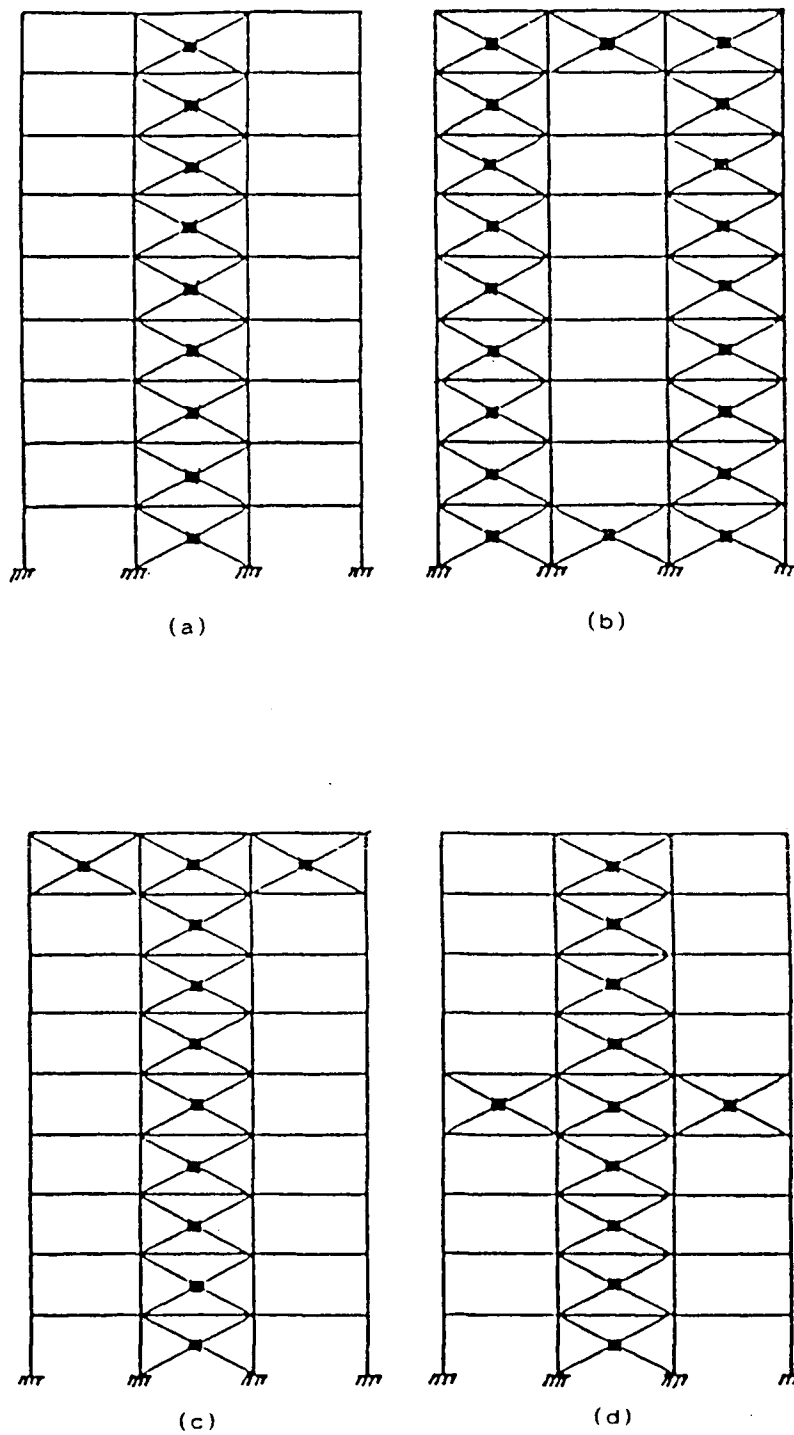
Figure 2.4 Possible Arrangements of Friction Damped Braced Frames (from Ref.:3)
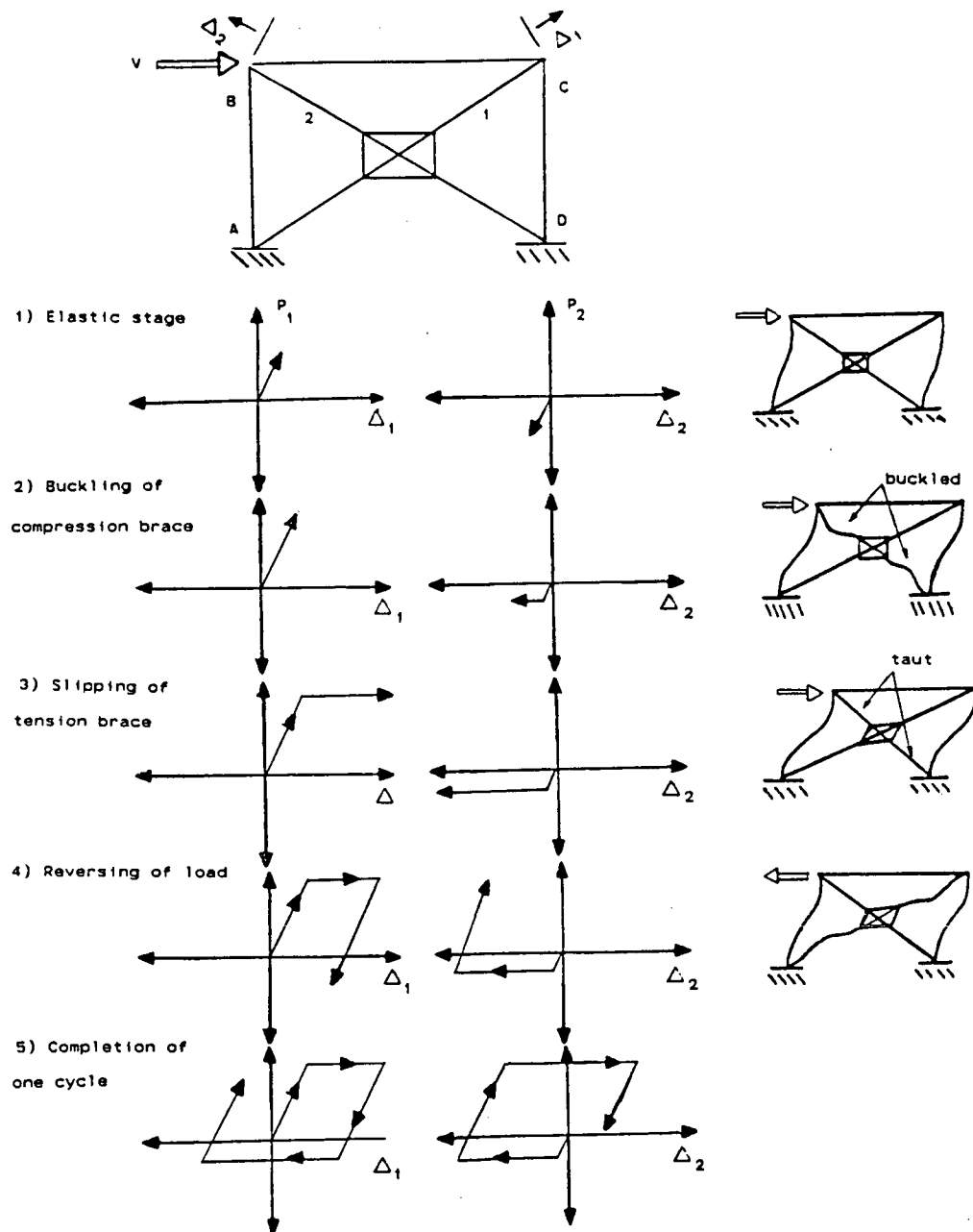
Figure 2.5 Hysteretic Behaviour of a Simple Friction Damped Braced Frame

Fyf=Fictitious yield stress in tension
    Corresponds to the stress in the tension brace at slipping

Fcr=Fictitious yield stress in compression
    Corresponds to the buckling stress of the compression brace
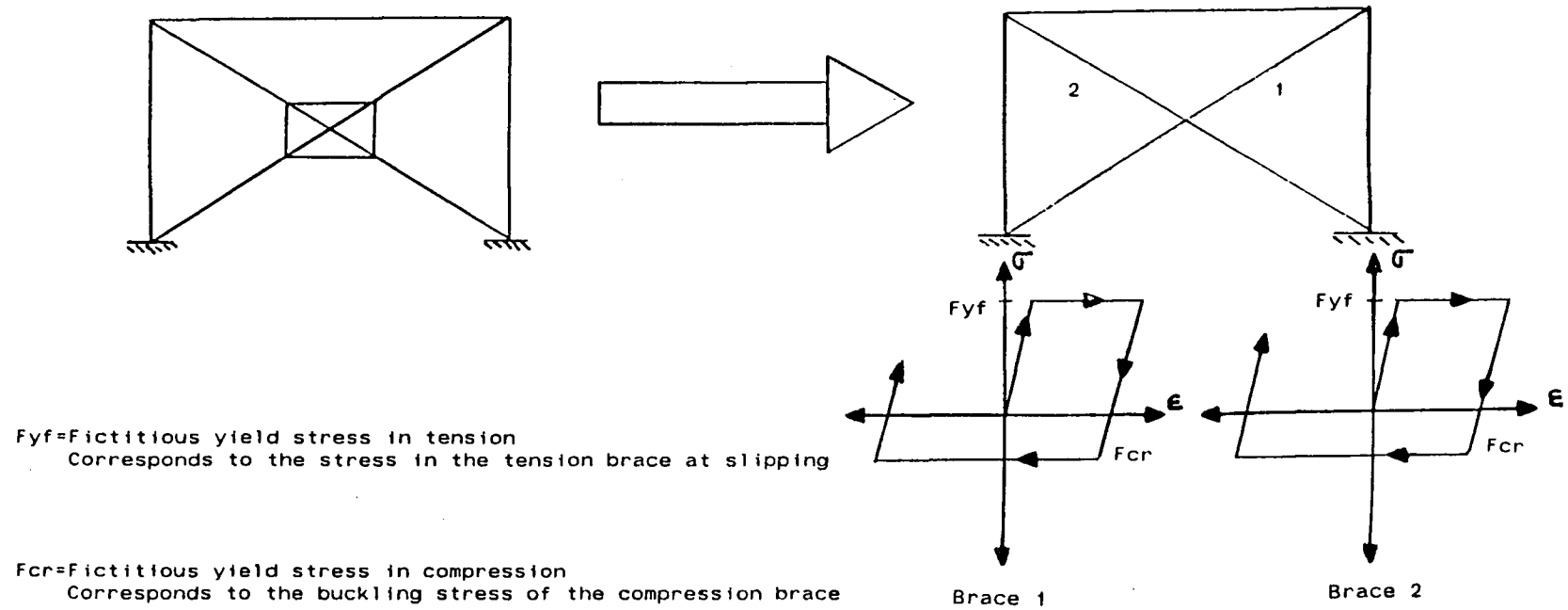
Figure 2.6 Simplified Model of a Friction Damped Braced Frame
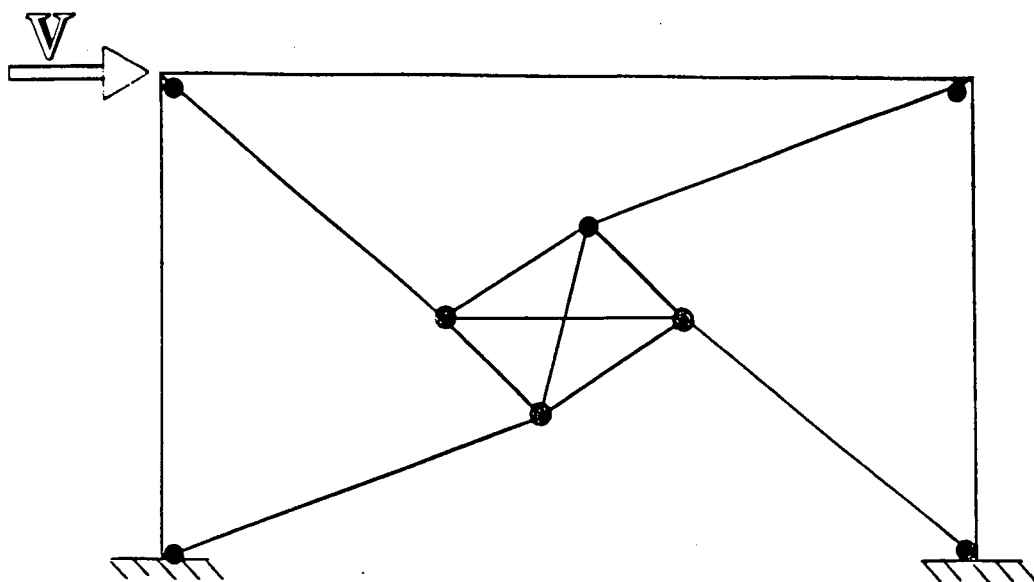
Figure 2.7 Unstable Mode of a Friction Damped Braced Frame
modeled with Truss Elements

Truss Elements

Beam Column Elements
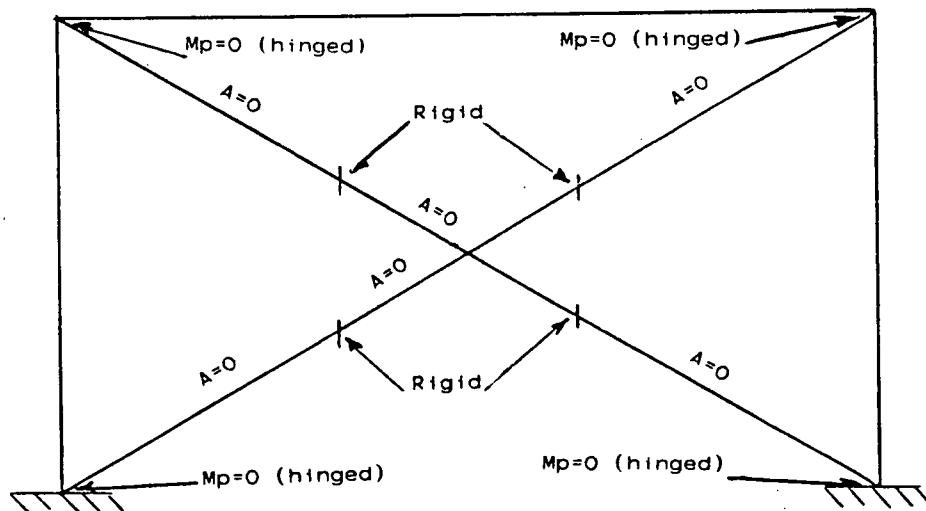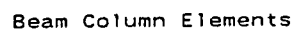
Figure 2.8 Refined Model of a Friction Damped Braced Frame
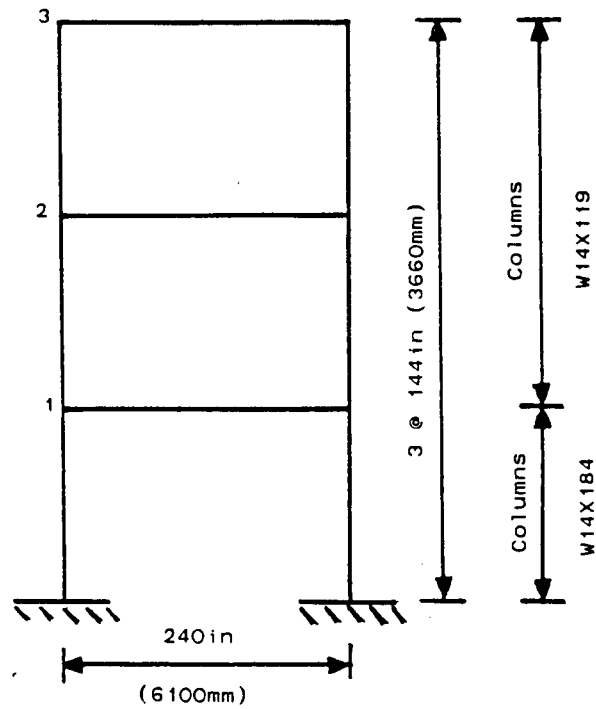
(a) Moment Resisting Frame (MRF)
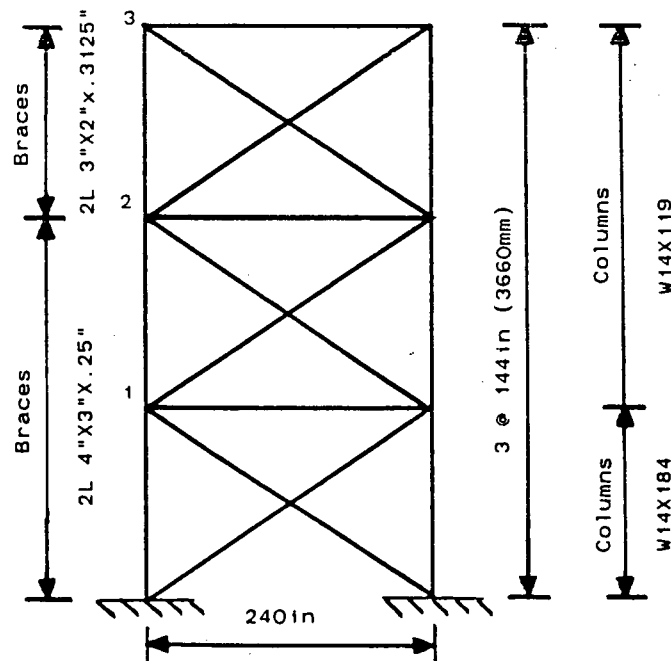
(b) Braced Moment Resisting Frame (BMRF)

Figure 3.1 Dimensions and Member Sizes of Prototype Structure (from ref.:8)

LIST OF MATERIALS

For One Frame   2 Frames Read

NO.	QTY.	DESCRIPTIONS	WEIGHT (IN)
1a	4	575X8 3563mm LONG	1182.92
2a	6	575X8 1974mm LONG	913.05
3B	6	525X8 1821mm LONG	657.86
4C	12	L...X5 1615mm LONG	695.07
5a	8	M.S. R 165X44X12	53.67
6a	4	M.S. R 160X140X6 mm	41.40
7a	20	M.S. R 100X45X6 mm	41.58
8a	20	M.S. R 100X45X6 mm	41.58
9a	4	M.S. R 6mm CUT AS SHOWN	14.44
10	8	M.S R 400X45X6 mm	66.54
11a	4	M.S. R 165X145X6 mm	44.22
12	4	M.S. R 6mm CUT AS SHOWN	22.11
13a	4	M.S. R 420X255X25 mm	824.76
14a	4	M.S. R 125X125X6 mm	28.88
15a	8	M.S. R 245X140X6 mm	126.79
16	6	M.S. R 180X75X6 mm	49.90
17a	4	M.S. R 115X44X12 mm	18.70
18	96	ASTM A-325 5/8"Ø HEX. BOLTS	160.10
19	16	ASTM A-325 3/4"Ø HEX. BOLTS	50.38
20	6	L...X... 1485mm LONG	321.05
21a	3	L...X... 1225mm LONG	132.42
22	6	M.S. R 170X140X6 mm	65.98
23	18	C 200X17 200mm LONG	601.20
24F	6	SHIM 6mm THICK 50X50	8.39

TOTAL WEIGHT: 6264.69

REFERENCE FRAME
2 Branches
GENERAL ARRANGEMENT

SCALE 1:10
DATE: 1/11/01
DRAWN BY LD.AF

A9255   PAGE 1 OF 6

NOTES:

LENGTHS IN MILLIMETRES
STEEL GRADE FOR 575X8: 300W

CLEAN TO SSPC-SP6
PAINT: 1 COAT ZINC RICHED
2ND PAINT AFTER 1.5 mm D.F.T.

4 WELDED SURFACES READ OF A1
WELDED ITEMS FOR A1 ARE MARKED WITH LOWER CASE "a"
AND ITEM NUMBER

BOLTED MEMBERS ARE MARKED WITH CAPITAL LETTER
AND ITEM NUMBER

2050   1175   1175   1175   1400

Figure 3.2 General Arrangement of Model Frame

DETAIL ①

TYPICAL BEAM-COLUMN CONNECTION
FLOORS 1 AND 2

DETAIL ②

TYPICAL BEAM-COLUMN CONNECTION
FLOOR 2

NOTES :

LENGTHS IN MILLIMETRES
WELDING USING ELECTRODES E480XX
ALL HOLES : 11/16" DIA.
ALL BOLTS : ITEM 18
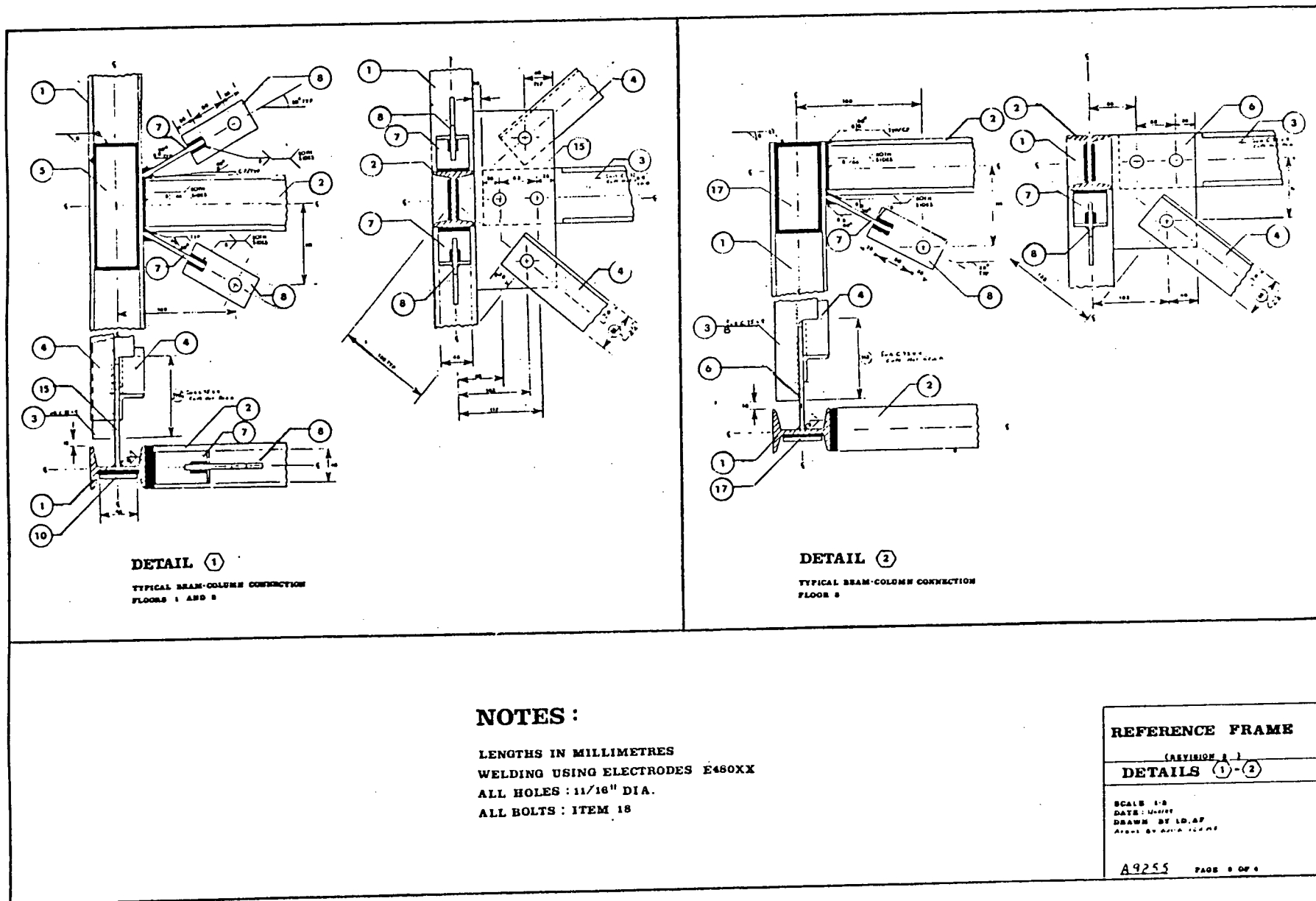
Figure 3.3 Details 1-2 of Model Frame

DETAIL ③

TYPICAL BASE-COLUMN CONNECTION

DETAIL ④

LATERAL BRACING
TYPICAL CORNER CONNECTION

NOTES:

LENGTHS IN MILLIMETRES

WELDING USING ELECTRODES E48UXX
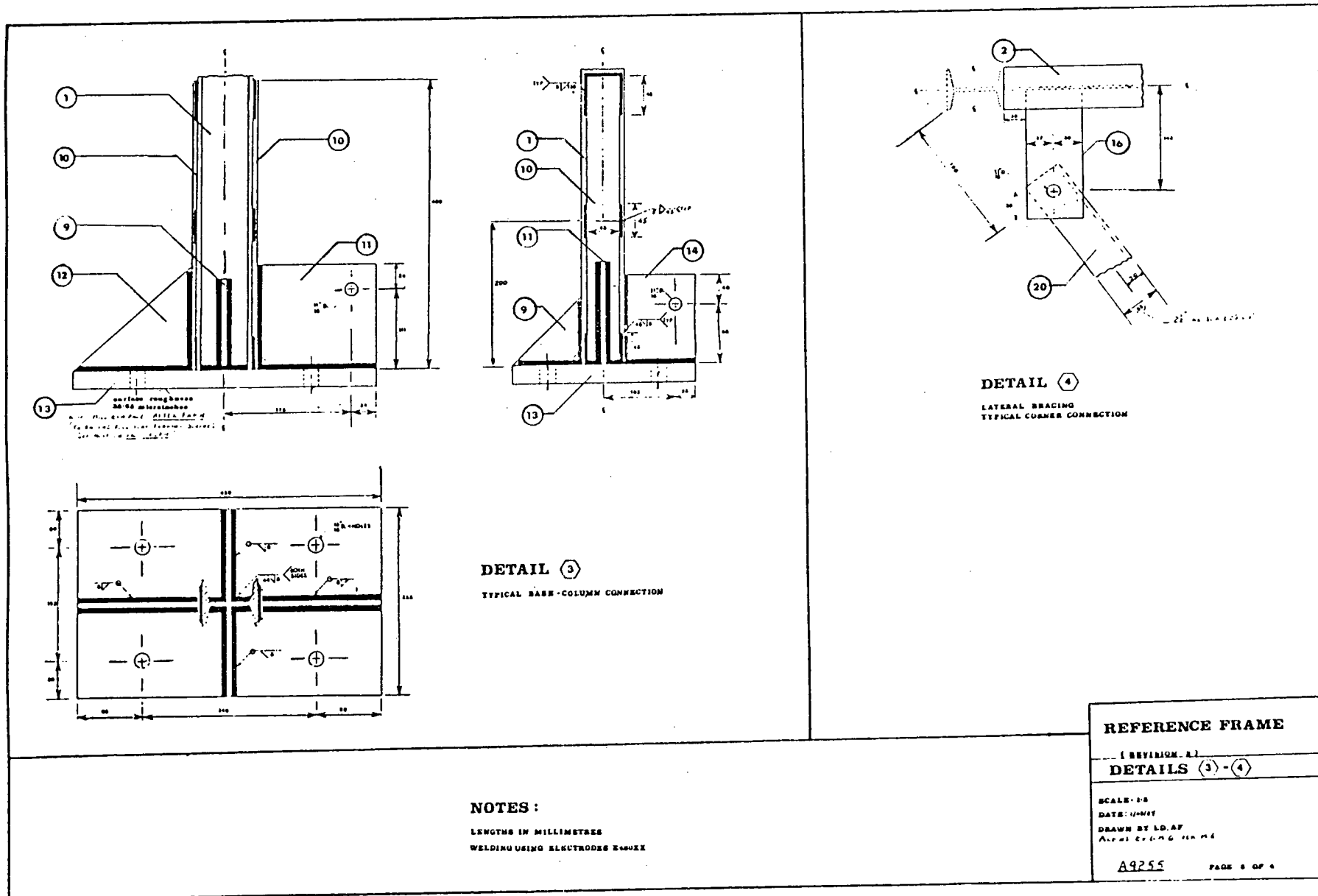
Figure 3.4 Details 3-4 of Model Frame
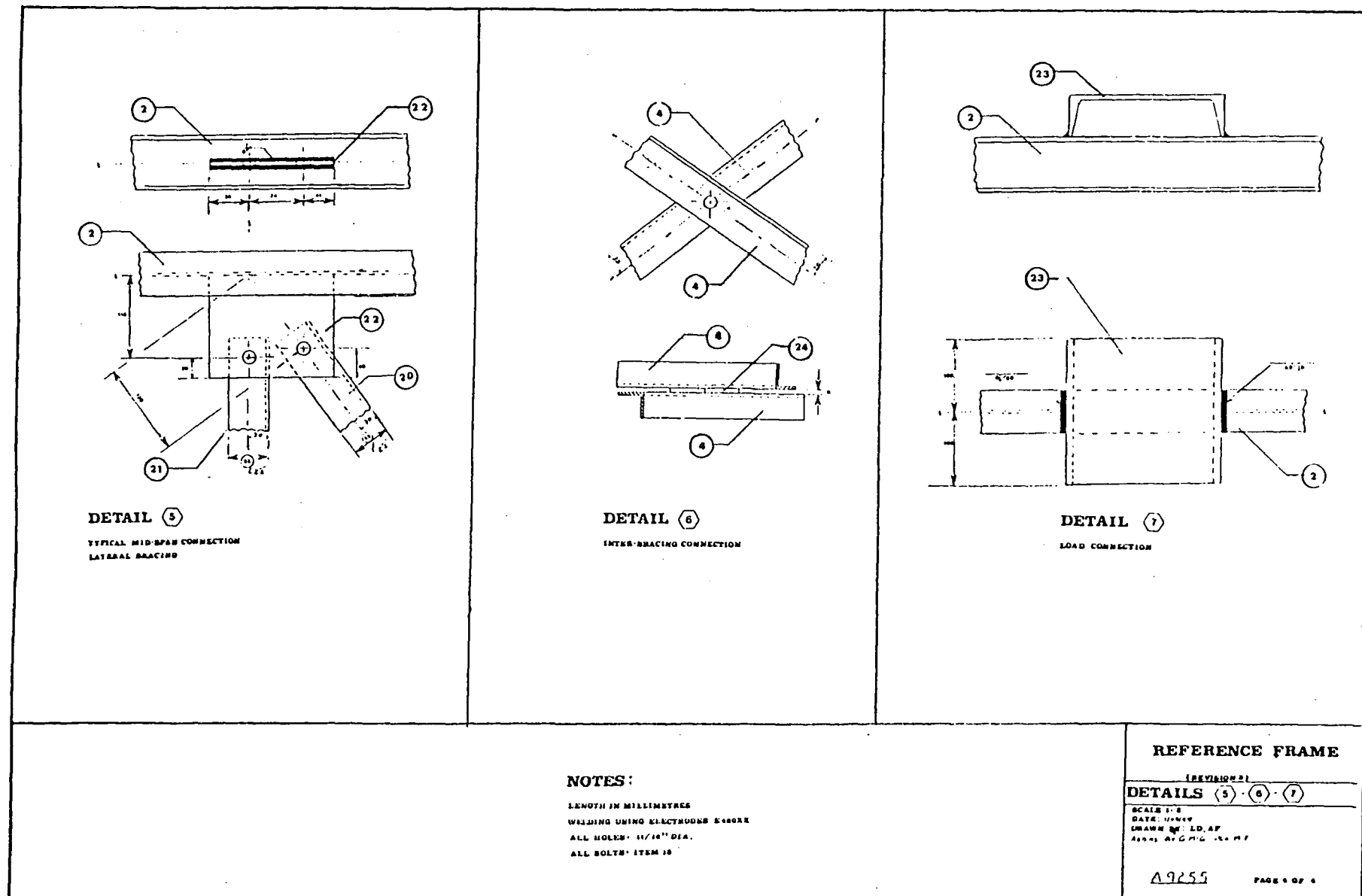
Figure 3.5 Details 5-6-7 of Model Frame

Figure 3.6 Model Frame mounted on the Shaking Table
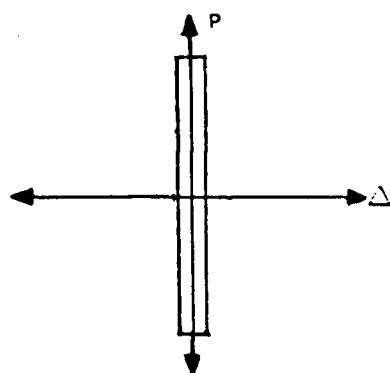
(a) High slip load
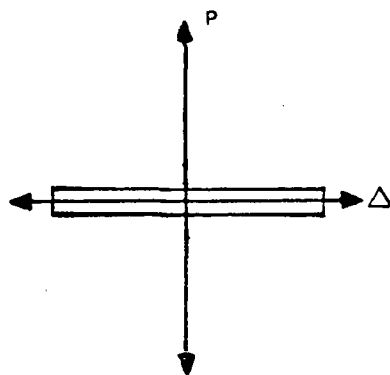
(b) Low slip load
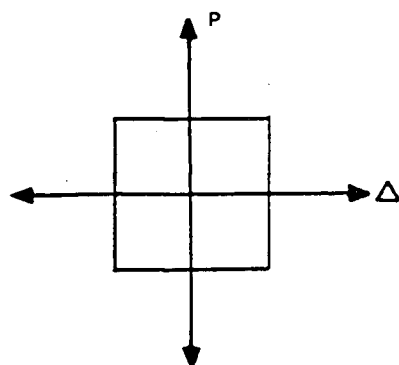
(c) Optimum slip load

Figure 4.1 Concept of Optimum Slip Load

$$P_g = 2P_\ell - P_{cr}$$
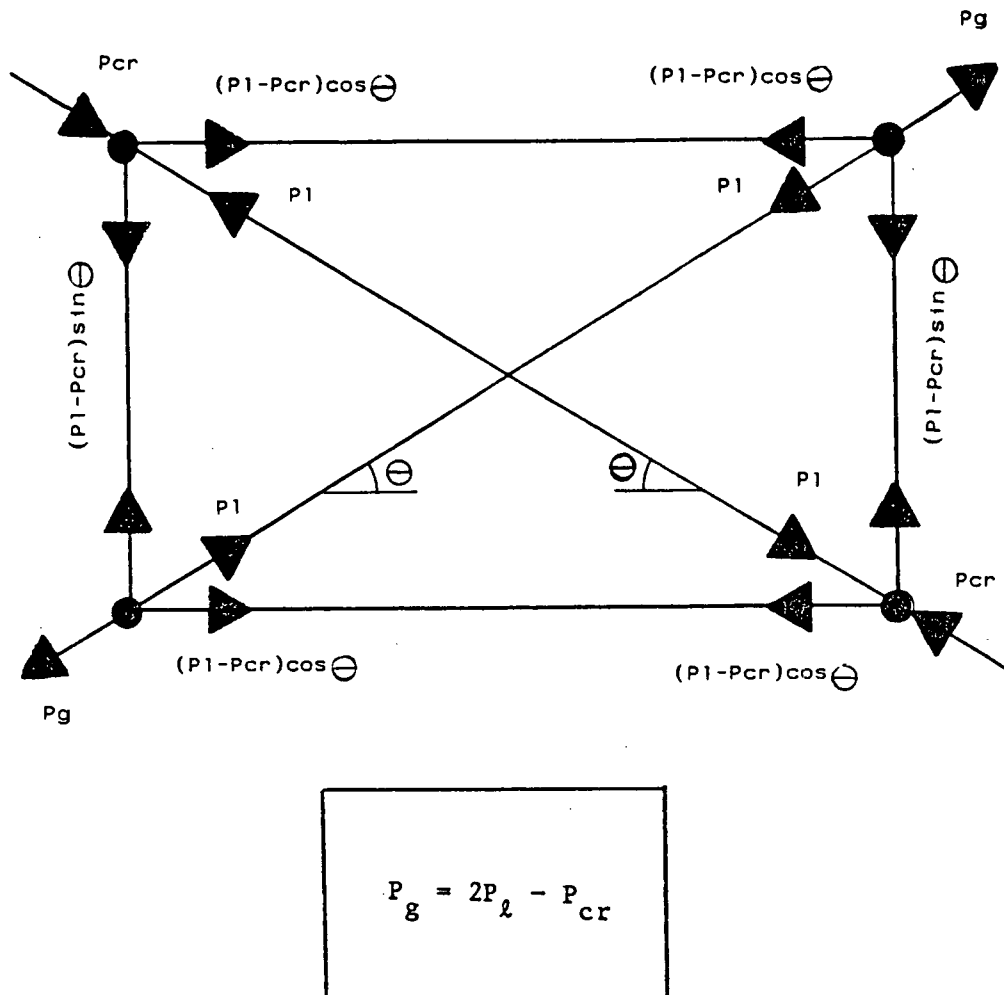
Figure 4.2 Free Body Diagram of a Friction Device at Slipping

129.

(a) Beams and columns

S75X8

321kN

48kN

M

-48kN

-9.57kN-m

9.57kN-m

-321kN
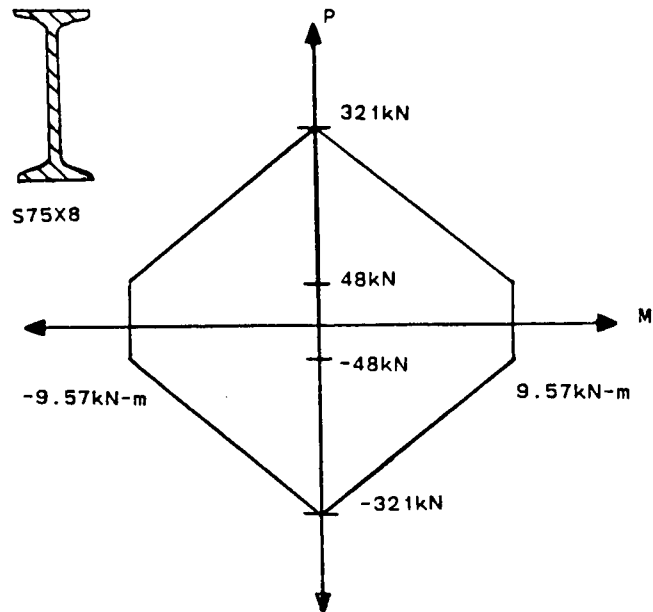
(b) Reinforced base columns

S75X8

6mm Plate

483kN

72kN

M

-72kN

-16.02kN-m

16.02kN-m

-483kN
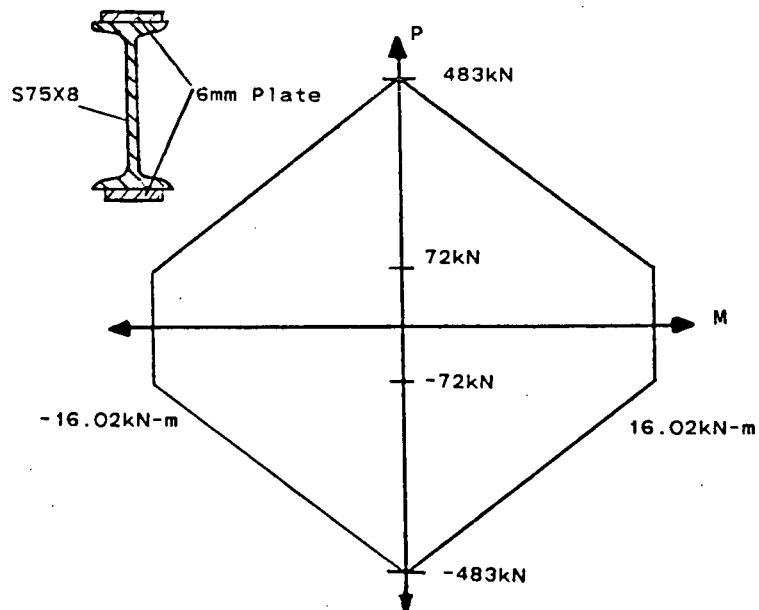
Figure 4.3 Yield Interaction Surfaces for Model Frame

(a) El Centro (SOOE) (0-6sec.)

(b) Parkfield (N65E) (0-9sec.)

(c) Newmark-Blume-Kapur artificial earthquake
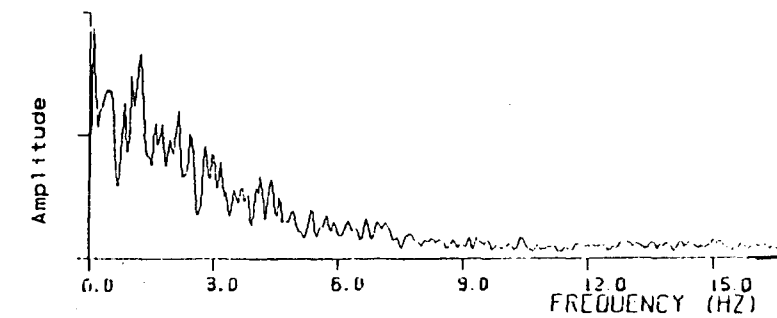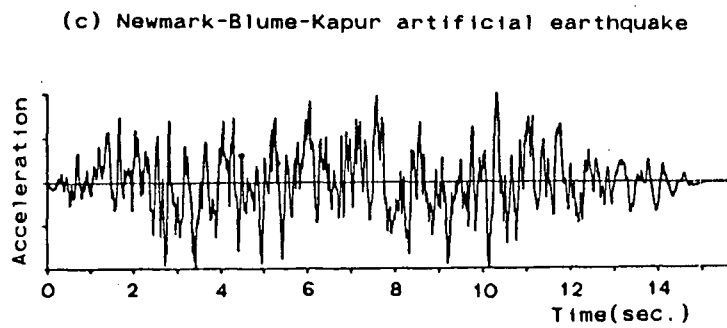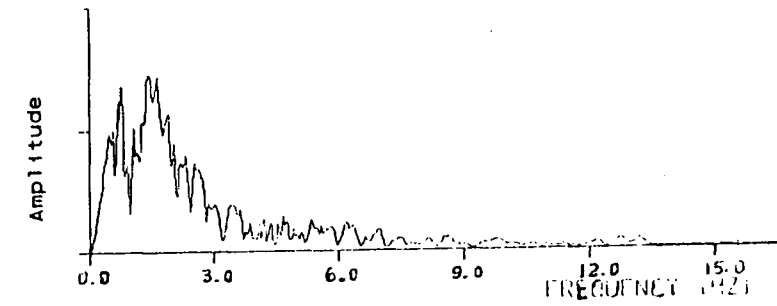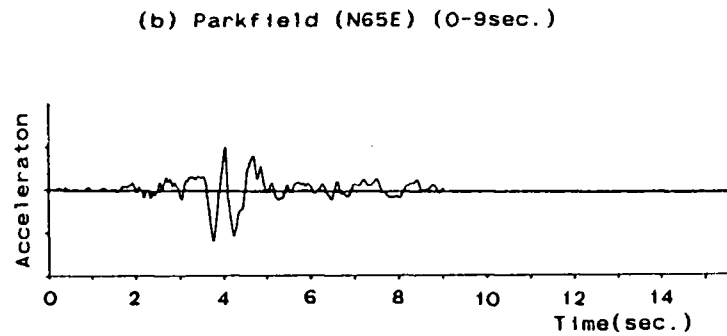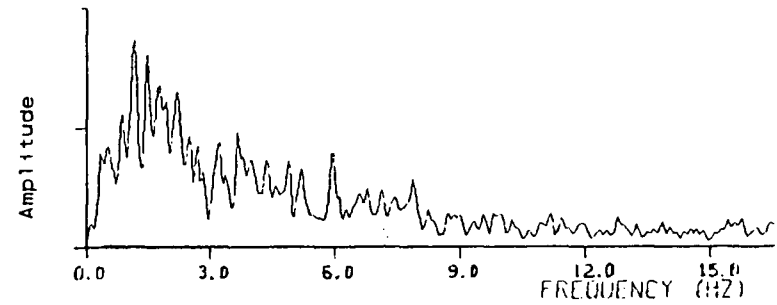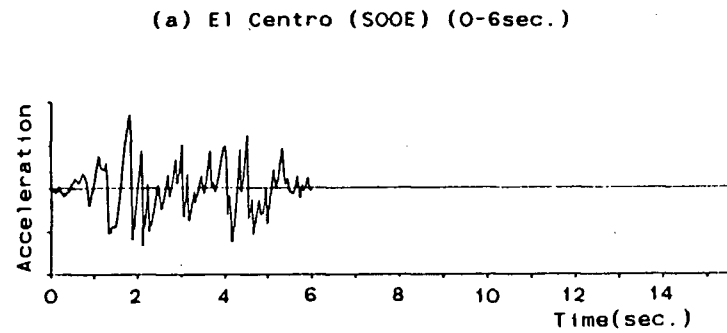
Accelerograms

Fourier Spectra

Figure 4.4 Earthquakes used for the Optimum Slip Load Study

(a) Envelope of bending moments in the beams

(c) Envelope of lateral deflections

(b) Envelope of bending moments in the columns

(d) Envelope of shear forces in the columns
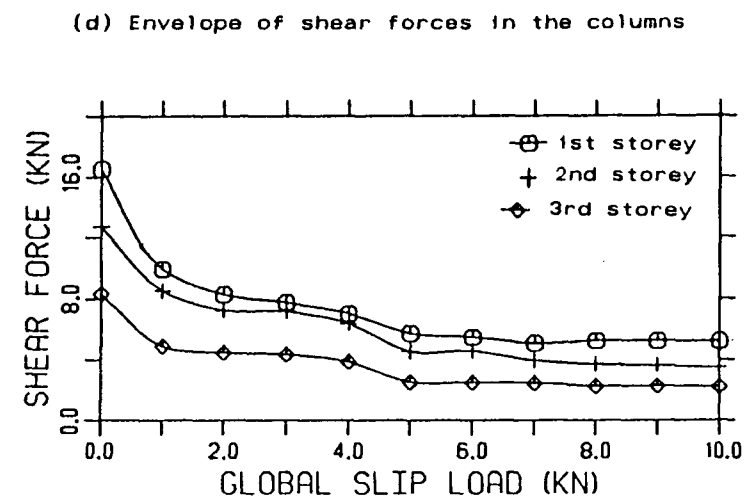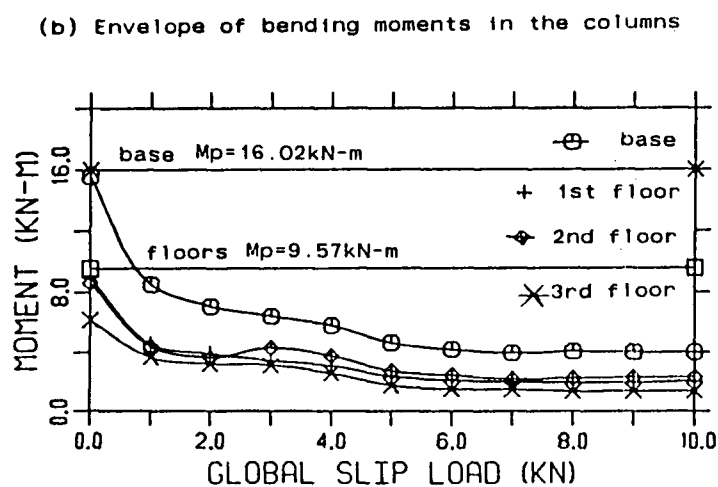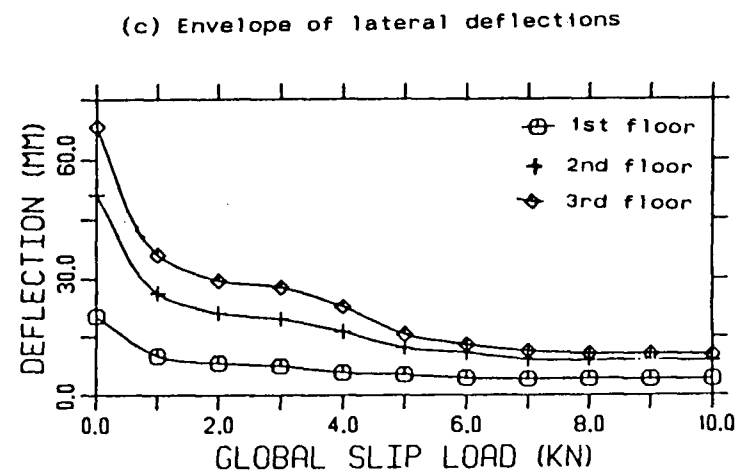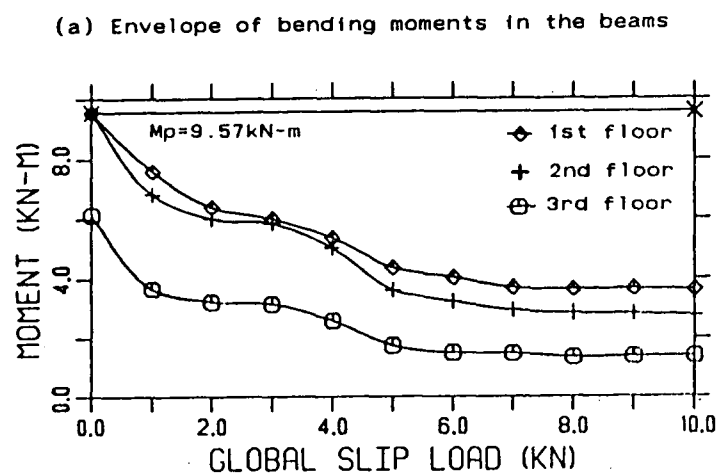
Figure 4.5 Results of Optimum Slip Load Study, El Centro Earthquake

(a) Envelope of bending moments in the beams

(b) Envelope of bending moments in the columns

(c) Envelope of lateral deflections

(d) Envelope of shear forces in the columns
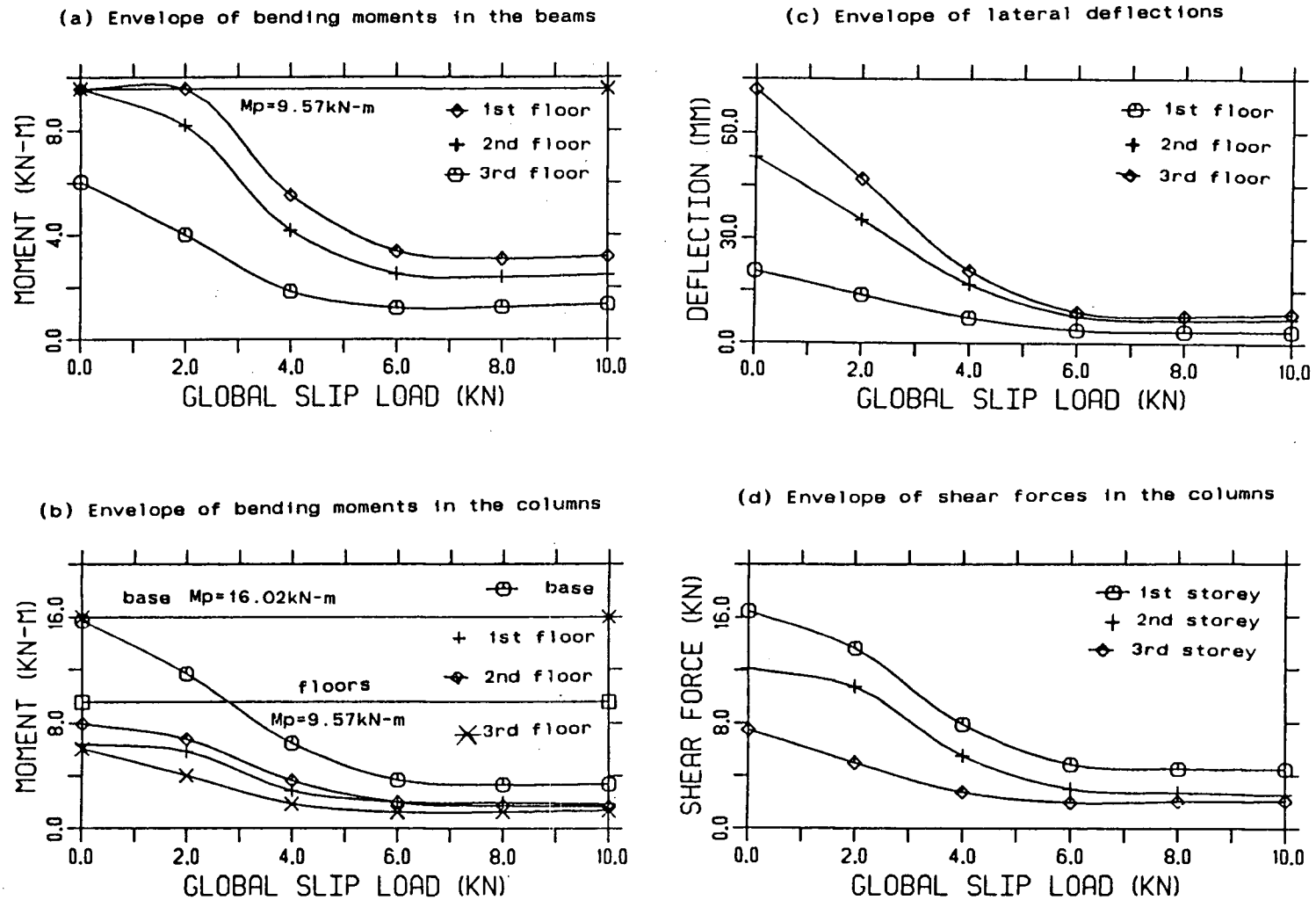
Figure 4.6 Results of Optimum Slip Load Study, Parkfield Earthquake
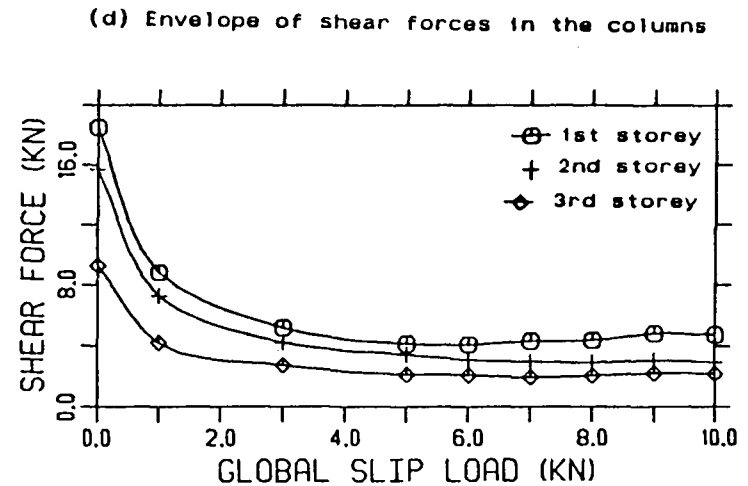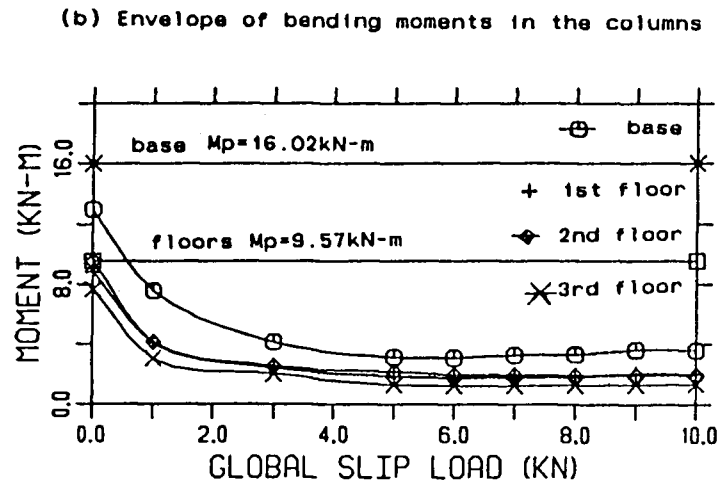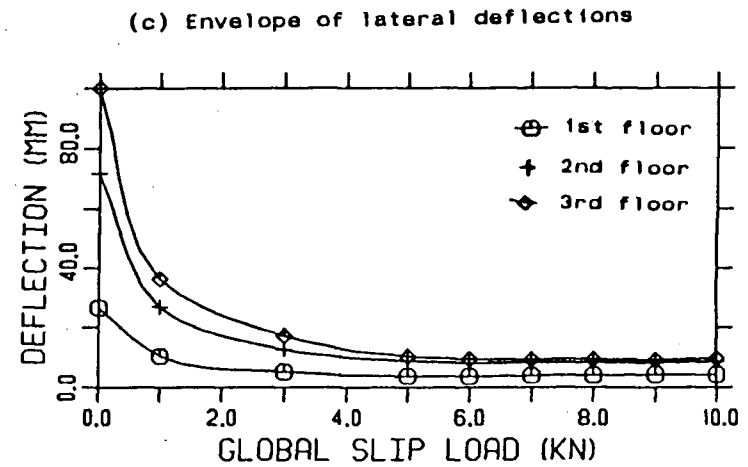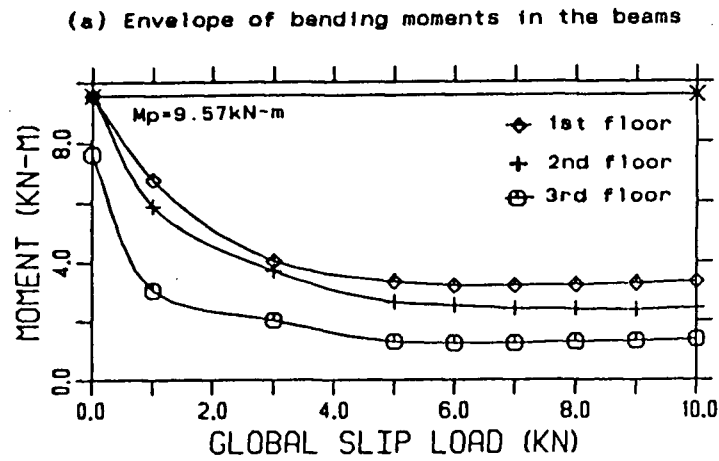
Figure 4.7 Results of Optimum Slip Load Study, Artificial Earthquake
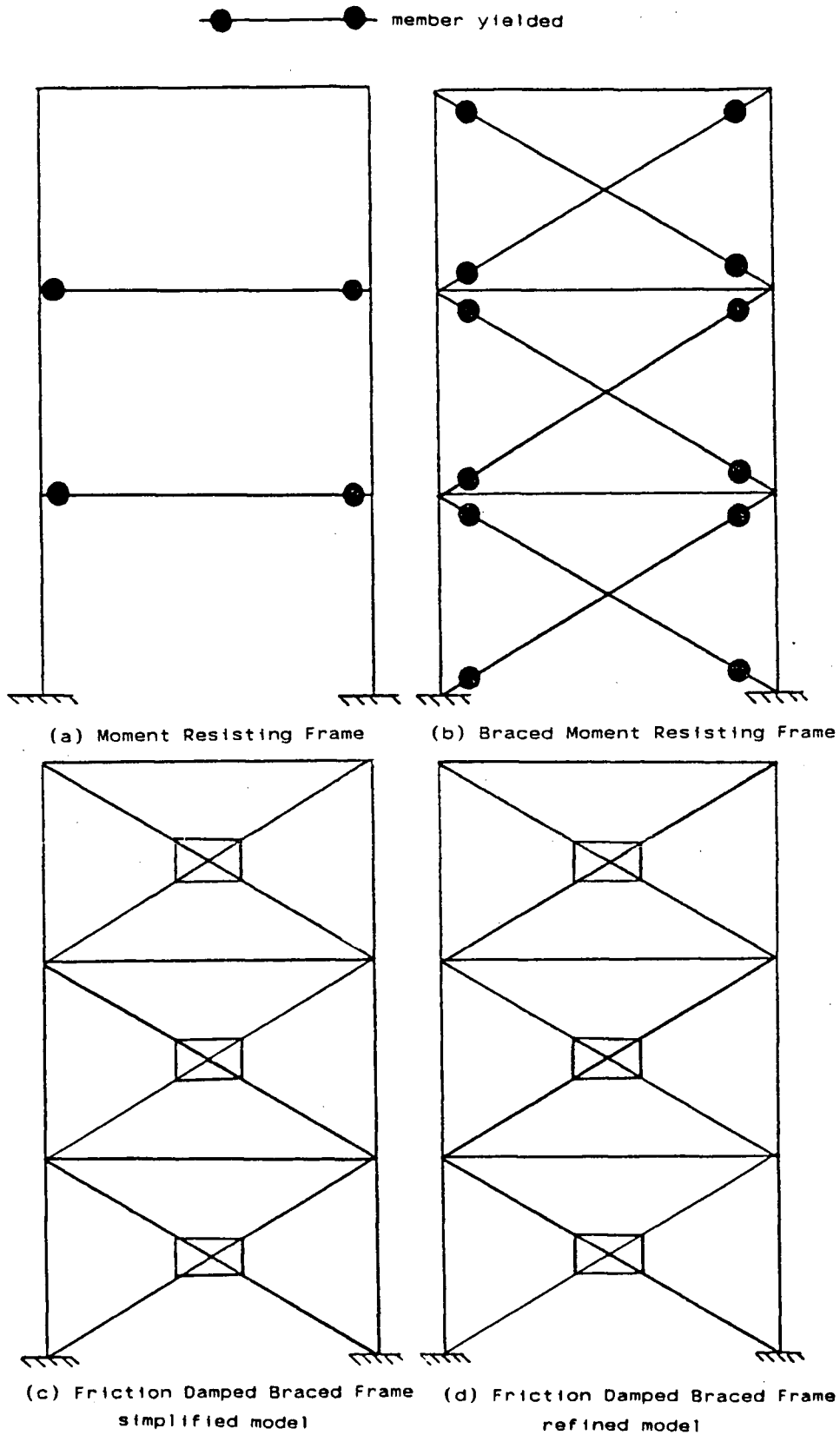
Figure 4.8 Structural Damage after El Centro Earthquake
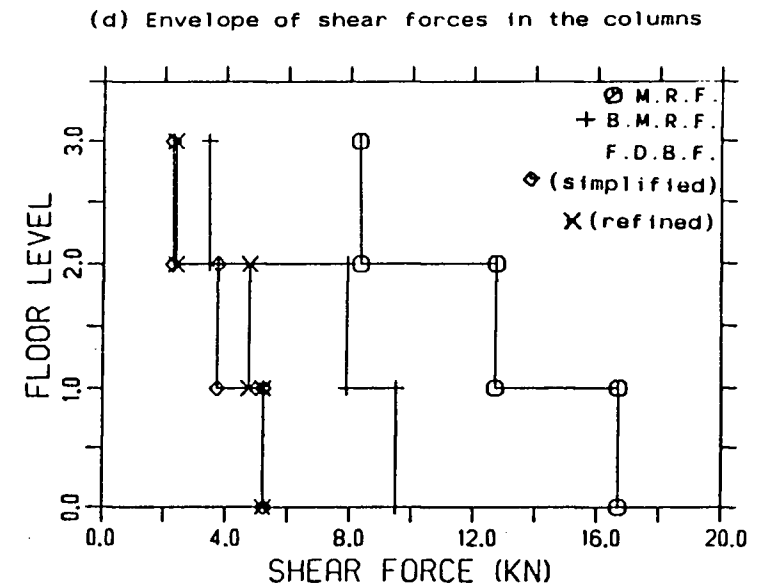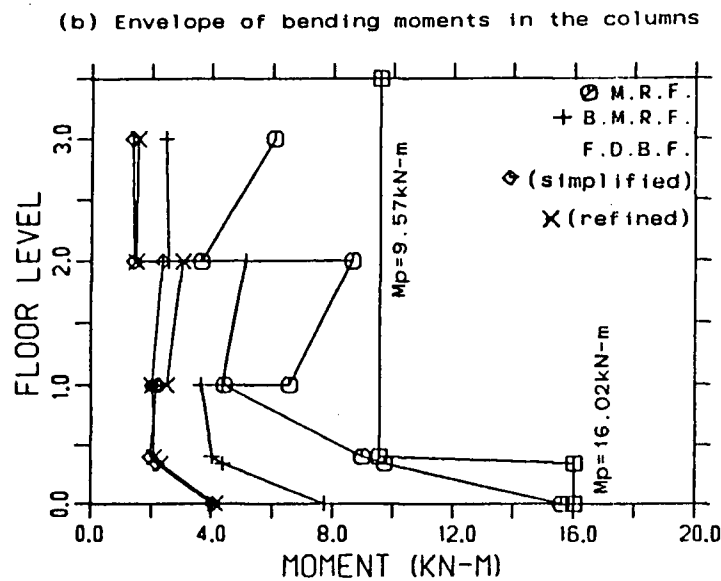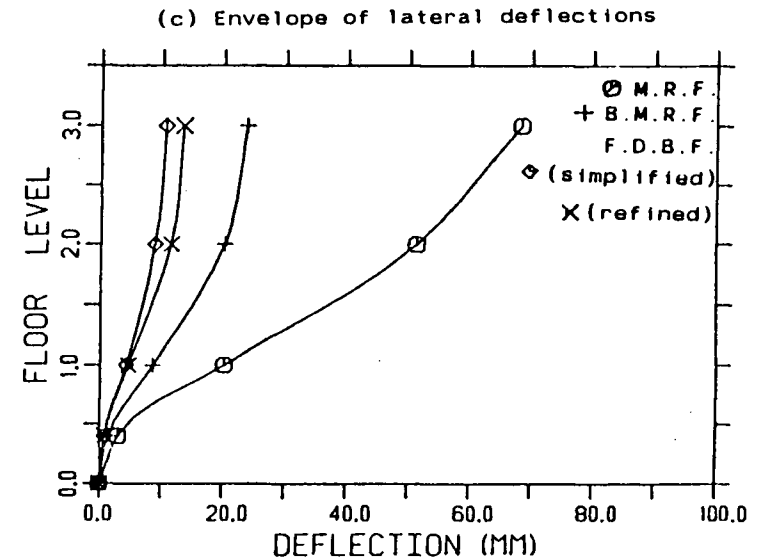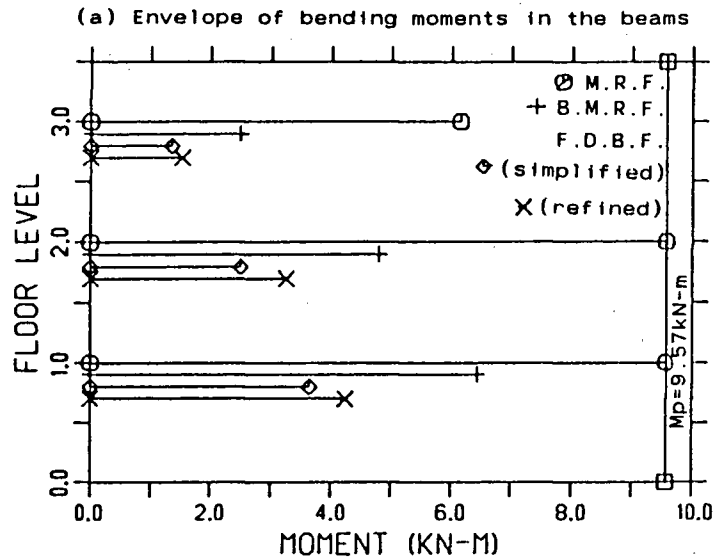
Figure 4.9 Results Envelope for El Centro Earthquake

(a) Acceleration Record
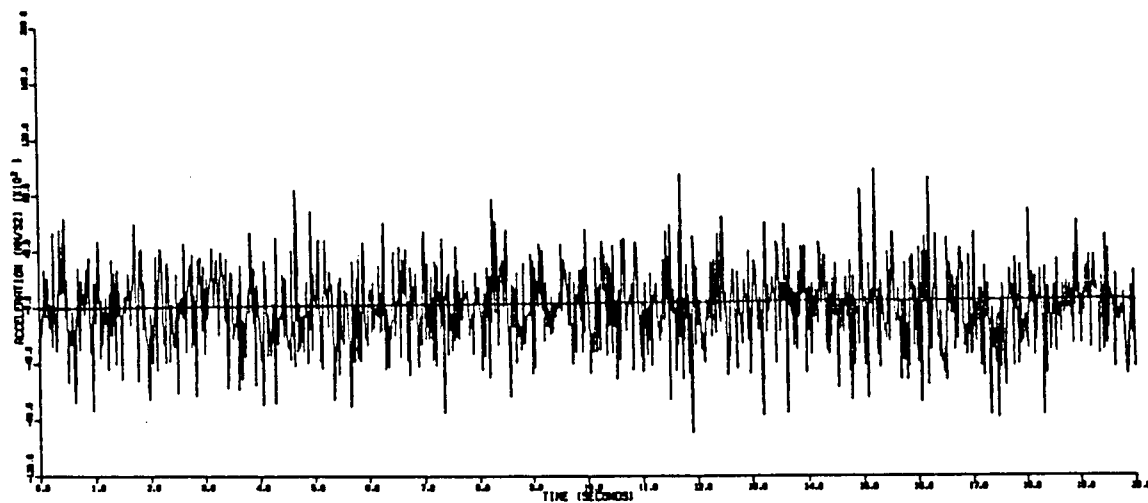
(b) Power Spectral Density Function
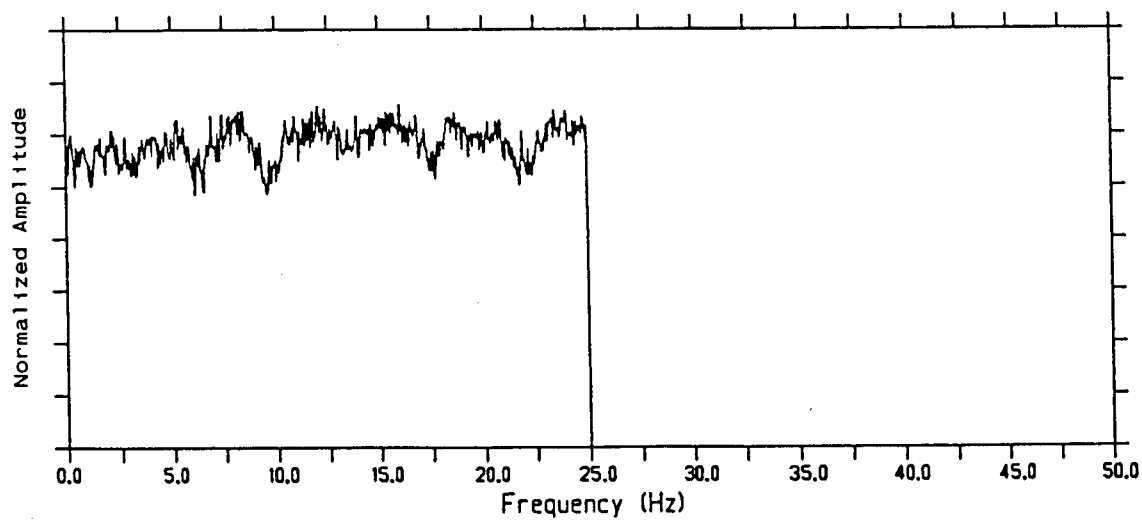
Figure 4.10 Band Limited (0-25Hz) White Noise Record
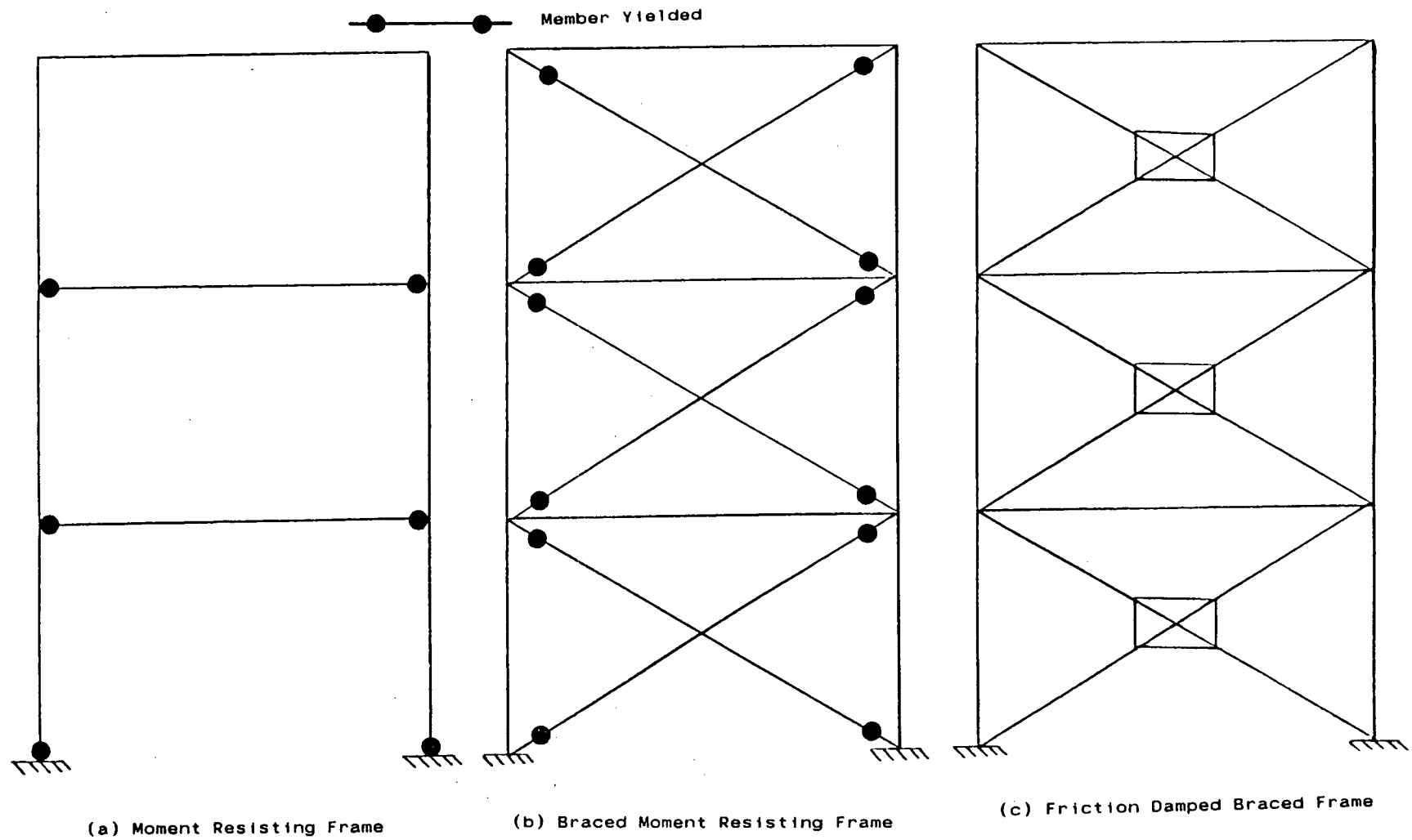
Figure 4.11 Structural Damage after White Noise Excitation

(a) Envelope of Bending Moments in the Beams

(b) Envelope of Bending Moments in the Columns

(c) Envelope of Lateral Deflections

(d) Envelope of Shear Forces in the Columns
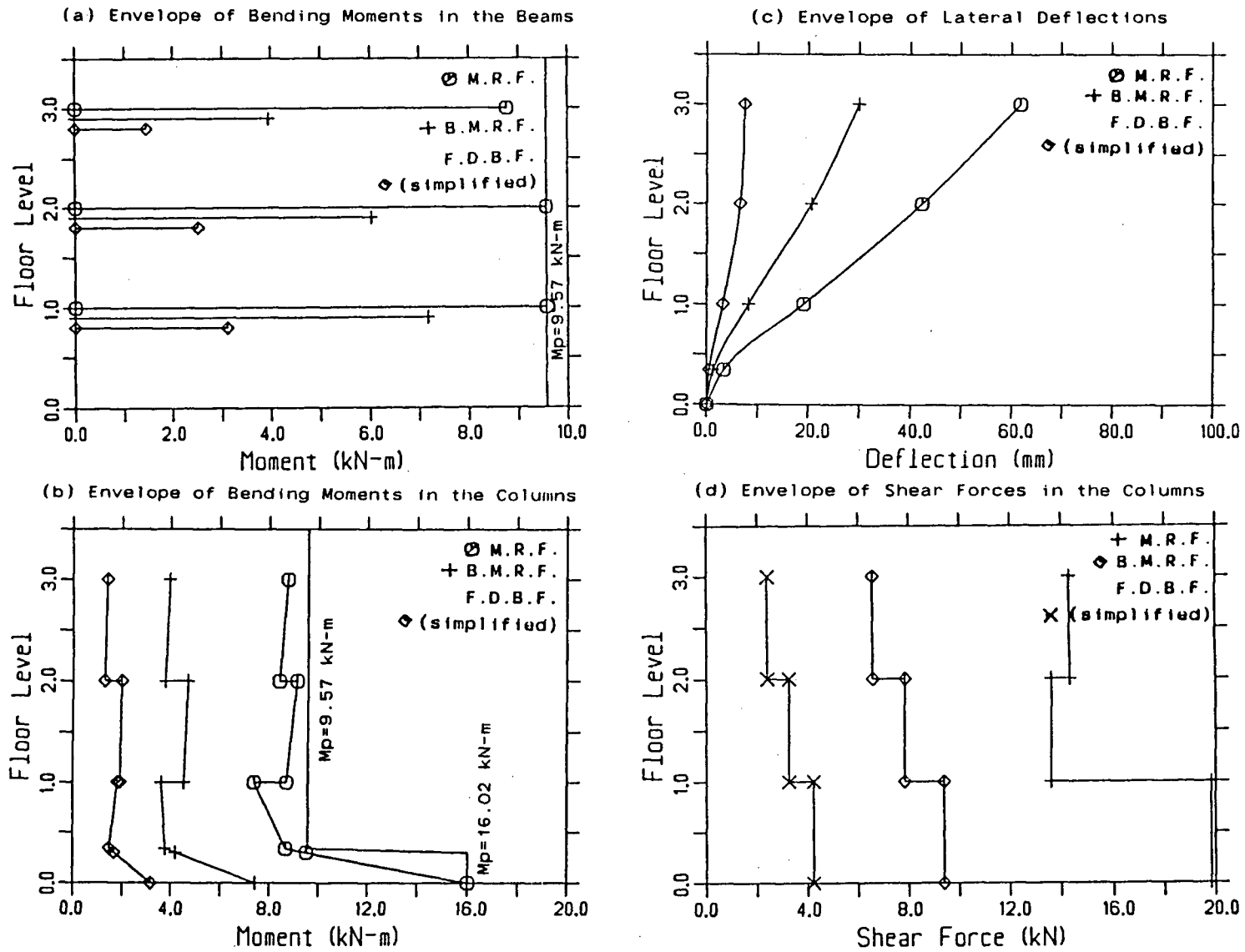
Figure 4.12 Results Envelope for White Noise Excitation
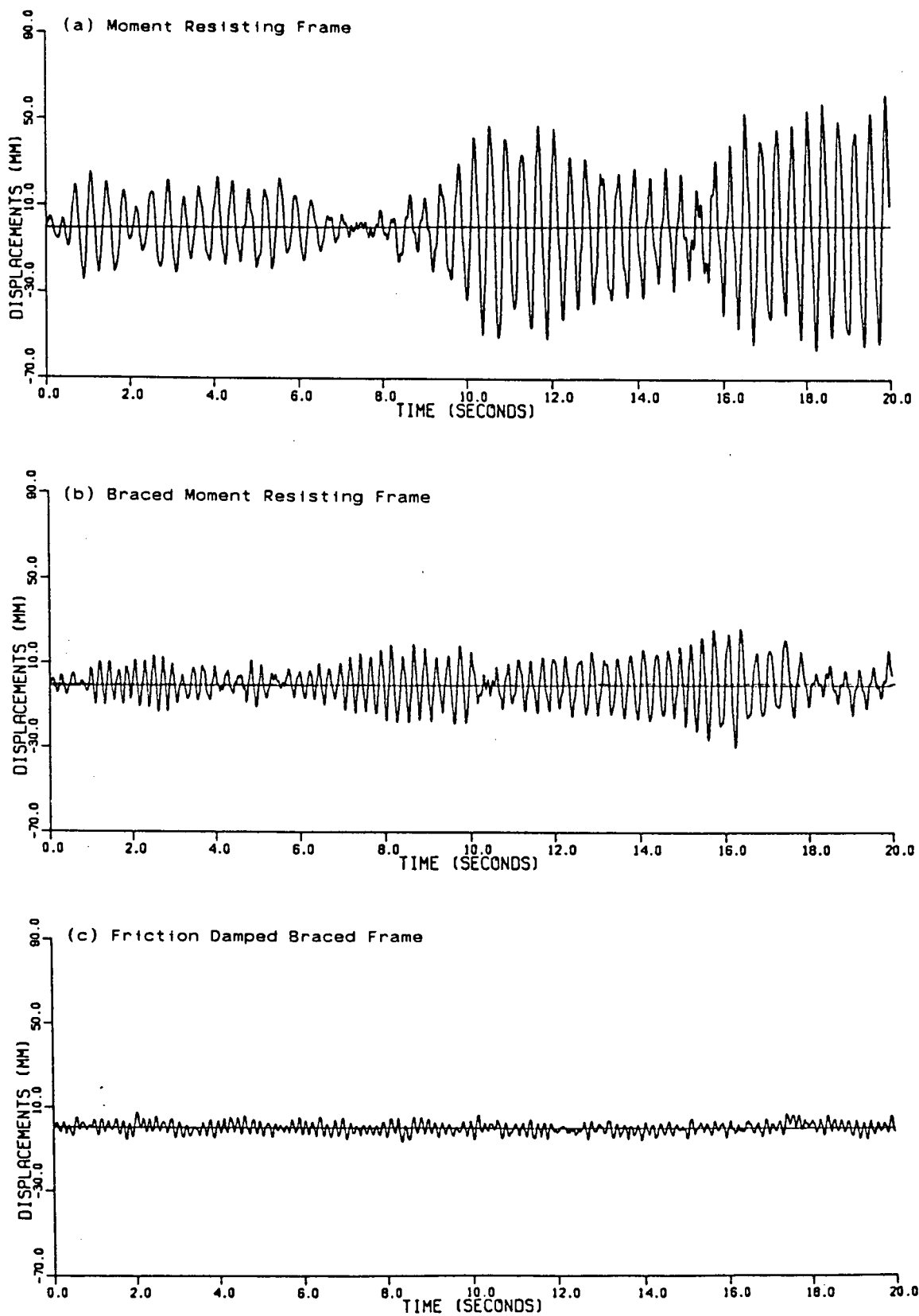
Figure 4.13 Time Histories of Third Floor Deflection for White Noise Excitation
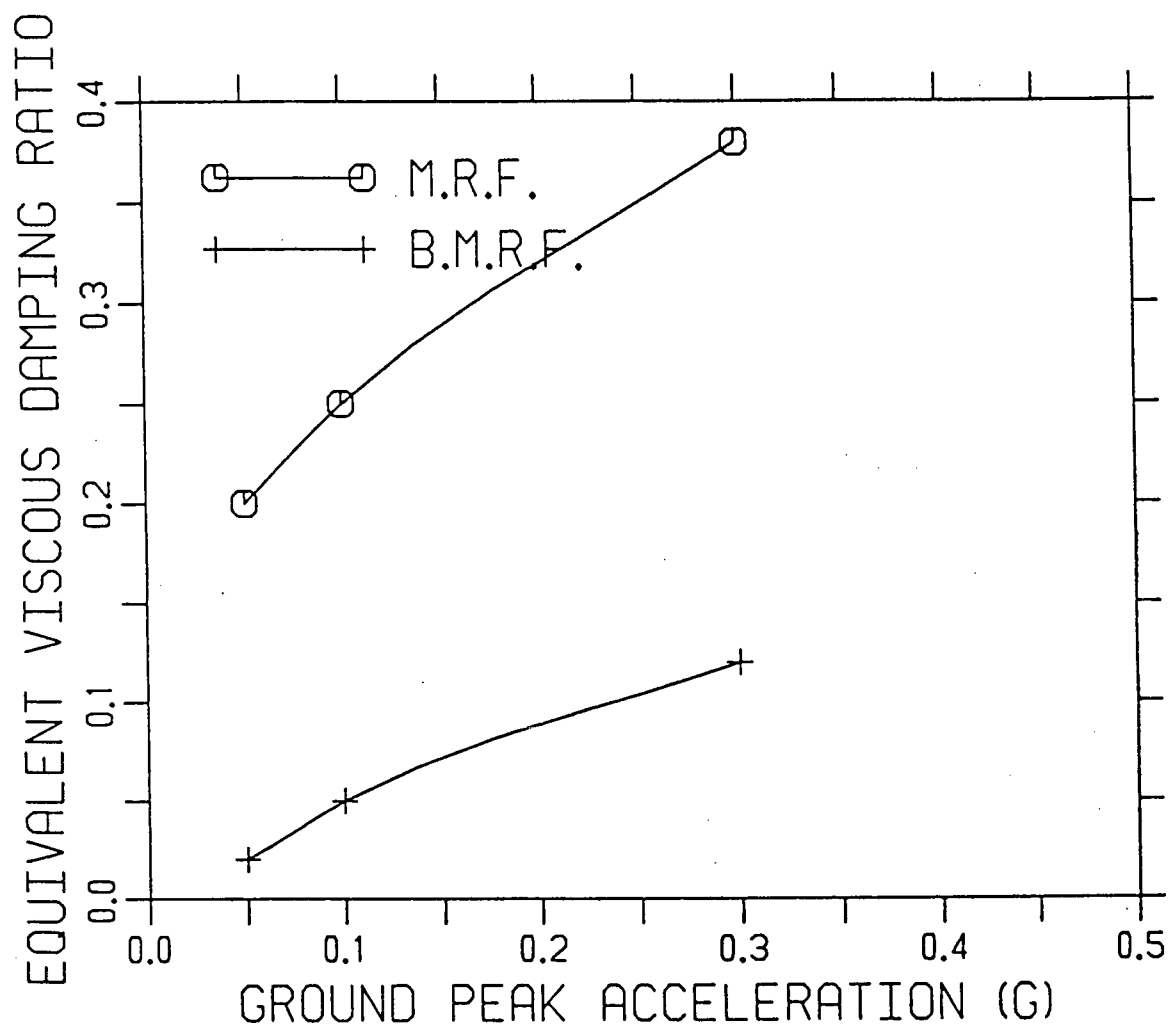
Figure 4.14 Equivalent Viscous Damping Study,Newmark-Blume-Kapur
Artificial Earthquake

Figure 5.1 General Arrangement of Friction Device

Figure 5.2 Details of Friction Device
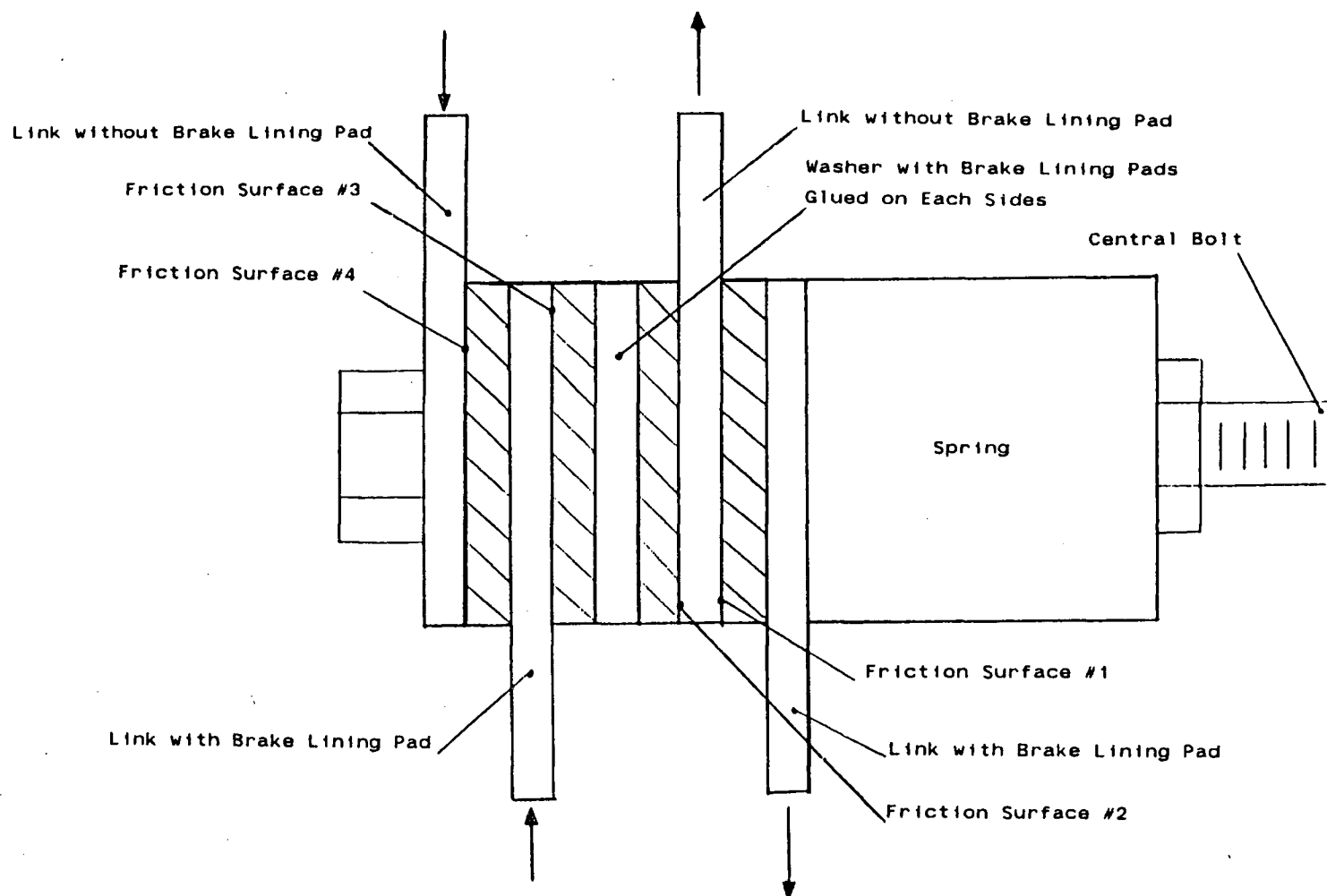
Figure 5.3 Friction Surfaces of Friction Device
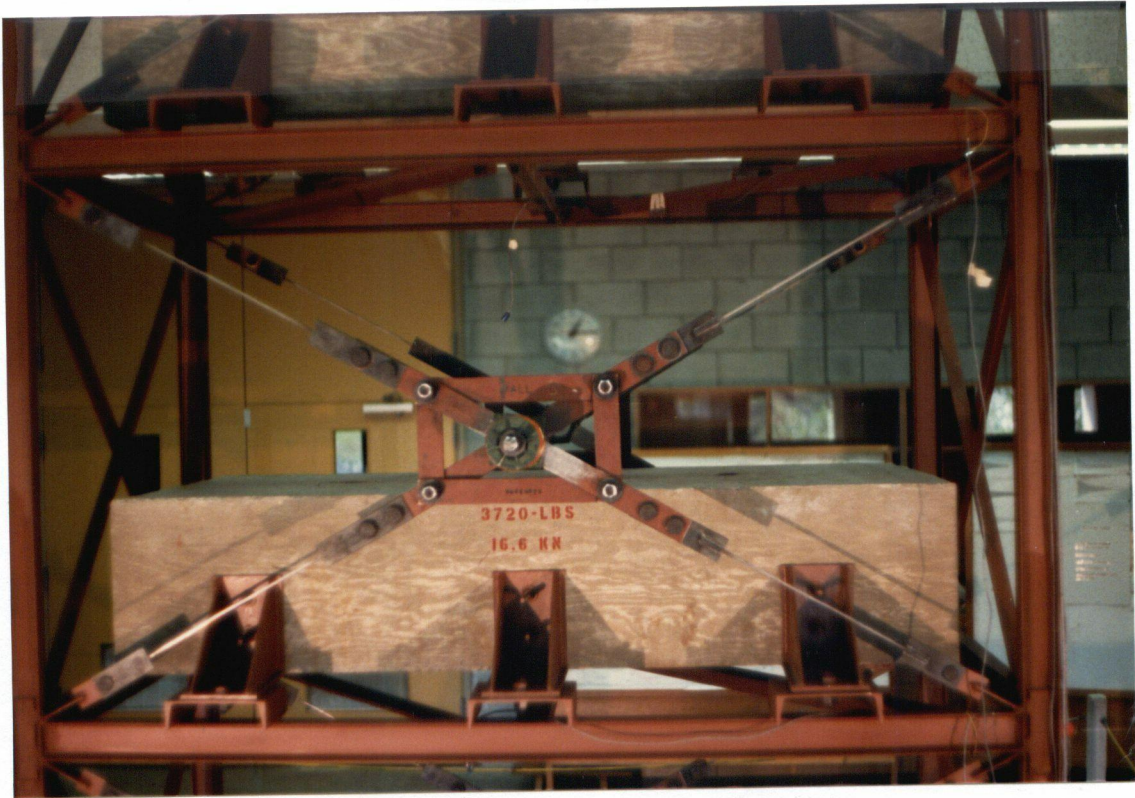
Figure 5.4 Friction Device on Model Frame
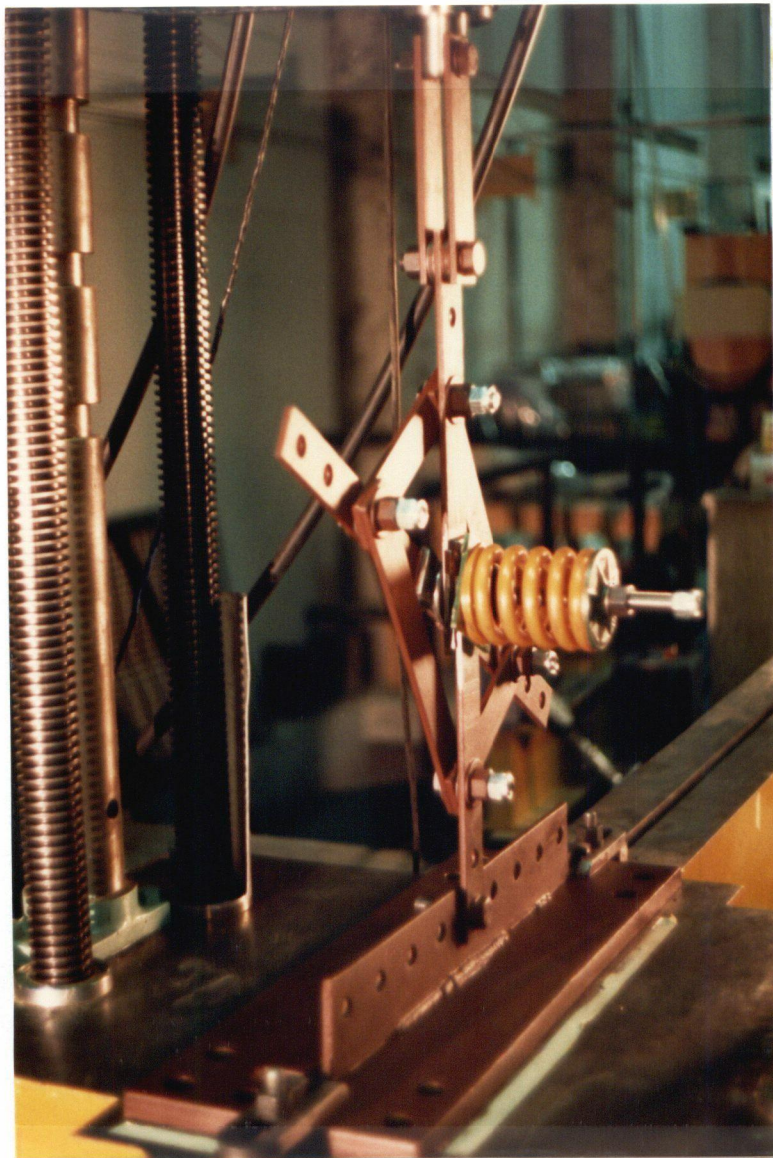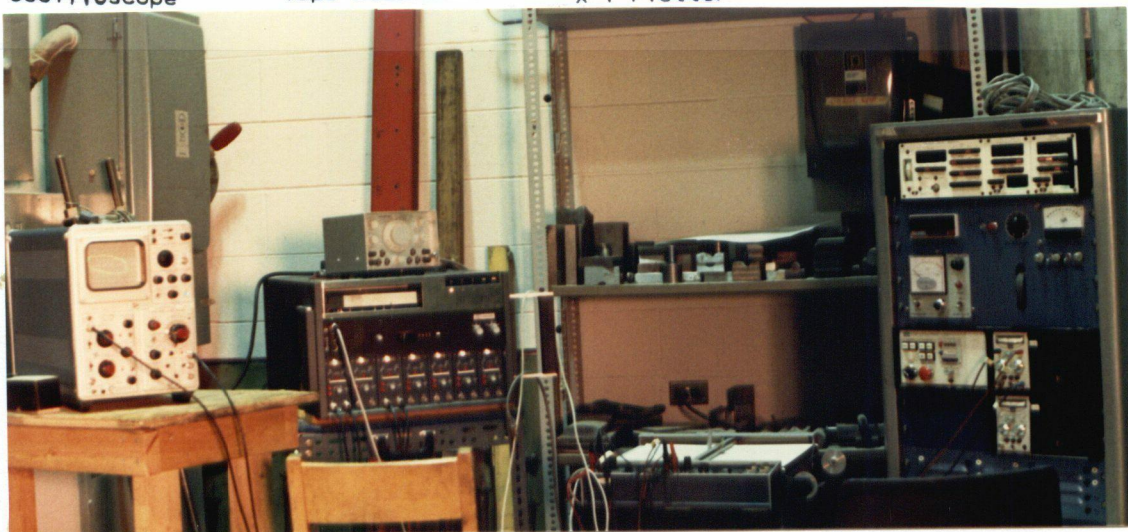
Figure 5.5 Experimental Set Up for Cyclic Tests of Friction Devices
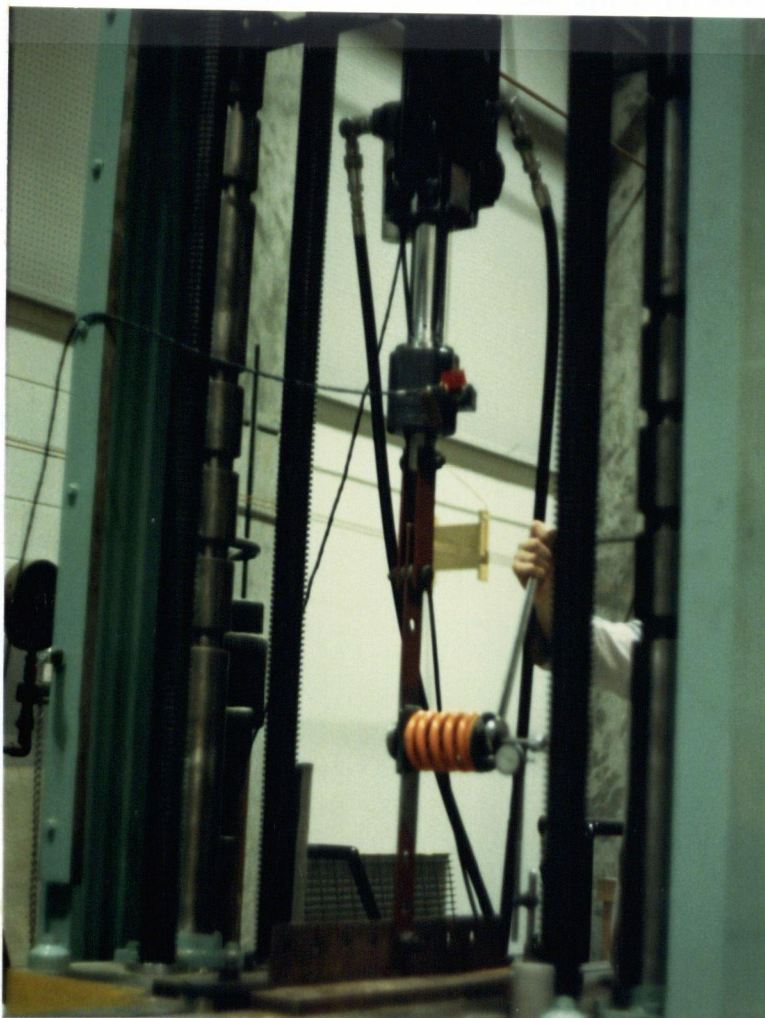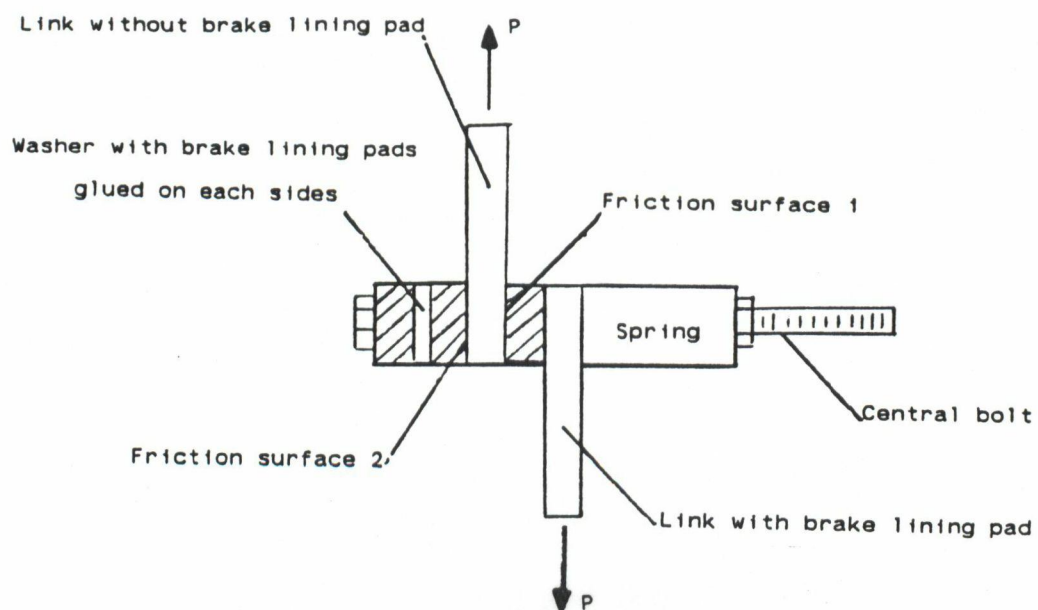
Figure 5.6 Experimental Set Up for Stability Tests
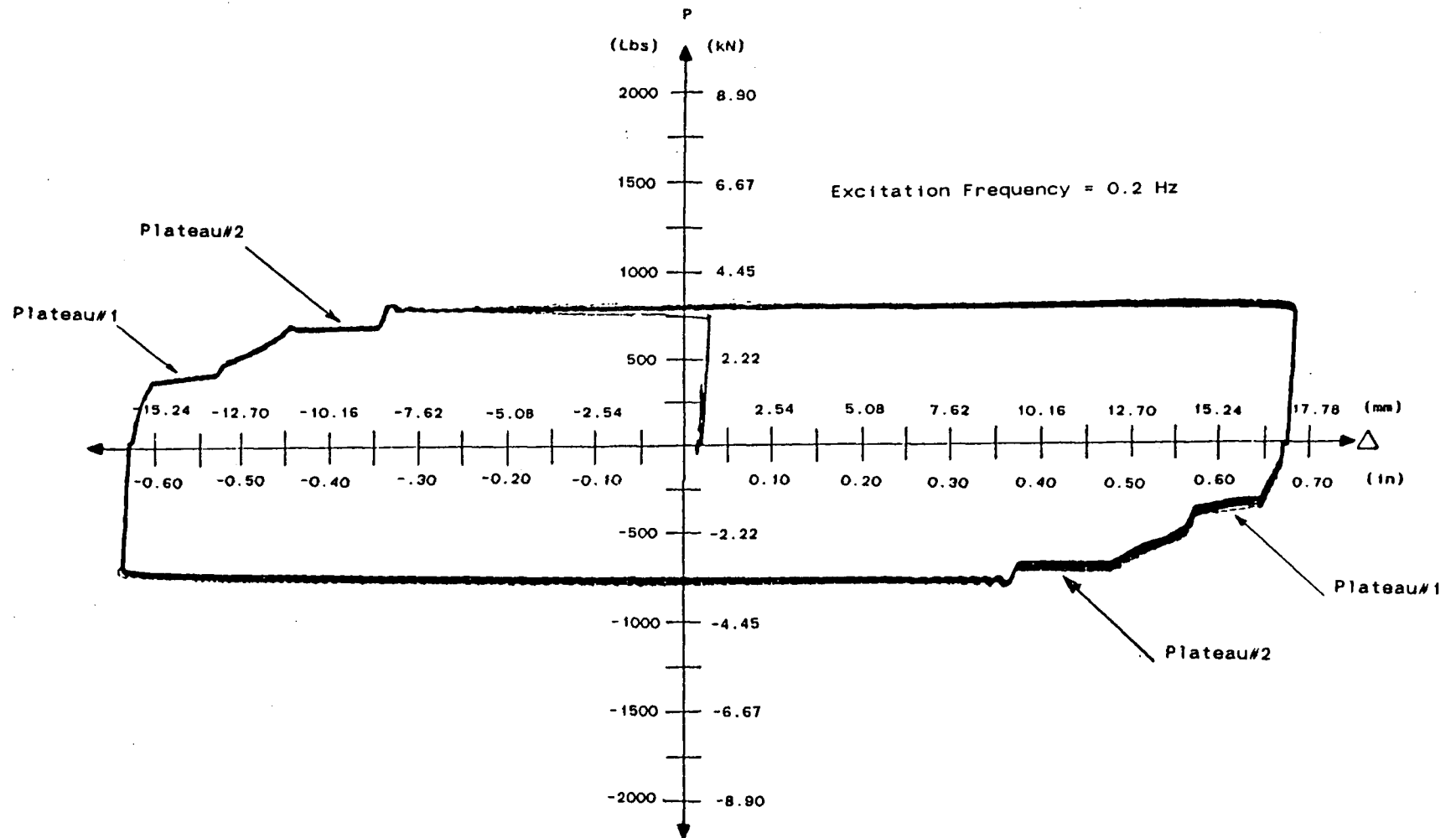
Figure 5.7 Typical Hysteresis Loop From Stability Tests
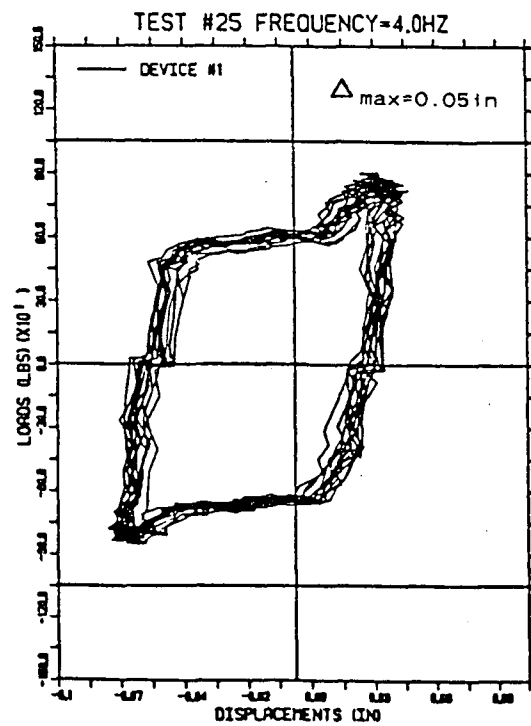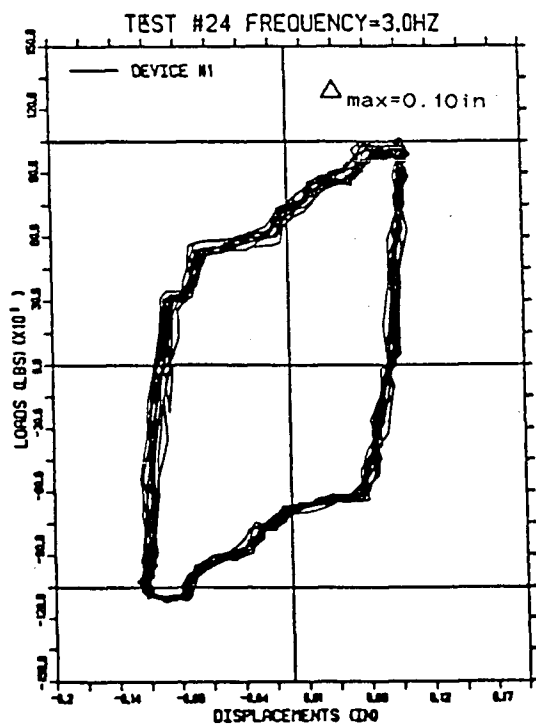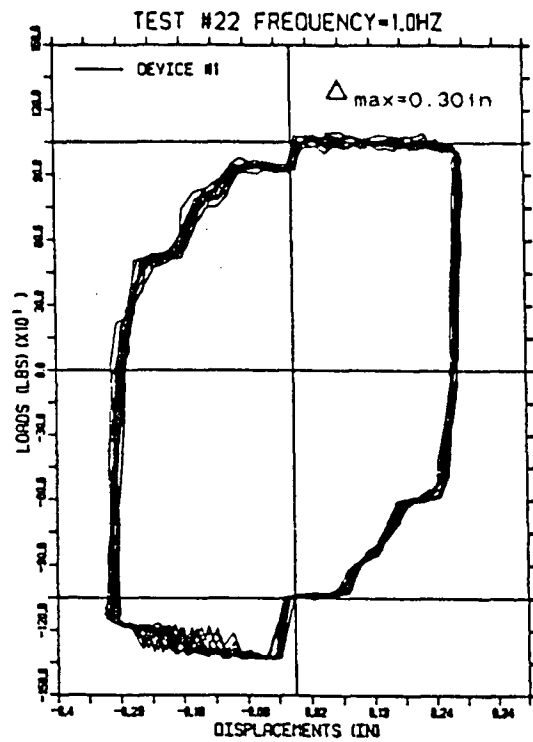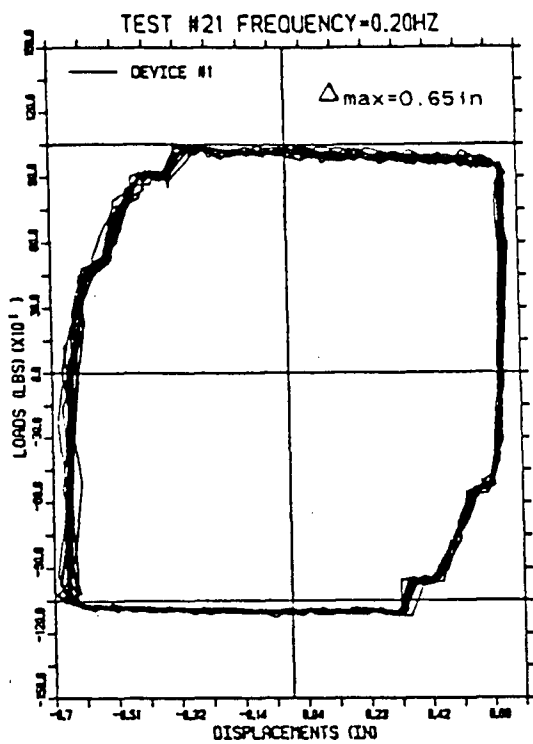
Figure 5.8 Results of Stability Tests for Various Frequencies
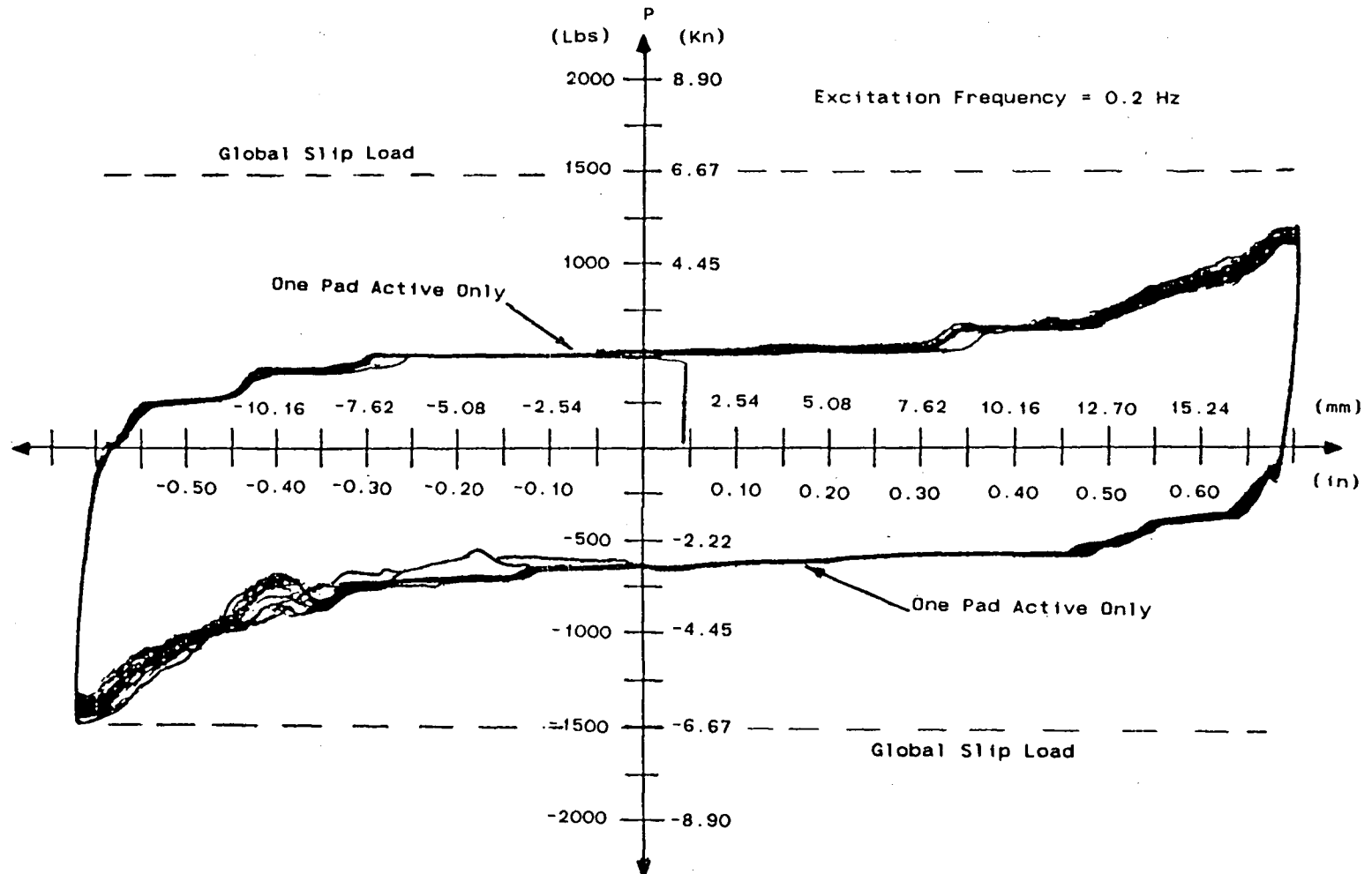
Figure 5.9 Hysteresis Loop from Original Device
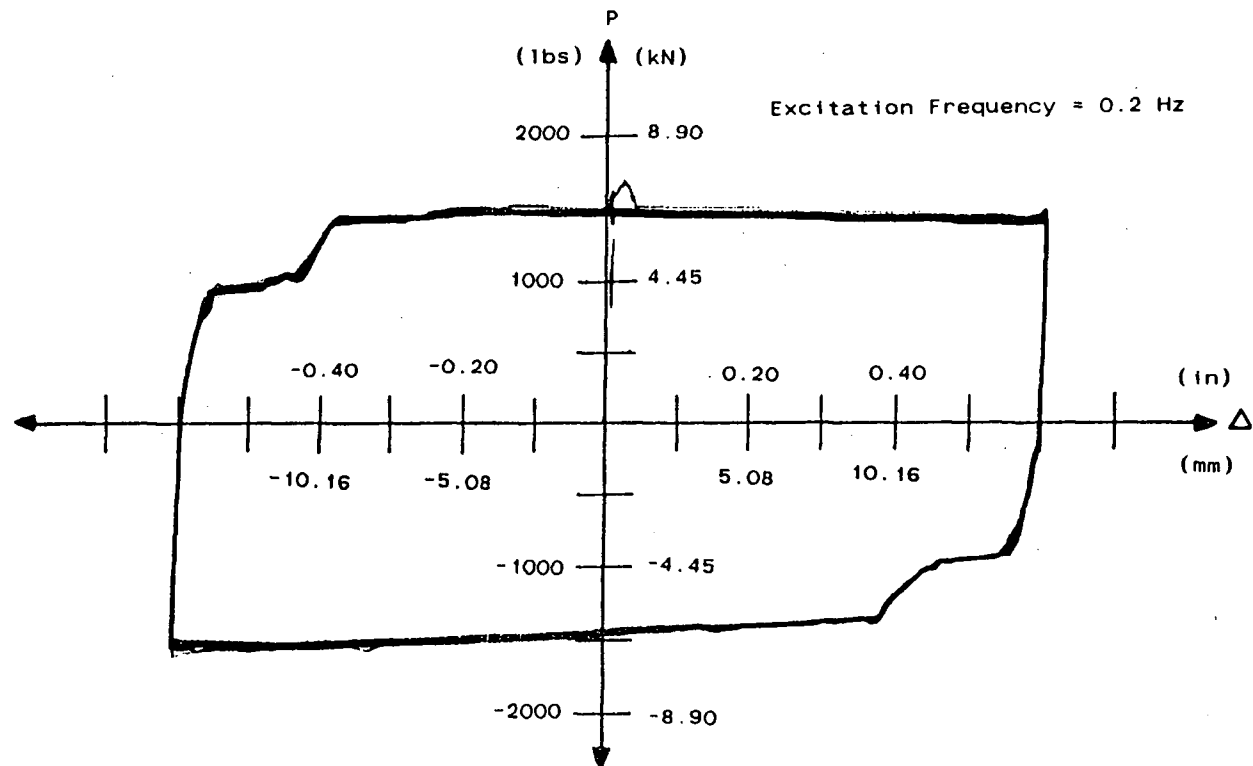
Figure 5.10 Hysteresis Loop from Modified Device
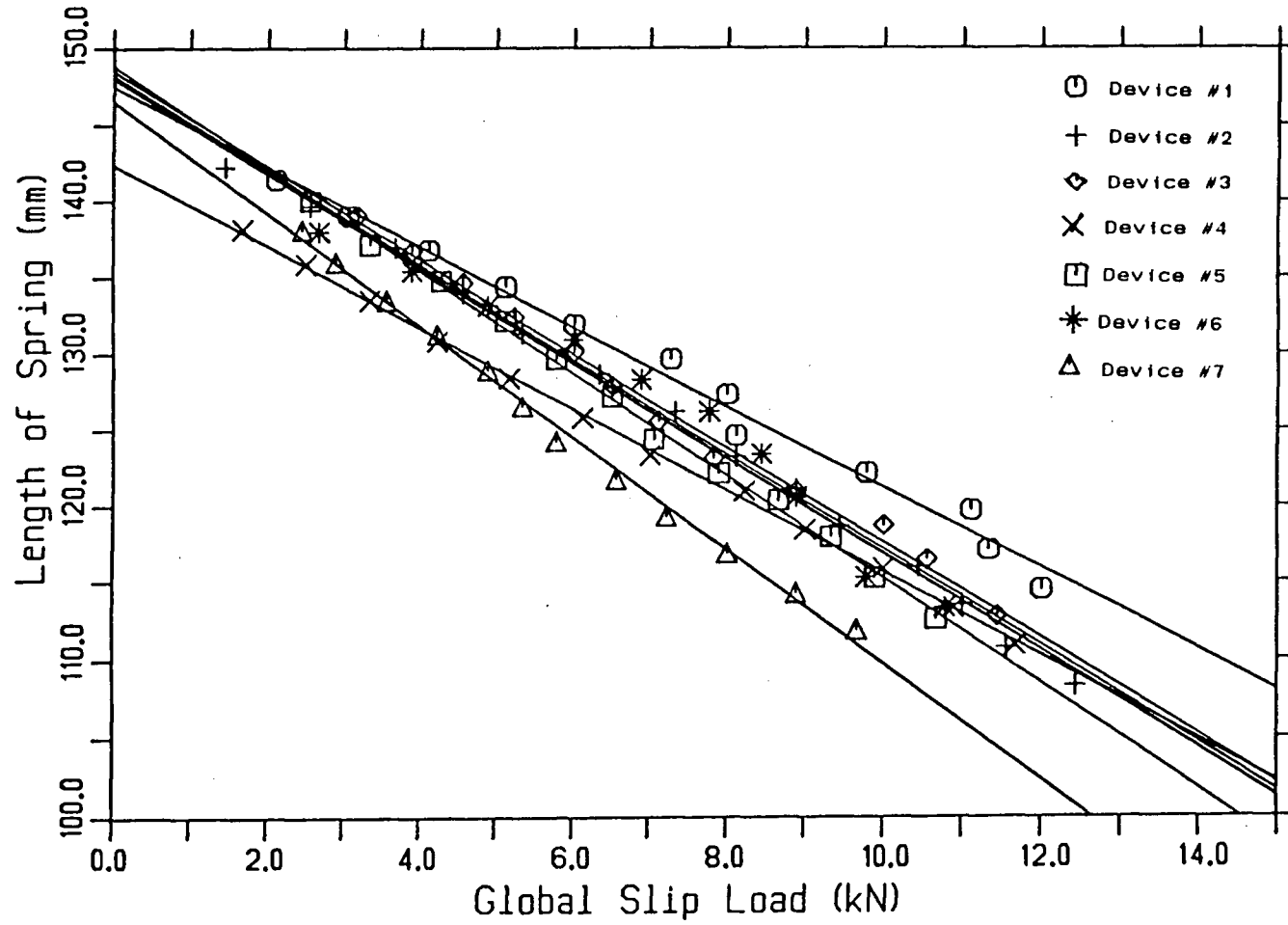
Figure 5.11 Calibration Curves of Friction Devices

All Dimensions in mm

item # 25
description: BRACES FOR FDBF
quantity: 30
scale: AS INDICATED
date: 25/03/85
drawn by ld, af

Page 1 of 2
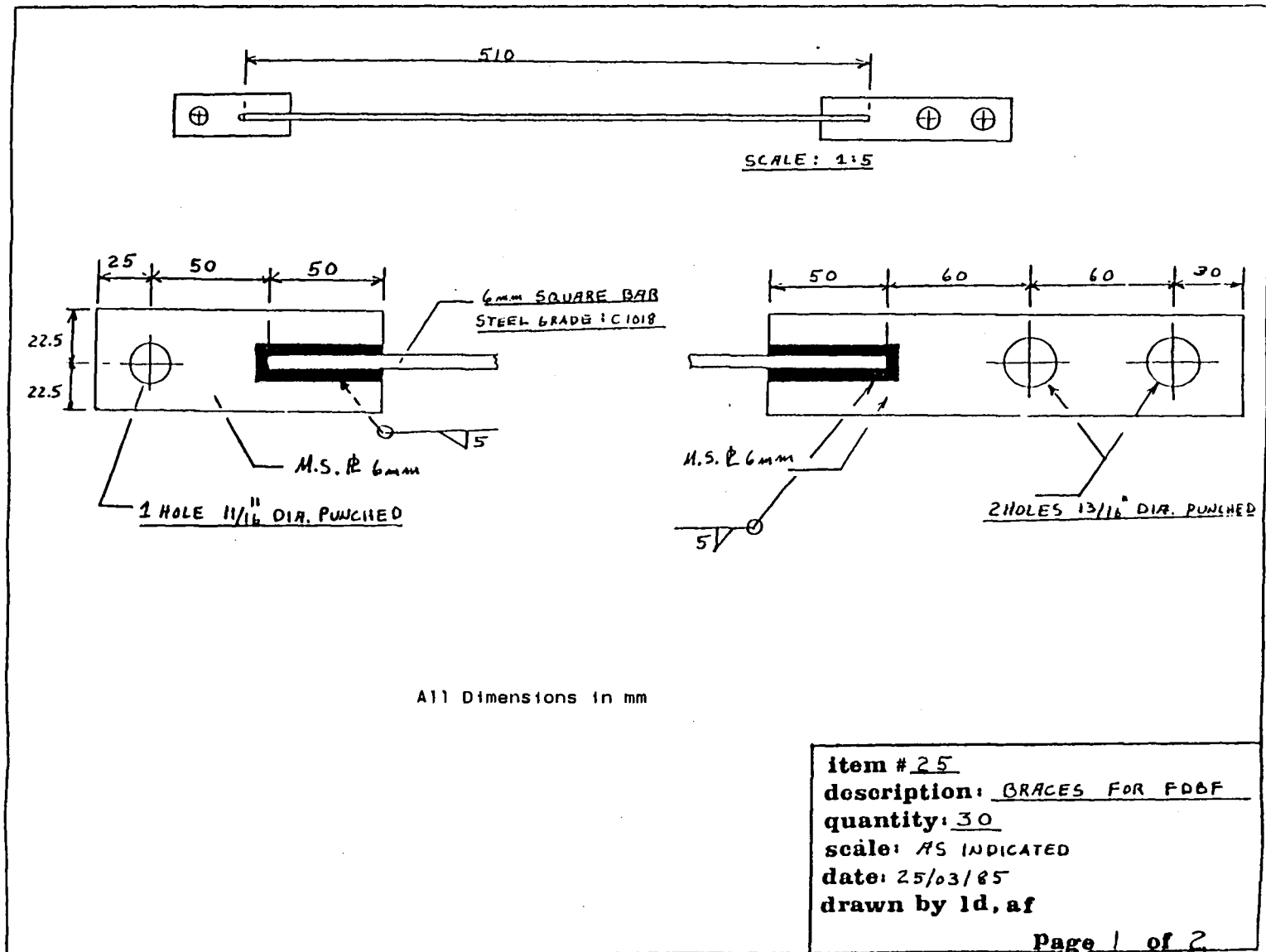
Figure 6.1 Detail of Brace Unit Used on the Friction Damped Braced Frame
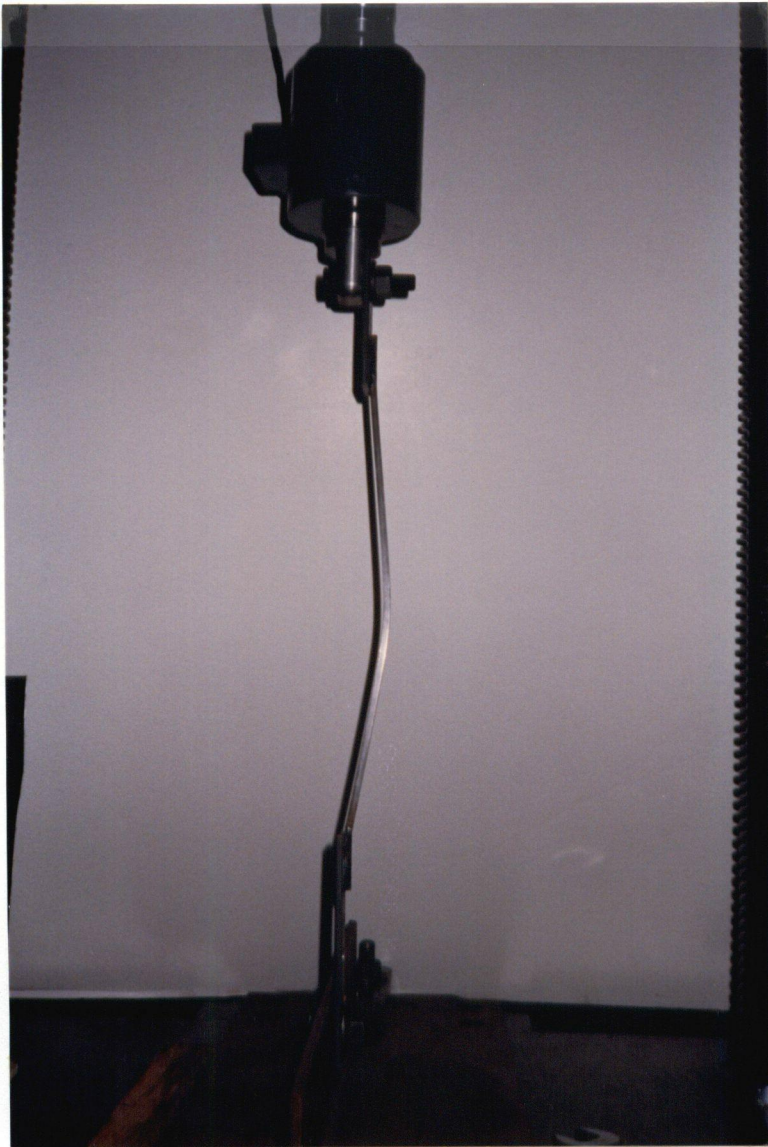
Figure 6.2 Permanent Deformed Shape of Brace Unit after Uniaxial Test #1
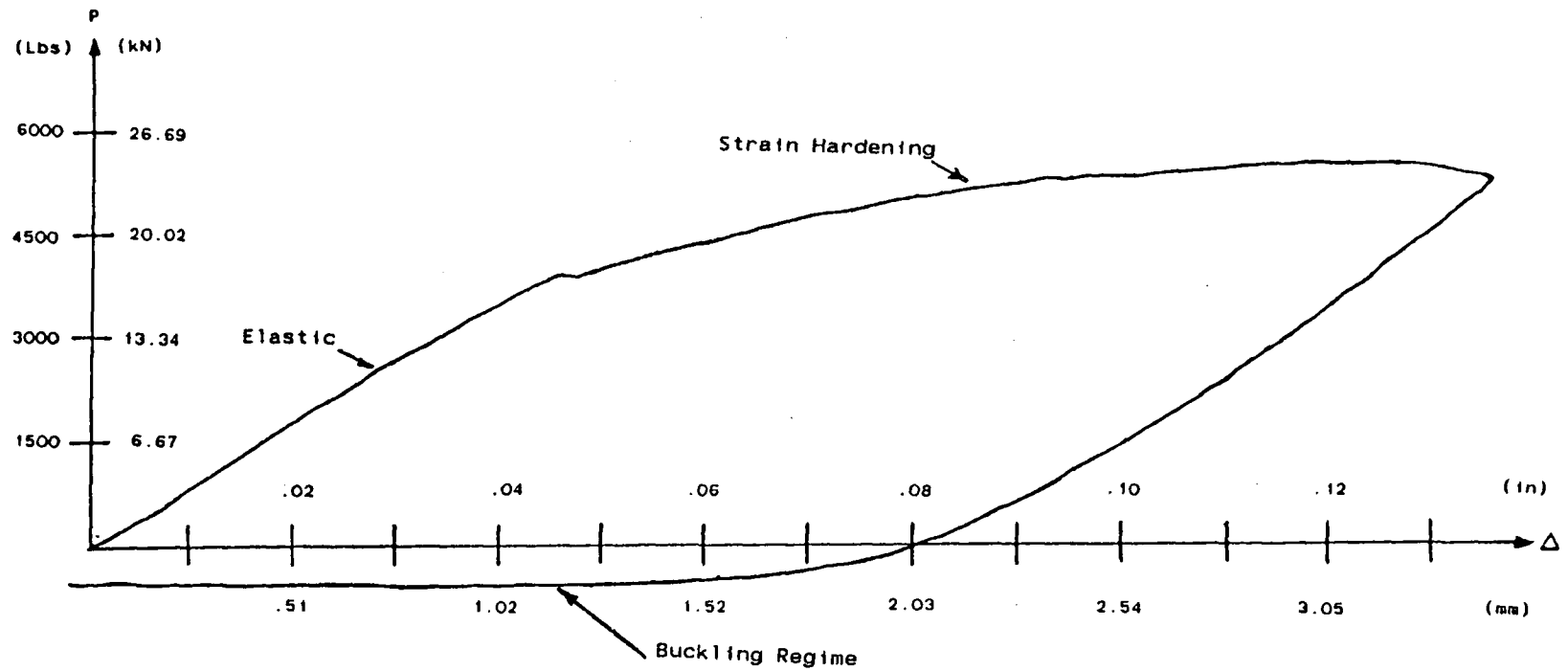
Figure 6.3 Load-Deformation Curve from Uniaxial Test #1 on Brace
Unit
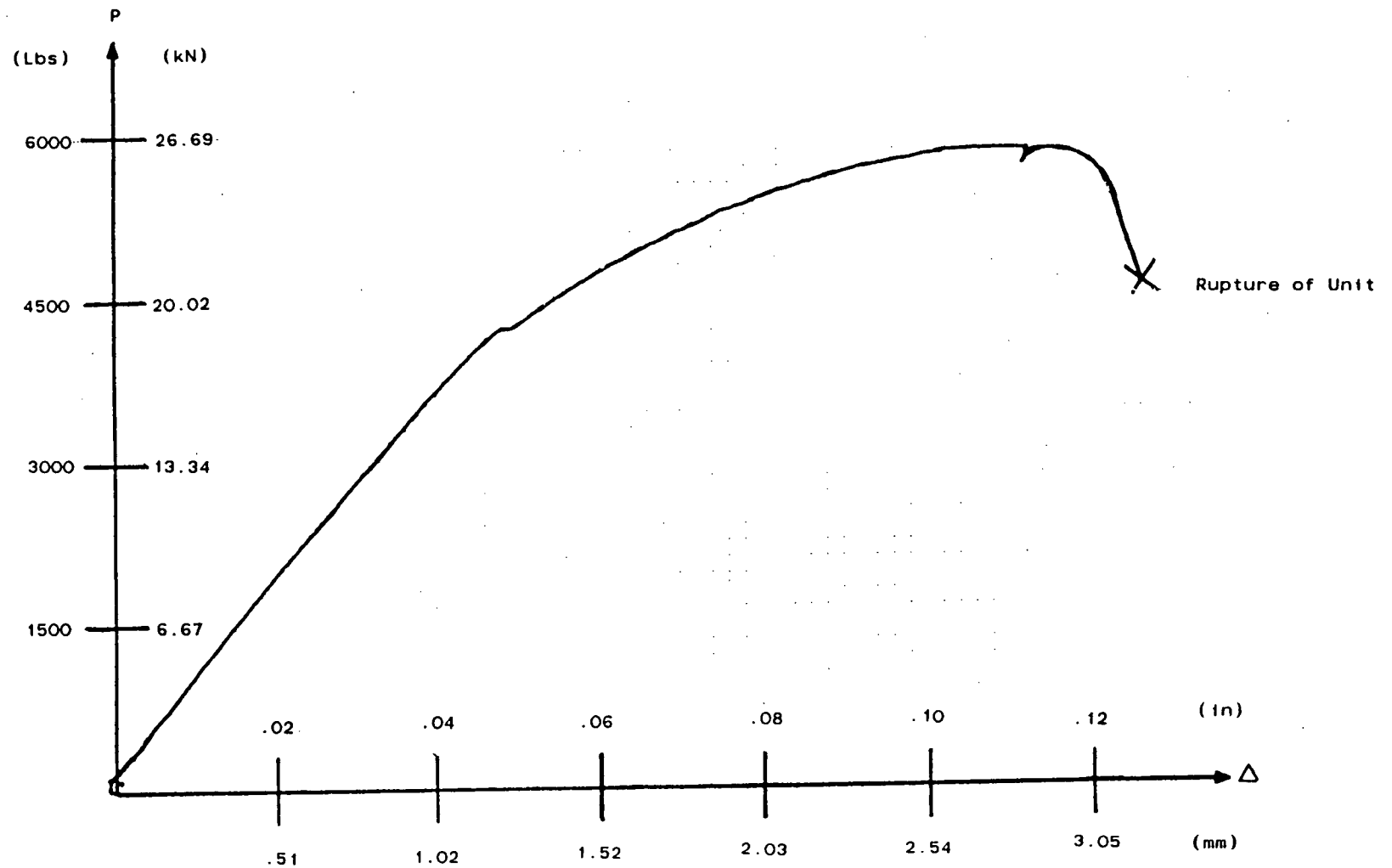
Figure 6.4 Load-Deformation Curve from Uniaxial Test #2 on Brace
Unit
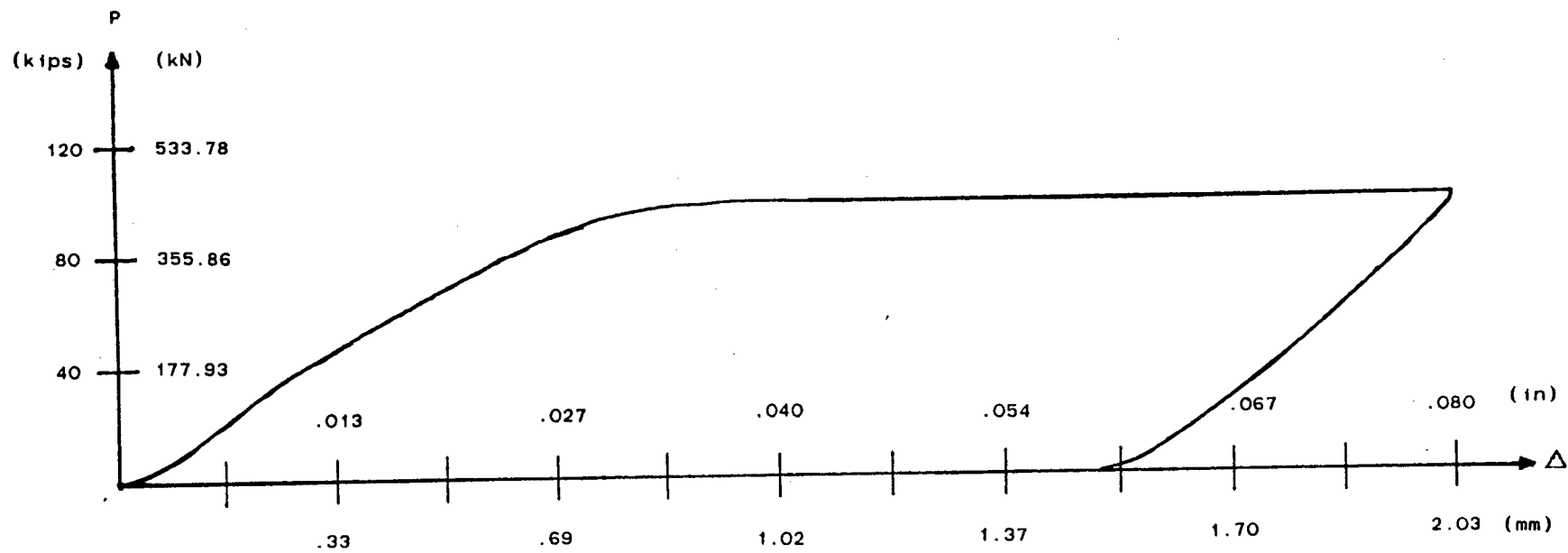
Figure 6.5 Load-Deformation Curve from Uniaxial Test on Main
Members (S75X8)
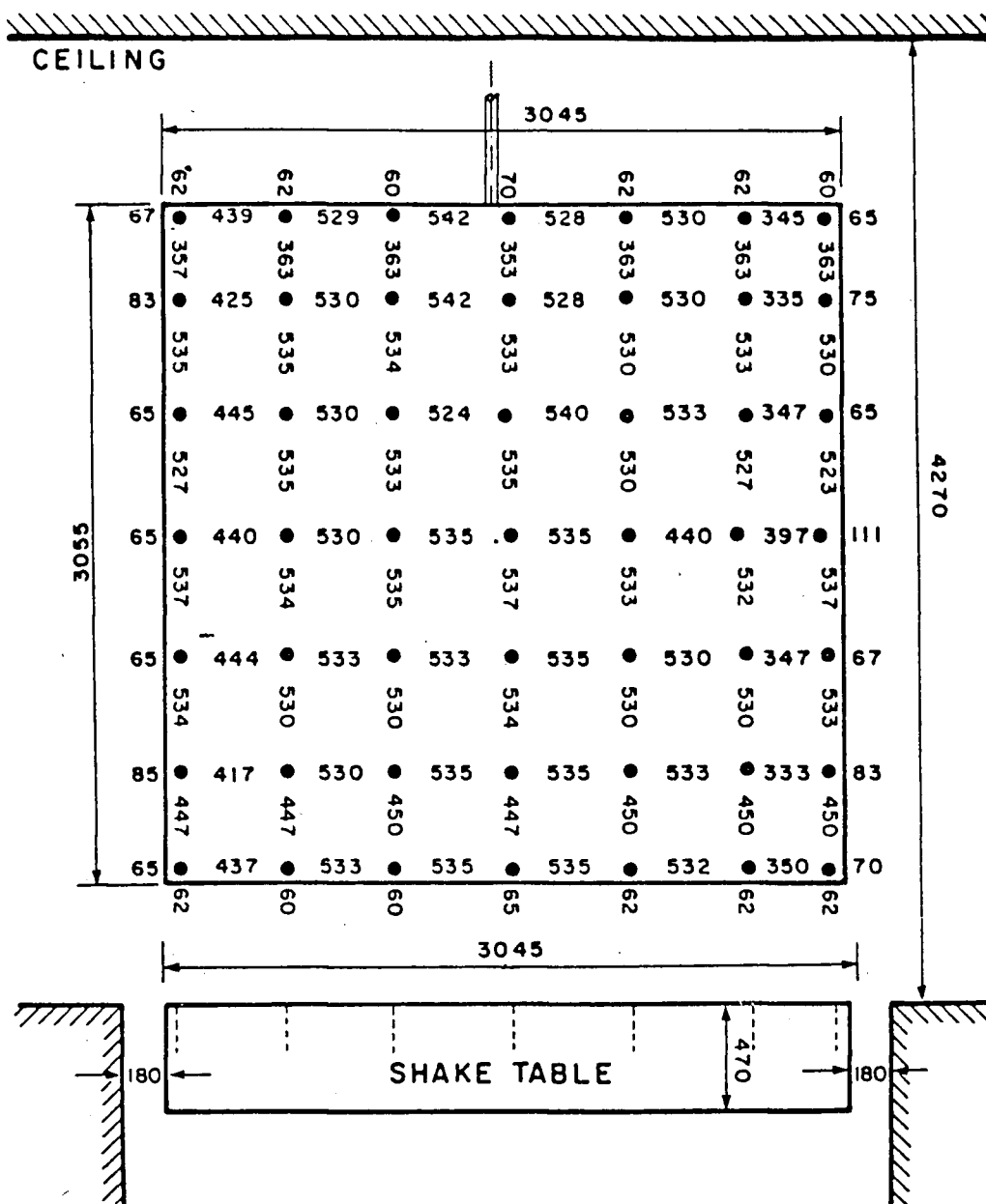
Figure 7.1 General Arrangement of Earthquake Simulator Table
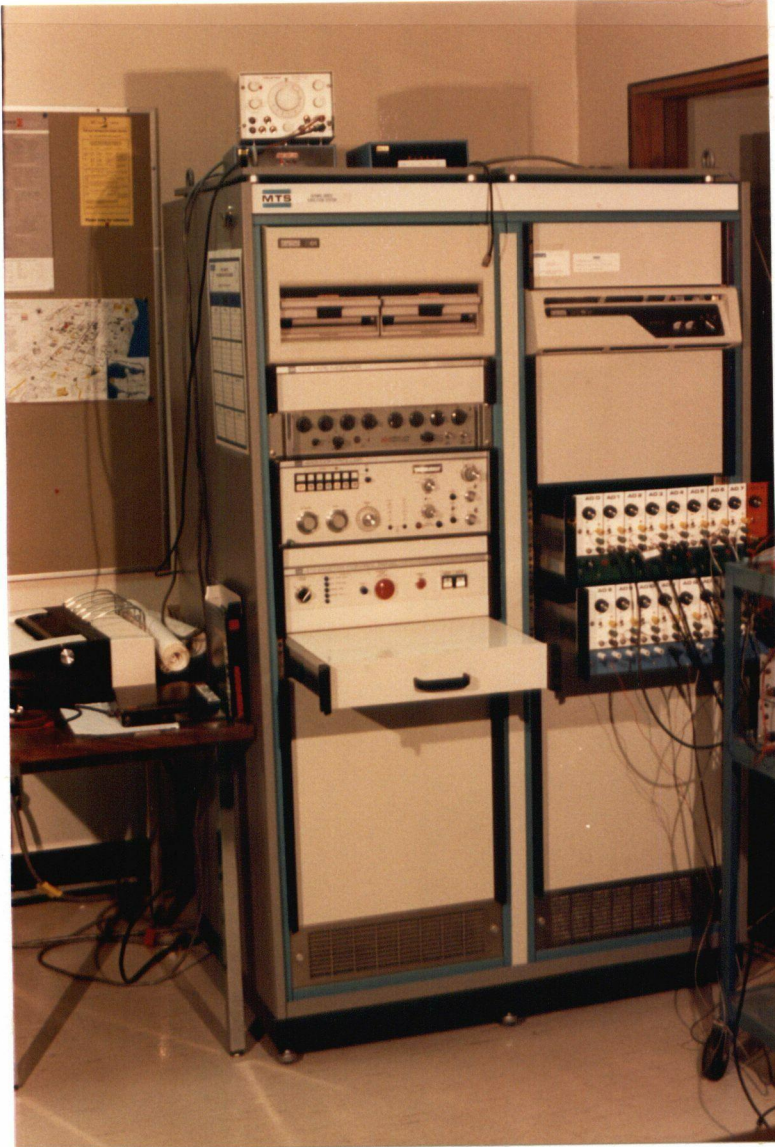
Figure 7.2 Physical Arrangement of Data Acquisition System for
Earthquake Simulator Table
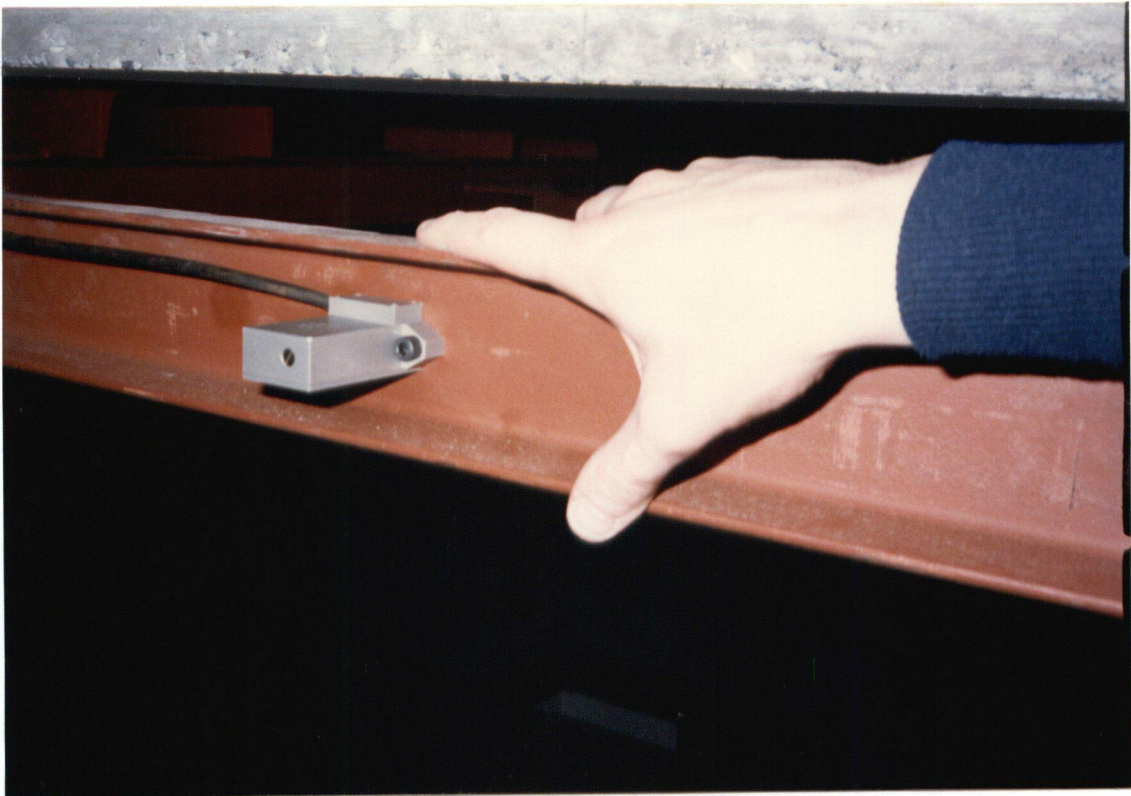
Figure   7.3   Strain Gage Accelerometer on First Floor Cross-Beam
of Model Frame
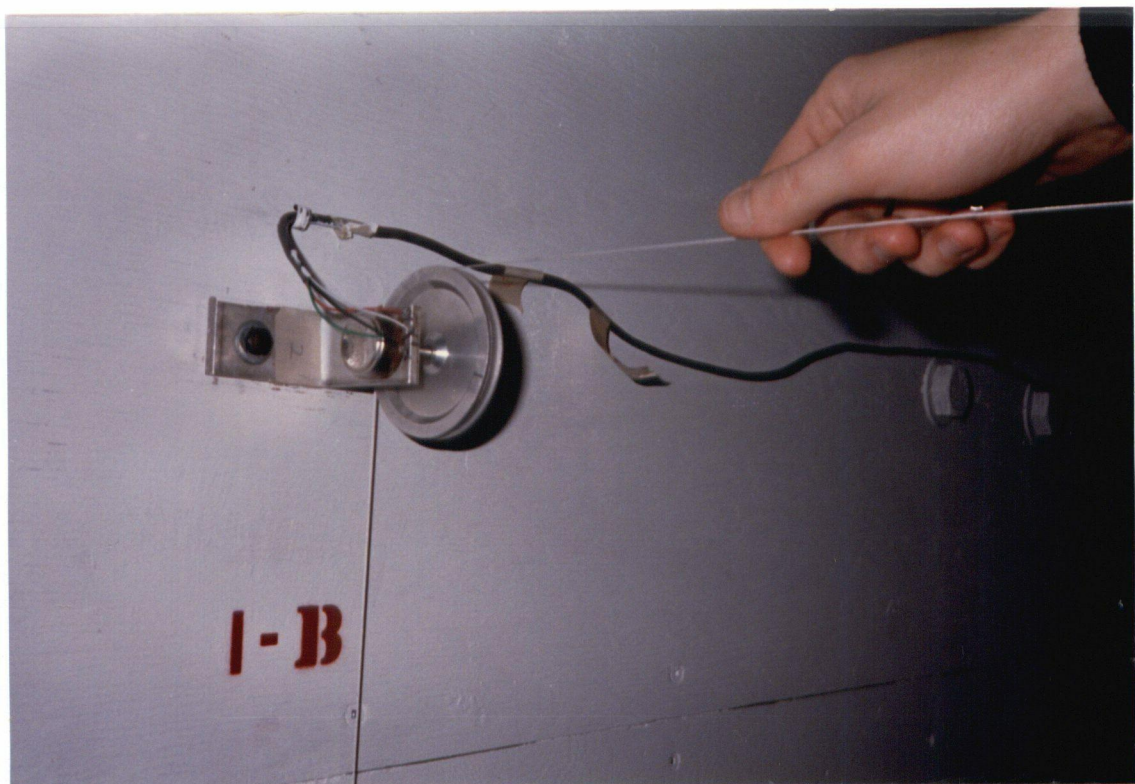
Figure 7.4 Potentiometer Used to Measure   Absolute   Displacement
of Model Frame

Figure 7.5 Strain Gages Unit on Base Column of Model Frame
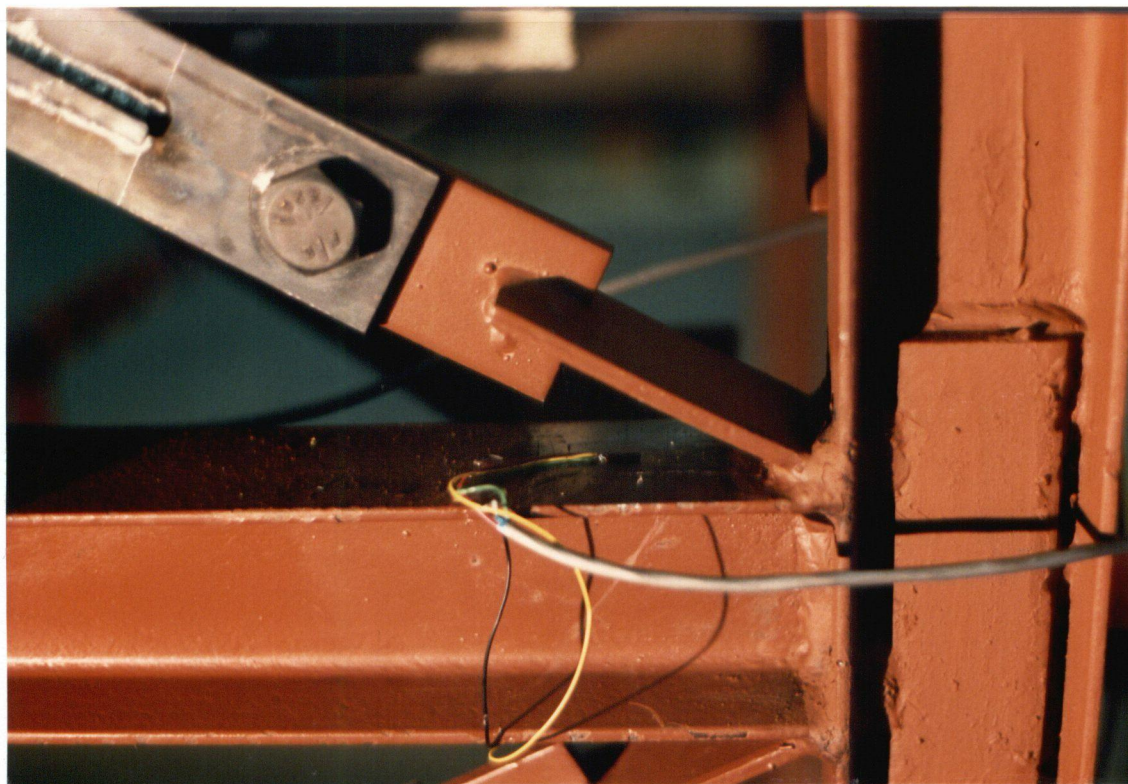
Figure 7.6 Strain Gages Unit on First Floor Beam of Model Frame
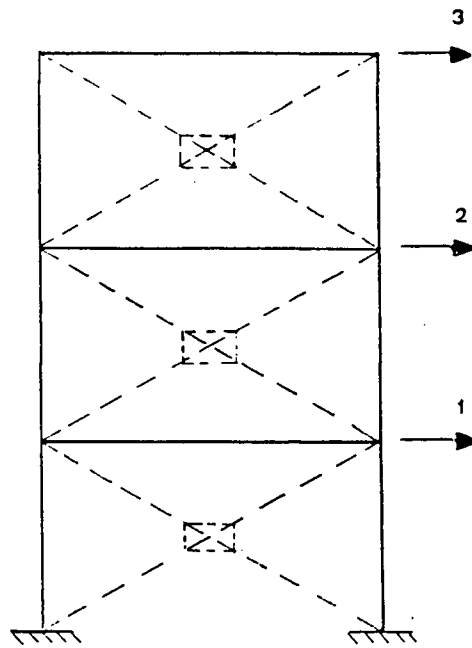
Figure 8.1 Degrees of Freedom Considered to Determine the Experimental Mode Shapes of the Model Frames
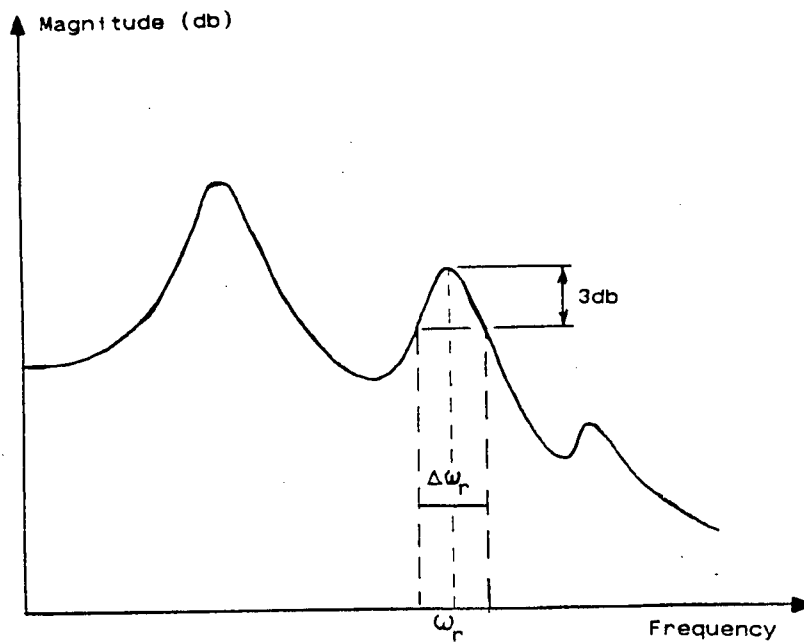
Figure 8.2 Bandwidth Method Applied to a Multi-Degree-of-Freedom System
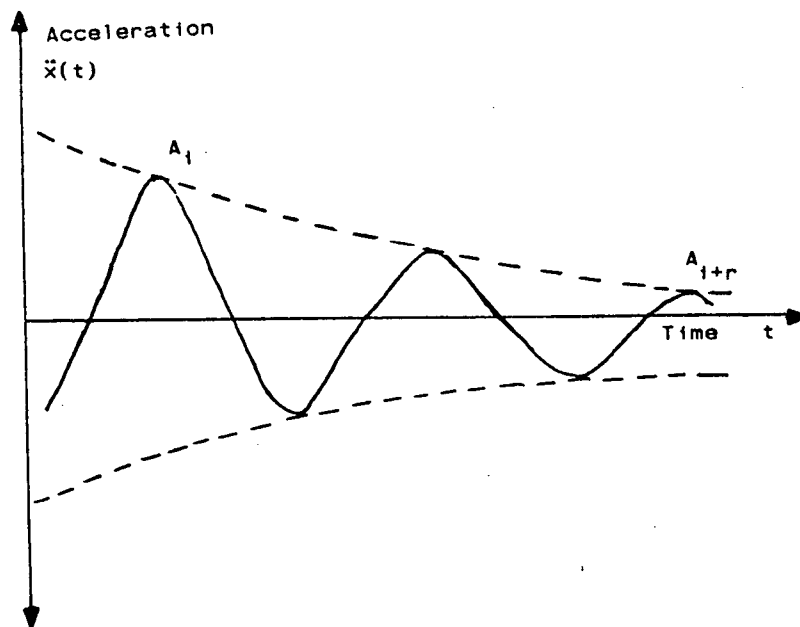
Figure 8.3 Typical-Acceleration-Decay Record

Figure 9.1 Moment Resisting Frame on Shaking Table
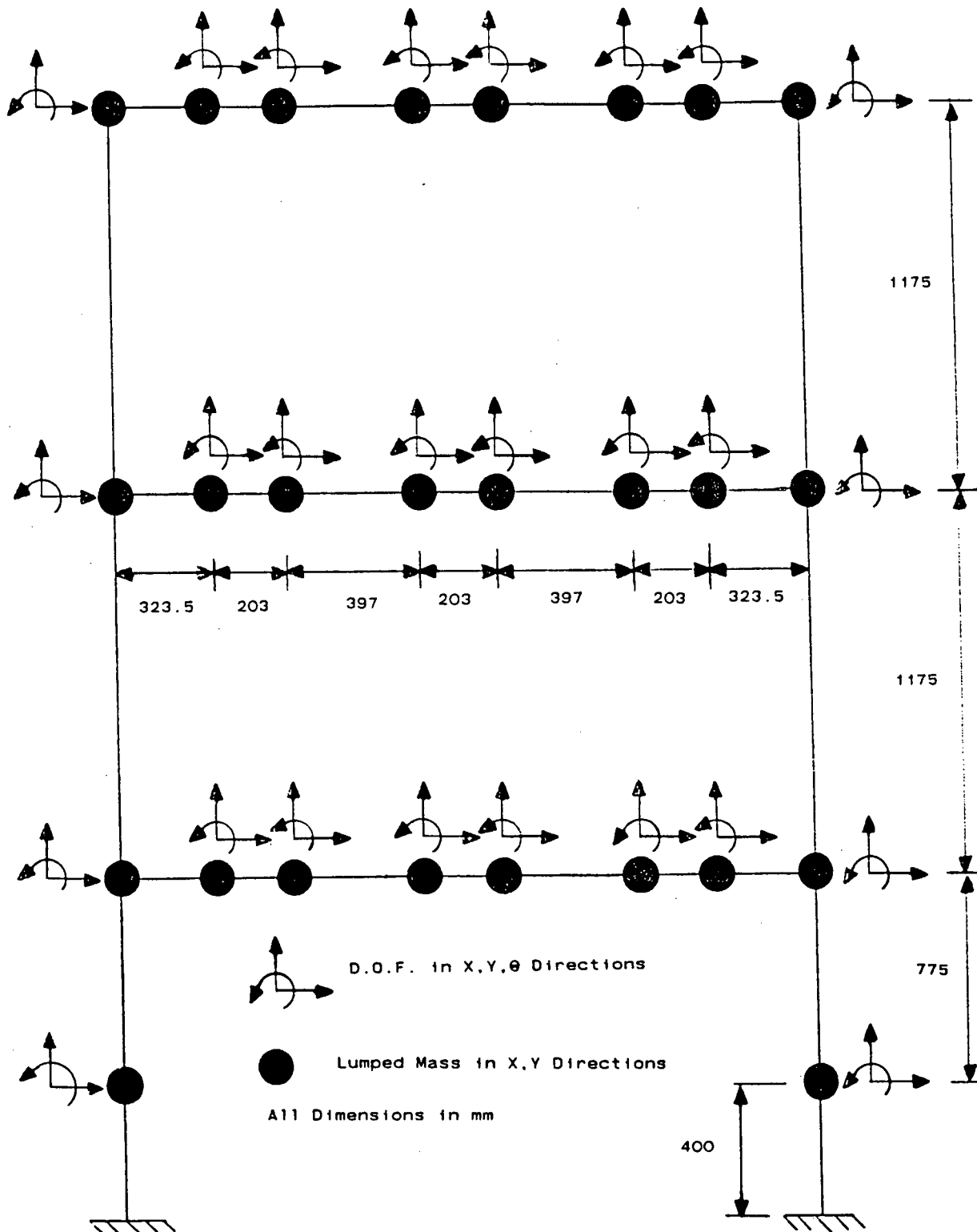
Figure 9.2 Computer Model Used for the Free Vibration Analysis of the Moment Resisting Frame

Mode#1, 17.788 rad/s

Mode#2, 57.642 rad/s

Mode#3, 87.336 rad/s

Mode#4, 95.756 rad/s

Mode#5, 99.965 rad/s

Mode#6, 100.091rad/s
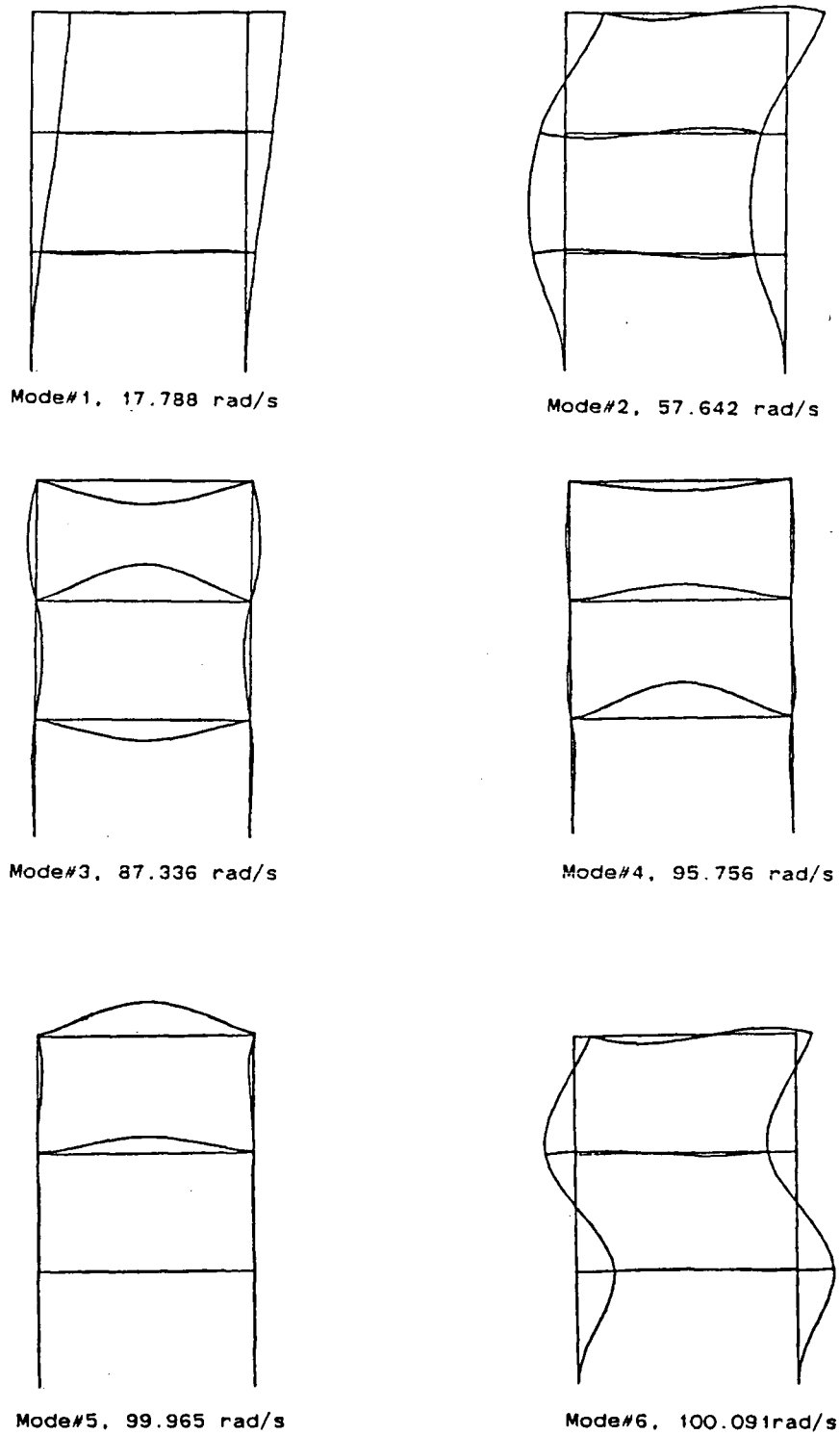
Figure 9.3 Predicted Natural Frequencies and Mode Shapes of the
Moment Resisting Frame
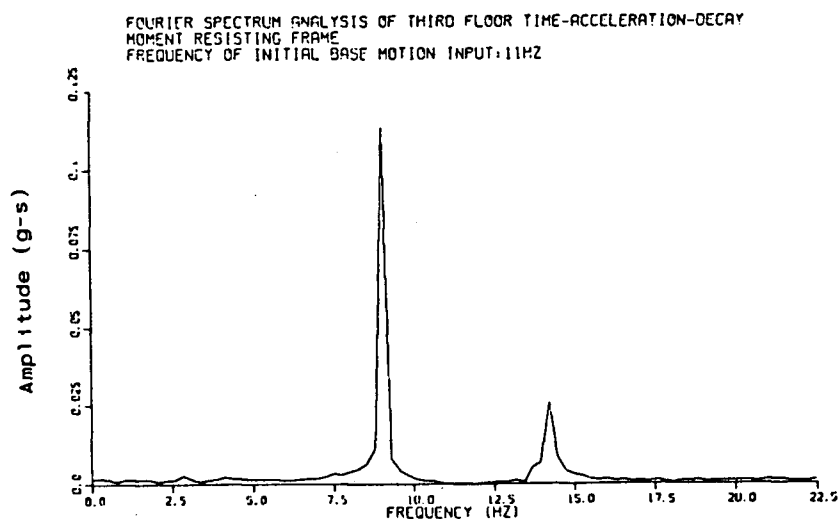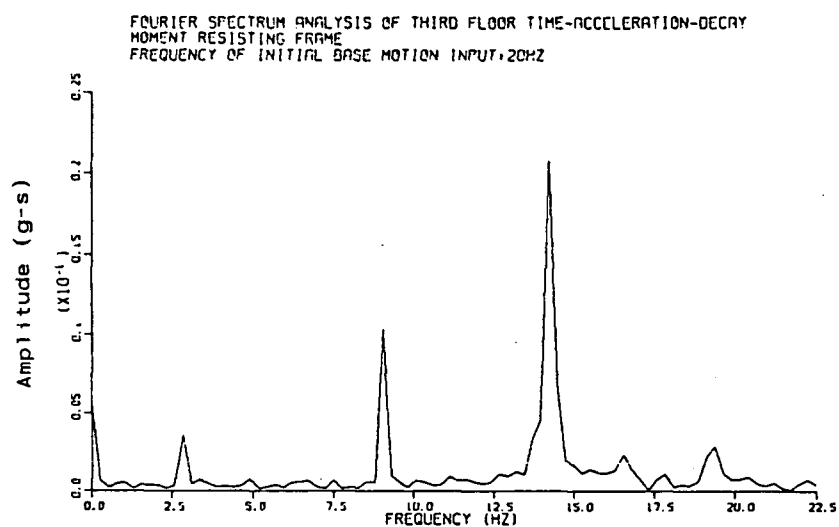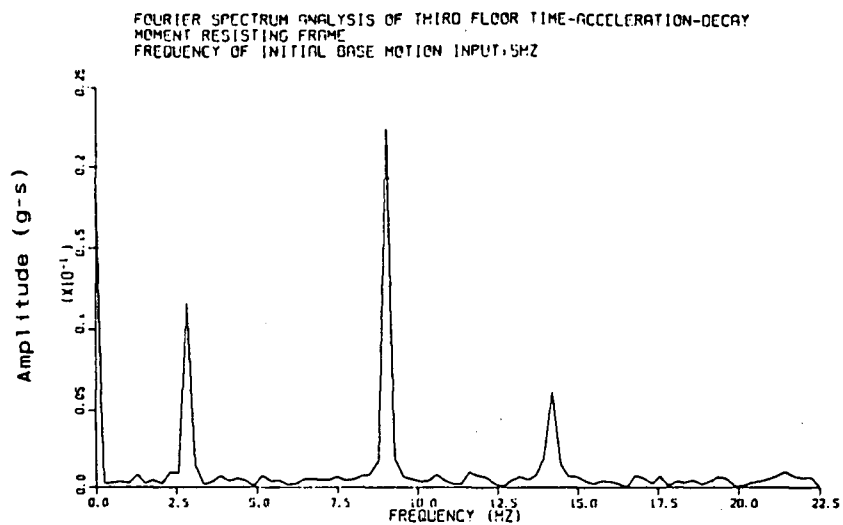
Figure 9.4 Fourier Spectrum Analysis of the Moment Resisting
Frame
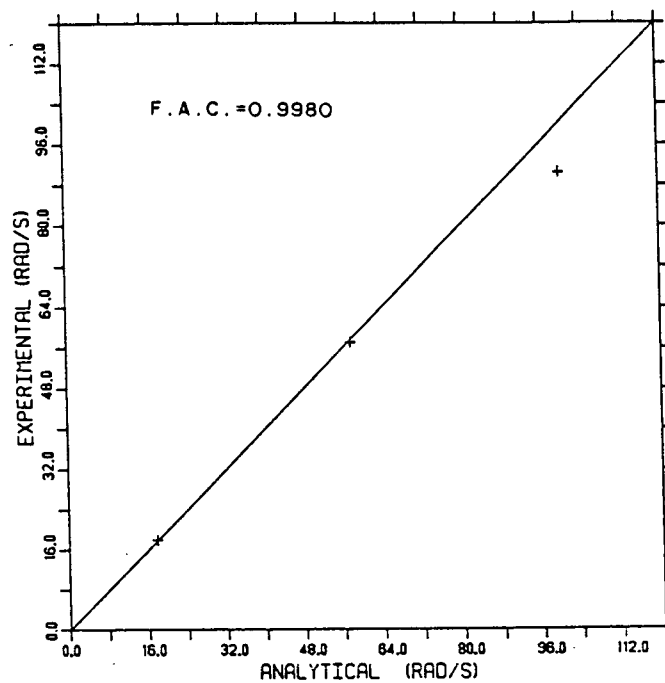
Figure 9.5 Measured vs Predicted Natural Frequencies of the Moment Resisting Frame
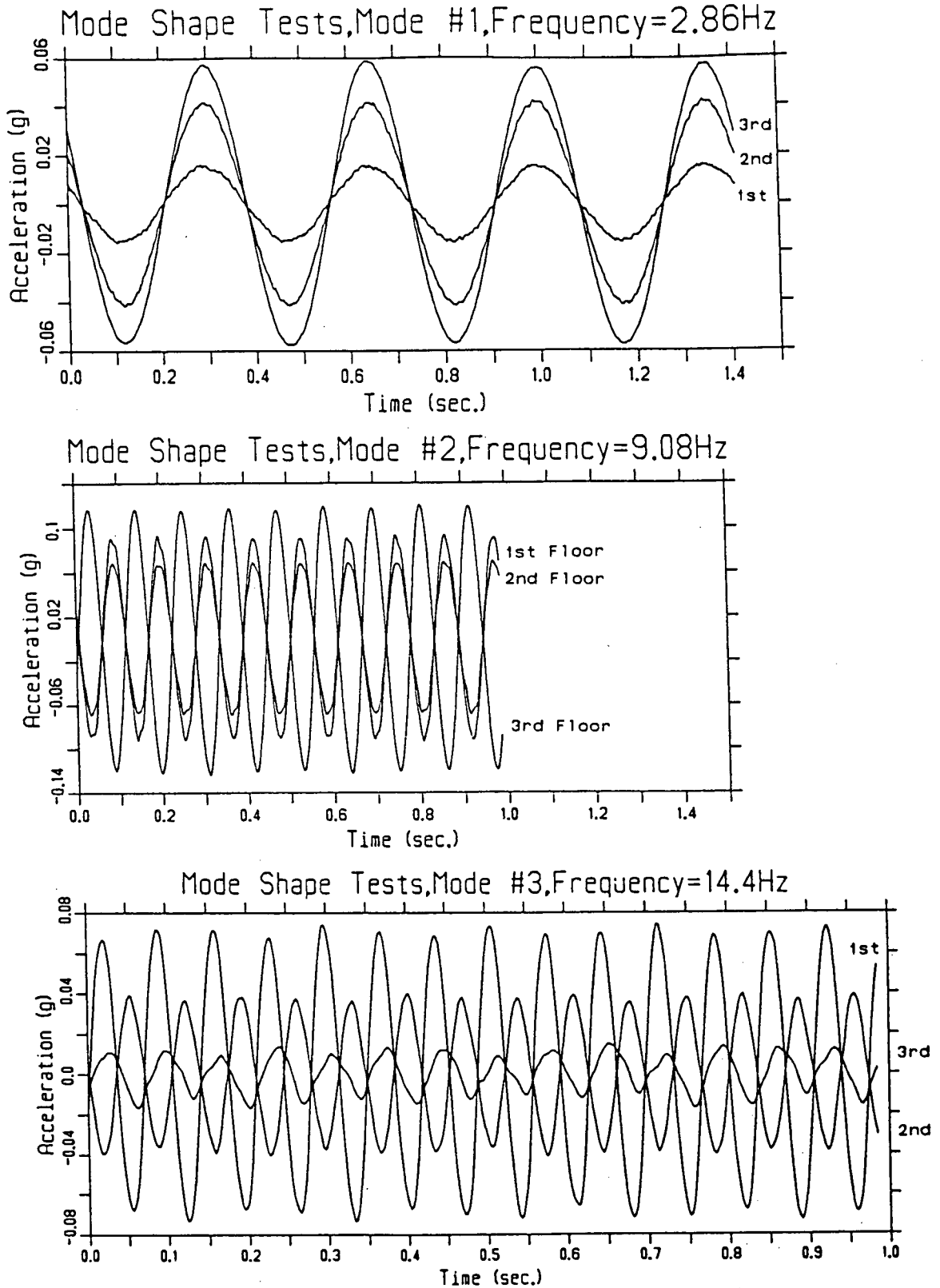
Figure 9.6 Estimation of Mode Shapes for the Moment Resisting Frame
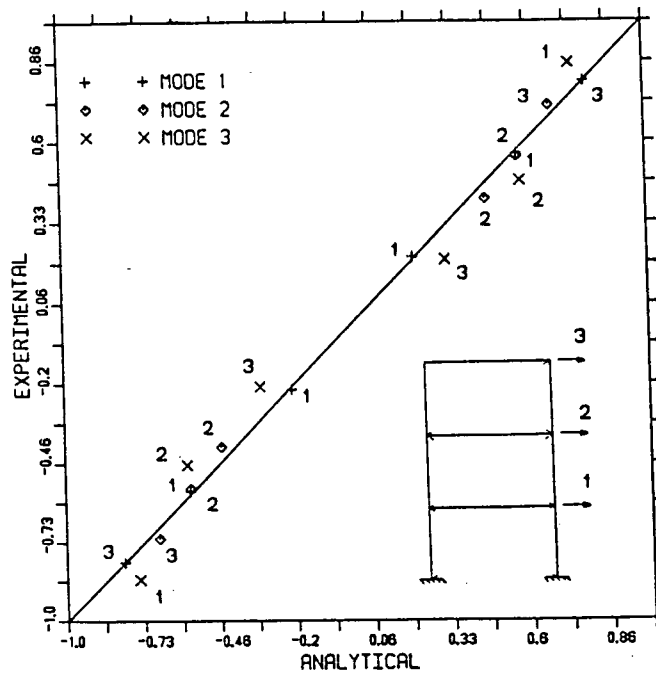
Figure 9.7 Measured vs Predicted Mode Shapes of the Moment Resisting Frame
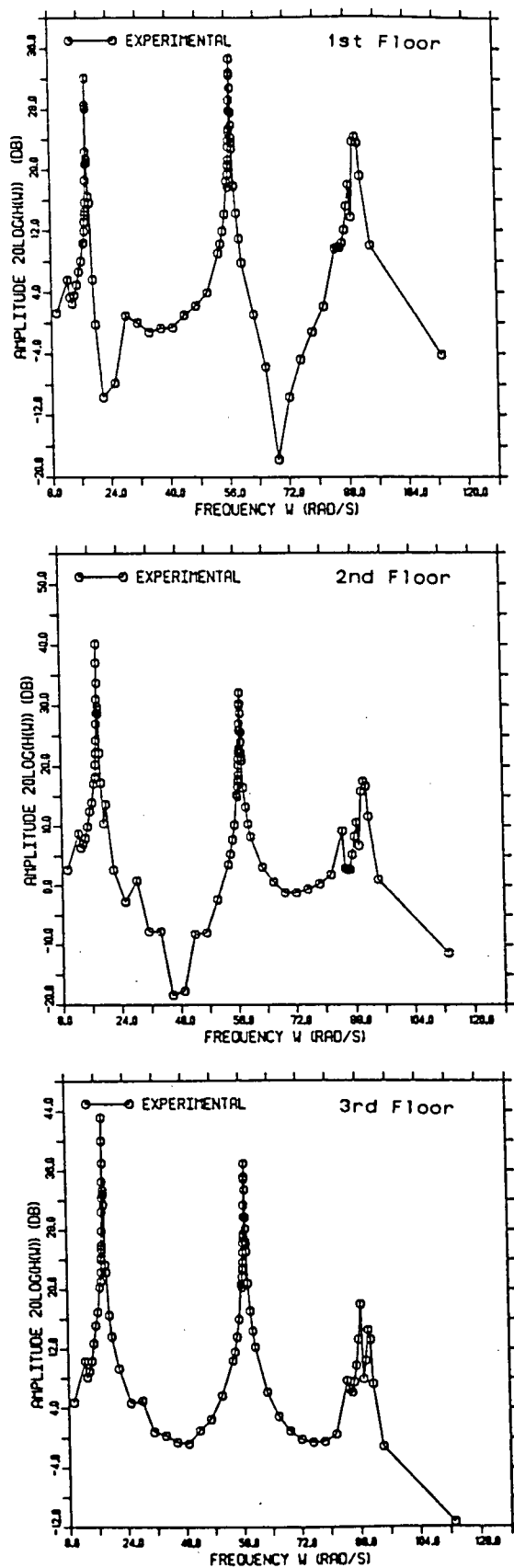
Figure 9.8 Experimental Mobility Functions for the Moment Resisting Frame
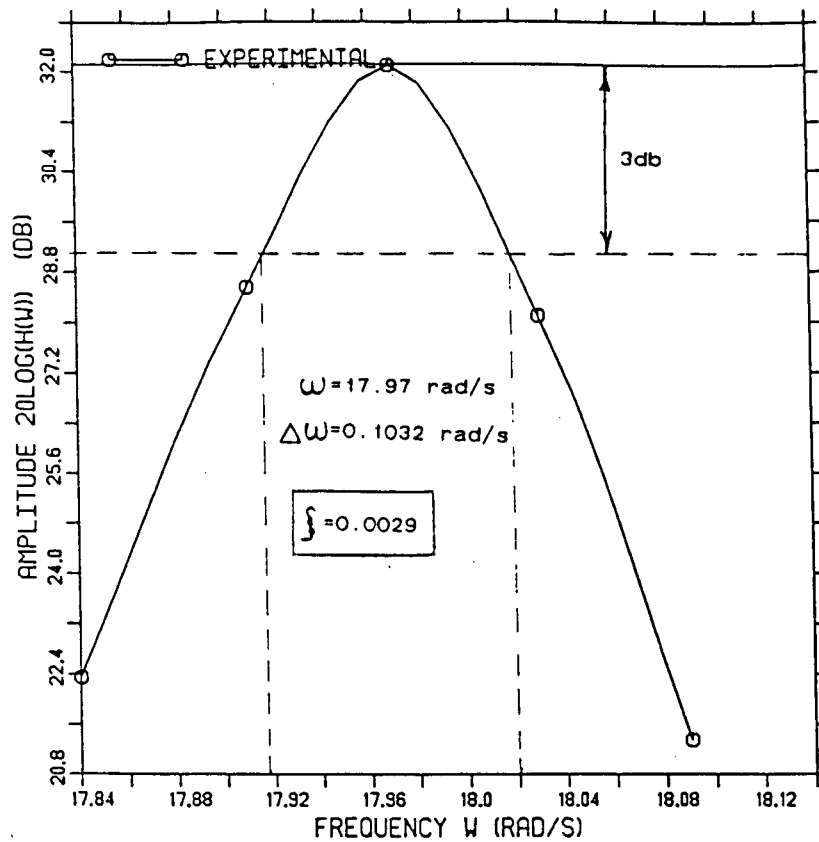
Figure 9.9 Bandwidth Method Applied to the First Floor Mobility Function of the Moment Resisting Frame
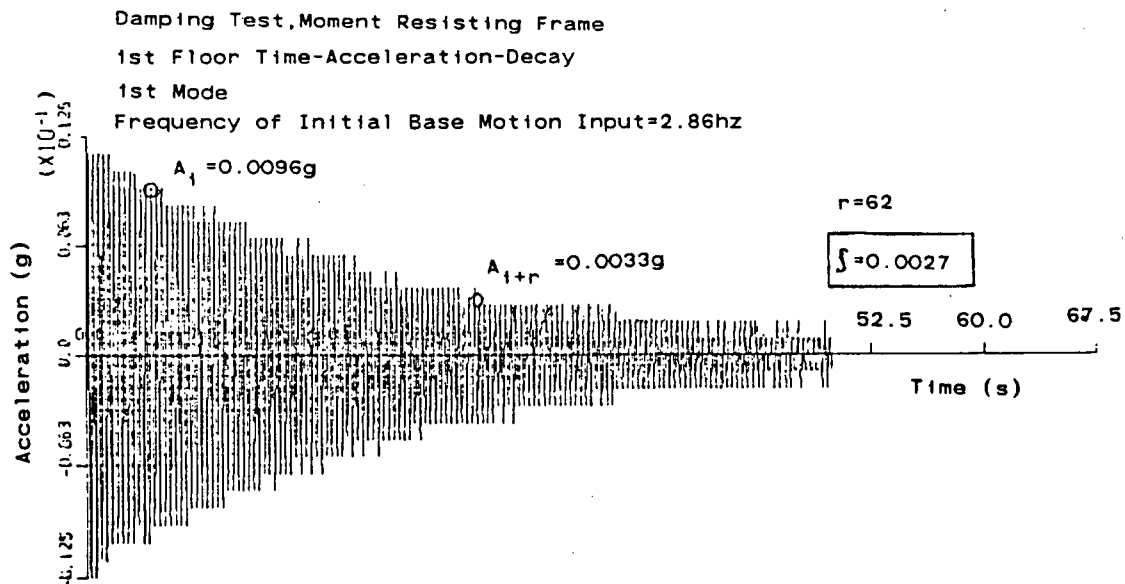
Figure 9.10 Logarithmic Decrement Method Applied to the First Floor Time-Acceleration-Decay of the Moment Resisting Frame
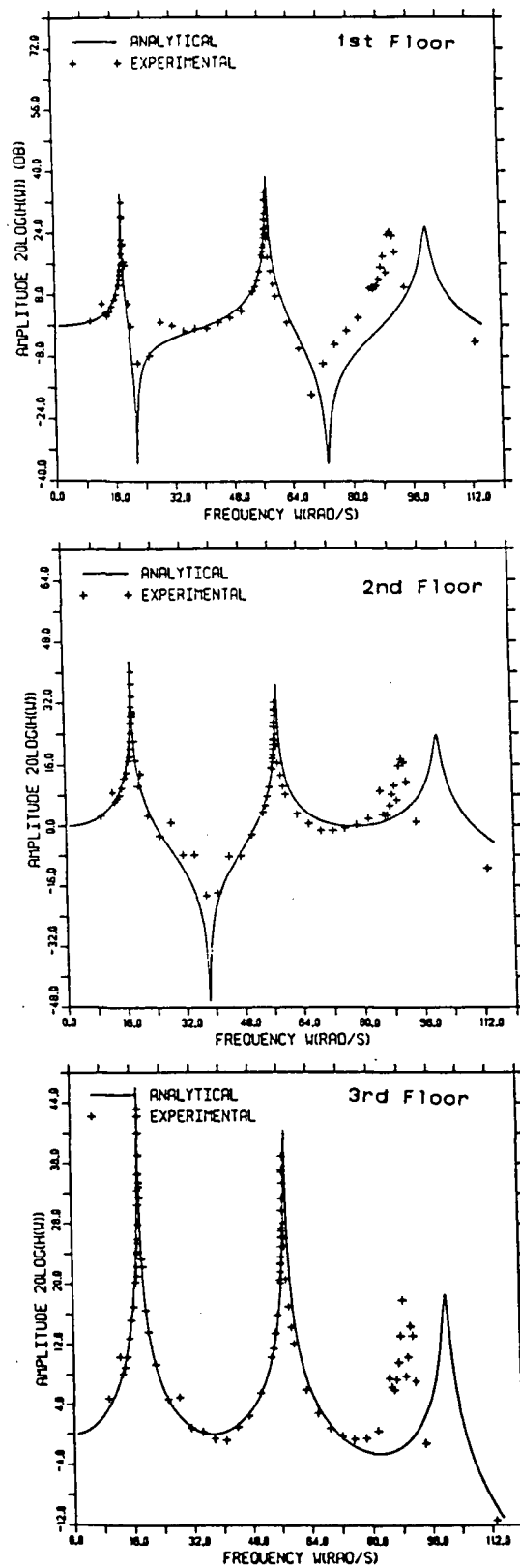
Figure 9.11 Predicted vs Measured Mobility Functions of the Moment Resisting Frame

174.
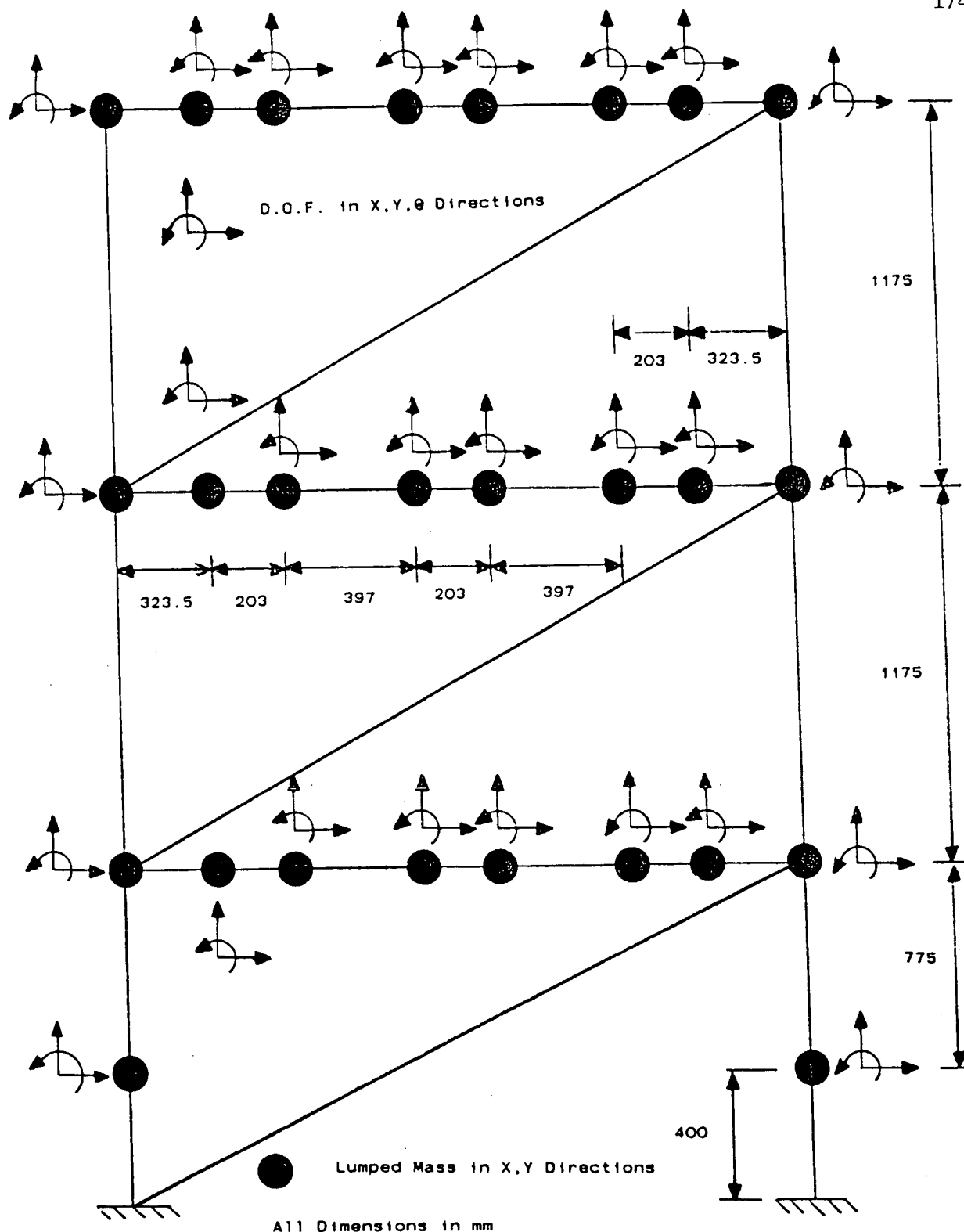
Figure 10.1 Computer Model Used for the Free Vibrations Analysis of the Braced Moment Resisting Frame
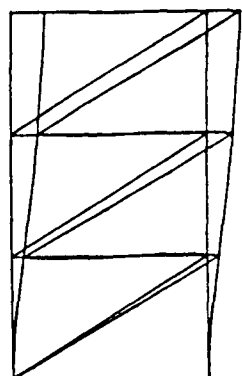
Mode #1, 31.962 rad/s
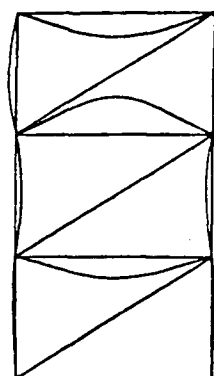
Mode #2, 87.331 rad/s
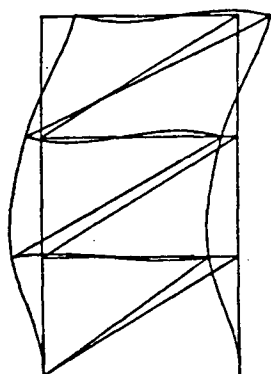
Mode #3, 91.617 rad/s
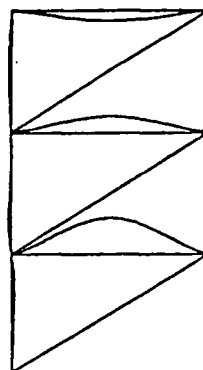
Mode #4, 95.730 rad/s
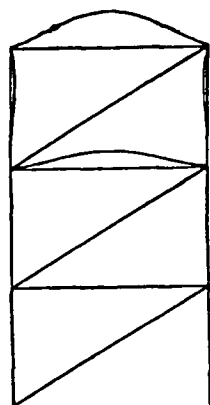
Mode #5, 99.956 rad/s
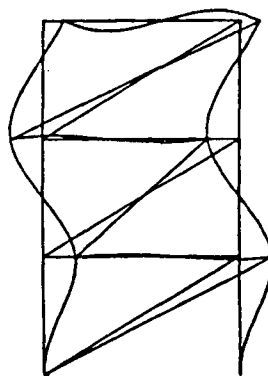
Mode #6, 138.389 rad/s

Figure 10.2 Predicted Natural Frequencies and Mode Shapes of the Braced Moment Resisting Frame

FOURIER SPECTRUM ANALYSIS OF THIRD FLOOR TIME-ACCELERATION-DECAY
BRACED MOMENT RESISTING FRAME
FREQUENCY OF INITIAL BASE MOTION INPUT:18HZ
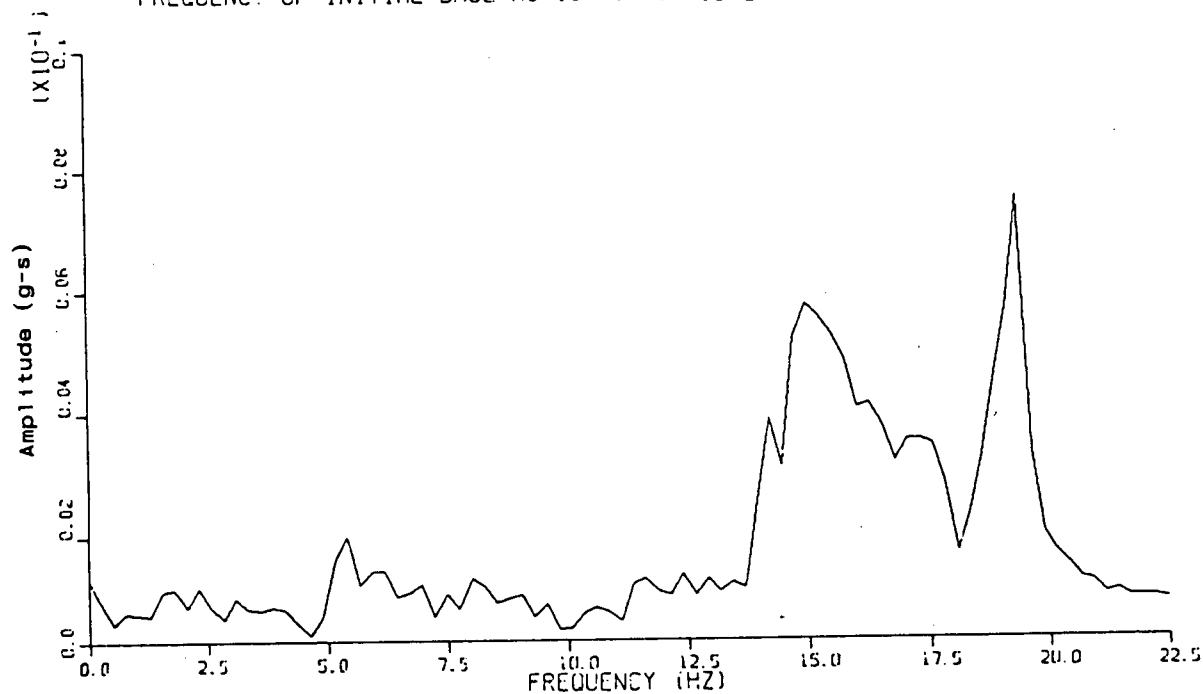
FOURIER SPECTRUM ANALYSIS OF THIRD FLOOR TIME-ACCELERATION-DECAY
BRACED MOMENT RESISTING FRAME
FREQUENCY OF INITIAL BASE MOTION INPUT:8HZ
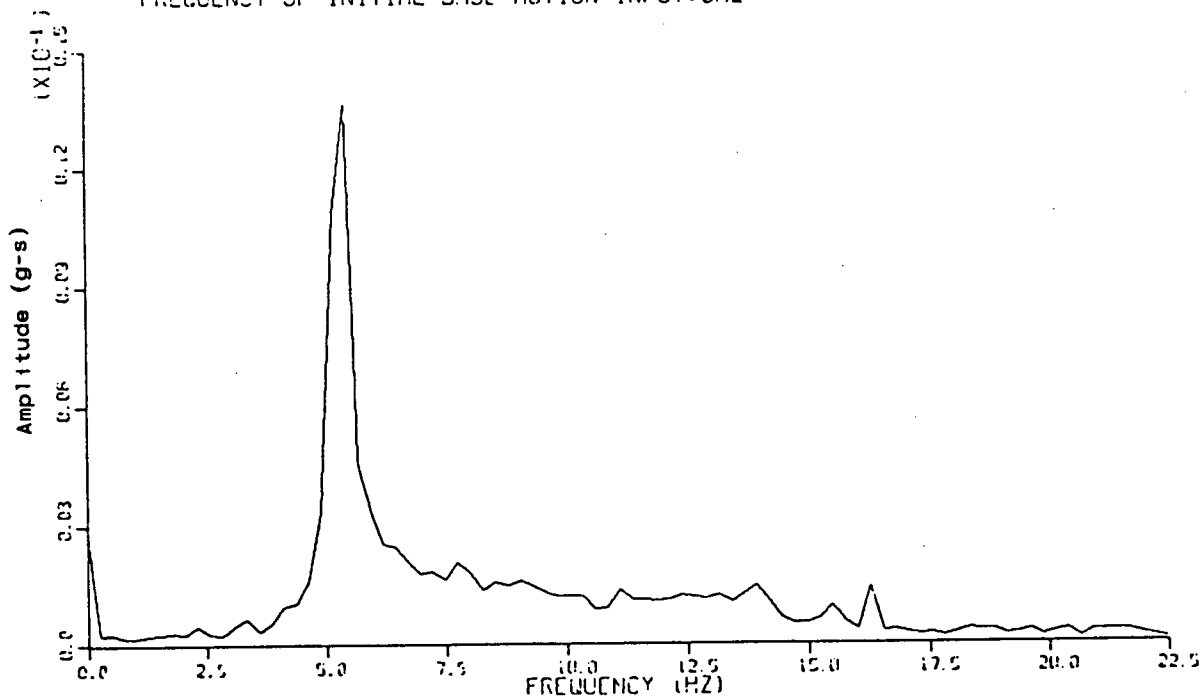
Figure 10.3 Fourier Spectrum Analysis of the Braced Moment
Resisting Frame
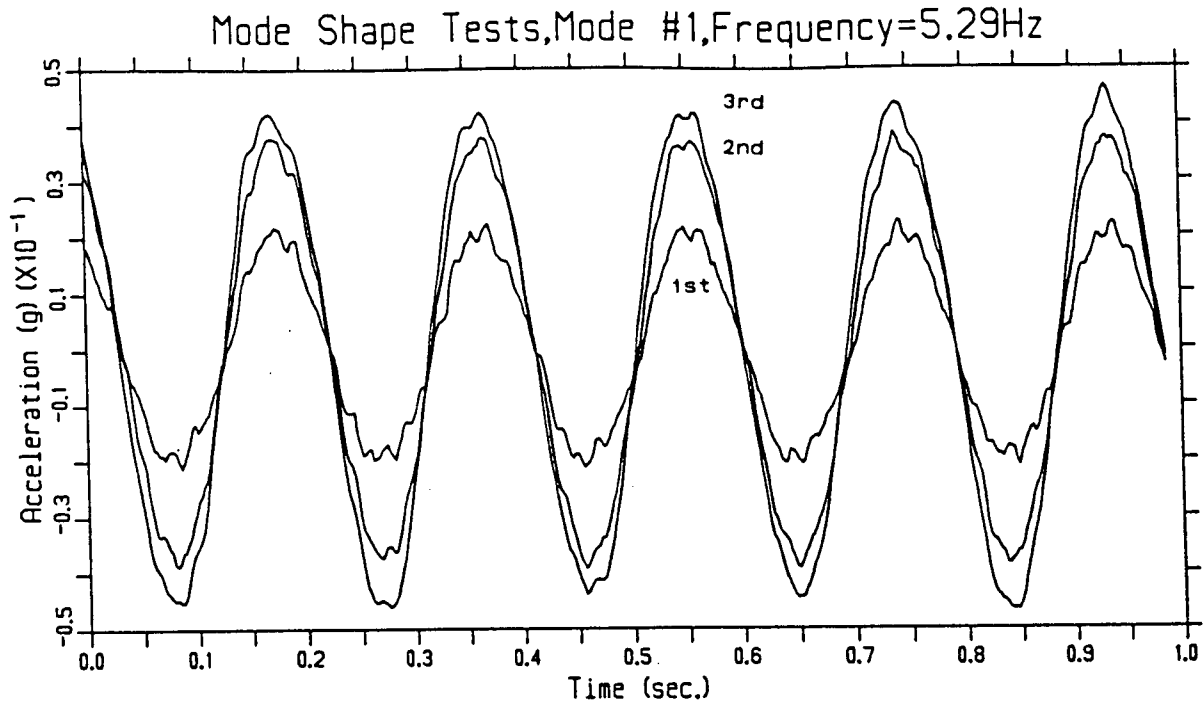
Figure 10.4 Estimation of Mode Shapes for the Braced Moment
Resisting Frame
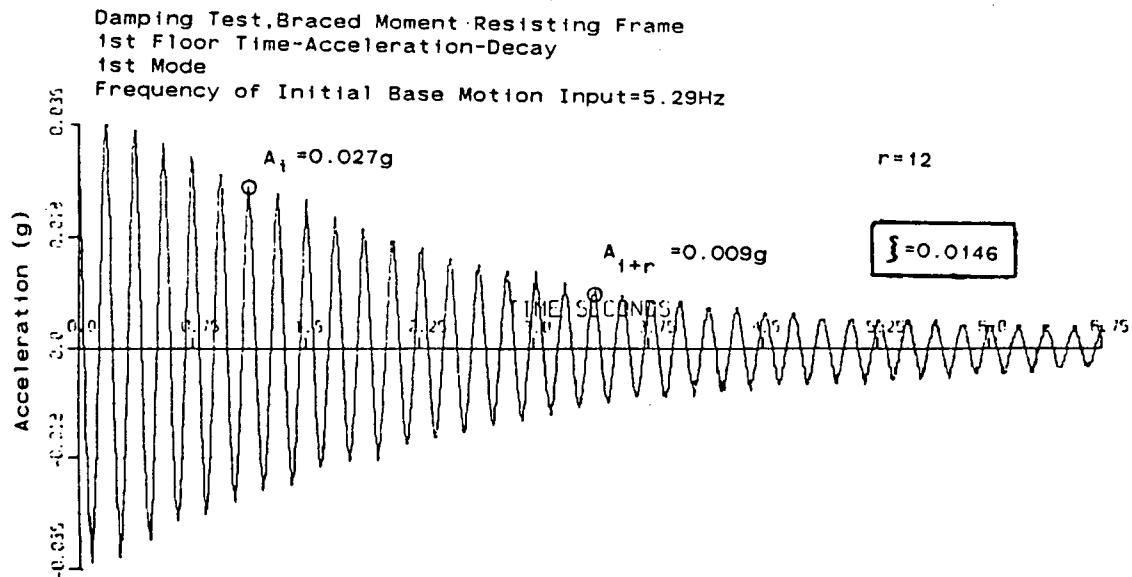
Figure 10.5 Logarithmic Decrement Method Applied on the First
Floor Time-Acceleration-Decay of the Braced Moment Resisting
Frame
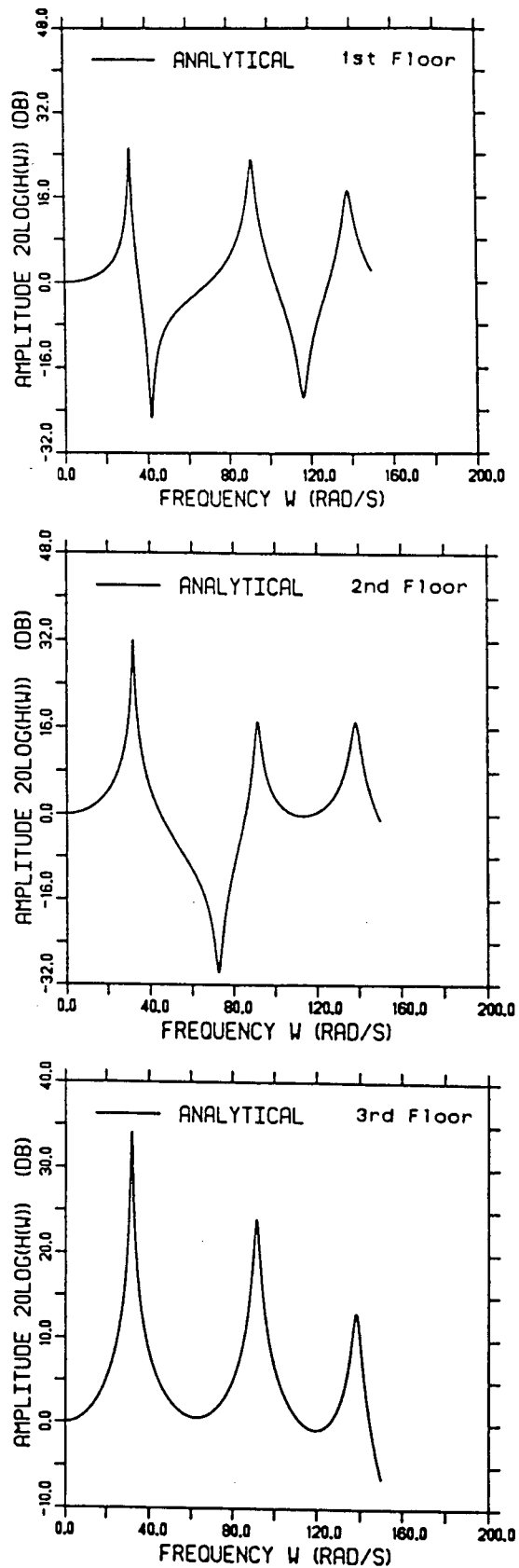
Figure 10.6 Predicted Mobility Functions of the Braced Moment Resisting Frame
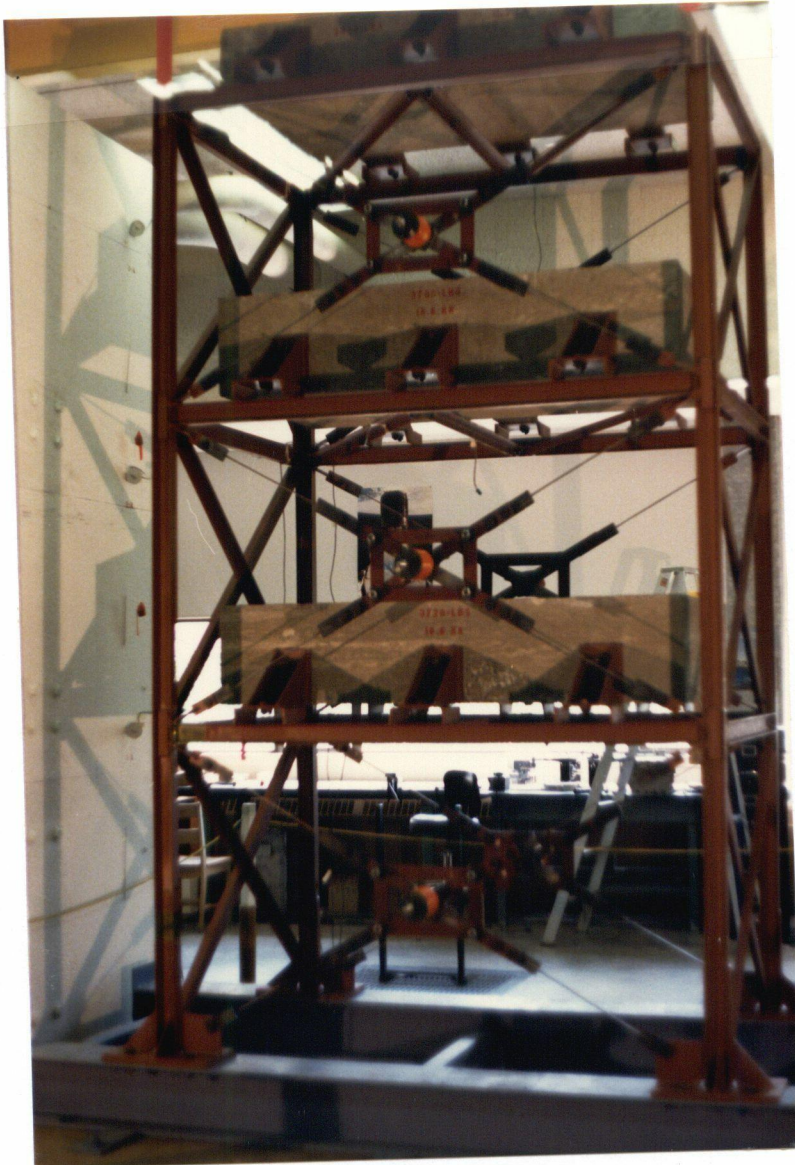
Figure 11.1 Friction Damped Braced Frame on Shaking Table
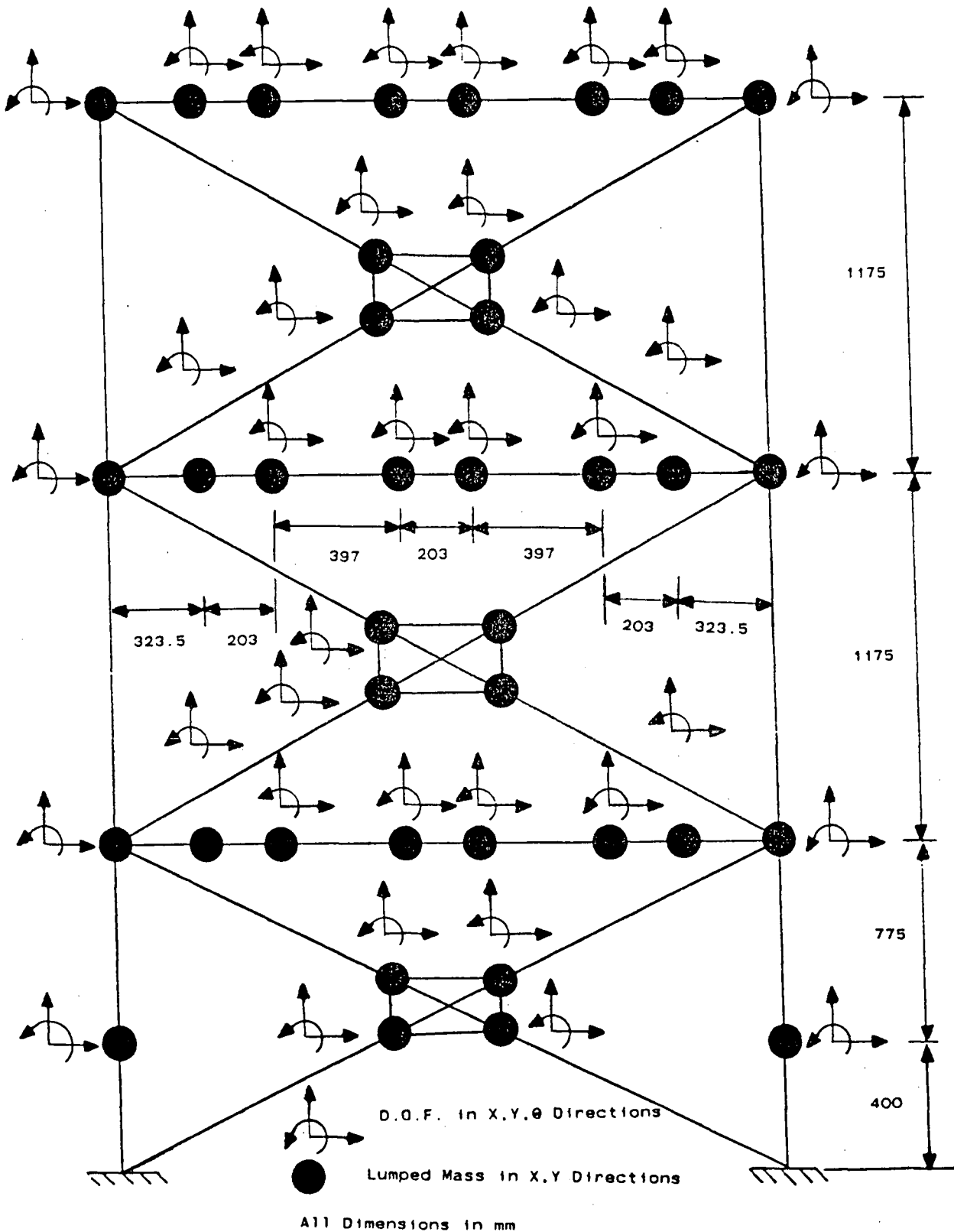
Figure 11.2 Computer Model Used for the Free Vibrations Analysis of the Friction Damped Braced Frame Under Low Amplitude Excitations
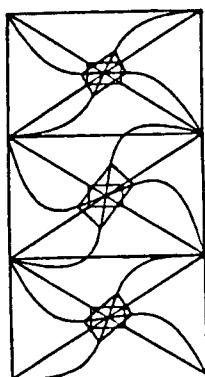
Mode#1, 24.448 rad/s
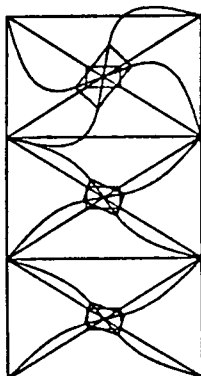
Mode#2, 24.746 rad/s
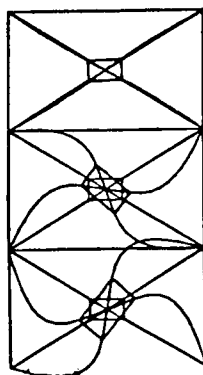
Mode#3, 24.829 rad/s

Figure 11.3 Predicted Natural Frequencies and Mode Shapes of the Friction Damped Braced Frame Under Low Amplitude Excitation,Modes#1-#3
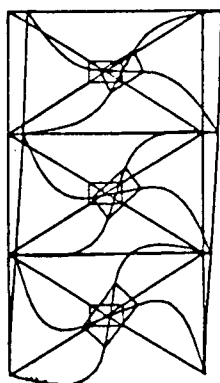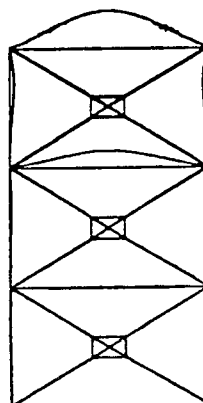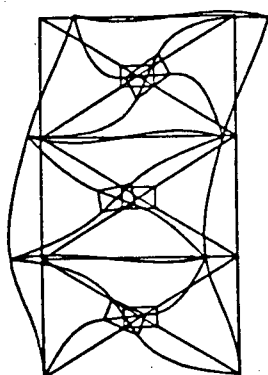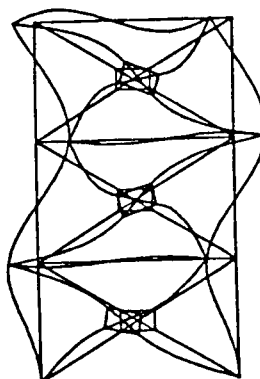
Mode#4, 44.059 rad/s
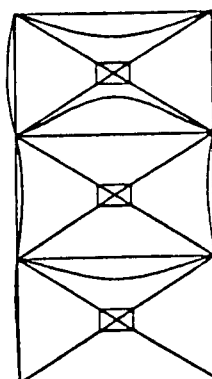
Mode#5, 87.332 rad/s
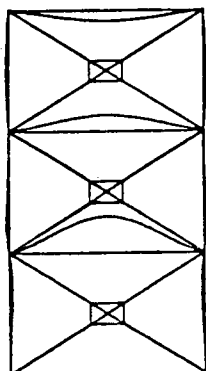
Mode#6, 95.732 rad/s
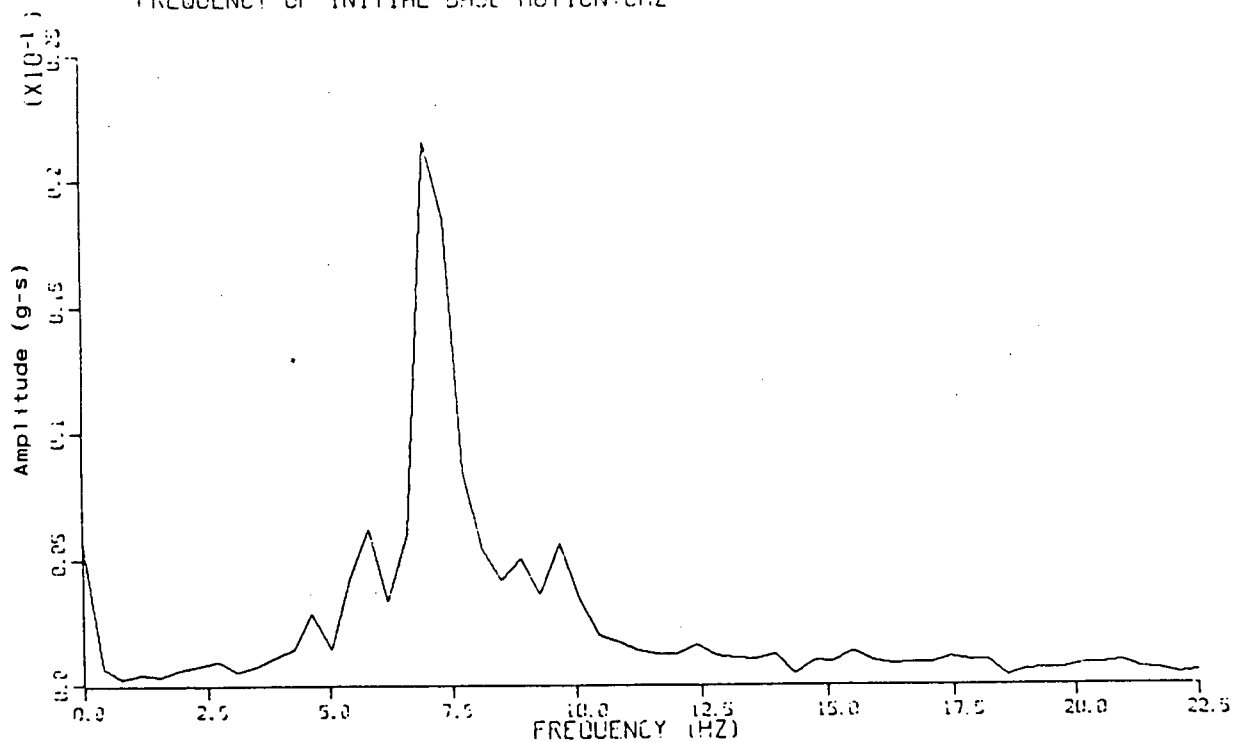
Mode#7, 99.956 rad/s

Mode#8, 122.348 rad/s

Mode#9, 177.919 rad/s

Figure 11.4 Predicted Natural Frequencies and Mode Shapes of the Friction Damped Braced Frame Under Low Amplitude Excitation,Modes#4-#9

FOURIER SPECTRUM ANALYSIS OF THIRD FLOOR TIME-ACCELERATION-DECAY
FRICTION DAMPED BRACED FRAME
FREQUENCY OF INITIAL BASE MOTION:8HZ

FOURIER SPECTRUM ANALYSIS OF THIRD FLOOR TIME-ACCELERATION-DECAY
FRICTION DAMPED BRACED FRAME
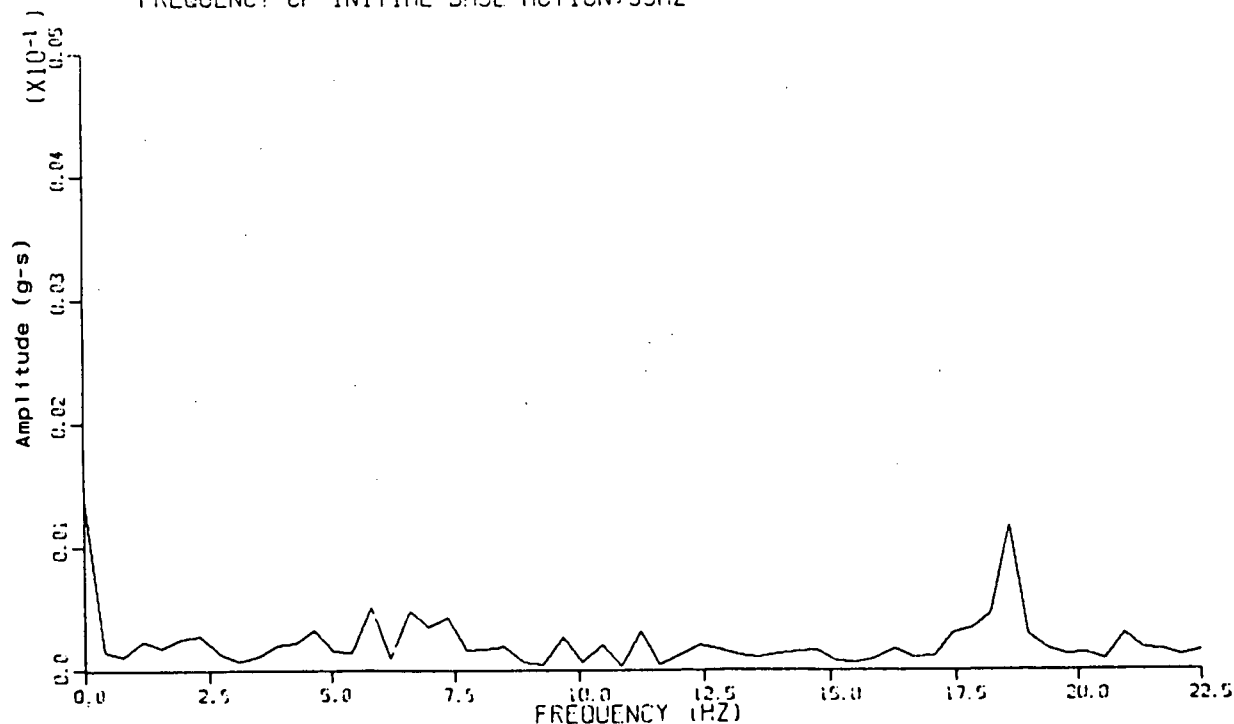FREQUENCY OF INITIAL BASE MOTION:35HZ

Figure 11.5 Fourier Spectrum Analysis of the Friction Damped
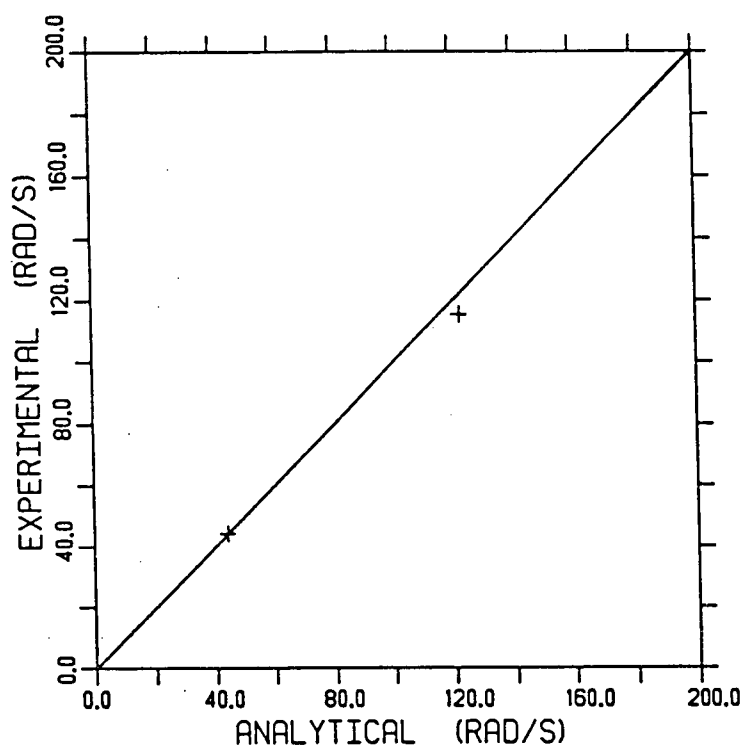Braced Frame Under Low Amplitude Excitations

Figure 11.6 Measured vs Predicted Natural Frequencies of the Friction Damped Braced Frame Under Low Amplitude Excitations
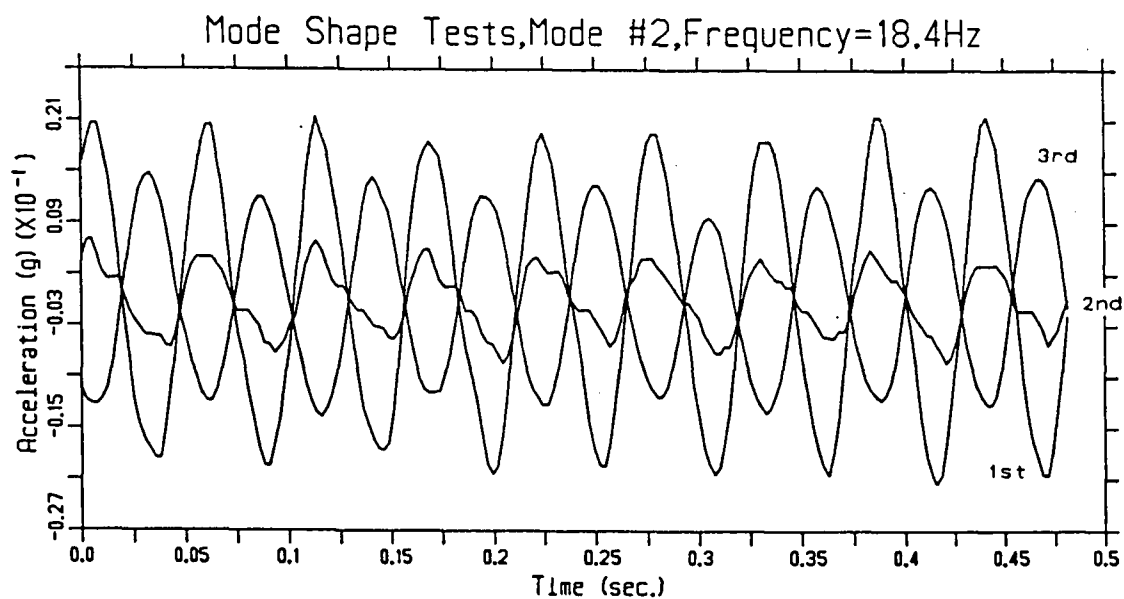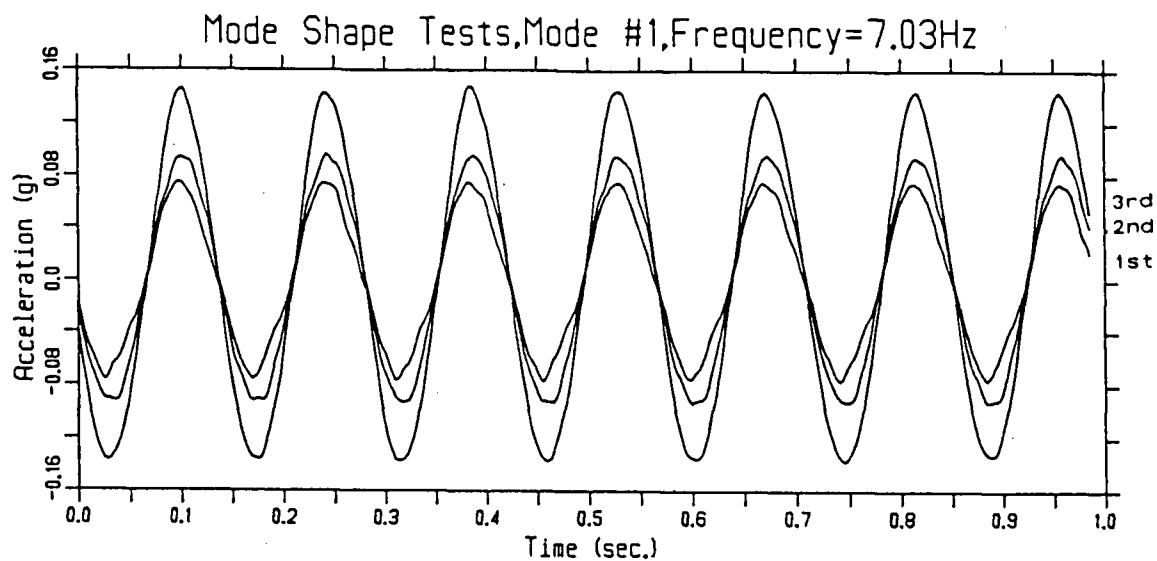
Figure 11.7 Estimation of Mode Shapes for the Friction Damped Braced Frame Under Low Amplitude Excitations
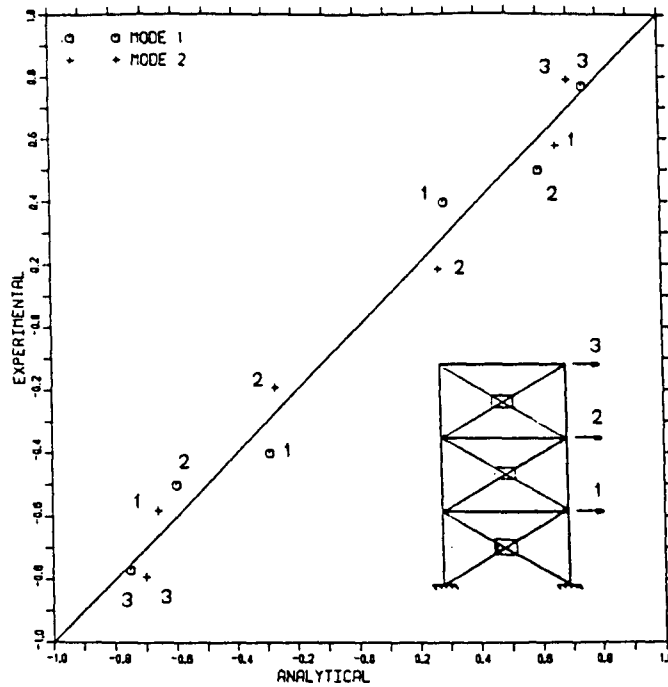
Figure 11.8 Measured vs Predicted Mode Shapes of the Friction Damped Braced Frame Under Low Amplitude Excitations
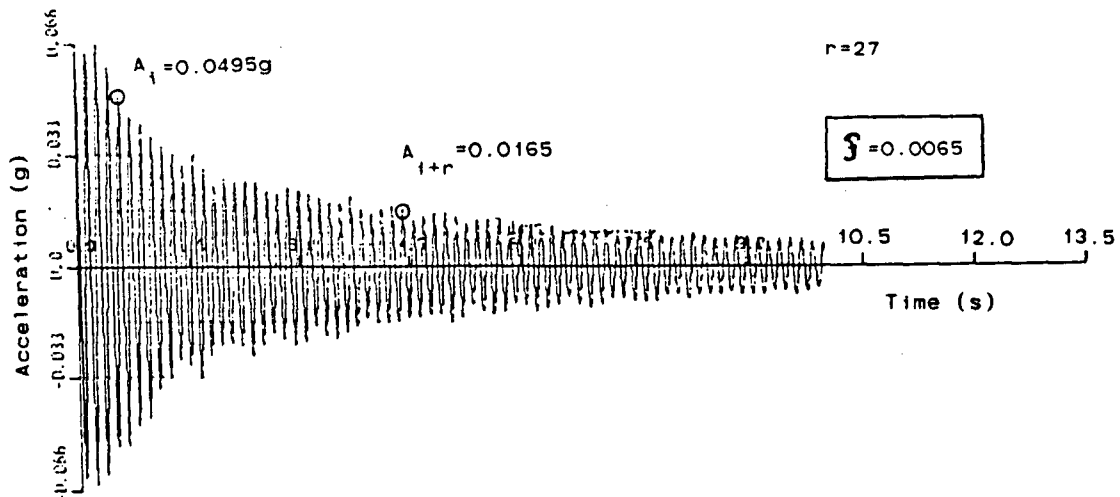
Figure 11.9 Logarithmic Decrement Method Applied to the First Floor Time-Acceleration-Decay of the Friction Damped Braced Frame

(a) Moment Resisting Frame

Intensity 1
Mmax/Mp=0.34

Intensity 2
Mmax/Mp=0.57

Intensity 3
Mmax/Mp=1.00

(b) Braced Moment Resisting Frame

Intensity 1
Mmax/Mp=0.16
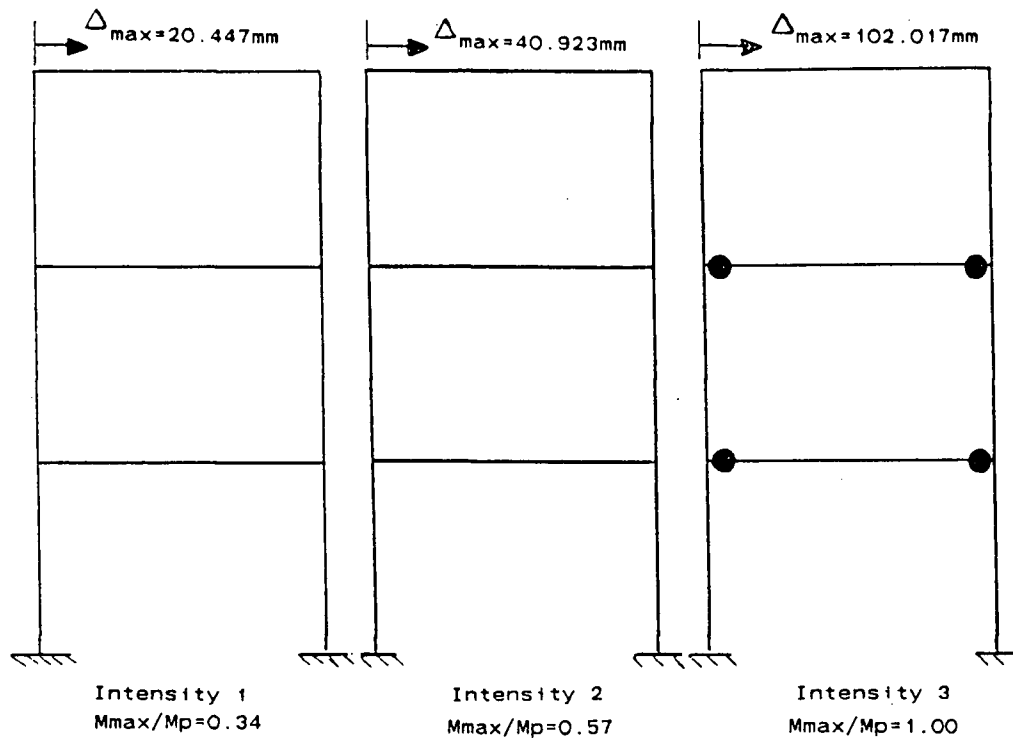
Intensity 2
Mmax/Mp=0.20

Intensity 3
Mmax/Mp=0.36
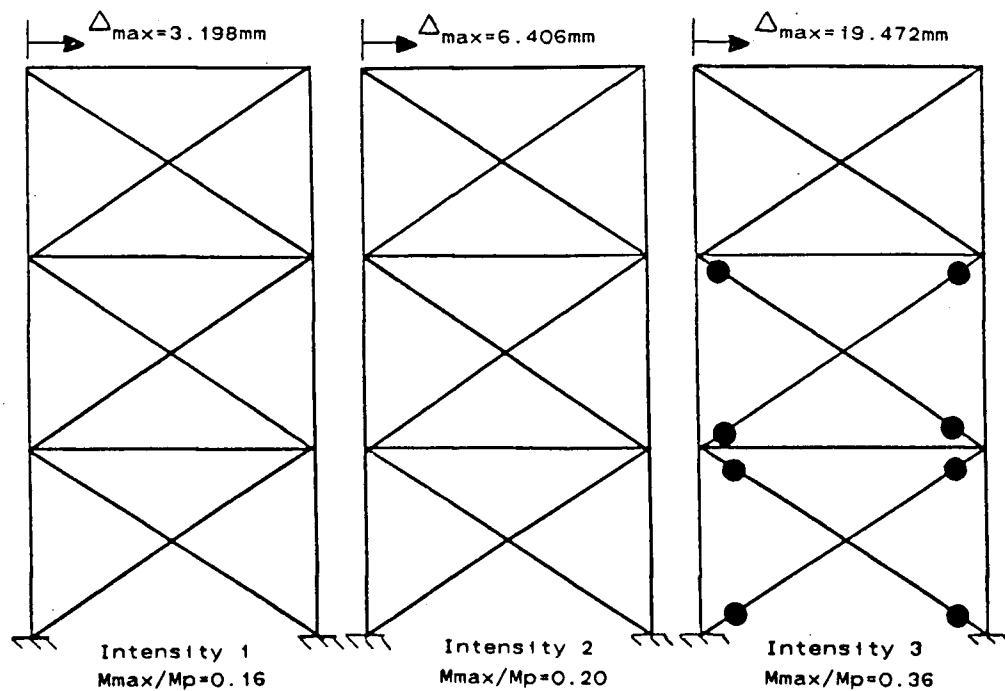
Figure 12.1 Predicted Structural Damage After Artificial Earthquake, Intensities 1,2,3

Figure 12.2 Shaking Table Performance, Newmark-Blume-Kapur Artificial Earthquake
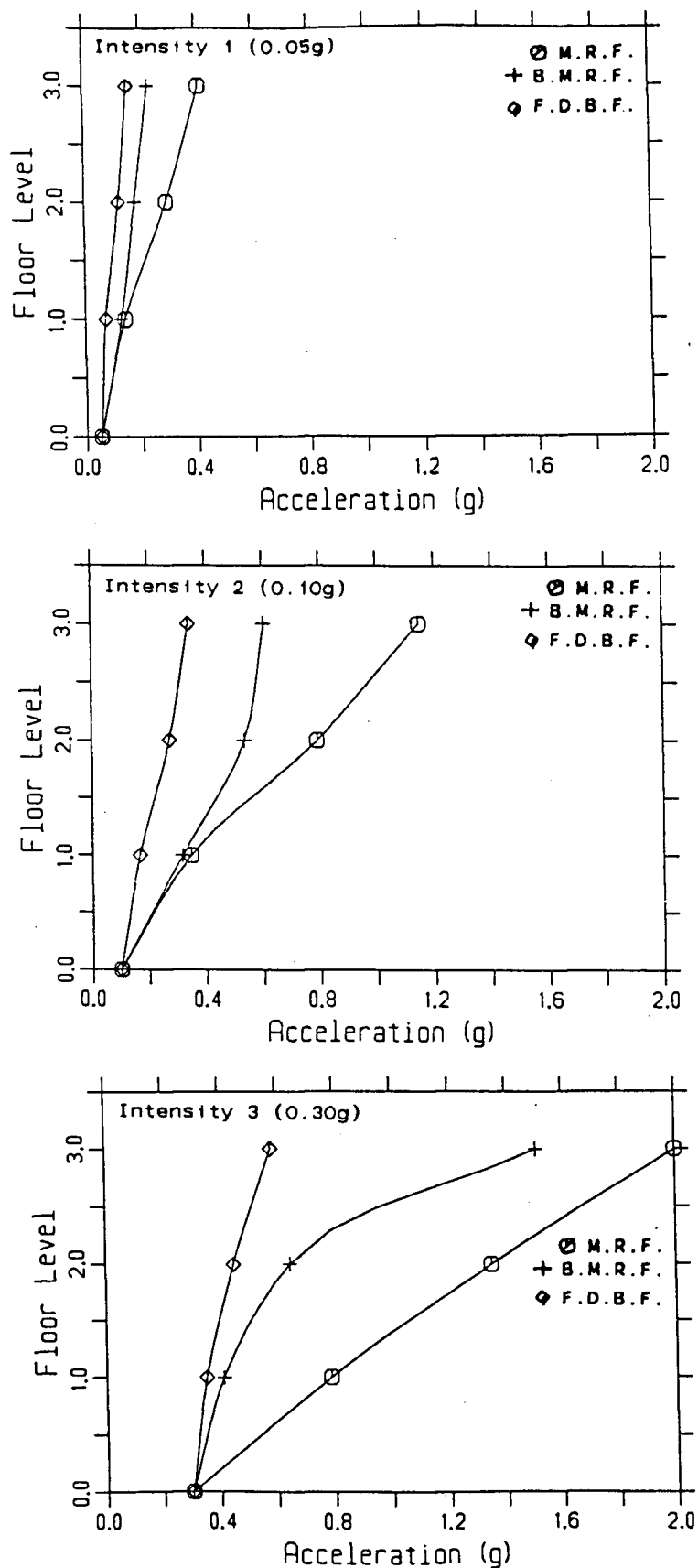
Figure 12.3 Envelopes of Measured Horizontal Accelerations, Newmark-Blume-Kapur Artificial Earthquake,Intensities 1,2,3
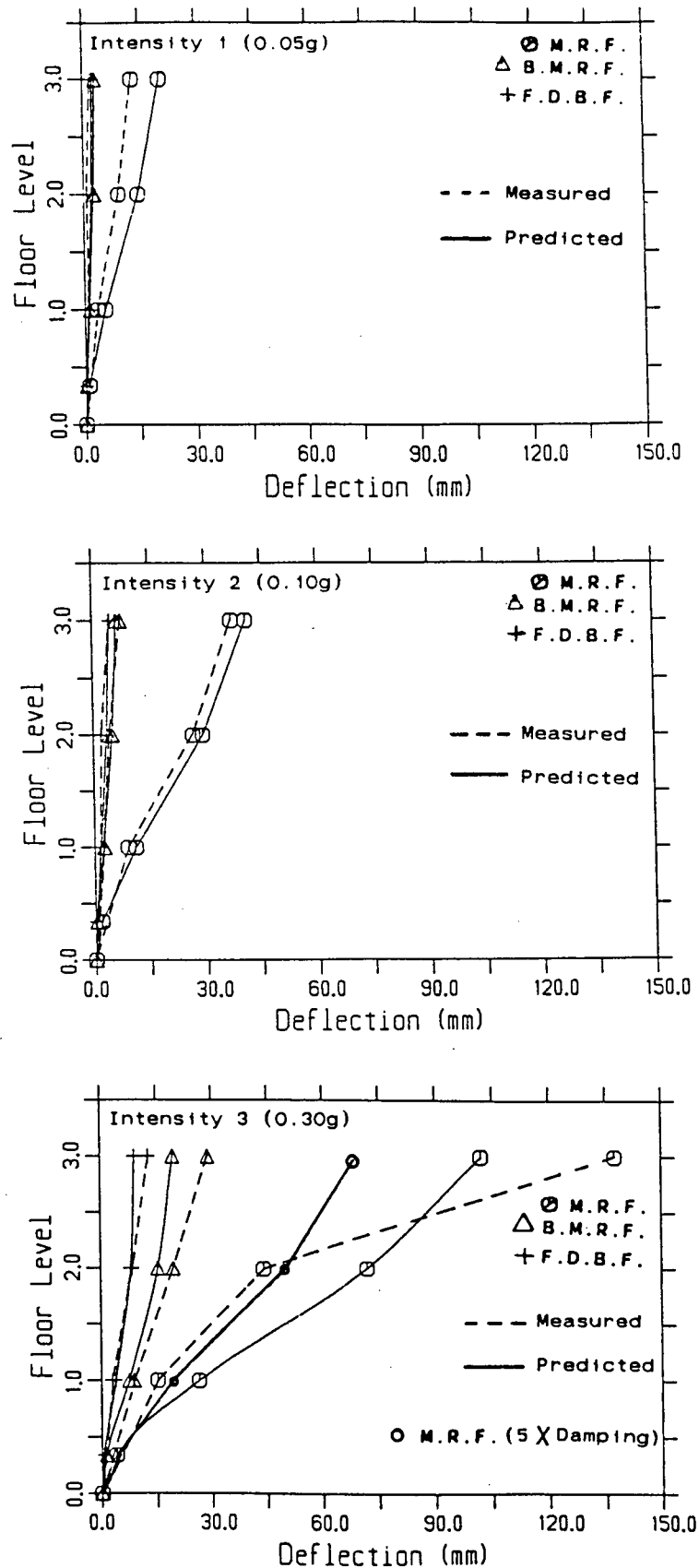
Figure 12.4 Envelopes of Lateral Deflections,Newmark-Blume-Kapur
Artificial Earthquake,Intensities 1,2,3
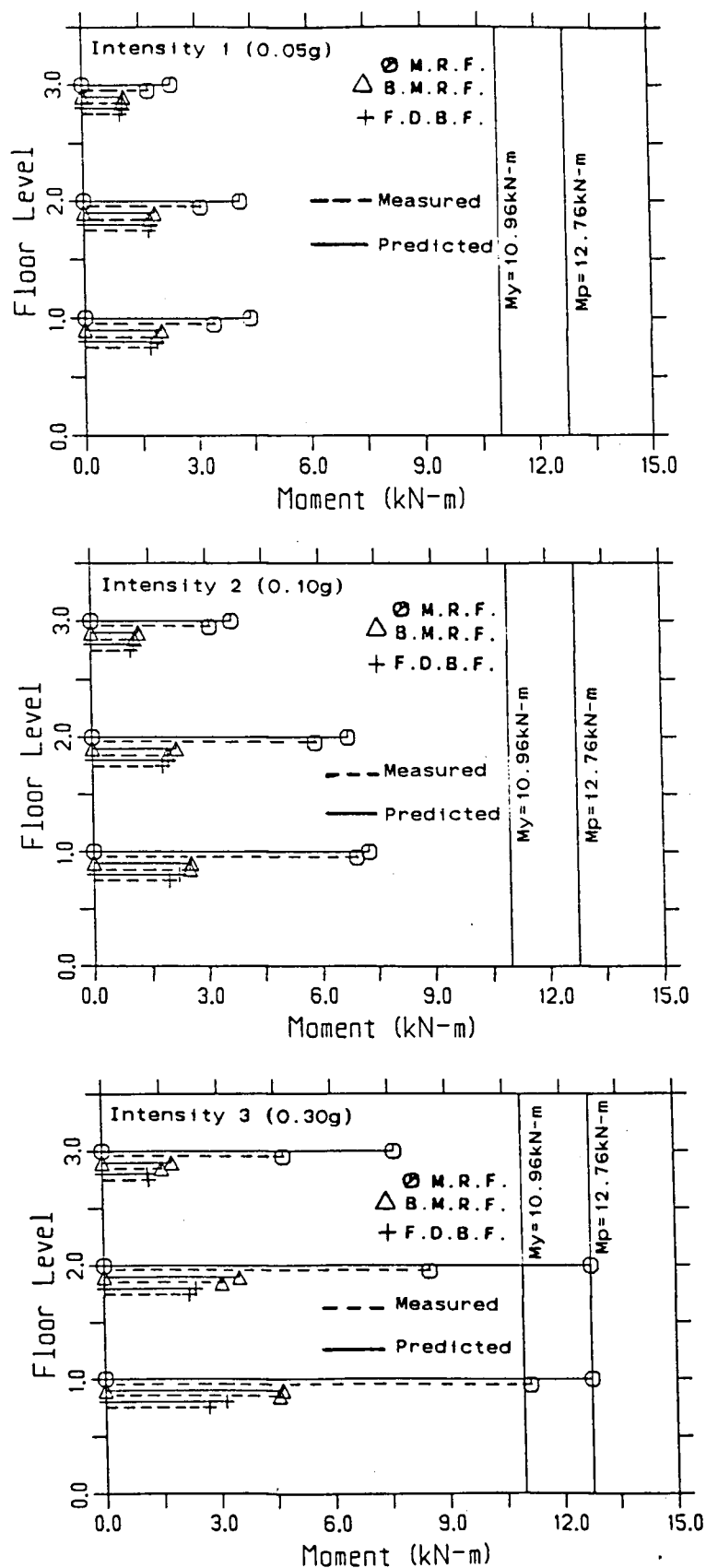
Figure 12.5 Envelopes of Bending Moments in the Beams,Newmark-Blume-Kapur Artificial Earthquake,Intensities 1,2,3

(a) Moment Resisting Frame

(b) Braced Moment Resisting Frame

(c) Friction Damped Braced Frame
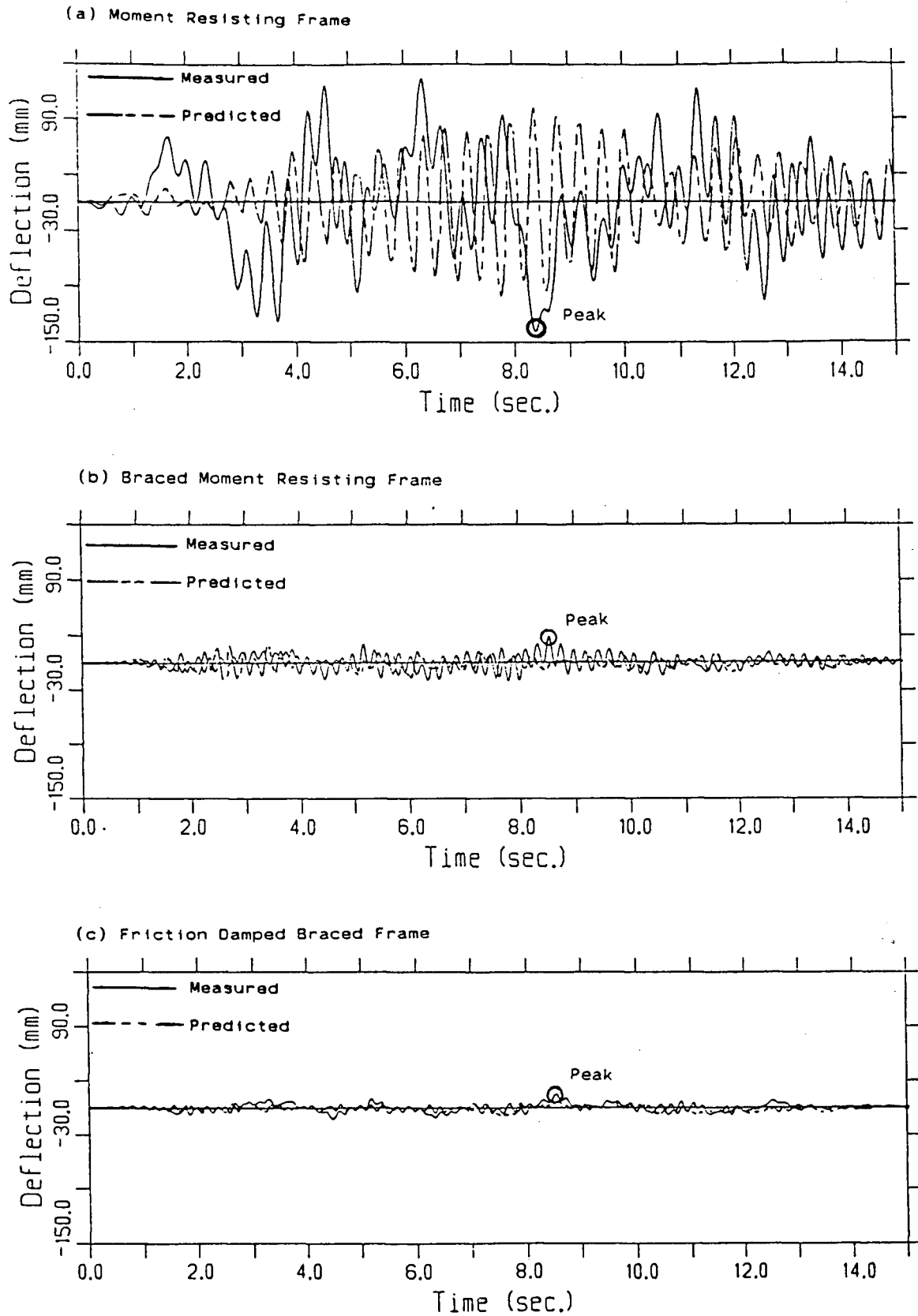
Figure 12.6 Time-Histories of Third Floor Deflection, Newmark-Blume-Kapur Artificial Earthquake, Intensity 3
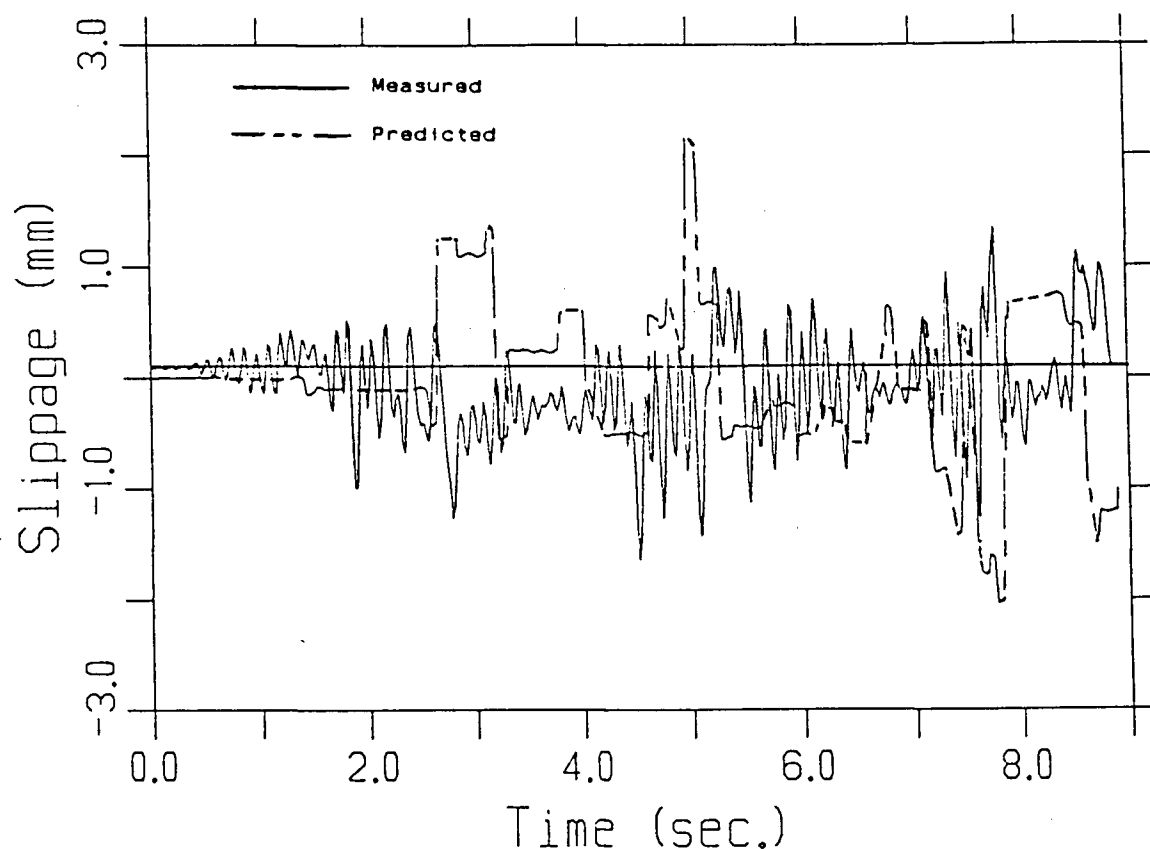
Figure 12.7 Slippage Time-Histories of Second Floor Device,Newmark-Blume-Kapur Artificial Earthquake,Intensity 3
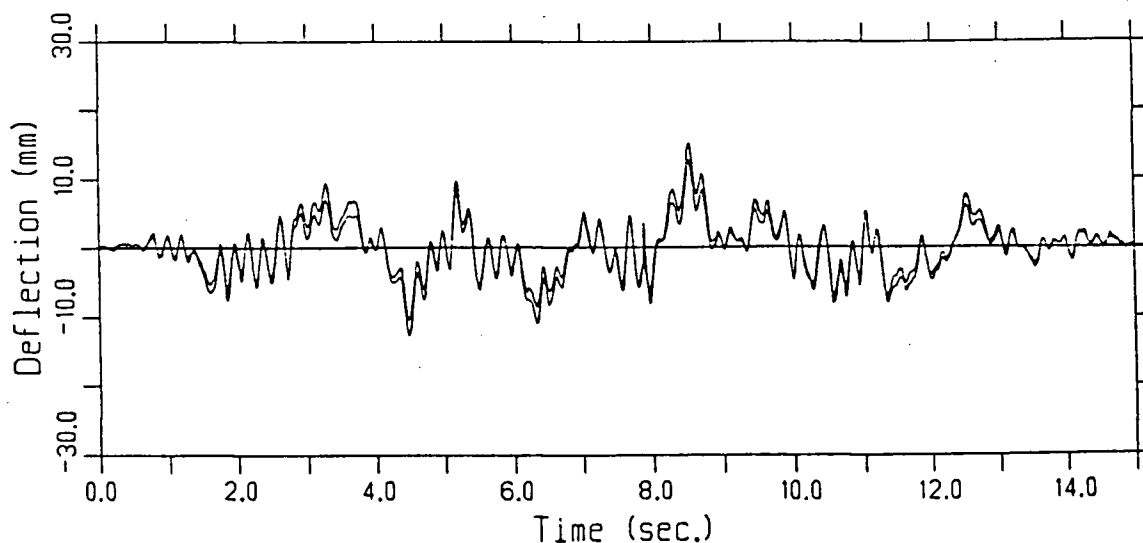
Figure 12.8 Recorded Time Histories of Third Floor Deflection From Both Potentiometers of the Friction Damped Braced Frame,Newmark-Blume-Kapur Artificial Earthquake,Intensity 3

Acceleration Record,Actual Earthquake
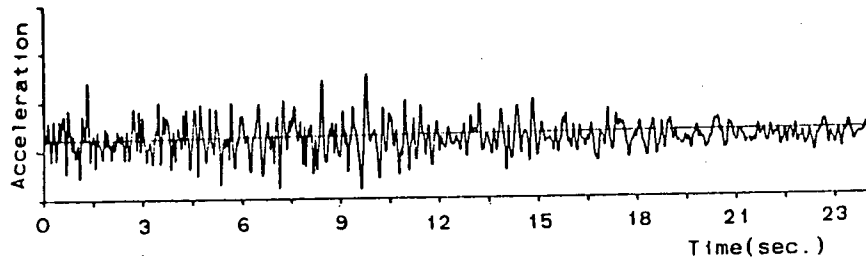
Fourier Amplitude Spectrum,Actual Earthquake
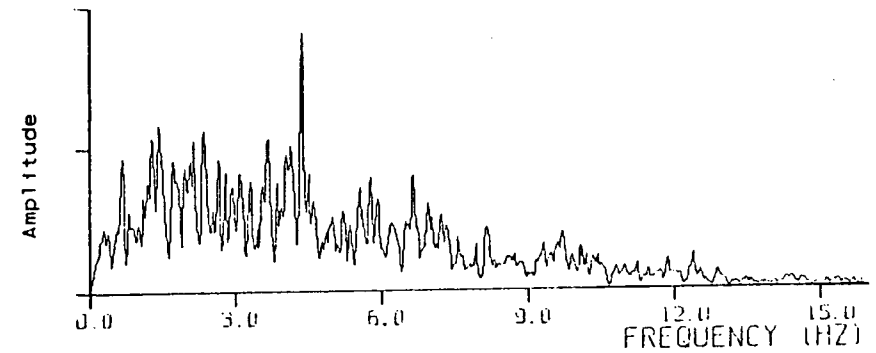
Recorded Table Acceleration
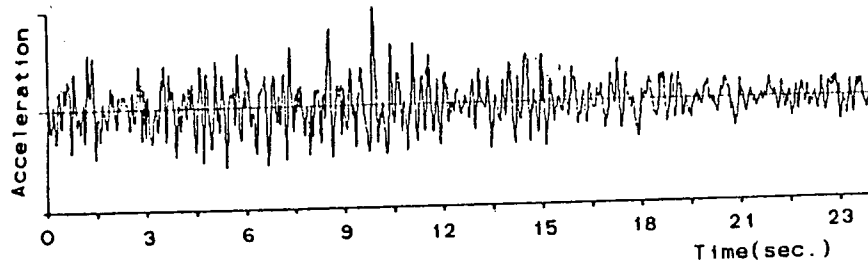
Fourier Amplitude Spectrum,Table Acceleration
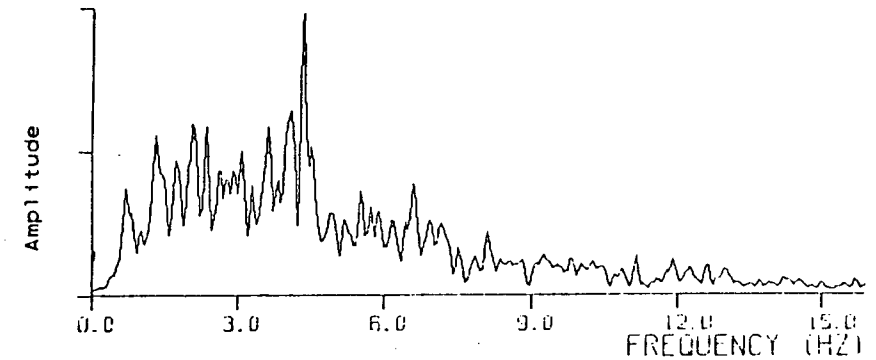
Figure 12.9 Shaking Table Performance,Taft Earthquake
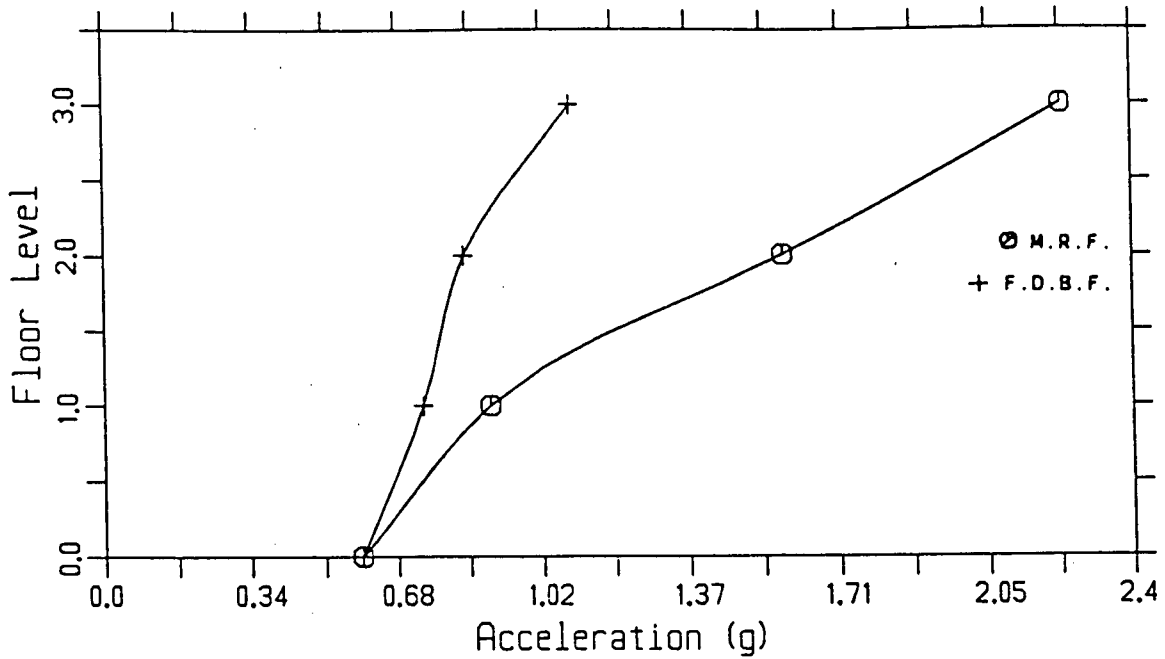
Figure 12.10 Envelope of Measured Horizontal Accelerations,Taft Earthquake (0.60g)
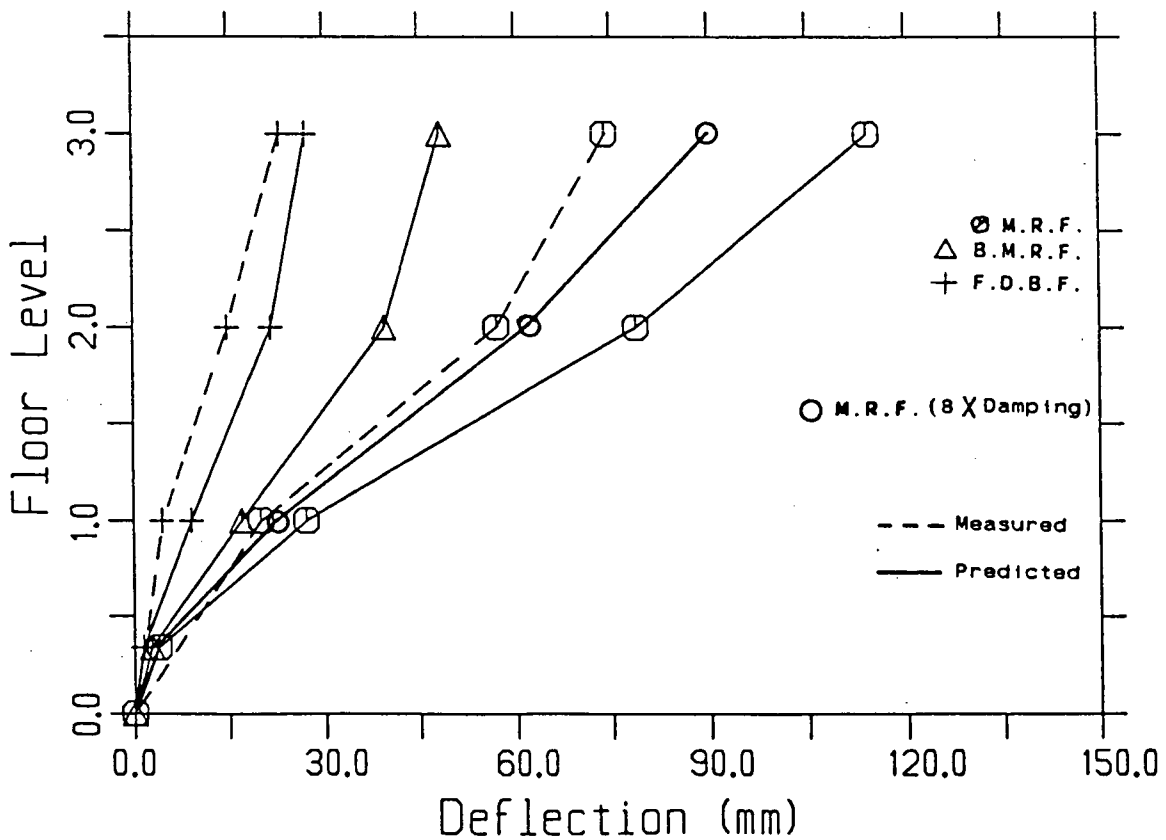
Figure 12.11 Envelope of Lateral Deflections,Taft Earthquake (0.60g)
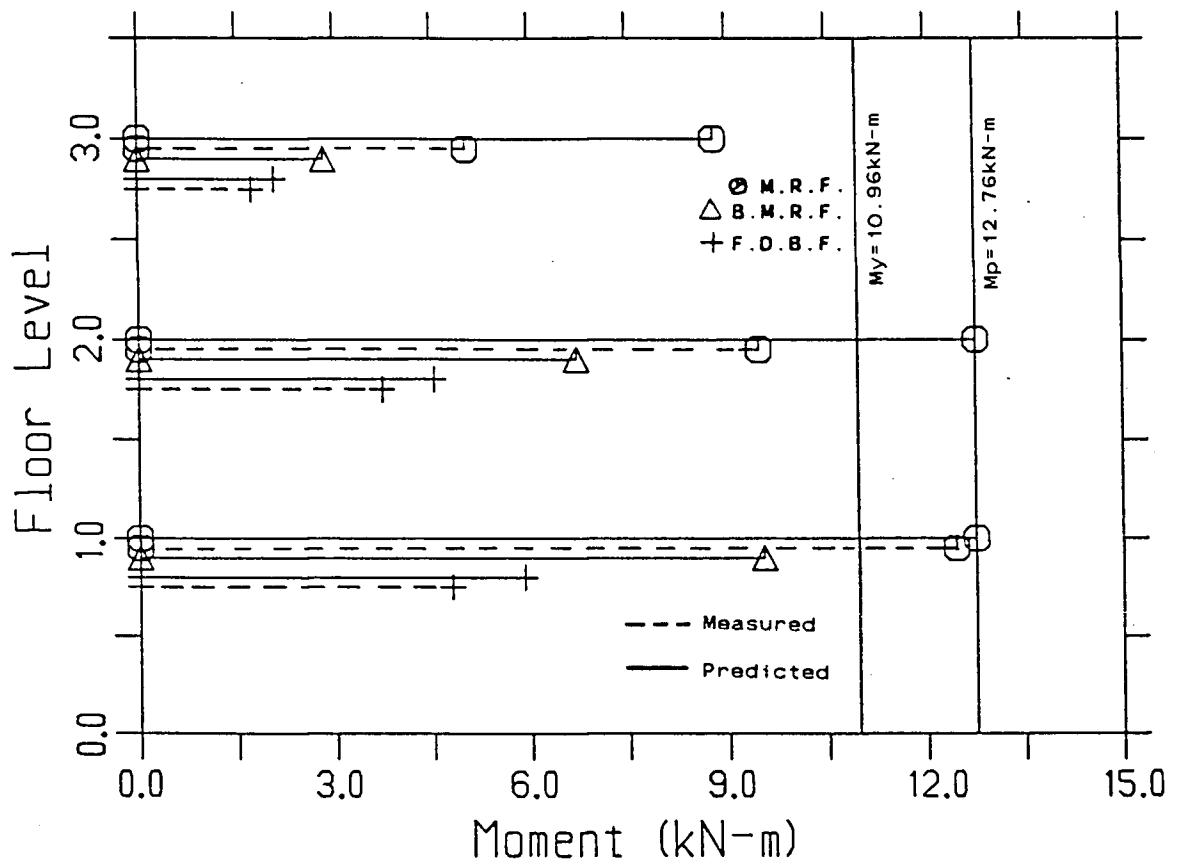
Figure 12.12 Envelope of Bending Moments in the Beams,Taft Earthquake (0.60g)
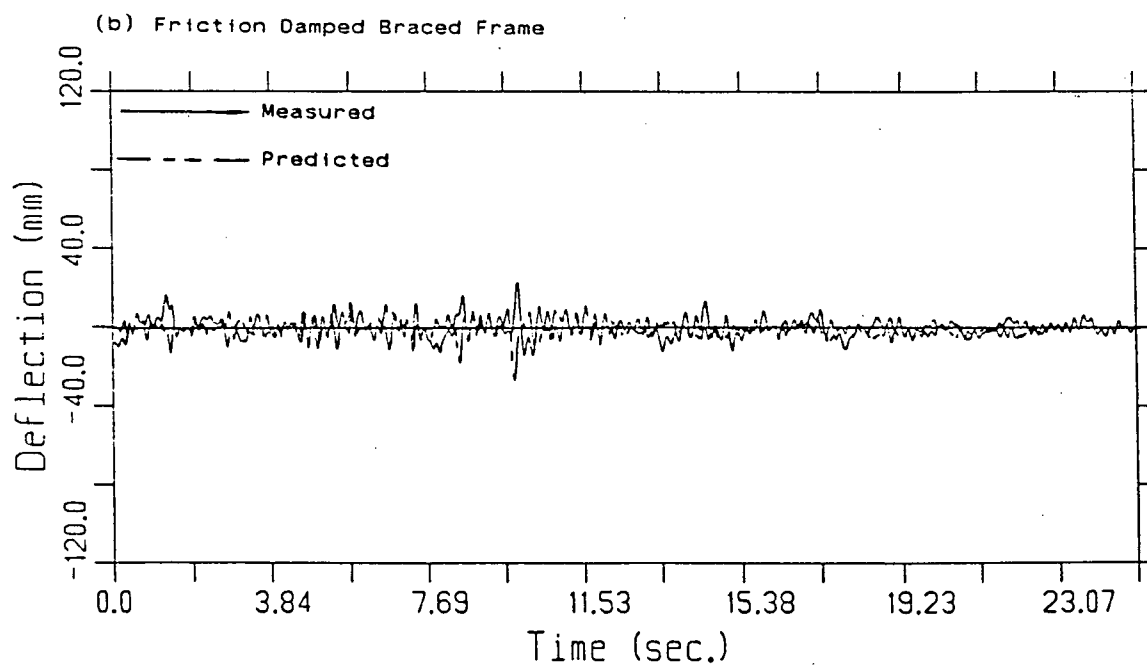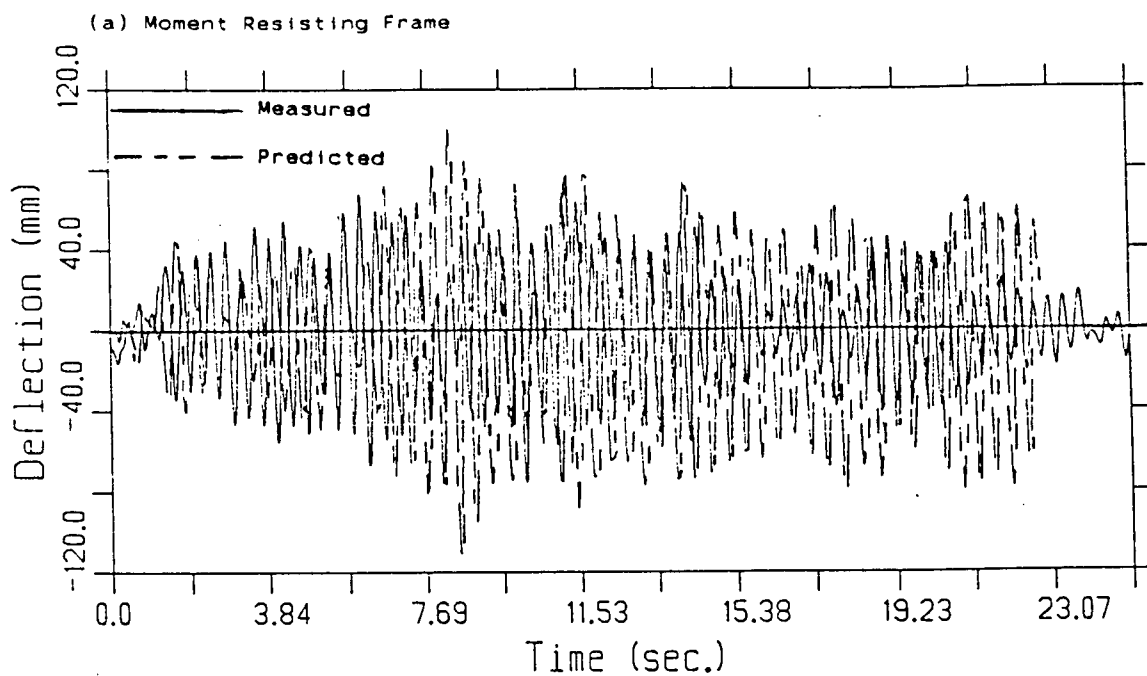
Figure 12.13 Time-Histories of Third Floor Deflection,Taft Earthquake (0.60g)
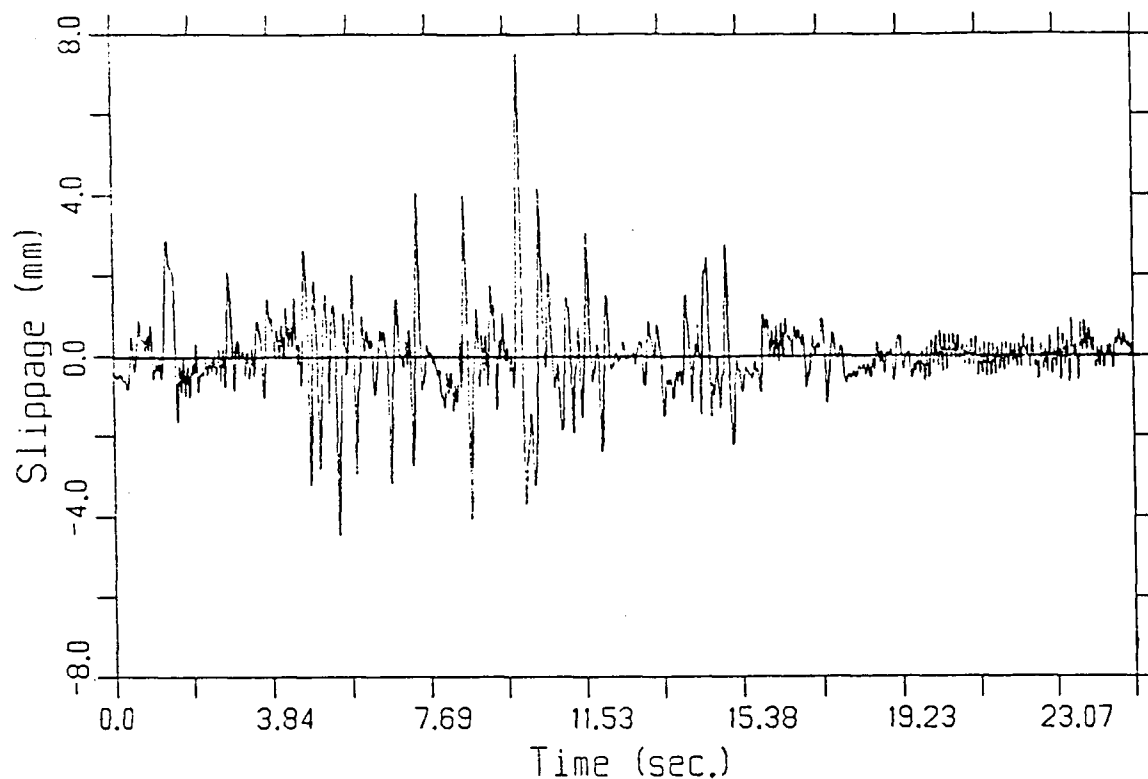
Figure 12.14 Recorded Slippage Time-History of Second Floor Device, Taft Earthquake (0.60g)
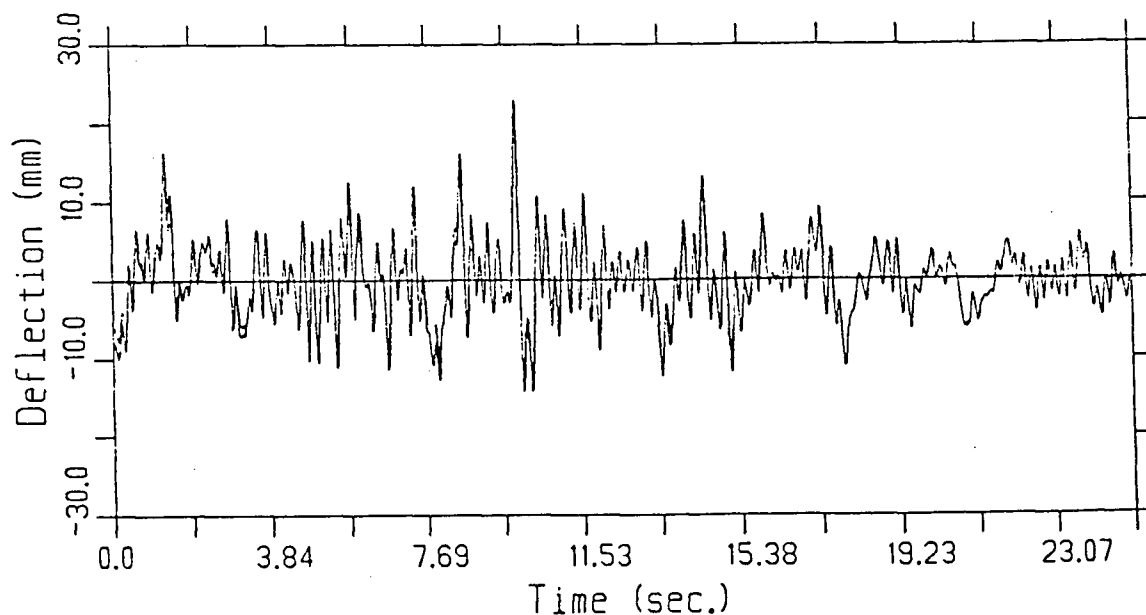
Figure 12.15 Recorded Time-Histories of Third Floor Deflection From Both Potentiometers of the Friction Damped Braced Frame , Taft Earthquake (0.60g)
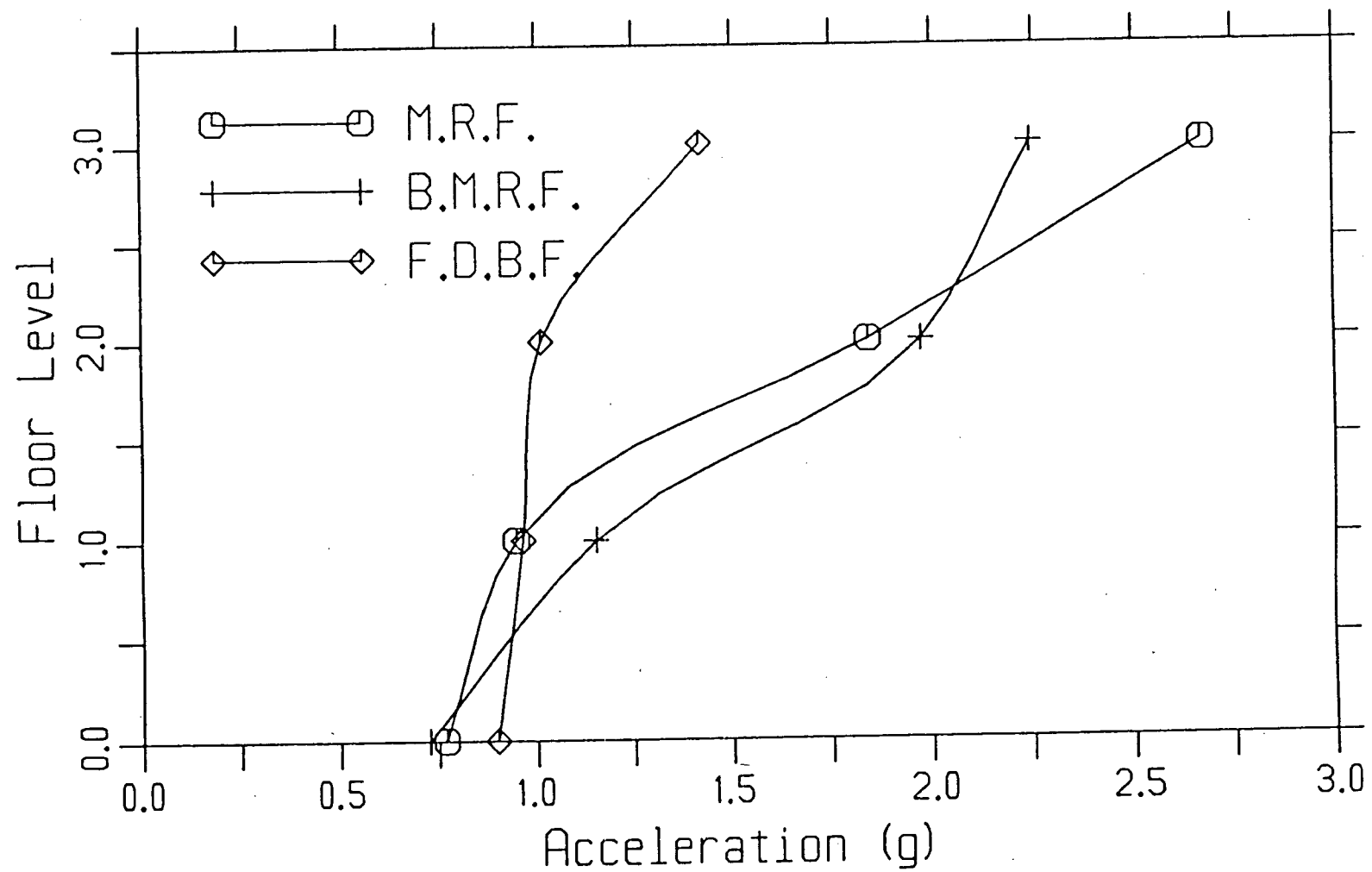
Figure 12.16 Envelope of Measured Horizontal Accelerations,Taft
Earthquake (0.9g)

(a) Moment Resisting Frame
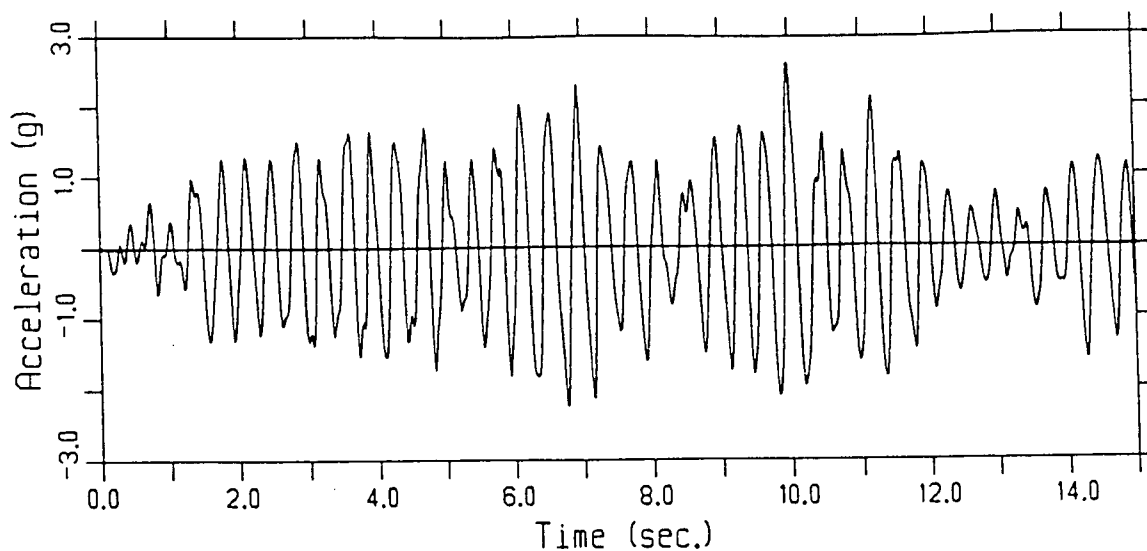
(b) Braced Moment Resisting Frame
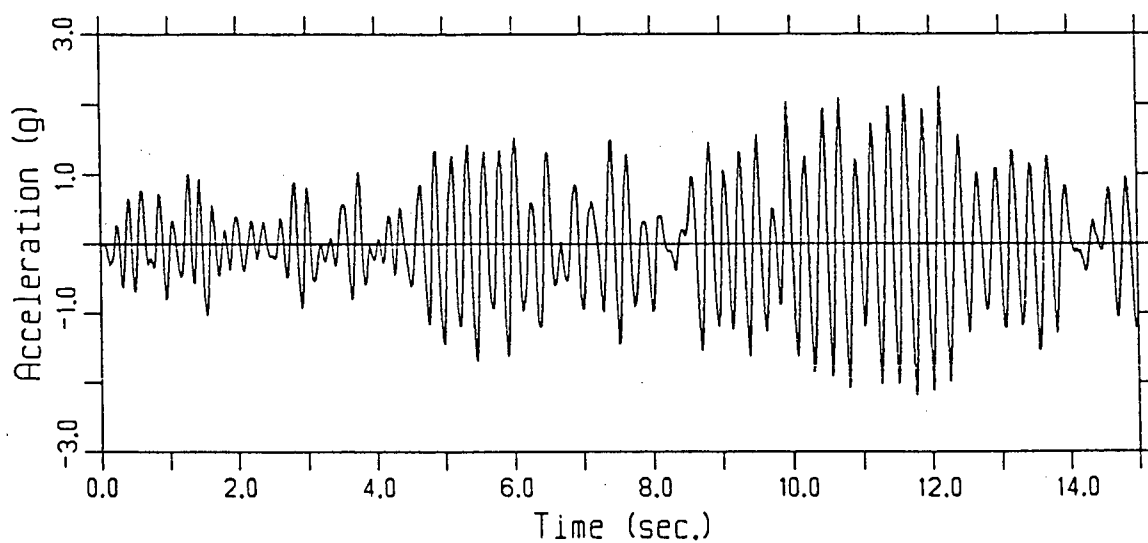
(c) Friction Damped Braced Frame
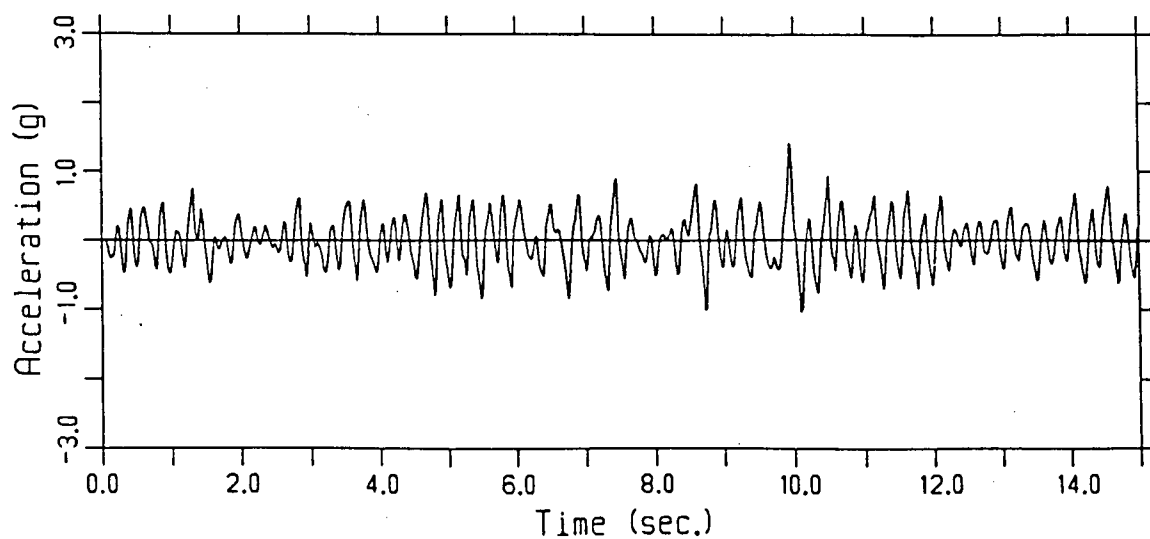
Figure 12.17 Time-Histories of Third Floor Accelerations,Taft Earthquake (0.9g)

(a) First Floor Device

(b) Second Floor Device

(c) Third Floor Device
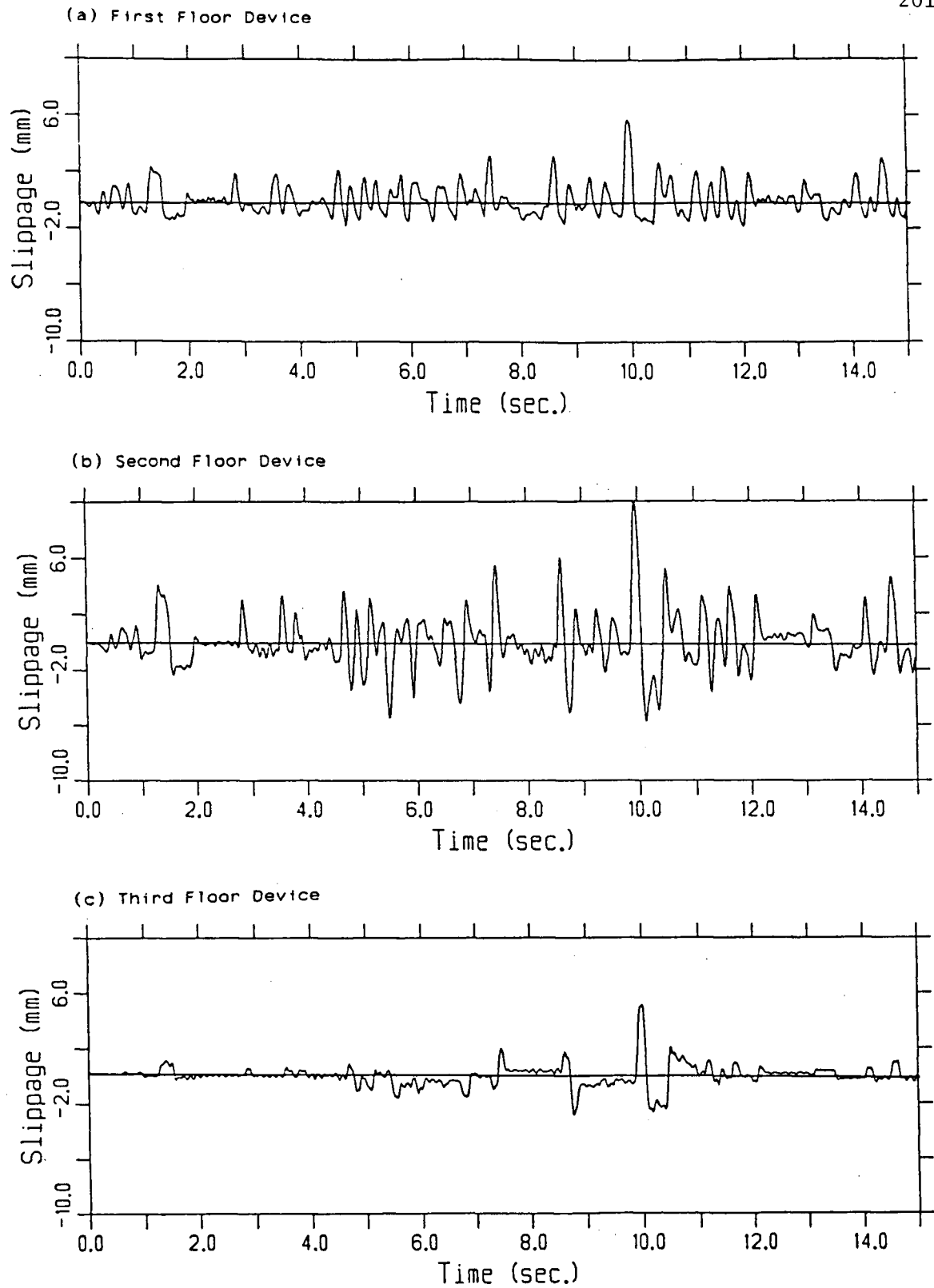
Figure 12.18 Slippage Time-Histories of Friction Devices, Taft Earthquake (0.9g)
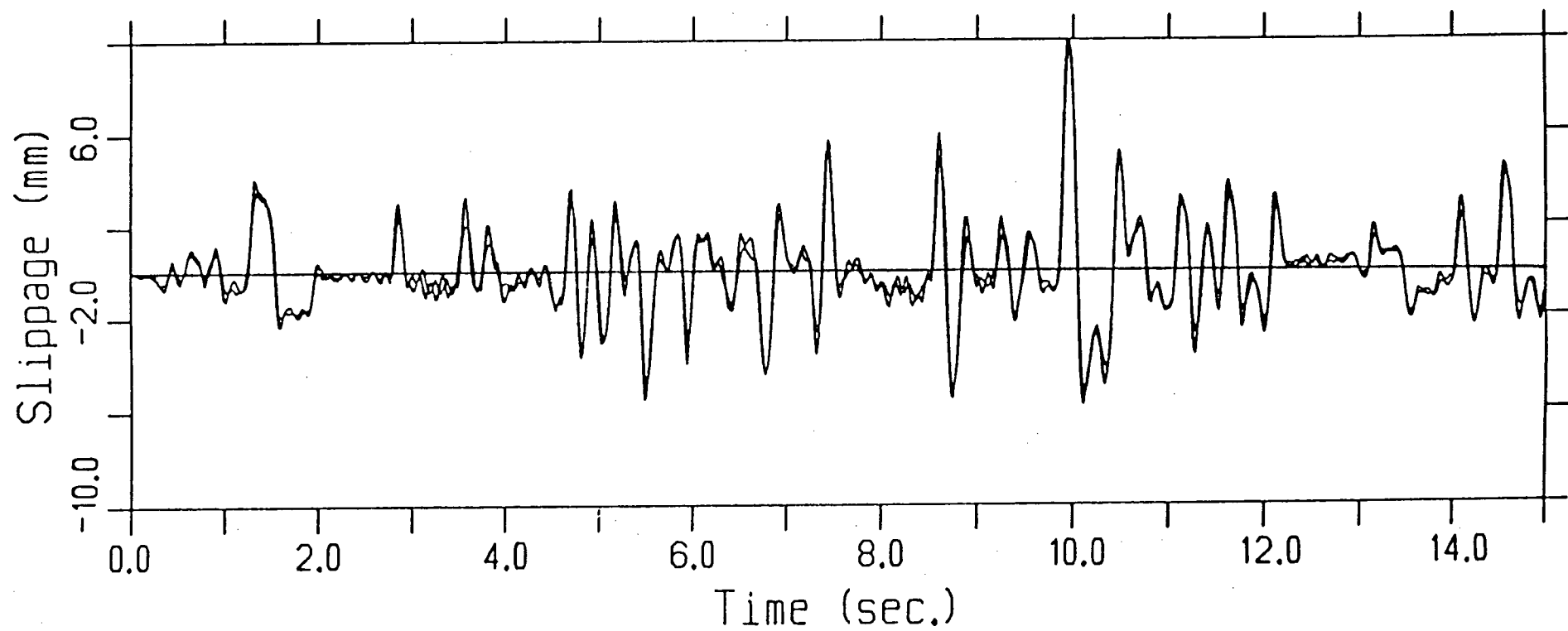
Figure 12.19 Slippage Time-Histories of Both Second Floor Devices,Taft Earthquake (0.9g)
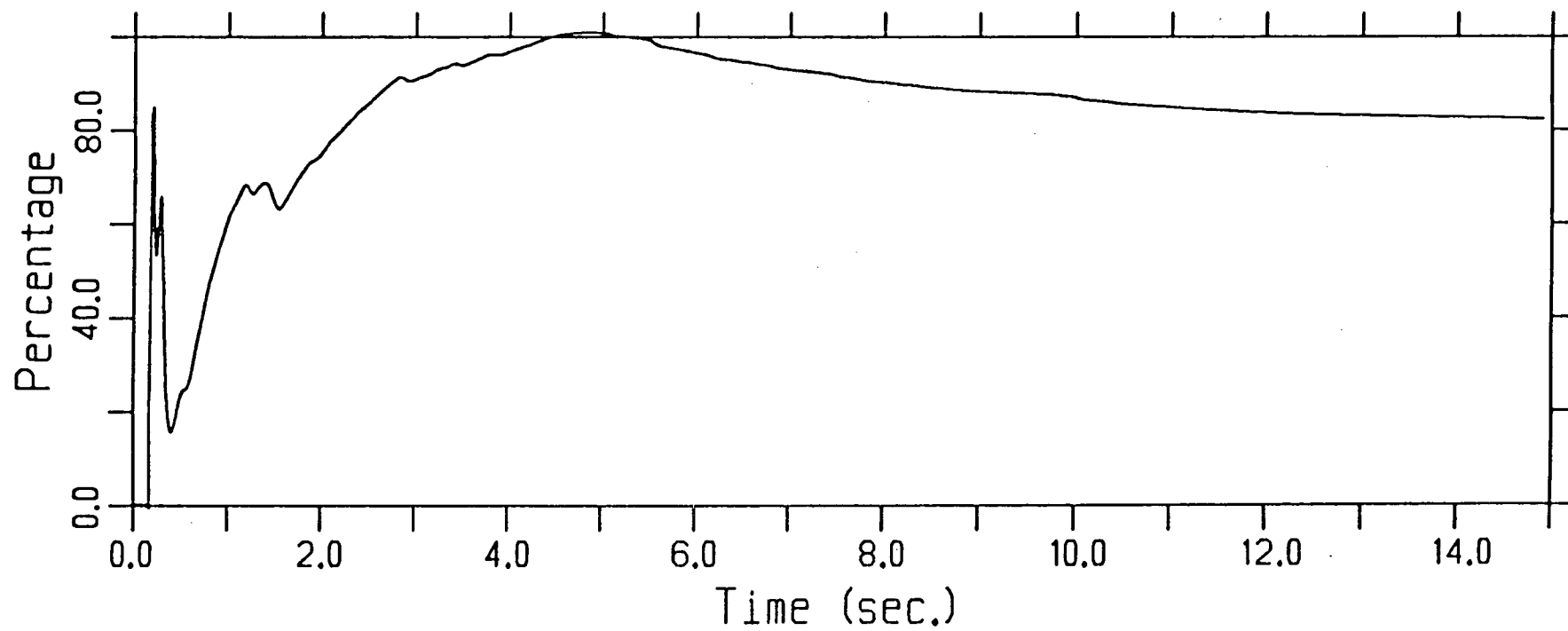
Figure 12.20 Time-History of the Percentage of Energy Dissipated by the Friction Devices,Taft Earthquake (0.90g)

	Dimensions	
Quantity	Absolute System	Engineering System
Length, l	L	L
Force, Q	MLT^{-2}	F
Modulus of elasticity, E	$ML^{-1}T^{-2}$	FL^{-2}
Poisson's ratio, ν		
Mass density, ρ	ML^{-3}	FT^2L^{-4}
Deflection, δ	L	L
Stress, σ	$ML^{-1}T^{-2}$	FL^{-2}
Frequency, f	T^{-1}	T^{-1}
Acceleration, g	LT^{-2}	LT^{-2}

Table 3.1 Dimensions of Governing Variables for Vibration of Elastic Structure (from ref.:7)

			Scale Factors	
Group (1)	Quantity (2)	Dimension (engineering units) (3)	Exact Scaling (4)	Gravity Forces Neglected (5)
Loading	Force, Q	F	$S_E S_l^2$	$S_E S_l^2$
	Gravitational acceleration, g	LT^{-2}	1	1
	Time, t	T	$S_l^{1/2}$	S_l
Geometry	Linear dimension, l	L	S_l	S_l
	Displacement, δ	L	S_l	S_l
	Frequency, f	T^{-1}	$S_l^{-1/2}$	S_l^{-1}
Material properties	Modulus, E	FL^{-2}	S_E	S_E
	Stress, σ	FL^{-2}	S_E	S_E
	Poisson's ratio, ν		1	1
	Density, ρ	FL^{-3}	S_E/S_l	Neglected

Table 3.2 Similitude Requirements for Vibration of Elastic Structure (from ref.:7)

Response parameter	Simplified model	Refined model	Refined / Simplified
1st floor max. deflection	4.249mm	4.616mm	1.09
2nd floor max. deflection	8.909mm	11.497mm	1.29
3rd floor max. deflection	10.559mm	13.434mm	1.27
1st floor beam max. moment	3.634kN-m	4.234kN-m	1.17
2nd floor beam max. moment	2.496kN-m	3.257kN-m	1.30
3rd floor beam max. moment	1.354kN-m	1.521kN-m	1.12
1st storey column max. moment	4.039kN-m	4.143kN-m	1.03
2nd storey column max. moment	2.360kN-m	3.055kN-m	1.29
3rd storey column max. moment	1.354kN-m	1.521kN-m	1.12
1st storey max. shear	5.227kN	5.224 N	1.00
2nd storey max. shear	3.719kN	4.747kN	1.28
3rd storey max. shear	2.263kN	2.356kN	1.04
1st storey max. axial force	27.138kN	28.531kN	1.05
2nd storey max. axial force	16.394kN	17.527kN	1.07
3rd storey max. axial force	6.580kN	7.790kN	1.18
C.P.U. Time	81.293sec.	292.116sec.	3.59

Table 4.1 Comparison between Simplified and Refined Models, El Centro Earthquake

Device #	Linear Regression	Correlation Coefficient
1	L=-3.12P+148.02	-0.9941
2	L=-2.63P+147.53	-0.9979
3	L=-3.09P+148.47	-0.9971
4	L=-2.67P+142.41	-0.9996
5	L=-3.36P+148.83	-0.9987
6	L=-3.10P+148.19	-0.9811
7	L=-3.68P+146.53	-0.9977

P=Global Slip Load (kN)   L=Length of Spring (mm)

Table 5.1 Results of Linear Regressions for Calibration of Friction Devices

Mode	Natural Frequencies (hz)		Natural Frequencies (rad/s)		Difference (%)
	Measured	Predicted	Measured	Predicted	
1	2.86	2.831	17.97	17.788	-1.05
2	9.08	9.174	57.05	57.642	1.04
3	14.4	15.930	89.22	100.091	10.63

Table 9.1 Comparison Between Measured and Predicted Natural
Frequencies of the Moment Resisting Frame

Mode	Mode Shapes		M.A.C.
	measured	predicted	
1	{0.22,0.56,0.80}	{0.21,0.57,0.80}	0.9996
2	{0.55,0.41,-0.72}	{0.57,0.46,-0.68}	0.9998
3	{0.86,-0.47,0.21}	{0.75,-0.58,0.32}	0.9823

Table 9.2 Comparison of Measured and Predicted Mode Shapes of the Moment Resisting Frame

Mode	Floor	Method	Modal Damping Ratio
1	1	Bandwidth	0.0029
1	1	Log-Decrement	0.0027
1	2	Bandwidth	0.0025
1	2	Log-Decrement	0.0030
1	3	Bandwidth	0.0025
1	3	Log-Decrement	0.0029
2	1	Bandwidth	0.0023
2	1	Log-Decrement	0.0017
2	2	Bandwidth	0.0025
2	2	Log-Decrement	0.0017
2	3	Bandwidth	0.0024
2	3	Log-Decrement	0.0017
3	1	Bandwidth	0.0109
3	1	Log-Decrement	0.0041
3	2	Bandwidth	0.0103
3	2	Log-Decrement	0.0041
3	3	Bandwidth	0.0076

Table 9.3 Measured Modal Damping Ratios of the Moment Resisting Frame

Mode	Floor	Method	Modal Damping Ratio
1	1	Log-Decrement	0.0146
1	2	Log-Decrement	0.0125
1	3	Log-Decrement	0.0109

Table 10.1 Measured Modal Damping Ratios of the Braced Moment Resisting Frame

Mode	Natural Frequencies (hz)		Natural Frequencies (rad/s)		Difference (%)
	Measured	Predicted	Measured	Predicted	
1	7.03	7.012	44.17	44.059	-0.26
2	18.4	19.472	115.6	122.348	5.83
3	*	28.316	*	177.919	-

TABLE 11.1 Comparison Between Measured and Predicted Natural Frequencies of the Friction Damped Braced Frame Under Low Amplitude Excitations

* Unable to Verify Experimentally

Mode	Mode Shapes		M.A.C.
	predicted	measured	
1	{0.29,0.60,0.75,}	{0.40,0.50,0.77}	0.9661
2	{0.66,0.27,-0.70}	{0.58,0.19,-0.79}	0.9972

Table 11.2 Comparison of Measured vs Predicted Mode Shapes of the Friction Damped Braced Frame Under Low Amplitude Excitations

Mode	Floor	Method	Modal Damping Ratio
1	1	Log-Decrement	0.0065
1	2	Log-Decrement	0.0060
1	3	Log-Decrement	0.0056
2	1	Log-Decrement	0.0043
2	3	Log-Decrement	0.0034

Table 11.3 Measured Modal Damping Ratios of the Friction Damped Braced Frame

Intensity	Type of Frame	Bending Moment (kN-m)	
		Measured	Predicted
1	M.R.F.	1.48	2.11
	B.M.R.F.	0.47	0.46
	F.D.B.F.	0.22	0.34
2	M.R.F.	4.05	4.18
	B.M.R.F.	1.06	0.96
	F.D.B.F.	0.45	0.70
3	M.R.F.	7.07	10.01
	B.M.R.F.	2.61	2.82
	F.D.B.F.	0.94	1.47

Table 12.1 Envelopes of Bending Moments in the Base Column at Location of Strain Gages,Newmark-Blume-Kapur Artificial Earthquake,Intensities 1,2,3

Frame	Bending Moment (kN-m)	
	Measured	Predicted
F.D.B.F.	2.70	3.50
B.M.R.F.	6.50	*
M.R.F.	9.60	10.30

* Unable to Verify Experimentally

Table 12.2 Envelope of Bending Moments in the Base Column at Location of Strain Gages,Taft Earthquake (0.60g)

Frame	Mode	Natural Frequencies (Hz)		
		Predicted	Measured	
			Frame#1	Frame#2
M.R.F.	1	2.831	2.86	2.81
	2	9.174	9.08	8.91
	3	15.93	14.4	13.90
B.M.R.F.	1	5.087	5.29	6.10
	2	14.581	*	*
	3	22.025	*	*
F.D.B.F.	1	7.012	7.03	6.00
	2	19.472	18.4	*
	3	28.316	*	*

*Unable to Verify Experimentally

Table 12.3 Comparison of Natural Frequencies for the Two Model Frames

Frame	Mode	Modal Damping Ratio	
		Frame#1	Frame#2
M.R.F.	1	0.0028	0.0026
	2	0.0021	0.0023
	3	0.0074	0.0040
B.M.R.F.	1	0.0127	0.0058
	2	*	*
	3	*	*
F.D.B.F.	1	0.0060	0.0058
	2	0.0039	*
	3	*	*

* Unable to Verify Experimentally

Table 12.4 Comparison of Damping Ratios for the Two Model Frames

	Frame	Cross-Section	Mp(kN-m)	Δ_{max}(mm)	Md/Mp	Mi/Mp	Mmax/Mp
Original Size	M.R.F. *	S75x8	9.57	102.02	0.16	0.84	1.00
	B.M.R.F. *	S75x8	9.57	19.47	0.16	0.32	0.48
	F.D.B.F. *	S75x8	9.57	9.05	0.16	0.17	0.33
Reduced Size	F.D.B.F.	SLP-3"	5.89	10.48	0.25	0.19	0.44
	F.D.B.F.	HSS 38.1x38.1x4.78mm	2.76	13.87	0.54	0.10	0.64
	F.D.B.F.	HSS 38.1x38.1x2.54mm	1.80	14.32	0.82	0.12	0.94

* Tested on Shaking Table

Mp=Plastic Moment

Md=Maximum Moment From Dead Load

Mi=Maximum Moment From Inertia Load

Mmax=Maximum Moment From Inertia Forces + Dead Load

Δ_{max}=Maximum Third Floor Lateral Deflection

Table 13.1 Design of a Reduced Size Friction Damped Braced Frame,Newmark-Blume-Kapur Artificial Earthquake (0.30g)

Appendix A: Listing of Program "VIBRATION"

```
C*********************************************************************
C        PROGRAM VIBRATION
C        BY ANDRE FILIATRAULT
C        APRIL 1985
C        UNIVERSITY OF BRITISH-COLUMBIA
C
C        GENERATION OF THE AMPLITUDE FREQUENCY RESPONSE FUNCTION
C        FOR AN ELASTIC M.D.O.F.S. WITH MODAL VISCOUS DAMPING
C        UNDER HARMONIC BASE EXCITATION IN PHASE
C        LOGICAL UNIT 5:DATA-FILE CONTAINING THE NO. OF DEGREES
C                         OF FREEDOM,THE NATURAL FREQUENCIES,MODE
C                         SHAPES,DAMPING RATIOS AND FREQUENCY RANGE
C        LOGICAL UNIT 6:OUTPUT FILE
C*********************************************************************
      IMPLICIT REAL*8(A-H,O-Z)
      DIMENSION A(3,3),AINV(3,3),D1(3,3),D2(3,3),G(3),H(3),HW(1000,3)
      DIMENSION W(1000),WN(3),ZETA(3),DA(3,3),ADA(3,3),IPERM(6)
C
C     READ DATA FROM DATA-FILE
C
      READ(5,100)N
      READ(5,101)(WN(I),I=1,N)
      DO 10 I=1,N
      READ(5,102)(A(J,I),J=1,N)
  10 CONTINUE
      READ(5,103)(ZETA(I),I=1,N)
      READ(5,111) W1,W2
 100 FORMAT(I5)
 101 FORMAT(3F7.2)
 102 FORMAT(3F7.2)
 103 FORMAT(3F6.4)
 111 FORMAT(2F7.2)
C
C     WRITE DATA IN OUTPUT FILE
C
      WRITE(6,104)
      WRITE(6,105)
      WRITE(6,106)N
      WRITE(6,107)(WN(I),I=1,N)
      WRITE(6,108)
      DO 20 I=1,N
      WRITE(6,109)(A(I,J),J=1,N)
  20 CONTINUE
      WRITE(6,110)(ZETA(I),I=1,N)
      WRITE(6,116)W1,W2
      WRITE(6,104)
 104 FORMAT(//,80('*'),//)
 105 FORMAT(T25,'PROGRAM VIBRATION')
 106 FORMAT(T25,'NO. DEGREES OF FREEDOM CONSIDERED= ',I5)
 107 FORMAT(T25,'NATURAL FREQUENCIES (RAD/S)= ',3(F7.2,1X))
 108 FORMAT(T25,'MODAL MATRIX')
 109 FORMAT(T25,3(F4.2,1X))
 110 FORMAT(T25,'MODAL DAMPING RATIOS= ',3(F6.4,1X))
 116 FORMAT(T25,'FREQUENCY RANGE (RAD/S)= ',2X,F7.2,'TO ',F7.2)
C
C     CALL UBC MATRIX SUBROUTINE TO INVERSE THE MODAL MATRIX
C
      CALL INV(N,N,A,IPERM,N,AINV,DET,JEXP,COND)
C
```

```
C     SET UP FREQUENCY RANGE
C
      DO 25 I=1,N
      DO 26 J=1,N
      D1(I,J)=0.D0
      D2(I,J)=0.D0
   26 CONTINUE
   25 CONTINUE
      DELW=(W2-W1)/1000.D0
      WBAR=W1-DELW
C
C     STARTS LOOP THROUGH FREQUENCY RANGE
C
      DO 30 I=1,1000
      WBAR=WBAR+DELW
      DO 40 J=1,N
      DENO=DABS((WN(J)**2.D0-WBAR**2.D0))**2.D0
      DENO=DENO+(2.D0*ZETA(J)*WN(J)*WBAR)**2.D0
      D1(J,J)=(2*ZETA(J)*WN(J)*WBAR)/DENO
      D2(J,J)=(WN(J)**2.D0-WBAR**2.D0)/DENO
   40 CONTINUE
      CALL DGMULT(D1,AINV,DA,N,N,N,N,N,N)
      CALL DGMULT(A,DA,ADA,N,N,N,N,N,N)
      DO 50 J=1,N
      G(J)=0.D0
      DO 60 K=1,N
      G(J)=G(J)+ADA(J,K)
   60 CONTINUE
   50 CONTINUE
      CALL DGMULT(D2,AINV,DA,N,N,N,N,N,N)
      CALL DGMULT(A,DA,ADA,N,N,N,N,N,N)
      DO 70 J=1,N
      H(J)=0.D0
      DO 80 K=1,N
      H(J)=H(J)+ADA(J,K)
   80 CONTINUE
      H(J)=-H(J)
   70 CONTINUE
      DO 90 J=1,N
      HW(I,J)=(DABS(G(J))**2.D0+DABS(H(J))**2.D0)*WBAR**4.D0
      HW(I,J)=HW(I,J)+1.D0-(2.D0*H(J)*WBAR**2.D0)
      HW(I,J)=DSQRT(HW(I,J))
      HW(I,J)=20.D0*DLOG10(HW(I,J))
   90 CONTINUE
      W(I)=WBAR
   30 CONTINUE
C
C     WRITE RESULTS IN OUTPUT FILE
C
      WRITE(6,104)
      WRITE(6,112)
      DO 95 J=1,N
      WRITE(6,113)J
      WRITE(6,114)
      DO 97 K=1,1000
      WRITE(6,115) W(K),HW(K,J)
   97 CONTINUE
   95 CONTINUE
  112 FORMAT(T25,'RESULTS')
  113 FORMAT(//,'DEGREE OF FREEDOM NO. ',I2)
  114 FORMAT(T15,'FREQUENCY W (RAD/S) ',5X,'H(W)')
  115 FORMAT(T15,F7.2,T40,F7.2)
      STOP
      END
```

```
C
C     THIS PROGRAM CALCULATE THE ENERGY DISSIPATED
C     BY THE FRICTION DEVICES AND THE TOTAL ENERGY
C     INPUTED IN THE FRICTION DAMPED BRACED FRAME
C     DURING A SEISMIC TEST ON THE SHAKING TABLE
C     UNITS USED MUST BE CONSISTENT
C     UNIT 1=RECORDED FIRST FLOOR ACCELERATION
C     UNIT 2=RECORDED SECOND FLOOR ACCELERATION
C     UNIT 3=RECORDED THIRD FLOOR ACCELERATION
C     UNIT 4=RECORDED TABLE DISPLACEMENT
C     UNIT 6=OUTPUT FILE CONTAINING ENERGY INPUT
C     UNIT 7=RECORDED SLIPPAGE OF FIRST FLOOR DEVICE
C     UNIT 8=RECORDED SLIPPAGE OF SECOND FLOOR DEVICE
C     UNIT 9=RECORDED SLIPPAGE OF THIRD FLOOR DEVICE
C     UNIT 10=OUTPUT FILE CONTAINING ENERGY DISSIPATED BY FRICTION
C     UNIT 11=OUTPUT FILE CONTAINING % ENERGY DISSIPATED
C
C
      IMPLICIT REAL*8(A-H,O-Z)
      DIMENSION A1(5000),A2(5000),A3(5000),XG(5000),S1(5000),S2(5000),S3
     *(5000),WM(3),EI(3),ED(3),P(3)
C
C     READ DATA
C
      WRITE(5,100)
  100 FORMAT('ENTER NUMBER OF DATA POINTS')
      READ(5,*) N
      WRITE(5,101)
  101 FORMAT('ENTER THE MASS OF EACH CONCRETE BLOCK')
      READ(5,*)(WM(I),I=1,3)
      WRITE(5,102)
  102 FORMAT('ENTER LOCAL SLIP LOAD OF FRICTION DEVICES')
      READ(5,*) PSLIP
      WRITE(5,111)
      READ(5,*) DELTAT
  111 FORMAT('ENTER SAMPLE INTERVAL ')
      AN=N/8
      NLINE=DINT(AN)

      DO 10 I=1,NLINE
      K=(8*I)-7
      K7=K+7
      READ(1,103)(A1(J),J=K,K7)
      READ(2,103)(A2(J),J=K,K7)
      READ(3,103)(A3(J),J=K,K7)
      READ(4,103)(XG(J),J=K,K7)
      READ(7,103)(S1(J),J=K,K7)
      READ(8,103)(S2(J),J=K,K7)
      READ(9,103)(S3(J),J=K,K7)
   10 CONTINUE
  103 FORMAT(8F10.5)
      N=NLINE*8
C
C     CALCULATE ENERGY
C
      WRITE(5,104)
      WRITE(6,104)
  104 FORMAT('***PROGRAM ENERGY***')
      WRITE(5,105) N
      WRITE(6,105) N
```

```
105 FORMAT('NUMBER OF DATA POINTS CONSIDERED',I5)
    DO 30 I=1,3
    WRITE(5,106) I,WM(I)
    WRITE(6,106) I,WM(I)
 30 CONTINUE
106 FORMAT('MASS OF FLOOR NO. ',I2,'=',F15.5)
    WRITE(5,107) PSLIP
    WRITE(6,107) PSLIP
107 FORMAT('LOCAL SLIP LOAD OF FRICTION DEVICES=',F15.5)
    WRITE(5,108)DELTAT
    WRITE(6,108)DELTAT
108 FORMAT('SAMPLE INTERVAL=',F15.5)
    WRITE(6,109)
    WRITE(10,115)
    WRITE(11,116)
115 FORMAT('TIME',5X,'ENERGY DISSIPATED')
116 FORMAT('TIME',5X,'% ENERGY DISSIPATED')
109 FORMAT('TIME',5X,'ENERGY INPUT')
    DO 15 I=1,3
    EI(I)=0.D0
    ED(I)=0.D0
 15 CONTINUE
    EITOT=0.D0
    EDTOT=0.D0
    DO 20 I=2,N
    DELTAX=-(XG(I)-XG(I-1))
    EI(1)=EI(1)+(WM(1)*(A1(I)+A1(I-1))*DELTAX)
C     MINUS SINCE TABLE LVDT CALIBRATED IN REVERSE WITH ACCELEROMETER
    EI(2)=EI(2)+(WM(2)*(A2(I)+A2(I-1))*DELTAX)
    EI(3)=EI(3)+(WM(3)*(A3(I)+A3(I-1))*DELTAX)
    ED(1)=ED(1)+DABS(S1(I)-S1(I-1))
    ED(2)=ED(2)+DABS(S2(I)-S2(I-1))
    ED(3)=ED(3)+DABS(S3(I)-S3(I-1))
    TIME=DELTAT*I
    EITOT=EITOT+((EI(1)+EI(2)+EI(3))/2.D0)
    EDTOT=EDTOT+((ED(1)+ED(2)+ED(3))*4.D0*PSLIP)
    PTOT=EDTOT/EITOT*100.D0
    WRITE(6,110) TIME,EITOT
    WRITE(10,110) TIME,EDTOT
    WRITE(11,110) TIME,PTOT
 20 CONTINUE
110 FORMAT(F7.4,F15.5)
    WRITE(5,112) EITOT
    WRITE(6,112) EITOT
    WRITE(5,113) EDTOT
    WRITE(6,113) EDTOT
    WRITE(5,114) PTOT
    WRITE(6,114) PTOT
112 FORMAT('TOTAL ENERGY INDUCED IN THE STRUCTURE=',F15.5)
113 FORMAT('TOTAL ENERGY DISSIPATED BY FRICTION=',F15.5)
114 FORMAT('% TOTAL ENERGY DISSIPATED BY FRICTION=',F15.5)
    STOP
    END
```